SYNTHESIS OF ORGANOFLUORINE COMPOUNDS USING A FALLING FILM MICROREACTOR: PROCESS DEVELOPMENT AND KINETIC MODELLING

Kuveshan Padayachee

[BSc Eng, UKZN]

University of KwaZulu-Natal

Howard College

A dissertation submitted in fulfilment of the requirements for the degree

Master of Science in Engineering in Chemical Engineering,

School of Engineering, College of Agriculture, Engineering and Science,

University of KwaZulu-Natal

June 2016

Supervisors: Doctor David Lokhat and Professor Deresh Ramjugernath

As the candidate's supervisor I agree to the submission of this dissertation:

Dr. D. Lokhat	Prof. D. Ramjugernath

DECLARATION

I, Kuveshan Padayachee declare that:

The research reported in this dissertation/thesis, except where otherwise indicated, is my original work.

1. The research reported in this thesis, except where otherwise indicated, is my original research.
2. This thesis has not been submitted for any degree or examination at any other university.
3. This thesis does not contain other persons' data, pictures, graphs or other information, unless specifically acknowledged as being sourced from other persons.
4. This thesis does not contain other persons' writing, unless specifically acknowledged as being sourced from other researchers. Where other written sources have been quoted, then:
    i. Their words have been re-written but the general information attributed to them has been referenced
    ii. Where their exact words have been used, then their writing has been placed in italics and inside quotation marks, and referenced.
5. This thesis does not contain text, graphics or tables copied and pasted from the Internet, unless specifically acknowledged, and the source being detailed in the thesis and in the References sections.

Signed: _____

Date: _____

ACKNOWLEDGEMENTS

This research is aligned with the aims of the Fluorochemical Expansion Initiative (FEI) endorsed and funded by the Department of Science and Technology. This project was supported by the South African Research Chairs Initiative of the Department of Science and Technology and, the National Research Fund, as well as Pelchem (a subsidiary of the South African Nuclear Energy Corporation) as part of the FEI programe.

This work would have not been possible without the technical help and support of a number of individuals throughout its duration. Firstly, I would like to thank my supervisor Professor D. Ramjugernath for his wealth of knowledge and experience shared. My deepest gratitude is extended to my co-supervisor, Dr. D. Lokhat whose support, knowledge and friendship will forever be appreciated. I would also like to thank the technical and laboratory staff at the School of Chemical Engineering at the University of KwaZulu-Natal for their assistance and advice, namely Nomthandazo Hadebe, Sadha Naidoo and Ayanda Kanyile.

I would also like to acknowledge all my post-graduate colleagues for their support, encouragement, knowledge and always welcomed sense of humour, Navar Singh, Perinban Govender, Ashveer Domah, Reshlin Moodley, Nalika Ojageer, Jesita Reddy, Thabo Magubane, Piniel Bengesai, Emmanuel Gande, Devash Rajcoomar, Philani Biyela, Rowen Gyan and Ashir Daya.

Lastly, I would like to thank Nadia Ismail, my sister (Denisha), mother (Rajas) and father (Vinesh) as well as Shaneel Ragoo, Saira, Grace and Ahmed Ismail for their love and support throughout my tertiary education, without whom, none of this would have been possible.

ABSTRACT

South Africa is rich in valuable ore, including fluorspar (calcium fluoride), a principle feedstock used to synthesize hydrofluoric acid and a wide range of other fluorochemicals. As part of a wider initiative to promote local beneficiation of fluorspar, the primary purpose of this investigation was the synthesis of two valuable fluorochemicals, namely 1,1,2,3,3,3-hexafluoropropyl methyl ether (HME) and methyl-2,3,3,3-tetrafluoro-2-methoxypropionate (MTFMP). A secondary objective was to develop and identify suitable kinetic models as well as the associated kinetic parameters for the systems by means of least squares regression of experimental data.

Two reactors were used in this study: the first, a gas-liquid continuously stirred semi-batch glass reactor was used for preliminary investigations (prior to the commencement of this work) to investigate the synthesis of HME. The second, a falling film microreactor (FFMR), a much more efficient medium for gas-liquid reactions, was used for the kinetic study. The FFMR was chosen as it has remarkable high rates of heat and mass transfer allowing for stringent control of reaction conditions as well as allowing for continuous process operation to be achieved.

HME was produced by the reaction of methanol and hexafluoropropene in the presence of potassium hydroxide. MTFMP was similarly synthesized by the reaction of methanol and hexafluoropropene oxide in the presence of potassium and sodium hydroxide. The HME system was initially investigated in the gas-liquid glass reactor where the presence of HME as well as by-products of the reaction were successfully identified and quantified using gas chromatography-mass spectroscopy and gas chromatography (with the internal standard method), respectively. Results revealed that the reaction was rapid and highly exothermic and brought about negligible solid formation which deemed the system suitable for a FFMR. The yield of HME in the glass reactor varied between 19.21 and 53.32% with respect to moles of hexafluoropropene gas introduced into the system. The yields of the by-products were also quantified and the yield of alkenyl ether was found to vary between 0.07 and 1.03% while alkyl tetrafluoropropionate varied from 2.42 to 5.10%. These experiments were conducted at reactor temperatures between 12 and 28 °C, hexafluoropropene mole fractions in the feed between 0.41 and 0.83 and an inlet potassium methoxide concentration between 0.40 and 0.80 $mol \cdot L^{-1}$.

The novel synthesis of HME and MTFMP using a FFMR was then undertaken with the reactor operating in counter current mode. A 4 factor circumscribed Box-Wilson central composite design was used to design experiments, the four factors of interest being reaction temperature, liquid flowrate, either potassium or sodium hydroxide concentration, and finally, hexafluoropropene (for

the HME system) and hexafluoropropene oxide (for the MTFMP system) mole fraction in the reactant gas.

HME yields were found to be greater in the FFMR varying from 11.60 to 71.47% with the yields of the by-products varying from 0.11 to 6.99% for the alkenyl ether and 0.75 and 6.24% for the alkyl tetrafluoropropionate. Experiments were conducted at temperatures between 2 and 22 °C, hexafluoropropene mole fraction in the feed of 0.17 and 0.88, potassium methoxide concentration of 0.25 and 0.61 $mol \cdot L^{-1}$ and a liquid flow rate of 0.50 and 5.50 $mL \cdot min^{-1}$.

The MTFMP system was handled similarly with its presence in the product being identified and quantified using gas chromatography-mass spectroscopy and gas chromatography (with the internal standard method), respectively. The yield of MTFMP was found to vary between 0.00 to 23.62% with respect to the moles of hexafluoropropene oxide introduced over the reaction period. The low yields were due to an inherently slower reaction which was not ideal for a FFMR given its low liquid residence time. Experiments were conducted at temperatures between 30 and 40 °C, hexafluoropropene oxide mole fraction in the feed of 0.16 and 0.84, potassium methoxide concentration of 0.15 and 0.65 $mol \cdot L^{-1}$ and a liquid flow rate of 0.50 and 5.50 $mL \cdot min^{-1}$. Results of the experiments showed that the MTFMP system was not suitable for the FFMR due to the low residence time of the reactant in reactor.

A kinetic model was then developed for both the reactive systems from fundamental principles and executed in the MATLAB® environment (version R2012b, The MathWorks, Inc.). The kinetic model proposed for the HME system consisted of five reactions for which reference kinetic rate constants and activation energies were successfully identified. The resultant model did not predict HME concentrations adequately with an average absolute relative deviation percentage (AARD %) of 34.12 %. The reaction mechanism proposed for the MTFMP system was a two step reaction sequence which described the system satisfactorily well, the kinetic parameters required for this system was a reference kinetic rate constant, activation energy and Sechenov coefficient which were all successfully identified. The effect of reaction order on the pertinent reactions was also investigated and it was found that a second order description best fit the experimental data. The MTFMP model fit experimental data less agreeably with an AARD % of 170.00 % which was heavily weighted by data points with errors in excess of 500%, analysing the results exclusive of these points lead to an AARD % of 17.80 %.

TABLE OF CONTENTS

LIST OF FIGURES

Chapter 2:

Chapter 3:

Chapter 4:

Chapter 5:

Appendix A:

Appendix B:

LIST OF TABLES

Appendix A:

Appendix B:

Appendix C:

LIST OF PHOTOGRAPHS

NOMENCLATURE

Symbol	Description	Units
A_i	Area of peak i, pre-exponential factor	-, varied
C_i	Concentration of species i	$mol \cdot m^{-3}$
C_P	Centrepoints	-
$D_{i,b}$	Diffusivity of species i in medium b	$m^2 \cdot s^{-1}$
E	Value of objective function, summed relative square error	-
E_F	Enhancement factor	-
$E_{A,i}$	Activation energy of reaction i	$kJ \cdot mol^{-1}$
k	Number of process variables	-
$K_{i,j}$ or $F_{i,j}$	Internal response factor between species i and j	-
K_s	Sechenov coefficient	$L \cdot mol^{-1}$
g	Acceleration due to gravity	$m \cdot s^{-2}$
Ha	Hatta number	-
H_i	Henry's Law constant	Pa
k_L	Liquid phase mass transfer coefficient	$m \cdot s^{-1}$
j_L	Mean velocity of liquid film	$m \cdot s^{-1}$
$\boldsymbol{j_L}$	Mass diffusion of component i	$kg \cdot m^{-2} s^{-1}$ or $mol \cdot m^{-2} s^{-1}$
M_i	Mass of species i	g
MM_i	Molar mass species i	$g \cdot mol^{-1}$
n_i	Moles of species i	mol
P	Pressure	Pa
R	Ideal gas constant	$J \cdot mol^{-1} \cdot K^{-1}$
Re_L	Liquid phase Reynolds number	-
S_i	Gas chromatograph response/signal of species i	-
Sc_L	Liquid phase Schmidt number	-
Sh_L	Liquid phase Sherwood number	-
t	Time	s
T	Temperature	K or °C
u_i	Standard uncertainty of value i	varied
V	Volume	mL or m^3
$\dot{V}$	Volumetric Flow rate	$mL \cdot s^{-1}$
x_i	Mass faction of species i	-
X_i	Experimental factor at level i	-

χ	Association parameter	-

GREEK SYMBOLS

Symbol	Description	Units
α	Rotatability of experimental design	-
β_0	Surface response coefficient – Intercept Term	-
β_i	Surface response coefficient – Linear Term	-
β_{ii}	Surface response coefficient – Squared Term	-
β_{ij}	Surface response coefficient – Interaction Term	-
δ_L	Liquid film thickness	m
$\lambda_{\pm}$	Limiting ionic conductance	$A \cdot cm^{-2}$
$\lambda_{i,HME}$	Weighting factor of species i with respect to HME	-
μ_i	Viscosity of species i	Pa·s
ν_i	Kinematic viscosity of species i	$m^2 \cdot s^{-1}$
ρ_i	Density of species i	$kg \cdot m^{-3}$
τ	Residence time	s

SUBSCRIPTS

0	Initial or reference
Act	Activation energy
EXP	Experimental
IS	Internal Standard
max	Maximum
$meth$	Methanol
min	Minimum
v	Vial

SUPERSCRIPTS

cc	Concentration based

M	Mixture
pc	Pressure based

ABBREVIATIONS

ANOVA	Analysis of Variance
BFM	Bubble Flow Meter
CCD	Central Composite Design
CSTR	Continuous stirred tank reactor
DoF	Degrees of Freedom
FID	Flame Ionisation Detection
GC	Gas Chromotography
GC-MS	Gas Chromotography Mass Spectroscopy
HFP	Hexafluoropropene
HFPO	Hexafluoropropene oxide
HME	1,1,2,3,3,3-hexafluoropropyl methyl ether
IS	Internal standard
KOH	Potassium hydroxide
MS	Mean squared
PTFE	Polytetrafluoroethylene
rpm	Revolutions per minute
SS	Sum squared
TCF	Temperature correction factor

1

CHAPTER ONE

1. INTRODUCTION

1.1 Previous work

It was an objective of the Reactor Technology Research Group at the school of Chemical Engineering (University of KwaZulu-Natal – Howard College) to develop an industrial scale continuous process for the production of 1,1,2,3,3,3-hexafluoropropyl methyl ether (HME). This was inspired by previous work on a gas-liquid continuously stirred semi-batch glass reactor where HME was successfully synthesized on a laboratory scale. Development of the industrial scale process required a thorough understanding of the reaction kinetics (a need addressed in this study) as well as process design; including separation and purification steps (work undertaken by Mr A. Domah).

1.2 Background and importance of topic

Fluorspar (or calcium fluoride (CaF_2)) is a naturally occurring mineral that is the main industrial source of elemental fluorine and hydrogen fluoride, and through these a number of important fluorochemical products (Simandl, 2009). South Africa has the world's largest fluorspar reserves at 17.1% and holds a 4.5 % share of the international fluorspar market which is comparatively small when considering the available reserves (Survey, 2013). Of the acid grade fluorspar mined in South Africa, 95% is exported while the remaining 5% is used to produce other fluorochemicals. This represents a large opportunity lost to process available acid grade fluorspar to higher value products (PELCHEM, 2011). The Fluorochemical Expansion Initiative (FEI) is an initiative endorsed by the Department of Trade and Industry which seeks to address this problem by increasing the beneficiation of South Africa's mined fluorspar by developing local fluorochemical technology and competence.

There are various research opportunities in the field of organofluorine chemistry to support the proposed increase in the fluorochemical value chain in South Africa. The investigation into the synthesis of new organofluorine compounds or revised synthesis procedures is a worthwhile

venture as these compounds may find uses in various industries and serve to make their commercial production more efficient and profitable (Banks et al., 1994).

This research focuses on the synthesis of two organofluorine compounds in particular, 1,1,2,3,3,3-hexafluoropropyl methyl ether (HME) and methyl-2,3,3,3-tetrafluoro-2-methoxypropionate (MTFMP) using a falling film microreactor (FFMR).

HME is a partially fluorinated dialkyl ether which is prepared by a gas-liquid reaction involving methanol (with dissolved catalytic amounts of potassium hydroxide) and hexafluoropropene. This results in the conversion of relatively cheap and available compounds into a higher value ether product which may be used as a solvent for the extraction of essential oils, for the synthesis of amides and as a foam blowing agent (Banks et al., 1994, Il'in et al., 2004).

MTFMP is a precursor to trifluorovinyl ethers (TFVEs) which are partially or fully fluorinated organofluorine compounds and are principally used as monomers or co-monomers for the synthesis of high value plastics, elastomers and membrane copolymers (Petrov, 2009, Spraul et al., 2006). MTFMP is synthesized by reacting methanol with either dissolved potassium hydroxide or sodium hydroxide with hexafluoropropene oxide in a gas-liquid reactor.

A FFMR consists of multiple thin falling films in microchannels which fall by gravity through the reactor and typically have a residence time of a few seconds. Structuring fluid flow into microchannels allows for high specific interfacial areas of up to 20 000 m^2/m^3 to be achieved in FFMRs (Al-Rawashdeh et al., 2008). This has proven to be remarkably greater than currently used gas-liquid contactors (Zhang et al., 2009). As a result of high specific interfacial areas, FFMRs display high heat and mass transfer rates which make them suitable for gas-liquid reactions that are highly exothermic, have fast kinetics and require stringent reaction temperature control.

Currently, HME and MTFMP are conventionally produced in a batch process and their synthesis using a FFMR has not been reported in the open literature (Dixon, 1959, Fritz et al., 1963, Lousenberg and Shoichet, 1997, Rendall, 1958). FFMRs allow reactions to be carried out in a continuous process which offers various advantages including being easier to operate and allowing for large scale production with the use of multiple FFMRs (Hessel et al., 2000, Vankayala et al., 2007).

1.3 Aims and objectives

The main aim of this research was the successful synthesis of HME by reaction of potassium hydroxide, methanol and hexafluoropropene and MTFMP by the reaction of sodium hydroxide or potassium hydroxide, methanol and hexafluoropropene oxide. In addition, literature appears to be devoid of information regarding the kinetics of these systems and thus an additional aim of this study was the development and identification of kinetic models for the synthesis of HME and MTFMP.

In order to achieve these aims the following objectives were set:

- Successfully synthesize HME and MTFMP and conduct qualitative and quantitative product analyses using gas chromatography-mass spectroscopy and gas chromatography, respectively.
- Develop a kinetic model to identify previously unknown kinetic parameters for both the HME and MTFMP systems by least squares regression of experimental data.

To ensure that these objectives were met a systematic approach was taken. This first step was carried out in preliminary investigations using a semi-batch gas-liquid stirred tank reactor. The purpose of these investigations was to confirm the presence of HME in the product mixture, determine the viability of the HME system for the FFMR and observe the effect of reaction conditions on reaction performance. Using the results obtained from preliminary investigations and information from the open literature a four factor experimental design was used to conduct investigations on a FFMR. This experimental data formed the foundation of the kinetic study and was subsequently used to identify a suitable model and associated kinetic parameters by least squares regression for both systems of interest.

1.4 Outline of thesis

This thesis consists of six chapters and six appendices. Chapter 1 gives a broad introduction to the current work, its relevance and importance. The overarching aims of the study are discussed as well as the set of objectives that served as benchmarked targets during the course of this work.

Chapter 2 delves into a general survey of the open literature pertaining to any relevant concepts and theory pertinent to the subject matter of this work. The literature survey focuses on the previous work conducted on the systems of interest, equipment characteristics and development as well as basic concepts of kinetic modelling.

In Chapter 3, the five main experimental aspects of this work are discussed. These are: instrument calibrations, preliminary investigations on a semi-batch gas-liquid glass reactor, FFMR equipment validation, FFMR experiments, and analytical techniques.

Chapter 4 discusses, the development of the kinetic models for both the systems of interest in this study. The model development encompasses the generation of a reaction model from fundamental equations in Chapter 2 as well as an overview on the operation of the kinetic models.

Chapter 5 presents all of the core results of the study as well as a discussion and interpretation of the findings, trends and challenges encountered. The main body of this thesis is then curtailed with the conclusions drawn from the results and recommendations for future work.

The appendices provide additional information such as instrument and analytical calibrations, raw data, sample calculations, MATLAB script files as well as chemical toxicology data sheets.

2

CHAPTER TWO

2. LITERATURE SURVEY

2.1 Organofluorine chemistry

The earliest published evidence of the synthesis of organofluorine compounds may be attributed to Dumas et al. who reacted potassium fluoride and dimethyl sulphate to produce methyl fluoride in 1835 (Banks et al., 1994). Various chemists continued to contribute to organofluorine chemistry but little progress was made until Moissan, who was the first to isolate elemental fluorine in 1886. This then paved the way for fluorination of various hydrocarbons by different methods to obtain fluoroplastics, fluorocarbon refrigerants such as Freon®, fluoroaromatic compounds and chlorofluorocarbons (Okazoe, 2009).

Today, the fluorochemical industry has expanded into a $16 billion market in which they are used in the synthesis of fluoropolymers, agricultural fertilizers, industrial solvents, refrigerants and in the medical diagnostics field (Banks et al., 1994).

Fluoropolymers alone have found application in various emerging fields, including use as a biomaterial suitable for the construction for medical prosthetics and internal supports. TFVE serves as an appropriate monomer for the production of fluoropolymers used as biomaterial due to the fact that it is not toxic, shows a lack of immunogenicity and has high mobility in water (Lousenberg and Shoichet, 1997).

The use of organofluorides as industrial solvents and refrigerants is especially important due to the ever increasing awareness of the environmental impact of chemicals and the need to replace ozone depleting chlorofluorocarbons as mandated by the Montreal Protocol (Velders et al., 2007). The solution to an alternative industrial solvent may be found in the use of partially fluorinated dialkyl ethers which have the advantage of having a high affinity to absorb oils (Il'in et al., 2004).

2.2 Organofluorine synthesis techniques

Mined fluorspar is classified based on the quality of the ore which is measured by its calcium fluoride content. Fluorspar is typically found in three grades; acid grade or *acidspar*, ceramic grade and lastly metallurgical grade or *metspar*. Acidspar has a minimum calcium fluoride content of 97 % and is principally converted to hydrofluoric acid which is a reagent in fluorochemical syntheses. Ceramic grade spar has a calcium fluoride content of between 80 and 96 % with silicon dioxide content under 3 % and is used to produce enamels and glass. Metspar has a minimum calcium fluoride content of 80% and can be found with up to 15 % silicon dioxide, it is used in steel making as well as in the production of aluminium (Bide, 2011, Finger et al., 1960, Kirsch, 2004).

From the three grades of fluorspar typically found, acidspar is the most versatile by having a multitude of uses, some of which involve the preliminary conversion to hydrofluoric acid.

2.2.1 The production of hydrofluoric acid

Although hydrofluoric acid is not an organofluorine it is very important in the synthesis of various fluorocarbons such as chlorofluorocarbons, agrochemicals, refrigerants and pharmaceuticals (Bide, 2011).

Anhydrous hydrofluoric acid is produced by an endothermic reaction (Equation 2.1) involving the addition of acid grade fluorspar to concentrated sulphuric acid at temperatures of approximately 300 °C in a rotary kiln reactor. The reaction produces gaseous hydrofluoric acid and calcium sulphate which is found as a solid. The reactor is usually operated at vacuum conditions as this has the dual advantage of reducing operating temperatures as well as aiding in the removal of the gaseous product.

The gaseous stream then undergoes various processing steps; thereafter anhydrous hydrofluoric acid with a purity of 99.98 % is produced. Aqueous hydrofluoric acid may be then obtained by the addition of water to the process stream. Figure 2.1 shows a simplified process flow diagram of the production process (Bide, 2011, Kirsch, 2004).

$$CaF_2 + H_2SO_4 \rightarrow 2\,HF + CaSO_4 \qquad (2.1)$$

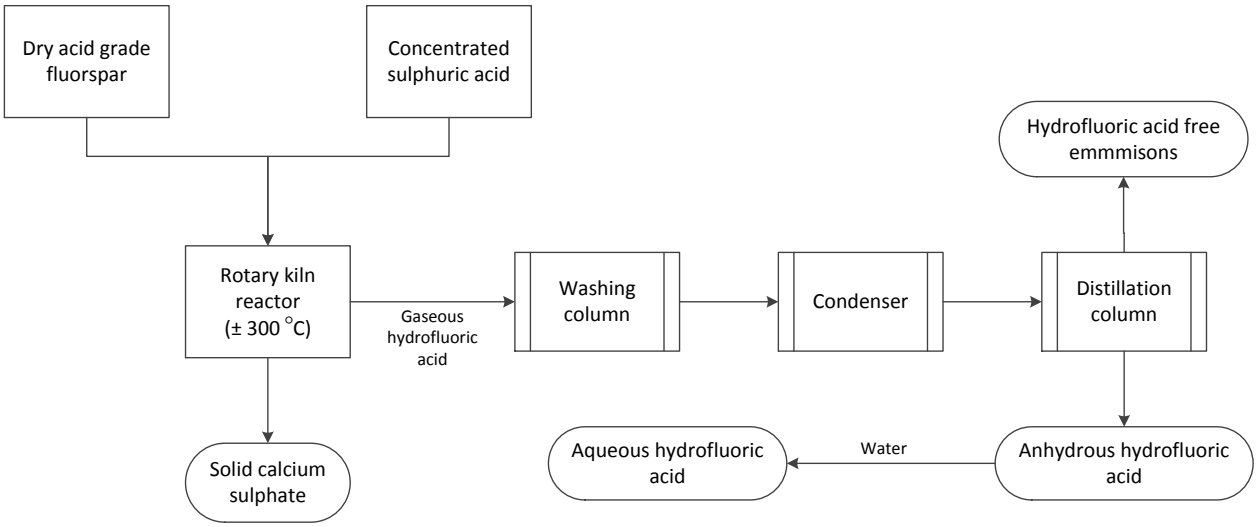

Figure 2.1: Simplified process flow diagram of the production of anhydrous and aqueous hydrofluoric acid from the reaction of acid grade fluorspar and concentrated sulphuric acid (Bide, 2011).

2.2.2 The production of chlorofluorocarbons

One of the most infamous groups of organofluorine compounds are chlorofluorocarbons (CFCs) whose negative effects on the ozone layer were highlighted by the Montreal Protocol of 1987 which subsequently placed legal limits on the use of CFCs, carbon tetrachloride, hydrofluoroethers, halons and various other ozone depleting chemicals (Auffhammer et al., 2005).

In the mid-1900s, CFCs were essential to everyday life, gaining popularity through their use as refrigerants, as insulation, in air conditioning systems, and later as solvents and in electronics. These chemicals were widespread because they were non-toxic, inert, could be produced in a range of boiling points (which made them desirable as refrigerants), were non-flammable, and non-carcinogenic (Haas, 1992).

In 1930 Midgley and Henne developed a continuous process for the production of dichlorodifluoromethane based on the work of F. Swarts. Dichlorodifluoromethane was produced by contacting carbon tetrachloride and anhydrous antimony bifluoride in the presence of antimony pentachloride according to Equation 2.2. The reaction proceeded with yields of up to 94% being readily achievable. Dichlorodiflоromethane was then easily separated from the product by fractional distillation (Midgley Jr and Henne, 1930).

$$3\ CCl_4 + 2\ SbF_2 \xrightarrow{SbCl_5} 3\ CCl_2F_2 + 2\ SbCl_4 \qquad (2.2)$$

2.2.3 The production of hydrofluorocarbons

Hydrofluorocarbons are another important organofluorine which gained great importance when restrictions on the use of CFCs were implemented by the Montreal Protocol. Hydrofluorocarbons served as replacement refrigerants to CFCs and although they were not potential ozone depleting chemicals, they are greenhouse gases (Kirsch, 2004).

Hydrofluorocarbons can be synthesised by combining two types of reactions hydrogenolysis of bromine or chlorine and Lewis acid-catalysed halogen isomerisation. Figure 2.2 shows three typical synthesis routes of how 1,1,1,2-tetrafluoroethane is produced by the reaction of tetrachloroethene and hydrofluoric acid.

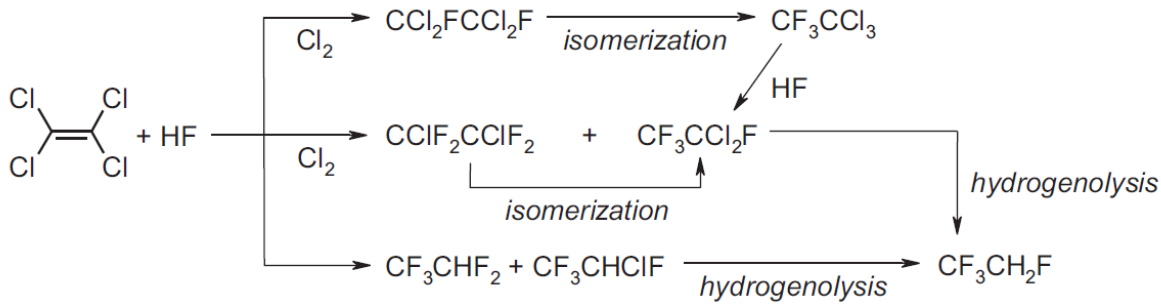

Figure 2.2: Typical synthesis routes to produce 1,1,1,2-tetrafluoroethane by the reaction of tetrachloroethene and hydrofluoric acid by the combination of two main reaction routes: hydrogenolysis of chlorine and Lewis-acid catalysed halogen isomerisation (Kirsch, 2004).

2.2.4 The production of fluoropolymers

A discussion of organofluorine synthesis would not be complete without the inclusion of fluoropolymers. Fluoropolymers were first discovered in the early 1930s by Ruff and Bretschnieder who synthesized gaseous tetrafluoroethylene, which later became a valuable monomer for perfluorinated fluoropolymer synthesis, such as polytetrafluoroethylene (PTFE). Tetrafluoroethylene is synthesized by the pyrolysis of chlorodifluoromethane in the reaction steps shown in Figure 2.3.

PTFE was discovered accidentally by Dr. Roy Plunkett at DuPont (one of the world leaders in fluoropolymer industry) in 1938. This would later be seen as the most monumental discovery in the fluoropolymers industry (Teng, 2012). PTFE is produced in a batch process by the addition polymerisation of tetrafluoroethylene. The reaction temperature may be up to 100 °C and between pressures of 0.7 and 3.5 MPa.

Chloroform step:

$$CH_4 + 3\,Cl_2 \longrightarrow CHCl_3 + 3\,HCl$$

Chlorodifluoromethane step:

$$CHCl_3 + 2\,HF \xrightarrow[(SbF_3\ \text{catalyst})]{} CHClF_2 + 2\,HCl$$

Tetrafluoroethylene synthesis:

$$CHClF_2 \xrightarrow[(\text{Pyrolysis})]{} CF_2CF_2 + 2\,HCl$$

Figure 2.3: Typical synthesis route to the commercial production of tetrafluoroethylene (Ebnesajjad, 2011).

Initially, research into fluoropolymers was not eagerly pursued due to its high melt viscosity and melt temperature as well as insolubility which made it difficult to process and dangerous to synthesize given the toxic nature of tetrafluoroethylene (Teng, 2012). This changed in the 1940s when fluoropolymers were seen as a viable material to be used in the purification of uranium hexafluoride during World War II, this meant that funding and equipment were readily available for this research.

The fluoropolymer industry continued to grow and today it is one of the largest global markets for fluorochemicals. The drivers of this market lie with the extremely desirable properties of fluoropolymers, such as low surface energy making it difficult for substances to adhere to them as well as being exceptionally chemically and thermally stable. These physical and chemical properties make them versatile and appropriate for use in electronics, chemical storage and transport, bio materials, coatings, textiles, construction and automotive industries (Ebnesajjad, 2011, Kirsch, 2004, Teng, 2012).

Fluoropolymers can be divided into two types; homopolymer and copolymers. Homopolyers are polymers which consist principally of a single repeating monomer whereas copolymers may consist of multiple monomers in each polymer segment. The polymers may then be further characterised by two different classes, namely; perfluoronated and partially fluorinated fluoropolymers. Perfluoronated fluoropolymers display the exceptional physical and chemical properties descried above, but this in turn decreases their processability. This inspired the innovation of partially fluorinated fluoropolymers which exhibited the necessary qualities of the perfluoronated fluoropolymers and was less difficult to process and mould.

2.3 Partially fluorinated dialkyl ethers

2.3.1 Previous work

The first recorded synthesis of 1,1,2,3,3,3-hexafluoropropyl methyl ether (HME) – one of the two organofluorine compounds of interest in this study – was in 1958 by Rendall et al. They were investigating the novel synthesis of various fluorinated carbon compounds. The authors discovered that partially fluorinated dialkyl ethers were produced by bubbling hexafluoropropene gas through a 10% potassium hydroxide in methanol solution at 30 ^{o}C. The resultant liquid was then poured over crushed ice resulting in two distinct layers forming. The bottom layer was separated. After fractionation of the bottom liquid layer the authors identified the major product of the reaction as HME (Rendall, 1958). The yield of HME was found to be 62.4wt% with respect to the hexafluoropropene gas introduced into the system.

Continuing on the work of Rendall et al. (1958), Il'in et al. (2004) performed a similar experiment by passing hexafluoropropene gas through a 5 % potassium hydroxide solution dissolved in methanol. The authors observed a large and rapid temperature increase of the reaction vessel from 20 to 40 ^{o}C and stopped passing hexafluoropropene through the potassium hydroxide solution when the heat release of the reaction had ceased. The reactor contents were then poured into water, decanted as before, and dried using calcium chloride ($CaCl_2$). The final product was obtained by distilling the product sample and analysis revealed a 98% yield of HME (Il'in et al., 2004).

2.3.2 Reaction Chemistry

Rendall et al. (1958) proposed that partially fluorinated dialkyl ethers may be synthesized by passing hexafluoropropene gas through an alcohol containing alkali ions. For the synthesis of HME, methanol is used as the alcohol and potassium hydroxide may be used to provide the required alkali ions. Hexafluoropropene gas serves as a suitable starting point for the synthesis of organofluorine compounds due to availability and affordability.

The reaction mechanism (shown in Figure 2.4) involves the addition of the alkoxy anion at the carbon-carbon double bond of the hexafluoropropene molecule which then leads to the formation of the reaction carbo-anion intermediate **I**. The proton made available from the alkoxy anion then bonds to the carbo-anion to produce the major product of the reaction HME, **II**.

Il'in et al. (2004) showed the presence of two other reaction products, an alkenyl ether (1,2,3,3,3-pentafluoro-1-methoxyprop-1-ene) **III** and an alkyl tetrafluoropropionate (methyl 2,3,3,3-tetrafluoropropionate) **IV**. Reaction product **III** is formed by elimination of fluorine from **I**.

Reaction products **II** and **III** then form the alkyl tetrafluoropropionate **IV** in the presence of water. Il'in et al. (2004) however found that the selectivity towards **II** was high with yield of reaction products **III** and **IV** not exceeding more than 5% in all experiments (Il'in et al., 2004).

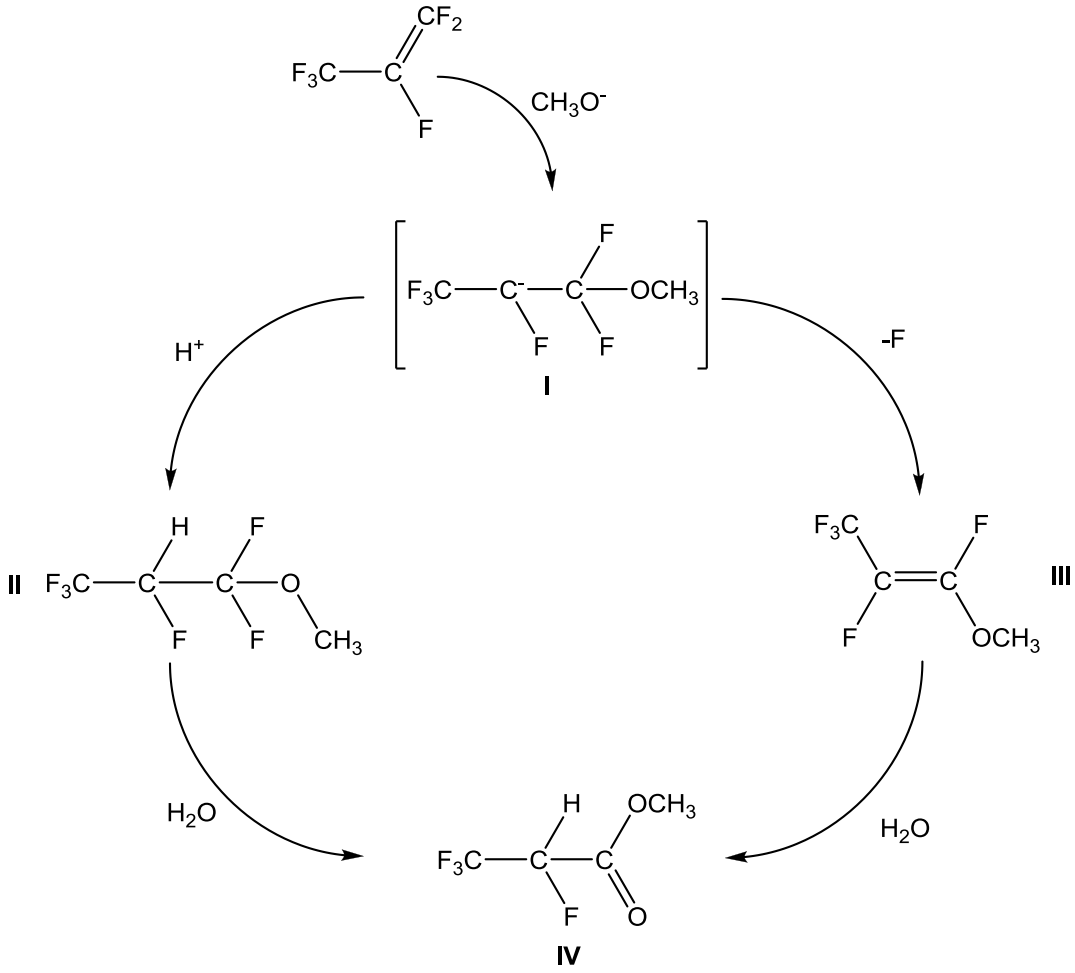

Figure 2.4: 1,1,2,3,3,3-hexafluoropropyl methyl ether (HME) reaction mechanism; addition of a methylalkoxy anion to a hexafluoropropene molecule to produce reaction intermediate **I**, protonation of **I** produces HME **II**. Defluoronation of **I** leads to an alkenyl ether **III** and in the presence of water **II** and **III** form an alkyl tetrafluoropropionate **IV** (Il'in et al., 2004).

2.4 Trifluorovinyl ethers

2.4.1 Previous work

TFVEs, that have MTFMP as a precursor, are partially or fully fluorinated organofluorine ether compounds which are principally used as monomers or comonomers for the synthesis of high value plastics, elastomers and membrane co-polymers (Petrov, 2009, Spraul et al., 2006). In addition to being used in the manufacturing of high value plastics there is precedence for the use of TFVEs as a biomaterial due to the fact that it is not toxic, shows a lack of immunogenicity and high mobility in water (Lousenberg and Shoichet, 1997).

TFVEs have been previously synthesised by two methods which avoid the need for chlorine, hydrogen fluoride or elemental fluorine (Lousenberg and Shoichet, 1997). Firstly, Dixon and Stanley (1959) synthesized TFVEs in a one-step reaction process which involved the reaction of an alkali metal alcoholate with tetrafluoroethylene, according to the following reaction scheme shown in Figure 2.2.

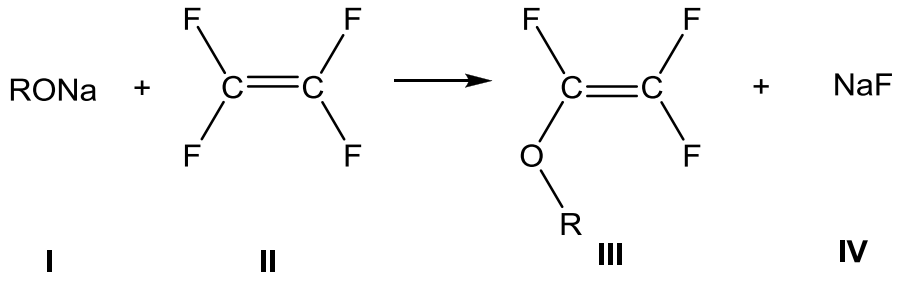

Figure 2.5: Reaction of alkali metal alcoholate **I** with tetrafluoroethylene **II** to produce trifluorovinyl ether **III** and alkali fluoride **IV** (Dixon, 1959).

Dixon and Stanley (1959) successfully synthesized various TFVEs with the **–R** group of compound **III** taking the identity of the alkyl or fluoroalkyl alcohol used in the reaction (**I**). There are however drawbacks to the one-step reaction sequence, including high operating pressure (up to 20 bar), long reaction times and low reported experimental yields of between 10 and 30 % (Dixon, 1959).

Fritz et al., (1963) later synthesized fully fluorinated vinyl ethers (perfluorinated vinyl ethers) by the one-step reaction sequence proposed by Dixon and Stanley (1959) which required the use of perfluorinated alcohols, i.e. where **–R** in compound **I** of Figure 2.5 is a fluoroalkyl. Fully fluorinated alcohols are however intrinsically unstable and consequently difficult to isolate, thus a

one-step reaction sequence is not viable for the production of perfluorinated vinyl ethers (Fritz et al., 1963).

Fritz et al., (1963) proposed an alternative means of synthesizing perfluorinated vinyl ethers by reacting an acid fluoride with hexafluoropropene oxide to produce an etherified acid fluoride according to the reaction scheme shown in Figure 2.6. The etherified acid fluoride may then be converted to a TFVE by thermolysis between 300 and 600 ^{o}C. Fritz et al., (1963) also proposed first converting the etherified acid fluoride to an alkali metal salt in order to lower the thermolysis temperatures to between 170 and 250 ^{o}C. Thermolysis in the presence of a polar solvent will also lead to a further reduction in the thermolysis temperature (Fritz et al., 1963).

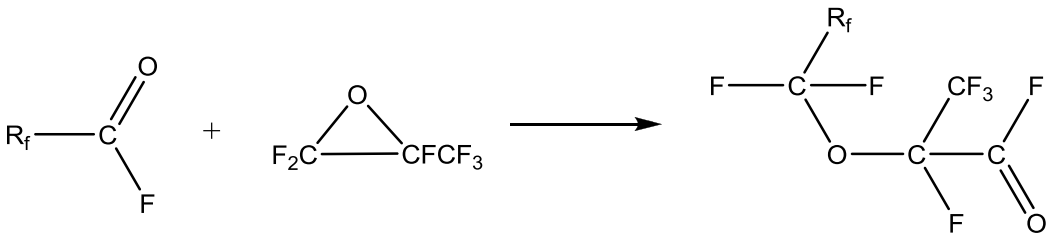

Figure 2.6: Reaction of acid fluoride with hexafluoropropene oxide to produce an etherified acid fluoride (Fritz et al., 1963).

The reaction product may be converted to the corresponding alkali metal salt by base hydrolysis, a suitable alkali base that may be used is potassium hydroxide (Fritz et al., 1963).

For example, perfluoromethyl perfluorovinyl ether was produced by the reaction of carbonyl fluoride and hexafluoropropene oxide at 75 ^{o}C for 4 hrs producing perfluoro-2-methoxypropionyl fluoride. The reaction product was then neutralised with potassium hydroxide in water and dried to obtain an alkali metal salt, potassium perfluoro-2-methoxyproprionate. Potassium perfluoro-2-methoxyproprionate was then thermolyzed in the presence of potassium fluoride to obtain the desired perfluoromethyl perfluorovinyl ether (Fritz et al., 1963). Carbonyl fluoride is, however, a hazardous gas which increases the danger of operation thus decreasing the appeal of this synthesis route for the production of TFVE (Tsai, 2005).

Lousenberg and Shoichet (1997) adopted the reaction procedure proposed by Fritz et al., (1963) to produce partially fluorinated trifluorovinyl ethers. The authors proposed the reaction of a sodium alkoxide with hexafluoropropene oxide and an alkali metal fluoride catalyst such as potassium or cessium fluoride to obtain a reaction intermediate. The intermediate or the corresponding alkali metal salt may then be thermolyzed directly to obtain a TFVE (Lousenberg and Shoichet, 1997).

2.4.2 Reaction chemistry

Lousenberg and Shoichet (1997) proposed the following reaction scheme (Figure 2.4):

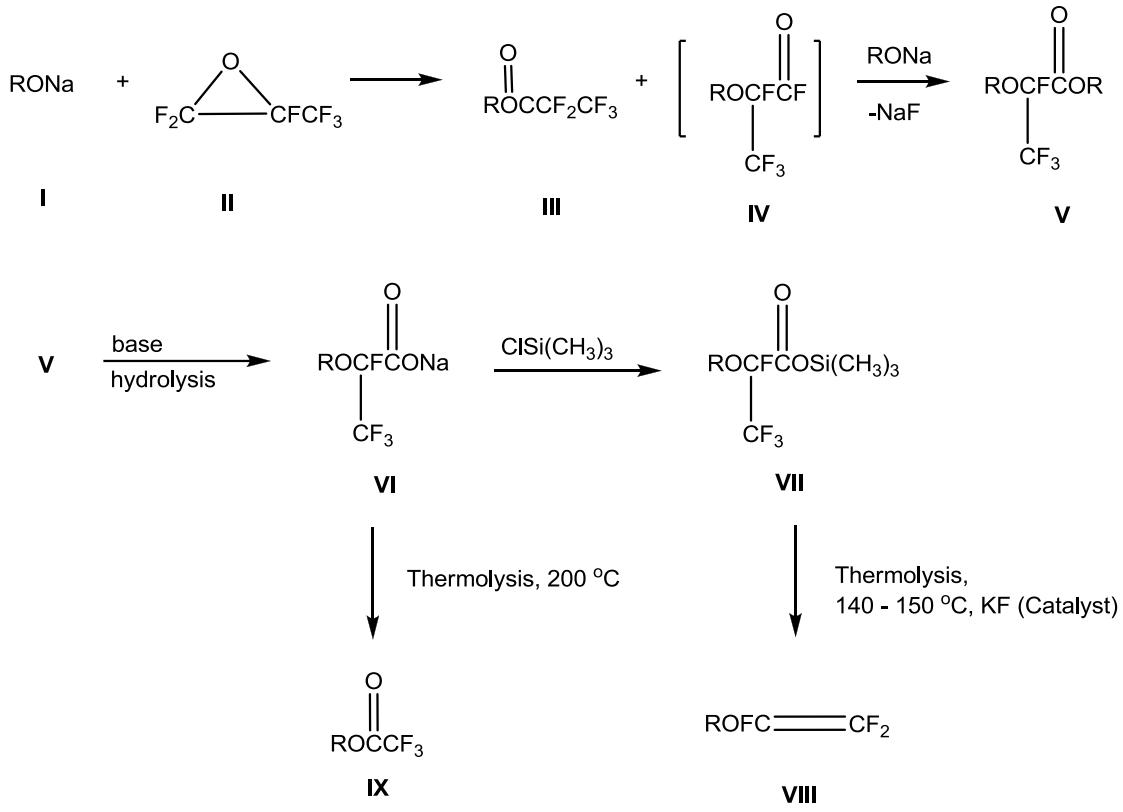

Figure 2.7: Reaction sequence for the production of trifluorovinyl ethers as investigated by Lousenberg and Shoichet (1997). Sequence shows the reaction of sodium alkoxide **I** and hexafluoropropene oxide **II** to obtain an undesired partially fluorinated propionate ester **III** and a desired partially fluorinated propionate methoxy ester **V**. Sodium carboxylate salt **VI** is produced by base hydrolysis of **V** which may be thermolyzed to a TFVE **IX**. Reaction of **VI** with trimethylsilyl chloride results in a partially fluorinated trimethylsilyl ester **VII**. This may then by thermolyzed to the desired TFVE **VIII**.

Lousenberg and Shoichet (1997) found that an undesired partially fluorinated propionate ester (**III**) and a desired partially fluorinated propionate methoxy ester (**V**) was produced by the reaction of sodium alkoxide (**I**) with hexafluoropropene oxide (**II**). The ester (**V**) was then converted to a sodium carboxylate salt (**VI**) which, when thermolyzed, forms a TFVE (**IX**) in low yields. A more desirable route was found when the sodium carboxylate salt (**VI**) was reacted with trimethylsilyl chloride to obtain a partially fluorinated trimethylsilyl ester (**VII**). This was then subjected to thermolysis between 140 to 150 ^{o}C in the presence of potassium fluoride to obtain the desired TFVE (**VIII**).

The initial reaction was found to be exothermic and resulted in the formation of esters **III** and **V**. The formation of the ester **III** is as a result of the alkoxide ion forcing ring opening of

hexafluoropropene oxide (**II**), while ester **V** is likely formed upon addition of another equivalent of the alkoxide ion to the intermediate compound **IV**. Lousenberg and Shoichet (1997) also found that the yield of the undesired ester may be influenced by reaction temperature and noted a decreased yield of the undesired ester with increased temperature, for example an experiment started at -78 ^{o}C resulted in a yield of 22% while a yield of 12% was noted at 0 ^{o}C (Lousenberg and Shoichet, 1997).

If compound **I** is sodium methoxide, then the resultant ester (**V**) can be identified as methyl-2,3,3,3-tetrafluoro-2-methoxyproprionate (MTFMP) and finally the desired TFVE (**VIII**) produced is 1,1,2-trifluoro-2-methoxyethene (TFME). TFME may then be converted to a higher value fully fluorinated vinyl ether by direct fluorination to obtain 1,1,2-trifluoro-2-(trifluoromethoxy)ethane, which is a useful monomer for the production of high-performance fluoroelastomers (Petrov, 2009).

It can be seen that the yield of TFME from the reaction scheme outlined in Figure 2.7 is greatly dependent on the yield of MTFMP and the partially fluorinated trimethylsilyl ester (**VII**) in the previous steps. The synthesis of TFME is beyond the scope of this study, however focus is instead placed on the synthesis of TFME precursors, viz. the formation of MTFMP by reaction of sodium methoxide and hexafluoropropene oxide.

2.5 Experimental equipment

This study set out to research the process development and kinetic modelling for the synthesis of two organofluorine compounds using a falling film microreactor (FFMR). However, the FFMR was not the only possible choice of equipment. A number of different types of reactors may be used to conduct kinetic data studies, each with their respective advantages and disadvantages Careful consideration is required, as the choice of reactor may affect ease, duration, accuracy/precision and cost of the research. There are two broad classes of reactors which may be used, namely, batch and continuous reactors. An overview of the potential choices is, therefore, of relevance here.

2.5.1 Batch reactor

The batch reactor is the simplest form of chemical reactors and is typically defined as a unit wherein the valid phases all have a spatially uniform concentration. Practically, this is achieved by using a mechanical or magnetic stirrer within the reactor vessel. The batch reactor is usually a very attractive option in laboratory studies due to its simplicity, as a chemical reaction in a beaker may easily be seen as a batch reactor. The batch reactor may be used to carry out gas-liquid

reactions by continuously recycling and bubbling the vapour phase through the liquid phase. Conversely however, the simplicity of the batch reactor is simultaneously its main disadvantage (Froment et al., 1990, Nauman, 2008).

Due to the nature of the batch reactor there are some common problems with regards to utilising the reactor for kinetic studies, these include temperature control and controlling start and end of reaction.

Considering the first of these problems, the reaction temperature may be controlled by submerging the reaction vessel in a liquid bath set at the reaction temperature or circulating liquid through an external jacket at the reaction temperature. It is also important to consider the nature of the reactive system. The batch reactor is usually not suitable for reactions which are rapid and thus undergo rapid temperature changes, but control can be achieved by using an external heating medium and an internal cooling coil to regulate the temperature (Wojciechowski and Rice, 2003). A temperature sensor must also be carefully positioned so that efficient temperature control is achieved.

The second problem arises when the reaction temperature is high and requires that the reagents be heated to the desired temperature. It is difficult to stop a fraction of the reaction proceeding before the desired temperature is reached. This may be overcome by heating the reagents separately and introducing them to the reactor once they have both reached the desired reaction temperature (Wojciechowski and Rice, 2003).

Analysis of the reactor product may also present problems as sampling significant quantities from the vessel is not advisable and thus an *in situ* sampling method may need to be considered. The sampling period will also need to be rapid due to the fact that the batch reactor is inherently a transient reactor and replicate samples are often only possible if the reaction is repeated which is time consuming and resource intensive (Wojciechowski and Rice, 2003). Owing to its limitations, the batch reactor was not considered for this research.

2.5.2 Lewis cell type reactor

Another reactor which is commonly used for kinetic studies between two phases is the Lewis cell reactor. The Lewis cell is essentially a batch reactor with the added advantage of having a clearly defined interfacial area between the phases. The reactor consists of two cavities, one above the other, with an interfacial plate separating these cavities. The interfacial plate defines the contact area between the phases.

A Lewis cell reactor can be used for liquid-liquid or gas-liquid reactions as in the works of (Baldascini et al., 2001, Molina and Bouallou, 2012, Molina and Bouallou, 2013). The phases are continuously mixed by stirrers in each phase to ensure uniform concentration while samples can be taken using sampling points in each compartment. For gas phases a pressure sensor is fitted to the top compartment which allows the pressure to monitored over time which is used in absorption and desorption reaction experiments(Molina and Bouallou, 2012, Molina and Bouallou, 2013). This reactor was still considered too limited for our purposes.

2.5.3 Continuously stirred tank reactor

The continuously stirred tank reactor (CSTR) differs from the batch reactor in that liquid is continuously removed from the system at the same rate at which it is introduced. In this configuration it is imperative that the contents of the reaction vessel be well mixed, because the reactor relies on the fact that the outlet concentration is an exact representation of the reactor contents. This involves immediately mixing the contents of the reactor with the new fluid entering the vessel (Bird et al., 2007).

Temperature control in the CSTR is affected in the same way as it was with the batch reactor; however the inclusion of an internal cooling system becomes increasingly difficult with the presence of a rapidly moving impeller or mixer.

The greatest advantage of the CSTR is that the product is a representation of the reaction occurring at a constant reactant concentration and so the rate of reaction is directly obtainable from analysis of the reactor product while allowing multiple samples to be taken for consistency. The CSTR thus combines the advantages of the batch reactor and the plug flow reactor.

The disadvantage of the CSTR is, however, that experiments may become very time consuming as it is not uncommon for systems to take longer than a day to reach steady-state conditions. Running the experiment for this amount of time may prove to be resource and energy intensive considering the amount of material which would be required to be processed. The CSTR has also proven to not be effective when it comes to multiphase reactions owing to the internal hydrodynamics of the reactor making it not suitable for gas-liquid reactions (Wojciechowski and Rice, 2003).

A modification can, however, be made whereby the gas phase is sparged into the liquid phase. This ensures that there is sufficient contact between the gas and liquid phases, which allows the reaction to proceed. Despite this modification, it was not deemed suitable for our purposes.

2.5.4 Bubble column reactors

Bubble column reactors are tall cylindrical vessels with a gas distributor at the base of the vessel. They are versatile multi-phase reactors which have a wide range of applications such as the petrochemical, biochemical, bulk chemical and metallurgical industries (Degaleesan et al., 2001). One of the most recognised uses of bubble column reactors is in the Fischer-Tropsch process which converts carbon monoxide and hydrogen to useful hydrocarbons (Meyers and Meyers, 2004).

This reactor type has gained a significant amount of focus over the last few decades due to their large industrial application and appeal. Some of the main advantages of bubble column reactors are their versatility, durability, low maintenance costs, ease of operation and high heat and mass transfer rates (Kantarci et al., 2005). A large portion of the research conducted in recent years has been to the design and operation of bubble column reactors with particular emphasis on fluid regime identification as well as the effect of reactor geometries on performance.

Findings of these studies have shown that the performance of the reactor is greatly dependent on the dominant flow regime, the three most commonly observed flow regimes are *heterogeneous* (churn-turbulent), *homogeneous* (bubbly flow) and *slug flow* regime. The choice of the correct operating region may differ based on the system. As a result, the prediction of the conditions of each flow regime is difficult as they vary for each bubble flow column, based on reactor dimensions and sparger type. Industrial reactors are typically found to operate in the heterogeneous flow regime even though it has been shown that heat and mass transfer rates are higher when flow is in the homogeneous regime (Schumpe and Grund, 1986).

Implementation of such a reactor requires that the vessel be carefully designed and this requires various hydrodynamic parameters such as axial dispersion coefficients of the gas and the liquid, sauter mean bubble diameter, mass transfer coefficients for the gas species, gas hold-ups as well heat and mass transfer coefficients. Since there has not been a large amount of research conducted on the systems of interest in this study, a large portion of these parameters are unknown and design of such a reactor is beyond the scope of this study (Kantarci et al., 2005).

2.5.5 Falling film microreactor

The last 20 years has seen increasing interest by academics and industrialists in microreactor technology due to the process versatility and process intensification potential of microstructured reactors (Chen et al., 2008, Hessel et al., 2000, Zanfir et al., 2005).

Microreactors are especially useful for gas-liquid and gas-liquid-solid catalytic reactions. These reactors principally operate by directing liquid flow through microchannels that may be as thin as 300 μm and allow gas to flow either con- or co-currently above the liquid flow, this creates a constant and uniform interfacial area between the gas and liquid phases along the length of the microchannel (Hessel et al., 2000).

The falling film microreactor (FFMR) used in this study is a well-known and well-studied microstructured reactor which was invented by the Institut für Mikrotechnik Mainz GmbH and has successfully shown its ability to maintain thin liquid films of up to 100 μm (Al-Rawashdeh et al., 2008). The FFMR consists of a cooling plate, a reaction plate with etched microchannels and a sight-glass which encloses the gas headspace (Figure 2.8). This design allows for specific interfacial areas of up 20 000 $m^2.m^{-3}$ to be achieved, which is noticeably higher than other gas-liquid contacting reactors as can be seen in Table 2.1 below (Hessel et al., 2000, Yue et al., 2007, Ziegenbalg et al., 2010). The high specific areas made available by the reactor design allow for high heat and mass transfer rates to be achieved which make FFMRs an efficient tool for rapidly exothermic gas-liquid reactions. FFMRs offer higher selectivities as reaction conditions may be more stringently controlled when compared to other gas-liquid contacting reactors. In addition, FFMRs allow for easier operation and increased process safety when dealing with hazardous or dangerous systems (Chen et al., 2008). Researchers have exploited the high heat and mass transfer rates of FFMRs for reactions such as catalysed hydrogenation (Yeong et al., 2003), direct fluorination of toluene (Jähnisch et al., 2000) and direct synthesis of hydrogen peroxide (Inoue et al., 2007).

Table 2.1: Comparison of mass transfer rates, specific areas and mass transfer coefficient of several gas-liquid reactors (Sobieszuk and Pohorecki, 2010, Yue et al., 2007)

Reactor Type	$k_L \cdot 10^5$ ($m.s^{-1}$)	a ($m^2.m^{-3}$)	$k_La \cdot 10^2$ (s^{-1})
Bubble columns	10–40	50–600	0.5–24
Couette-Taylor flow reactor	9–20	200–1200	3–21
Impinging jet absorbers	29–66	90–2050	2.5–122
Packed columns, concurrent	4–60	10–1700	0.04–102
Packed columns, countercurrent	4–20	10–350	0.04–7
Spray column	12–19	75–170	1.5–2.2
Static mixers	100–450	100–1000	10–250
Stirred tank	0.3–80	100–2000	3–40
Tube reactors, horizontal and coiled	10–100	50–700	0.5–70
Tube reactors, vertical	20–50	100–2000	2–100
Gas-liquid microchannel	40–160	3400–2000	30–2100

Various works have been published on the principle operations of FFMRs which include studies on the hydrodynamics and mass transfer capabilities of the unit. Zanfir et al., (2005) studied the absorption of carbon dioxide in a sodium hydroxide solution with the intention of developing a model for the system. The authors used 2-dimensional computational fluid dynamics to successfully model the reaction system for low concentrations of sodium hydroxide (0.1 and 1 M solutions) (Zanfir et al., 2005). Zanfir et al., (2005) also presented another important finding; that the resistance to mass transfer predominantly lays on the liquid side of the interface based on the diffusion-convection-reaction step.

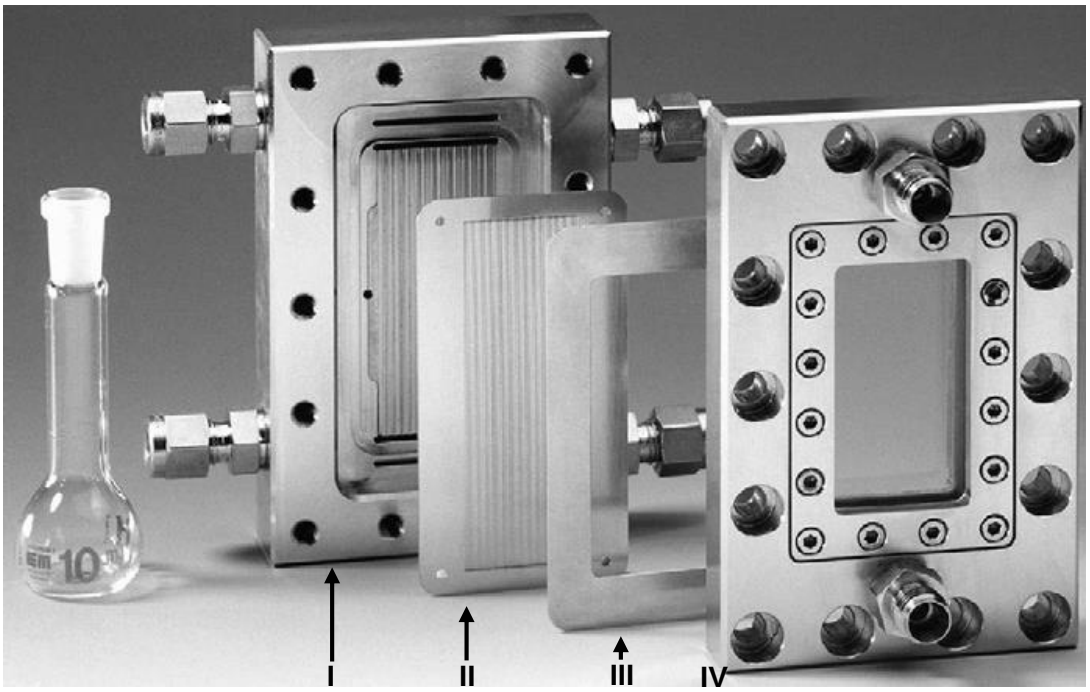

Figure 2.8: Falling film microreactor – Standard designed by the Institut für Mikrotechnik Mainz GmbH. Exploded view from left; integrated heat exchanger **I**, reaction plate **II**, washer **III** and reactor housing **IV** (Al-Rawashdeh et al., 2008).

Further development of the 2 dimensional model proposed by Zanfir et al., (2005) was undertaken by Al-rawashdeh (2008) with the aim to better understand and describe liquid phase behaviour as this, particularly, was found to present the major rate limiting step to reactions in the FFMR. The authors were able to study the effect of fabrication imprecisions and channel mal distribution which they found had an 11% and 2% effect on reaction conversion respectively (Al-Rawashdeh et al., 2008).

Zhang et al., (2009) studied the hydrodynamics and mass transfer of two-phase gas-liquid flow in a FFMR and found three predominant flow regimes that result as the liquid flow rate is increased; these were "*corner-rivulet flow*", "*falling film flow with dry patches*" and "*complete falling film*

flow". Complete falling film flow was found to be the best flow regime for gas-liquid reactions as this provides the best use of available reactor volume. Flow regimes such as corner-rivulet flow and falling film flow with dry patches do not ensure complete wetting of the reactor microchannel. Bearing in mind that gas-liquid reactions occur in the liquid phase, the presence of dry patches reduces the wetted interfacial area between the gas and liquid phases thus lowering the yield of the reaction.

In addition to liquid flow rate, liquid surface tension affects the formation of the liquid film in microchannels. This liquid meniscus also forms due to the surface tension and hydrophobicity properties of the reactor fluid; with the low flow rates in this study we do however assume a flat film. Zhang et al., (2009) found that liquid side mass transfer coefficients increased with decreased surface tension. The authors were also able to propose the following empirical correlation by least squares regression of experimental data:

$$\mathrm{Sh_L} = 0.0145 \cdot \mathrm{Re_L^{0.69}} \cdot \mathrm{Sc_L^{0.57}} \tag{2.3}$$

Where $\mathrm{Sh_L}$, $\mathrm{Re_L}$ and $\mathrm{Sc_L}$ represent the liquid-side Sherwood, Reynolds and Schmidt numbers, respectively. Each of these terms may be expressed by Equations 2.4, 2.5 and 2.8, respectively:

$$\mathrm{Sh_L} = \frac{\mathrm{k_L d_h}}{\mathrm{D_{G,b}}} \tag{2.4}$$

The Sherwood number indicates the relationship between convective and diffusive mass transfer in the liquid phase. The convective mass transfer is described by the liquid-side mass transfer coefficient (k_L) and the characteristic length (d_h) while the diffusive mass transfer is described the diffusivity of the gas phase in the liquid phase ($D_{G,b}$).

$$\mathrm{Re_L} = \frac{4\delta_\mathrm{L} \mathrm{j_L}}{\nu} \tag{2.5}$$

The Reynolds number indicates the flow regime within the microchannel and is calculated by incorporating the liquid film thickness (δ_L), mean velocity of the liquid film (j_L) and the kinematic viscosity of the liquid phase (ν). The liquid film thickness and the mean velocity of the liquid film are calculated using Equations 2.6 and 2.7, respectively.

$$\delta_\mathrm{L} = \sqrt[3]{\frac{3\mathrm{Q_L}\nu}{\mathrm{n \cdot b \cdot g}}} \tag{2.6}$$

$$j_L = \frac{g \cdot \delta_L^2}{3\nu} \tag{2.7}$$

Q_L, n, b, and g denote the volumetric flow rate of the liquid phase, the number of channels, the width of the microchannel and the acceleration due to gravity, respectively.

The Schmidt number is used to indicate the ratio between the viscosity (μ_L) and the mass diffusivity ($D_{G,b}$) and may be calculated using Equation 2.8.

$$Sc_L = \frac{\mu_L}{\rho_L \cdot D_{G,b}} \tag{2.8}$$

FFMRs also afford the opportunity for continuous operation which makes the prospect of industrial scale processes a promising venture. The transition from pilot or laboratory scale systems to an industrial scale process may be achieved by the numbering-up of microstructured units or relevant flow features such as number of channels or channel length (Chen et al., 2008, Ziegenbalg et al., 2010).

2.6 Experimental design

Experimental design is the basis of comprehensive experimental work as proper planning can allow for investigation and analysis of interaction between test variables as well as the quantity and quality of the deductions that may be made thereof (Berty, 1999).

The most comprehensive means of investigating the interaction of all factors and levels of each factor to be varied is by use of a full factorial design (FFD) (Antony, 2003). FFD looks to investigate the experiment at all permutations of the experimental conditions. Although this may be the most thorough means of investigation, resources or time constraints may limit the amount of experimental work that may be performed, hence FFD may not always be the most attractive experimental design technique.

Valuable interaction data for experiments which involve the investigation of various factors at multiple levels is, however, obtainable by following alternative experimental designs such as Box-Wilson and Box-Behnken central composite designs. These design methods allow for interaction data to be obtained without the need for a FFD to be performed thus greatly reducing the number of experimental runs required.

2.6.1 Box-Wilson central composite design

Box-Wilson central composite design (more commonly referred to as central composite design) involves investigating three classes of experimental conditions, viz. *cubic design points*, *axial design points* and *central design points*. Considering the range of interest for a particular design variable (i.e. temperature, catalyst concentration, flow rate, etc.) and expressing the bounds of this range as the -1 and +1 levels, the centre of this range may be expressed as the 0 level. Cubic design points may then be described as levels -1 and +1 of a particular design variable. Central design points may then be described as the set of experimental conditions at the 0 level of the design variable. The axial design points are experimental conditions which lie outside of the initial parameter range selected and are located at the ± α level. α quantifies the rotatability of the experimental design and is based on the number of factorial points which are investigated, if a full factorial design is used then α may be calculated using Equation 2.9 (Lazić, 2004). *F* is the number of design variables to be varied throughout the experimental study.

$$\alpha = (F)^{1/4} \tag{2.9}$$

The concept of rotatability was first introduced by Box and Hunter (1957) and is used to ensure that reasonable predictions of responses are made throughout the investigation region. One way of ensuring this is to ensure that the variances at all points (cubic, central and axial) are equal. When this is achieved the experimental design is then termed a rotatable design (Box and Hunter, 1957, Montgomery, 2008).

From Equation 2.9, the experimental conditions of the axial design points may be calculated by substituting -α and +α into Equation 2.10. X_{min} and X_{max} represent the initial range of the design variable chosen (i.e. the -1 and +1 levels).

$$X_i = \frac{\alpha.(X_{max} - X_{min}) + X_{max} + X_{min}}{2} \tag{2.10}$$

An important aspect during experimentation is a test of the variability and consistency of the experiment which can be evaluated by repeating a set of experimental conditions and observing the deviations thereof. Central composite design accounts for the variability of experiments by specifying replicate experiments of the central design points. The number of replicates to be performed is at the discretion of the experimenter, but it is recommended that a minimum of 3 replicates be performed (Lazić, 2004).

There are three types of central composite designs, namely; c*ircumscribed*, *inscribed* and *face centred* designs. A circumscribed experimental design is the original method of employing central composite designs. It positions the axial design points a distance ± α from the central design point and is based on the number of factors of interest. α for a circumscribed experimental design is greater than 1 thus the axial design points form the new bounds of the experimental region of investigation (Sematech, 2006).

An inscribed experimental design is employed when the limits of investigation are clearly defined and the axial design points are positions at the edges of the design space. An inscribed design is thus a circumscribed experimental design which has been scaled down by α (Sematech, 2006). Circumscribed and inscribed central composite designs require five levels for each design variable i.e. the $-\alpha$, -1, 0, +1 and $+\alpha$ levels of the design variable.

A face centred design has three levels for each process variable where the axial design points are located at the middle of each face thus the value of α is approximately 1. Figure 2.9 provides an illustrative example of the location of these design points for a design which has two factors.

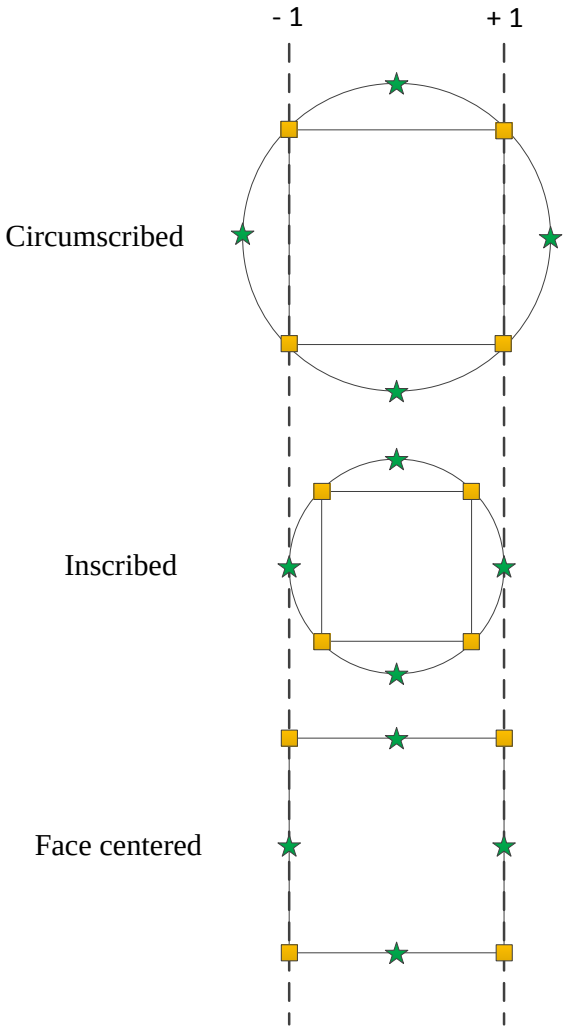

Figure 2.9: Illustrative example of a circumscribed, inscribed and face centred Box-Wilson central composite design for a two factor experiment. Axial design points (★) and cubic design points (■).

It is important to note that the circumscribed central composite design spans the greatest design space as can be seen in Figure 2.9 and is thus the most useful when trying to gauge the effect of experimental conditions over a large design space (Sematech, 2006).

The number of experimental runs required for a full central composite experimental design may be determined by Equation 2.11 where k is the number of process variables to be varied while C_p refers to the number of central design points chosen (Souza et al., 2005).

$$N = 2^k + 2k + C_p \tag{2.11}$$

2.6.2 Box-Benhken experimental design

A Box-Behnken experimental design is another example of a multivariate technique used in optimization studies and consists of experimental conditions chosen at the midpoint of the chosen

range for a particular design variable (Figure 2.10). A Box-Behnken experimental design only consists of the central and midpoint design points and thus consists of less experimental runs which utilises resources more efficiently (Sematech, 2006). The number of experimental runs required may be determined using Equation 2.12 (Souza et al., 2005).

$$N = k^2 + k + C_p \tag{2.12}$$

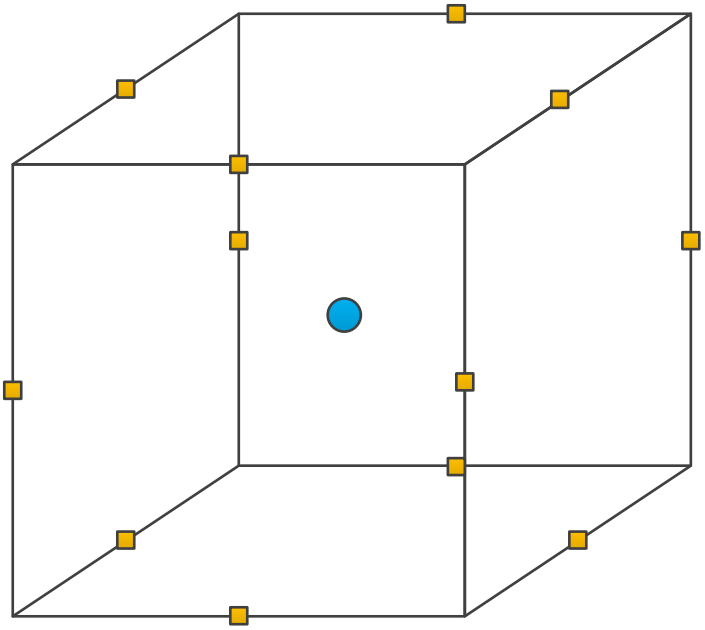

Figure 2.10: Illustrative example of three factor Box-Behnken experimental design. Central design points (●) and midpoints design points (■).

2.7 Kinetic modelling

Vital components of almost all chemical processes are chemical reactors which are responsible for the beneficiation of raw materials into higher value products. The performance of the reactor is crucial to the overall performance of the process often dictating whether the process is economically viable or not. To ensure that the reactor is performing optimally a thorough design of the reactor is integral and requires a comprehensive understanding of the reactive system, the mechanism, chemical kinetics and kinetic parameters. Reliable kinetic data is invaluable to industry as it allows the creation of lucrative opportunities for new and existing chemical processes (Gunawan et al., 2002, Wojciechowski and Rice, 2003).

In summary, the identification of a suitable kinetic model involves developing a reactor model, a reaction model (which incorporates a rate expression) and finally, fitting the model predictions to

experimental data. The model requires initial estimates which become improved estimates of the kinetic parameters once fit to experimental data (Gunawan et al., 2002).

2.7.1 Reactor model formulation

The reactor model is the first stage in the model formulation and is responsible for computing the hydrodynamics and the physical parameters of the system. The model may be constructed using software such as Microsoft Excel (Microsoft Corporation), MATLAB® (The MathWorks, Inc.), Mathematica (Wolfram Research) and Python (Python Software Foundation) which are very similar in many ways all having built-in functions which makes the programming language simpler and more efficient. MATLAB® (The MathWorks, Inc.) was used for all model development in this study.

A. Material balances

Model formulation begun with a statement of the governing equations, for fluid flow problems this is the continuity equation. Equation 2.13 is the differential form of the continuity equation illustrating an intrinsic physical law: the law of conservation of mass (Bird et al., 2007, Darby, 2001, Rice and Do, 2012).

$$\frac{\partial \rho}{\partial t} + \nabla(\rho \mathbf{v}) = 0 \tag{2.13}$$

The individual component continuity equations may be presented as:

$$\frac{\partial \rho_i}{\partial t} = -\mathbf{v}(\nabla \rho_i) - (\nabla \mathbf{j_i}) + R_i \tag{2.14}$$

Where ρ_i is the volume density of component *i*, $\boldsymbol{v}$ is the average mass velocity of the fluid, $\boldsymbol{j_i}$ is the mass diffusion of component *i* and R_i is the net rate of production or consumption of component *i* per unit volume. Equation 2.14 is seldom used in this form and adaptations are commonly made for ease of use. In this work the choice was made to express Equation 2.14 in terms of the measurable species concentrations:

$$\frac{\partial C_i}{\partial t} = -\mathbf{v}(\nabla C_i) - (\nabla \mathbf{j_i}) + R_i \tag{2.15}$$

Where C_i is the concentration of component i and $\boldsymbol{j_i}$ is now the molar diffusion of component i. The molar diffusion is then expressed by the Fick's Law (Henley et al., 2011):

$$\mathbf{j_i} = -\mathrm{D_{im}} \nabla \mathrm{C_i} \tag{2.16}$$

Where D_{im} is the molar diffusional coefficient of component i in medium m. A generalised mass balance for component *i* is then obtained by combining Equations 2.15 and 2.16.

$$\frac{\partial \mathrm{C_i}}{\partial \mathrm{t}} = \nabla\left(-\mathbf{v}\mathrm{C_i} + \mathrm{D_{i,m}} \nabla \mathrm{C_i}\right) + \mathrm{R_i} \tag{2.17}$$

The net rate of production and/or consumption of species i (R_i) is the sum of the n rates of production and/or consumption of i in all of the relevant reactions in the system.

$$\mathrm{R_i} = \sum_{\mathrm{a=1}}^{\mathrm{n}} \mathrm{r_a} \tag{2.18}$$

In the case of gas-liquid multiphase systems which have fast liquid phase reactions the consideration of mass transfer between the valid phases is essential and may be represented by (Nauman, 2008):

$$\text{Rate of mass transfer} = \mathrm{E_F K}\left(\mathrm{C^*_{j,L}} - \mathrm{C_{j,L}}\right) \tag{2.19}$$

where E_F is the enhancement factor, K is the overall volumetric mass transfer coefficient across the liquid film, $C^*_{j,L}$ is the saturated concentration of gas j at the liquid film interface and $C_{j,L}$ is the concentration of gas j in the bulk liquid phase.

A simplification may be made to Equation 2.19 when applied to the FFMR in that the resistance to mass transfer lies predominantly on the liquid side of the interface. The overall mass transfer coefficient K may then be replaced by the liquid side mass transfer coefficient k_L (multiplied by the reactor specific interfacial area for mass transfer (a) as computed using Equation 2.4 (Section 2.5.5) (Zanfir et al., 2005).

A further modification of Equation 2.19 may be made to the saturated concentration of gas j at the liquid film interface, as it may be conveniently be calculated by finding the ratio of the concentration of gas j in the bulk gas phase and the concentration based Henry's Law constant (Henley et al., 2011). Thus:

$$\mathrm{C^*_{j,L}} = \frac{\mathrm{C_{j,G}}}{\mathrm{H}} \tag{2.20}$$

B. Momentum balance

In addition to the material balance the momentum balance is required to incorporate the appropriate hydrodynamics of the liquid phase. Previous work by Al-Rawashdeh, et al. (2008) indicate that the fluid flow in microchannels of the FFMR is laminar in nature which leads dictates that there is a liquid flow velocity profile which exists in each channel and can be described by the appropriate momentum balance (Al-Rawashdeh et al., 2008). A generalised system of equations exist that define the force-momentum balance for laminar fluid flow of Newtonian fluids known as the Navier-Stokes Equations (Holland and Bragg, 1995, Roberson and Crowe, 1985, Schiesser and Griffiths, 2009).

In general, the momentum balance is stated as follows (Equation 2.21):

$$(\rho\mathbf{v})_t + \nabla\cdot(\rho\mathbf{v}\mathbf{v}) + \nabla P = 0 \tag{2.21}$$

Now dissecting Equation 2.21 into its individual terms so as they can be simplified to a more usable form, we take the first term on the left-hand side of the equation where the time derivative of the product of the fluid density and velocity vector is necessary:

$$(\rho\mathbf{v})_t = \frac{\partial(\rho v_x)}{\partial x} + \frac{\partial(\rho v_y)}{\partial y} + \frac{\partial(\rho v_z)}{\partial z} \tag{2.22}$$

The second term on the left-hand side is dot product of the spatial unit vector and the product of the liquid velocity vector with itself (a second-order nine element matrix) which gives us Equation 2.23 below:

$$\nabla\cdot(\rho\mathbf{v}\mathbf{v}) = \begin{bmatrix} \mathbf{i}\left\{\frac{\partial(\rho v_x v_x)}{\partial x} + \frac{\partial(\rho v_x v_y)}{\partial y} + \frac{\partial(\rho v_x v_z)}{\partial z}\right\} \\ \mathbf{j}\left\{\frac{\partial(\rho v_y v_x)}{\partial x} + \frac{\partial(\rho v_y v_y)}{\partial y} + \frac{\partial(\rho v_y v_z)}{\partial z}\right\} \\ \mathbf{k}\left\{\frac{\partial(\rho v_z v_x)}{\partial x} + \frac{\partial(\rho v_z v_y)}{\partial y} + \frac{\partial(\rho v_z v_z)}{\partial z}\right\} \end{bmatrix} \tag{2.23}$$

Finally, the third term when expanded is:

$$\nabla P = \frac{\partial(P)}{\partial x} + \frac{\partial(P)}{\partial y} + \frac{\partial(P)}{\partial z} \tag{2.24}$$

Substituting Equations 22 to 24 into Equation 21 we get:

i component: $\frac{\partial(\rho v_x)}{\partial x} + \frac{\partial(\rho v_x v_x)}{\partial x} + \frac{\partial(\rho v_x v_y)}{\partial y} + \frac{\partial(\rho v_x v_z)}{\partial z} + \frac{\partial(P)}{\partial x} = 0$ (2.25a)

j component: $\frac{\partial(\rho v_y)}{\partial y} + \frac{\partial(\rho v_y v_x)}{\partial x} + \frac{\partial(\rho v_y v_y)}{\partial y} + \frac{\partial(\rho v_y v_z)}{\partial z} + \frac{\partial(P)}{\partial y} = 0$ (2.25b)

k component: $\frac{\partial(\rho v_z)}{\partial z} + \frac{\partial(\rho v_z v_x)}{\partial x} + \frac{\partial(\rho v_z v_y)}{\partial y} + \frac{\partial(\rho v_z v_z)}{\partial z} + \frac{\partial(P)}{\partial z} = 0$ (2.25c)

Considering only the velocity profile in the z-direction chosen to be the co-ordinate indicating length down the length of a micro-channel the Navier-Stokes equations above reduce to a two-dimensional Poisson Equation stated below in Equation 2.26 for the liquid phase and Equation 2.27 for the gaseous phase.

$$-\mu_l \left(\frac{\partial^2 v_{l,z}}{\partial x^2} + \frac{\partial^2 v_{l,z}}{\partial y^2}\right) = \rho_l g \tag{2.26}$$

$$-\mu_g \left(\frac{\partial^2 v_{g,z}}{\partial x^2} + \frac{\partial^2 v_{g,z}}{\partial y^2}\right) = \frac{\partial P}{\partial z} \tag{2.27}$$

C. Henry's law constants

Henry's Law is a simple formulation that is commonly used in chemical thermodynamics to estimate composition from pressure and temperature data of species in solution at low concentrations. Henry's law states that the partial pressure of a species is directly proportional to its mole fraction in the liquid phase, the proportionality constant of this relationship is known as the Henry's Law constant (Henley et al., 2011, Smith et al., 2001).

The Henry's law constant may be found in various units, a commonly used Henry's Law constant expression is:

$$H_i^{PC} = \frac{P_i}{C_{i,L}} \tag{2.28}$$

Where, H_i^{PC} is the pressure-concentration based Henry's Law constant of species i and P_i is the partial pressure of species i. The Henry's Law constant required for Equation 2.20 needs to be a dimensionless concentration based expression of the constant (Equation 2.29).

$$H_i^{CC} = \frac{C_{i,G}}{C_{i,L}} \tag{2.29}$$

Where, H_i^{CC} is the concentration based Henry's Law constant of species i. To facilitate the conversion from H_i^{PC} to H_i^{CC} the concentration of species i in the gas phase may be expressed by Equation 2.30 if the gas phase is assumed to behave as an ideal gas. Where $n_{i,G}$ is the number of moles of gas i, V_G is the volume of gas, P_i is the partial pressure of species i, R is the ideal gas constant and T is the system temperature.

$$\mathrm{C_{i,G}} = \frac{\mathrm{n_{i,G}}}{\mathrm{V_G}} = \frac{\mathrm{P_i}}{\mathrm{RT}} \tag{2.30}$$

Combining Equations 2.29 and 2.30 to replace the concentration of species i in the gas phase, we obtain:

$$\mathrm{H_i^{CC}} = \frac{\mathrm{P_i}}{\mathrm{C_{i,L}RT}} \tag{2.31}$$

Noting Equation 2.29 it can be seen that:

$$\mathrm{H_i^{CC}} = \frac{\mathrm{H_i^{PC}}}{\mathrm{RT}} \tag{2.32}$$

Equation 2.32 allows for the translation of a pressure-concentration defined Henry's Law constant to a dimensionless concentration based Henry's Law constant. The next step lies in obtaining the appropriate pressure-concentration defined Henry's Law constant.

This can be performed provided appropriate vapour-liquid equilibrium ($T-x-y$ or $P-x-y$) data for the system of interest is available. Assuming there is no excess volume of the liquid phase of the system the molar volume of a binary liquid mixture is:

$$\begin{aligned} \mathrm{V^M} &= \textstyle\sum_i \mathrm{x_i V_i} \\ &= \mathrm{x_a V_a} + \mathrm{x_b V_b} \\ &= \mathrm{x_a}\frac{\mathrm{M_a}}{\rho_a} + \mathrm{x_b}\frac{\mathrm{M_b}}{\rho_b} \end{aligned} \tag{2.33}$$

Where, x_i is the liquid phase mole fraction of species i and M_i is the molar mass of species i. Assuming a basis of 1 mole then allows for the determination of the liquid phase concentration of a species in the binary mixture by dividing the liquid mole fraction of species i by the total molar volume of a binary liquid mixture.

$$C_{i,L} = \frac{x_i}{V^M} \tag{2.34}$$

The partial pressure of species i may also be easily obtained from the vapour-liquid equilibrium data.

$$P_i = y_i P \tag{2.35}$$

H_i^{PC} is then easily calculated from vapour-liquid equilibrium data by dividing Equation 2.35 by 2.34 and this may then be conveniently translated to H_i^{CC} by Equation 2.32.

In order to increase the usability of the dimensionless concentration based Henry's Law constant in the model, vapour-liquid equilibrium data was translated to H_i^{CC} which was then regressed to the Valentiner equation (Equation 2.36) (Takenouchi et al., 2001). a, b and c are parameters of the equation.

$$\ln H_i^{CC} = a + \frac{b}{T} + c \ln T \tag{2.36}$$

Another consideration that needs to be catered for is the effect that the presence of the dissolved salt (potassium hydroxide) has on the solubility of the gas in the liquid phase. In general, the solubility of the gas decreases (salting-out effect) as the concentration of the salt increases, there are cases (however rare) where the converse is true (salting-in) and this hinges on the effect that the salt has on the solvent. A salt that organises the intermolecular structure of the solvent leads to salting-out and a salt that disorganises the intermolecular structure of the solvent leads to salting-in, as explained by Ruckenstein and Shulgin. A well accepted means of compensating for the change in gas solubility with concentration of salt is by adjusting the Henry's Law constant with the Sechenov coefficient (Ruckenstein and Shulgin, 2002).

$$\ln\left(\frac{H_{i,salt}^{CC}}{H_i^{CC}}\right) = K_s C_s \tag{2.37}$$

Where $H_{i,salt}^{CC}$ is the adjusted concentration based Henry's Law constant for the presence of a dissolved salt, C_s is the concentration of the salt and K_s is the Sechenov coefficient of the system. The Sechenov coefficient is unique for each system of gas, liquid and dissolved salt and was thus a fitting parameter in this investigation.

2.7.2 Reaction model

The next step in the kinetic model formulation is a description of the reaction chemistry of the system. A statement of the material balances for the relevant species in the system is required in differential form so that they may be solved simultaneously. It is necessary to solve equations simultaneously as behaviour in the reactor changes with respect to location in the reactor (in the case of the FFMR this is along the length of a microchannel). In addition, there exists some interdependence of the material balances requiring that they be computed at each point along the microchannel (Gunawan et al., 2002).

What follows is a brief introduction into some commonly witnessed types of reactions, some of which are observed in this study.

A. Elementary reactions

Elementary reactions result in reaction rate expressions which can easily be produced by looking at a balanced chemical reaction of the system. The order of the reaction follows the stoichiometric relationship between the reactants. For example, consider the general reaction below (Equation 2.38) where ν_i is the stoichiometric coefficient of species i.

$$\nu_A A + \nu_B B \rightarrow \nu_C C \tag{2.38}$$

The accompanying rate expression for the formation of species C is:

$$r_C = k\, C_A^{\nu_A}\, C_A^{\nu_A} \tag{2.39}$$

Where, r_i is the reaction rate of species i, C_i represents the concentration of species i and k is the kinetic rate constant of the reaction (Nauman, 2008).

B. Multiple elementary reactions

It is very often the case where a reactive system is a bit more complex than the previously mentioned and has multiple reactions in the system. The reactions could happen *consecutively* or *step-wise* (Nauman, 2008):

$$\nu_A A + \nu_B B \xrightarrow{k_1} \nu_C C \qquad r_C = k_1\, C_A^{\nu_A}\, C_A^{\nu_A} \tag{2.40}$$

$$\nu_C C + \nu_D D \xrightarrow{k_2} \nu_E E \qquad r_F = k_2\, C_D^{\nu_D}\, C_E^{\nu_E} \tag{2.41}$$

The reactions could also be completely *independent* (Nauman, 2008).

$$\nu_A A + \nu_B B \xrightarrow{k_1} \nu_C C \qquad r_C = k_1 C_A^{\nu_A} C_B^{\nu_B} \tag{2.42}$$

$$\nu_D D + \nu_E E \xrightarrow{k_2} \nu_F F \qquad r_F = k_2 C_D^{\nu_D} C_E^{\nu_E} \tag{2.43}$$

The reactions could also occur simultaneously and result in *competitive* reactions (Nauman, 2008).

$$\nu_A A + \nu_B B \xrightarrow{k_1} \nu_C C \qquad r_C = k_1 C_A^{\nu_A} C_B^{\nu_B} \tag{2.44}$$

$$\nu_A A + \nu_D D \xrightarrow{k_2} \nu_E E \qquad r_E = k_2 C_A^{\nu_A} C_D^{\nu_D} \tag{2.45}$$

For scenarios where we have competitive reactions in a system the net rate of change of a species would be the sum of the rates of consumption and production of that species. Consider the following system where A is consumed in Equations 2.46 and 2.47 but produced in Equation 2.48.

$$\nu_{A,1} A + \nu_B B \xrightarrow{k_1} \nu_C C \qquad r_C = k_1 C_A^{\nu_A} C_B^{\nu_B} \tag{2.46}$$

$$\nu_{A,2} A + \nu_D D \xrightarrow{k_2} \nu_E E \qquad r_E = k_2 C_A^{\nu_A} C_D^{\nu_D} \tag{2.47}$$

$$\nu_F F + \nu_G G \xrightarrow{k_3} \nu_{A,3} A \qquad r_A = k_3 C_F^{\nu_F} C_G^{\nu_G} \tag{2.48}$$

The net rate of production/consumption (R_A) of A is:

$$R_A = \frac{\nu_{A,1}}{\nu_C} r_C + \frac{\nu_{A,2}}{\nu_E} r_E + r_A \tag{2.49}$$

C. Gas-liquid reactions

Gas-liquid reactions are treated differently to homogeneous reactions as material balances need to be conducted for each phase in the reactor. There are various considerations that need to be made when dealing with a heterogeneous reactive system, the first of which is the hydrodynamics of the system. The valid phases can be assumed to be (Nauman, 2008):

i. Gas and liquid phases are well mixed

ii. A single phase is well mixed while the other is in plug flow
iii. Both phases are in co-current plug flow
iv. Both phases are in counter-current plug flow

Often the nature of the reactor forces one of the above flow regimes to be adopted.

Another important consideration is the mass transfer between the phases. The reaction typically occurs in one phase of the reactor (the liquid phase) and thus the reaction can only proceed at a rate proportional to the transfer of the gaseous reactant from the gas to the liquid phase. Equation 2.50 shows the quantification of the mass transfer rate between the gas and liquid phases (Astarita, 1967, Danckwerts, 1970, Henley et al., 2011).

$$\text{Rate of mass transfer} = \mathrm{E_F K}\left(\mathrm{C^*_{j,L}} - \mathrm{C_{j,L}}\right) \tag{2.50}$$

where E_F is the enhancement factor, K is the overall volumetric mass transfer coefficient across the liquid film, $C^*_{j,L}$ is the saturated concentration of gas j at the liquid film interface and $C_{j,L}$ is the concentration of gas j in the bulk liquid phase.

D. Reactions with intermediates

Finally, there exists a complex reaction mechanism whereby the reactants combine to form an intermediate which is short-lived in the reactor as it is immediately consumed in a consecutive reaction i.e. the rate of the consecutive reaction is much greater than the rate of formation of the intermediate. At equilibrium there thus exists a finite concentration of the intermediate as it is consumed and produced at approximately the same rate. In these cases the net rate of change in the amount of intermediate is assumed to be zero, this is known as the *quasi steady-state approximation.* Applying this assumption greatly simplifies the reaction rate description (Nauman, 2008, Roberts, 2009).

2.7.3 Solving the system of equations

The first step in trying to understand and model behaviour of physical systems is the development of the governing equations. This is an integral part of the process but bears little fruit until the equations can be simultaneously solved so that their output may be studied. In this study the governing equations consist of the momentum and material balances which span the full spectrum of the spatial domain, i.e. the x, y and z directions. The existence of the multivariate variables dictates that the equations are in fact partial differential equations (PDEs) which add an additional level of complication to the solution of the equations.

Unlike with PDEs, ordinary differential equations (ODEs), which are subject to only one independent variable and the derivative thereof, have a number of well-defined and fairly accurate numerical method techniques which allow them to be solved, namely; the Euler Method, Midpoint method and the Runge-Kutta method (Shampine, 1994, Suli, 2010). A method often employed for the numerical solution of PDEs is the Method-of-Lines (MOL) (Schiesser and Griffiths, 2009, Wouwer et al., 2014).

A. Initial and Boundary Conditions

Important to note are the concepts of initial and boundary conditions for the equations to be solved. For a system of equations to be fully defined for a system it needs to be supported by the correct number of initial and boundary conditions completing the mathematical definition of the problem. In general; the number of initial conditions required is equivalent to the order of the time-derivative and the number of boundary conditions required is equivalent to the sum of the order of all the spatial derivatives in the problem (Schiesser and Griffiths, 2009, Wouwer et al., 2014)

B. Method-of-Lines

The fundamental concept behind the MOL is to have the PDE approximated by a series of ODEs. The ODEs take their form from the original PDE by keeping the time-derivative intact and replacing all spatial derivatives with their respective finite difference approximation. Once this is done we can then apply the well-defined numerical methods used for ODE systems, which is one of the prominent features of MOL.

Intrinsically, the space is divided into *M* nodes over which MOL is defined, with each of these nodes represented by an ODE and appropriate finite difference approximations. The number of nodes used to define the space over is at the discretion of the user and can be optimised in order to get the desired balance between computation time and accuracy. Finite difference approximations are used to approximate the value of a derivate by estimation of the slope at a specific point by one of the following three approximations:

$$\frac{\partial \mathrm{u}_i}{\partial \mathrm{t}} = \frac{u(i)-u(i-1)}{\Delta t} \qquad \textbf{Backward difference} \qquad (2.51a)$$

$$\frac{\partial \mathrm{u}_i}{\partial \mathrm{t}} = \frac{u(i+1)-u(i-1)}{\Delta t} \qquad \textbf{Central difference} \qquad (2.51b)$$

$$\frac{\partial \mathrm{u}_i}{\partial \mathrm{t}} = \frac{u(i+1)-u(i)}{\Delta t} \qquad \textbf{Forward difference} \qquad (2.51c)$$

Similarly, for second order derivatives:

$$\frac{\partial^2 u_i}{\partial t^2} = \frac{2u(i)-u(i-1)}{\Delta t^2} \qquad \textbf{Backward difference} \quad (2.52a)$$

$$\frac{\partial^2 u_i}{\partial t^2} = \frac{u(i+1)-2u(i)+u(i-1)}{\Delta t^2} \qquad \textbf{Central difference} \quad (2.52b)$$

$$\frac{\partial^2 u_i}{\partial t^2} = \frac{2u(i+1)-u(i)}{\Delta t^2} \qquad \textbf{Forward difference} \quad (2.52c)$$

From Equations 2.51 and 2.52 an it is evident that one method of approximation can't be used for all nodes, i.e. at node 1 a *forward difference* approximation can be used which only requires the dependent variable input at nodes 1 and 2. Use of any other approximation would require a dependent variable input at node *i-1* (node 0) which is not a physical node and hence does not exist. Similarly for node *M*, a *backward difference* approximation is required which negates the need to access node *M+1* which is not in the bounds of the physical system.

Solving the ODEs can then easily be achieved using built-in functions in MATLAB® (The MathWorks, Inc.). An ODE solver which may be used is a variable order solver such as `ode45`, `ode23` and `ode15s`. The solvers utilise the Runge-Kutta formulation for solving initial value type problems. The numbers in the above mentioned functions indicate the how the error is estimated in each function. The error is calculated by comparing the Runge-Kutta formulations of different orders, for example; `ode45` computes its error by comparing 4th and 5th order Runge-Kutta formulations. The letter "`s`" after `ode15s` indicates that the solver is for *stiff functions*. Stiff functions are functions which change very quickly and thus a small step-size is required as the systems of equations are integrated. Stiffness has to do with the efficiency of the computation and a stiff solver allows for faster computation. Considering the aforementioned solvers `ode15s` was used for all integration.

Another very important aspect of the MOL implementation in this study was the adaption of all equations such that they are initial-value problems, i.e. the subsequent ODEs contain only 1 independent variable which is time. The ODEs were then solved over a sufficient time period to ensure that fluid behaviour had stabilised emulating stead-state conditions. This is significant as all analysis of the systems were at *steady-state* conditions which would imply that the governing equations are devoid of the time variable. Based on the above the model formulation in this study is termed *pseudo initial-value 3-D simulation.*

In summary, considering MOL implemented for a single micro-channel; the *x*, *y* and *z* physical spaces are segmented into a number of discrete nodes: M_x, M_y and M_z. Finite difference approximations are then used to transform the material balance PDE's for each system into a system of ODEs. The number of ODEs solved per species is equivalent to the number of nodes the physical space has been divided into i.e. $M_x \times M_y \times M_z$ nodes.

C. Model co-ordinate system

Figure 2.11 illustrates the co-ordinate system adopted in this study. Envisioning the cross-section of a microchannel as per below the *x*-direction demarcated the width of the channel (marked by W in Figure 2.11) with the null position being the left edge of the channel. The *y*-direction demarcated the depth of the channel (indicated by D in Figure 2.11) with the null position being the bottom of the reactor channel. Finally, the *z*-direction dictates the point along the length of the microchannel where the null position is the top of the channel (i.e. point of liquid flow inlet).

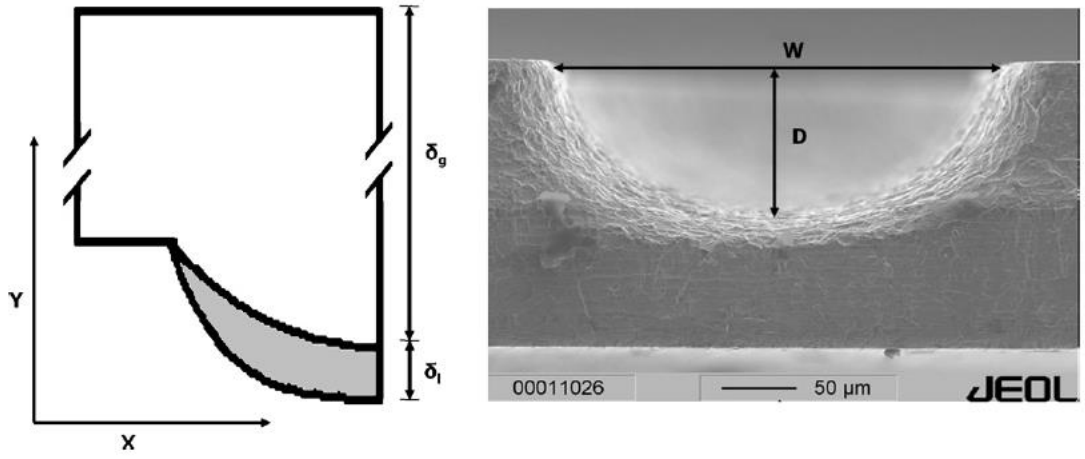

Figure 2.11: Falling-film microreactor channel cross-section images as presented by Al-Rawashdeh, et al. (2008).

D. Liquid film geometry

In general, microchannels are available in two different geometries; wider channel widths have the tendency to resemble a parabola/elliptic circle i.e. they have a wider base that is not completely circular. Having an irregular boundary which does not conveniently fit into the conventional Cartesian co-ordinate system adds complexity to the model formulation particularly with the implementation of MOL which requires discrete nodes across the physical system.

Considering the above as well as the animation of the liquid film in Figure 2.12 an assumption was made that the liquid film resembled a rectangular layer of thickness (δ_L) and width W.

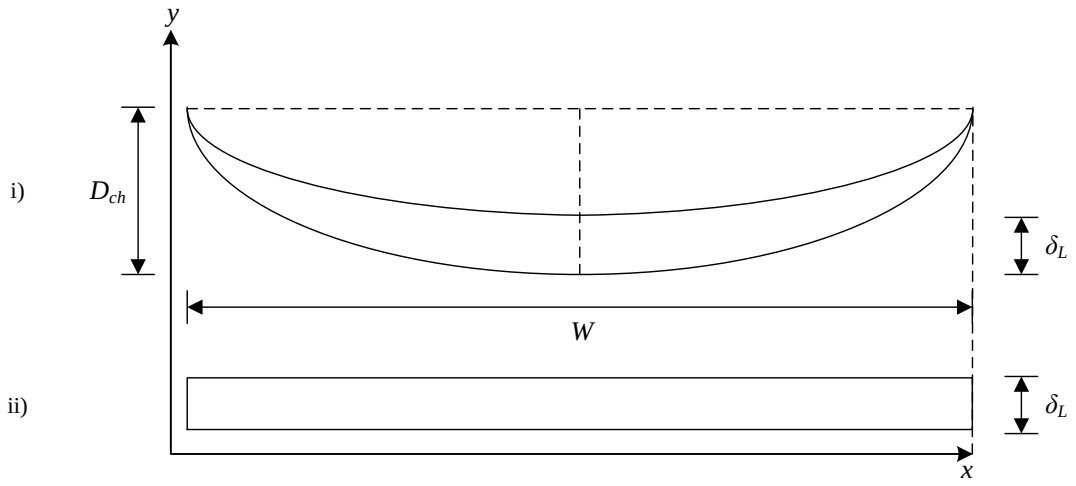

Figure 2.12: Liquid film cross section **i)** of elliptical approximation of liquid film shape and **ii)** rectangular approximation of liquid film shape ultimately used for kinetic model.

2.7.4 Kinetic model identification

The final step in the model formulation is the identification of an appropriate kinetic model. This involves evaluating the adequacy of the model when compared with experimental data. The comparison between the model results and the experimental data is gauged by a single value, the *objective function*, which is minimised to obtain the best model. Minimisation of the objective function occurs when the magnitudes of the kinetic parameters are varied. The variation of the kinetic parameters but is achieved using optimisation functions that are built into MATLAB® (The MathWorks, Inc.). These are discussed further in Section 4.1. The quality of the fit in this study was quantified using the following summed relative-square-error objective function:

$$\mathrm{E} = \sum \left(\frac{\mathrm{C_i^{EXP}} - \mathrm{C_i^{Pred}}}{\mathrm{C_i^{EXP}}} \right)^2 \tag{2.53}$$

Where E is the summed relative-square-error, C_i^{EXP} is the concentration of species i in the product as observed in experiments and C_i^{Pred} is the concentration of species i in the product as predicted by the kinetic model.

2.8 Response surface methodology

Response surface methodology is a statistical analytical technique used to evaluate the effect of control variables on one or more responses. Response surface methodology was pioneered by Box

and Wilson in 1951 and requires that a set of designed experiments (such as those mentioned in Section 2.6) be conducted and their responses fit to a polynomial model to determine an optimal response (Box and Wilson, 1951). The general form of the polynomial model may be seen in Equation 2.54.

$$Y = \beta_0 + \sum_{j=1}^{k} \beta_j X_j + \sum_{i<j} \beta_{ij} X_i X_j + \sum_{j=1}^{k} \beta_{jj} X_j^2 + \cdots \quad (2.54)$$

In Equation 2.54, Y is the predicted response, β_0 is the intercept coefficient, β_j are the linear term coefficients, β_{ij} are the coefficients for the interaction terms and β_{jj} are the coefficients of the quadratic terms. These beta coefficients may be determined by least squares multilinear regression. X_i and X_j represent the control variables of the experimental design (Istadi and Amin, 2007).

Box and Wilson further indicated that a quadratic model was sufficient to investigate the interaction between control variables, and thus Equation 2.54 may be truncated after the forth term for ease of use (Lazić, 2004).

The response function indicated in Equation 2.54 may be visually interpreted as the *response surface* of the k-th dimension (a hyper surface). For a more basic analysis of the interaction between control variables the system may be observed in two dimensions by varying two control variables and maintaining the remaining k-2 variables at a constant value (Lazić, 2004).

3

CHAPTER THREE

3. EXPERIMENTAL EQUIPMENT, PROCEDURE AND DESIGN

3.1 Preliminary investigations

3.1.1 Experimental equipment

Preliminary experiments were an integral part of this study as it allowed for a more comprehensive understanding of the reactive system and gave vital insight into an appropriate operating envelope for future experiments for the HME system. The experiments were conducted on a semi-batch gas-liquid stirred tank reactor that was commissioned by previous researchers at the Thermodynamic Research Unit (University of KwaZulu-Natal – Howard College). The equipment was appropriate for the preliminary experimentation of the HME system because it provided an agitated medium and a temperature controlled environmen.

In summary, the semi-batch reactor consisted of a glass vessel which enclosed a cooling coil, mechanical stirrer, temperature probe and a sintered gas sparger. Temperature control was affected by the use of an external heating jacket and an internal cooling coil. The flow of cooling water through the internal coil was regulated using a temperature controller to governor the reaction temperature (this was the temperature of the liquid phase in the reactor) which was monitored using an internal temperature probe. It was possible that the gas may entrain some of the liquid phase as it exits the system to be vented and so to reintroduce this entrained liquid to the system a reflux condenser was added, using chilled water as the cooling medium. Figure 3.1 shows a schematic of the experimental equipment with an accompanying picture seen in Photograph 3.1 in Section 3.1.2 below. A more detailed description of the above mentioned components follows below.

The gas reagent used in these experiments was hexafluoropropene which was diluted with nitrogen gas. The gases were fed through 2 separate precision rotameters connected in parallel before passing to 3-way ball valves (Swagelok, 316 SS, PTFE) on each line. The 3-way valve allowed for flow to be redirected to a bubble flow meter (BFM) which was used to calibrate the precision rotameters. The gas lines directed towards the reactor were then allowed to blend at a

mixing point before being directed to the sintered gas sparger which was submerged in the reactor contents during operation. The gas cylinders housing the reactant gases were fitted with pressure regulators and set to a discharge pressure of 2 bar.

The reactor was a 2 L clear glass vessel with a heating jacket and a discharge valve at the base of the vessel, which allowed for the reactor contents to be withdrawn. The reactor was mounted on a tripod stand to ensure stability and allow access to the discharge valve below the unit. A 4 port glass flange was fitted to the top of the glass vessel and sealed with vacuum grease. The four ports provided space for the mechanical stirrer (50 mm Teflon paddle), $^1/_4$″glass cooling coil, gas sparger and the temperature probe and reflux condenser (which required one port due to the use of a forked glass neck).

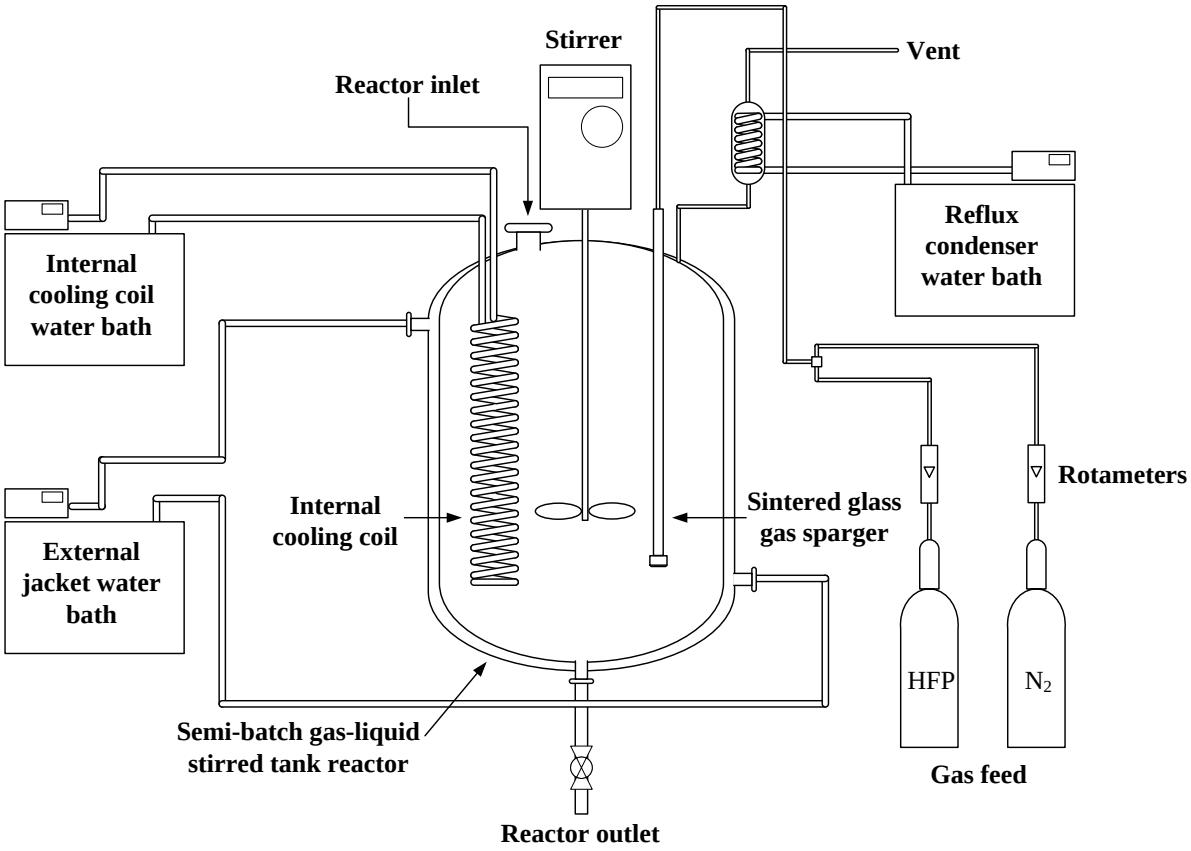

Figure 3.1: Schematic of fully commissioned semi-batch gas-liquid stirred tank reactor used for preliminary investigations into the synthesis of 1,1,2,3,3,3-hexafluoropropyl methyl ether.

As mentioned above, temperature control was affected by simultaneous use of an external heating jacket and internal cooling coil which was submerged in the reactor contents. Water was circulated through the external jacket at 35 °C for all experiments. This temperature was chosen as it was above the highest temperature investigated (28 °C) ensuring that heating would occur throughout all experiments. Higher external jacket temperatures were avoided as it was not

desired to excessively heat the reactor contents thus increasing the strain on the internal cooling system.

Water at a temperature of 2 °C was circulated through the internal cooling coil. This temperature was chosen as the reaction to produce HME was observed as highly exothermic and it was desired to have water at a cold enough temperature to be able to quickly remove heat from the liquid phase, i.e. the lower the coolant temperature, the greater the temperature driving force for heat removal. The last area which used cooling water was the reflux condenser; chilled water at 15 °C was circulated through this unit which is below the boiling point of methanol (64.7 °C).

3.1.2 Experimental procedure and materials

The synthesis of HME in a semi-batch gas-liquid stirred tank reactor required that hexafluoropropene gas be bubbled through methanol that contained dissolved potassium hydroxide (the solution is known as potassium methoxide). Hexafluoropropene, with an experimentally determined purity of 99.8 %, was sourced from the South African Nuclear Energy Corporation (NECSA). The reactant gas was diluted in order to allow variation of the inlet gas concentration, this was achieved using nitrogen gas with a specified purity of 99.999 % which was purchased from Afrox. Methanol was sourced from Laboratory Equipment and Supplies (purity of 99.6 %) and potassium hydroxide was purchased from Merck KGaA with a specified purity of 85 %. The purities of methanol and potassium hydroxide were appropriate, especially when considering the purity of raw materials which would be economically feasible for large scale production of HME.

A. Feed preparation

The reactor was charged with 1.5 L of methanol, this was to allow sufficient head space for unreacted hexafluoropropene and nitrogen gas to escape through the gas vent (Figure 3.1, Section 3.1.1) and to ensure that a sufficient amount of the internal cooling coil was submerged to guarantee adequate cooling. The mass of potassium hydroxide required for each experiment, to obtain the desired feed concentration, was weighed on an Adventurer™ Ohaus Corp. mass balance. The mass balance was calibrated by Trilab Support with an average absolute deviation of 0.001 g; this was considered to be the standard uncertainty of all mass readings recorded throughout this study. The catalyst was then added to the 1.5 L of methanol in the reaction vessel and agitated for 15 min at 450 rpm to ensure that all solid was well dissolved. All samples were prepared with an average percentage uncertainty of 0.33% on the concentration of the potassium methoxide feed stock.

B. Gas sparger preparation

Salt builds up on the surface and in the pores of the sintered gas sparger throughout the duration of the reaction which hinders the efficacy of the gas sparger. This salt is believed to be agglomerates of fine particles of potassium hydroxide and potassium fluoride (a possible by-product of the reaction). In order to ensure that the sparger was clean for every experiment it was removed from the glass reactor and placed in a beaker of deionised water while nitrogen gas was flushed through it for 5 min. This step was crucial to maintaining a high rate of bubbling for all experiments.

C. Reactor start-up

The reactor start-up procedure was essential to ensuring that each experiment proceeds at the required starting conditions. In order to guarantee this, the temperature of the two baths was set 1 hour prior to running an experiment. The temperature of the water circulated through the reactor jacket was set to 35.0 °C, while the temperature of the water to be circulated through the internal submerged cooling coil was set to 2.0 °C. The temperature controllers were not calibrated as their only effect was to regulate the temperature of the reactor; however, the submerged PT 100 temperature probe was calibrated and had an average percentage relative deviation of 0.07 % on display temperature. The standard uncertainties of these controllers are 0.7 °C. The reflux condenser cooling water bath was also prepared 1 hour prior to each experiment by setting the temperature controller to 15.0 °C.

D. Experimental procedure

Prior to the start of each reaction the temperatures of all 3 cooling baths (i.e. external heating jacket water bath, internal cooling coil water bath and reflux condenser cooling bath) were checked to ensure that they were at the required set point temperatures and additional time was allowed for stabilisation of temperatures if necessary. It was also ensured that all potassium hydroxide added to the liquid charge in the reactor was dissolved.

a. The first step of every experiment was ensuring that the liquid contents of the reactor were at the desired reaction temperature. This was done by setting the reaction temperature using the temperature controller (controller A – Photograph 3.1) and opening valve B (Photograph 3.1) 20 min prior to experiment commencement and setting the impeller speed to 450 rpm (controller C – Photograph 3.1).
b. The next step of every experiment was setting the flow meters to the required flow rates.

i. This was done by directing gas flow initially to the bubble flow meter (labelled BFM) using valves D and E as seen in Photograph 3.2 for hexafluoropropene and nitrogen, respectively.
ii. The nitrogen and hexafluoropropene precision rotameters (rotameters F and G – Photograph 3.2, respectively) were then set to the desired flow rate using the calibration charts generated for each rotameter (refer to Section 3.3 for calibration procedures and Appendix A for calibration plots).
iii. Once the temperature controller had stabilised at the desired reaction temperature the gas flow was re-directed to the reactor by turning valves D and E and a timer was simultaneously started.

The sum of the nitrogen and hexafluoropropene gas flow rates were maintained at 1.75 $L \cdot min^{-1}$ for all experiments on the glass reactor to control the bubbling from the sintered gas sparger whilst variation of the individual flow rates of the gas still allowed for reactant gas concentration to be altered. Each experiment was run for 30 min as it was observed that the reaction proceeded rapidly and this would ensure that quantifiable amounts of HME was formed while severe build-up of salt on the sparger was avoided. Salt builds up on the sparger throughout the duration of the reaction which affects the rate of bubbling, thus prolonging the reaction would result in deteriorating rates of bubbling which reduces the efficacy of the reactor.

c. Once the reaction had reached the 30 min mark the reaction was stopped. This was done by:
    i. Directing hexafluoropropene gas flow to the BFM using valve D and closing the hexafluoropropene rotameter (rotameter G).
    ii. The flow rate of nitrogen was increased to double its flow rate using rotameter F and allowed to run for 5 min. The purpose of this was to flush the system of any unreacted hexafluoropropene gas, thus terminating the reaction.
d. Finally, the reactor was emptied and products stored for analysis.
    i. Emptying the reactor required that valve H at the base of the glass vessel (Photograph 3.1) be opened and the contents drained into a 2 L glass beaker.
    ii. The empty weight of the glass beaker was measured and so was the weight inclusive of the reactor contents, this allowed for the mass of the reactor discharge to be determined.
    iii. A sample of the crude product was taken by drawing out approximately 1 mL of crude through a micropore filter (Millipore Millex-GV 0.22 µm filter) in order to remove any solid particles entrained in the liquid. The sample vial was cleaned and weighed prior to use. Samples were stored in a refrigerator until analysis was

conducted. Analysis was conducted using a Shimadzu 2010 Gas Chromatograph and Shimadzu QP 2010 Plus Quadropole Gas Chromatograph – Mass Spectroscopy. Specifics regarding the analytical techniques used are discussed in more detail in Section 3.4 and 3.5.

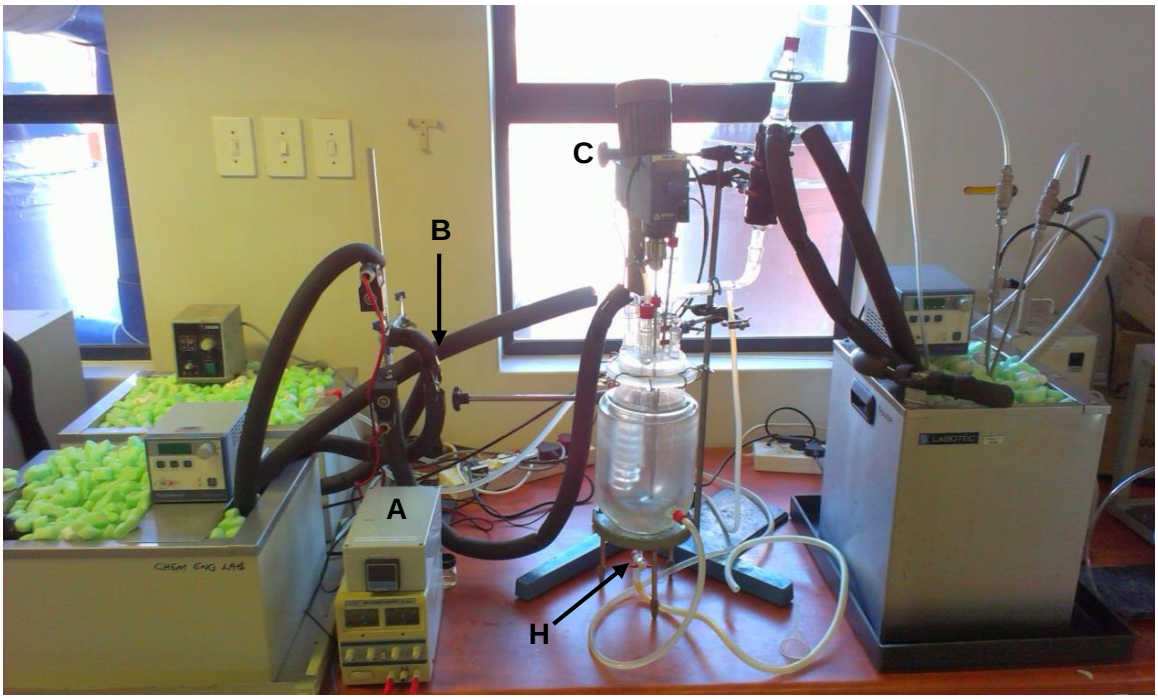

Photograph 3.1: Experimental set-up used for preliminary investigations into the synthesis of 1,1,2,3,3,3-hexafluoropropyl methyl ether using a semi-batch gas-liquid stirred tank reactor.

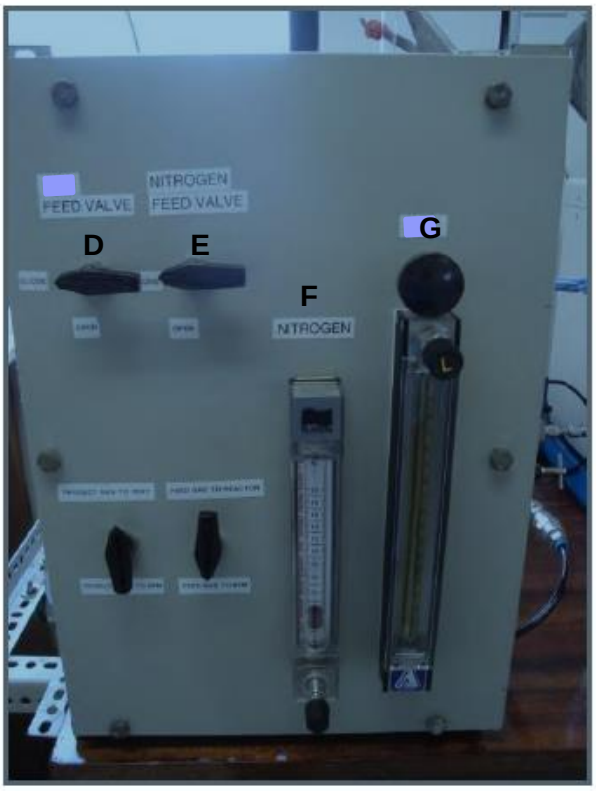

Photograph 3.2: Valve panel containing precision rotameters used to control nitrogen and hexafluoropropene gas flow rates as well as flow direction of gas (from cylinders to either reactor or bubble flow meter).

3.1.3 Experimental design

In order to ascertain the influence of various reaction conditions on the yield of HME, it was decided that a circumscribed central composite design with 3 design variables would be used. The 3 factors of interest were; potassium hydroxide concentration in methanol, hexafluoropropene gas mole fraction in the gaseous feed to the reactor as well as reaction temperature. The experimental design dictated that 20 experiments be carried out which included 6 centrepoints to assess the consistency of the experimental equipment. Table 3.1 shows the permutations of experimental conditions as required by a 3 factor circumscribed central composite design.

The experiments were carried out with the following parameter ranges; potassium hydroxide concentration 0.40 to 0.80 mol.L^{-1} (percentage uncertainty of 0.33% on the concentration of the potassium methoxide feed stock), hexafluoropropene mole fraction in the gas phase of 0.41 to 0.83 (percentage uncertainty of 3.5 % on hexafluoropropene mole fraction) and a temperature range from 12 to 28 ^{o}C (percentage uncertainty of 1.25 % of the display temperature). The temperature range used was benchmarked based on previous work by of Rendall et al. (1958) and Il'in et al. (2004). The concentration of the gas phase was varied by adjusting flow rates of hexafluoropropene and an inert gas. Nitrogen (N_2) gas was chosen.

Table 3.1: Permutations of experimental conditions required for a 3 factor circumscribed Box-Wilson central composite design. 0, ±1 and ±α indicates centrepoint, factorial and axial operating conditions.

	Manipulated variables		
Run Number	Feed gas mole fraction	Catalyst concentration	Reaction temperature
1	1	1	1
2	1	1	-1
3	1	-1	1
4	1	-1	-1
5	-1	1	1
6	-1	1	-1
7	-1	-1	1
8	-1	-1	-1
9	α	0	0
10	α	0	0
11	0	α	0
12	0	α	0
13	0	0	α
14	0	0	α
15	0	0	0
16	0	0	0
17	0	0	0
18	0	0	0
19	0	0	0
20	0	0	0

Table 3.2: Levels of operating conditions to be investigated in 3 factor circumscribed central composite design for 1,1,2,3,3,3-hexafluoropropyl methyl ether system on semi-batch gas-liquid stirred tank reactor. 0, ±1 and ±α indicates centrepoint, factorial and axial operating conditions.

	Levels				
Factors	-α	-1	0	+1	+α
Hexafluoropropene mole fraction	0.41	0.49	0.62	0.74	0.83
Catalyst concentration ($mol \cdot L^{-1}$)	0.40	0.48	0.60	0.71	0.80
Reaction temperature (^oC)	12.0	15.0	20.0	25.0	28.0

3.2 Falling film microreactor equipment validation

The validation of experimental equipment is crucial to ensure that it operates accurately, efficiently and safely. Equipment validation of the FFMR was performed based on previous work by Zanfir et al., (2005), Al-rawashdeh et al., (2008) and Zhang et al., (2009). As outlined in Section 2.4, Zanfir et al., (2005) and Al-rawashdeh et al., (2008) undertook investigations into the gas-liquid behaviour within FFMRs by generating models for reactive systems and validating these results experimentally (Al-Rawashdeh et al., 2008, Zanfir et al., 2005, Zhang et al., 2009).

The authors of these studies chose to observe the absorption and subsequent reaction of carbon dioxide in sodium hydroxide solution to produce sodium carbonate.

This reaction was chosen due to the fact that it has proven to be rapid and irreversible, which makes it ideal for study using a FFMR (Astarita, 1967, Danckwerts, 1970). The reagents are also relatively inexpensive and easily available which also makes them suitable for equipment validation experiments. The reaction system involves passing 12 wt% ethylene glycol in water mixture through the FFMR while carbon dioxide was passed through the gas chamber. The liquid outlet which contains absorbed carbon dioxide is passed into a beaker of 0.1 mol·L^{-1} sodium hydroxide solution. Thereafter, the absorbed carbon dioxide then reacts with the available sodium hydroxide to produce sodium carbonate. The reaction steps may be expressed as follows:

$$CO_{2\,(g)} \leftrightarrow CO_{2\,(abs)} \tag{3.1}$$

$$CO_{2\,(abs)} + OH^-_{(aq)} \leftrightarrow HCO^-_{3\,(aq)} \tag{3.2}$$

$$HCO^-_{3\,(aq)} + OH^-_{(aq)} \leftrightarrow CO^{2-}_{3\,(aq)} + H_2O_{(l)} \tag{3.3}$$

Overall reaction:

$$2NaOH_{(aq)} + CO_{2\,(g)} \leftrightarrow Na_2CO_{3\,(aq)} + H_2O_{(l)} \tag{3.4}$$

The amount of sodium hydroxide was determined by titration analysis using hydrochloric acid to neutralise the system. Titrations were carried out using a Metrohm 888 Titrandol autotritator. The titration analysis has two endpoints which can be identified by using phenolphthalein and methyl orange as indicators respectively (Zhang et al., 2009).

In order to ensure that absorbed carbon dioxide reacts completely Zanfir et al., (2005) and Al-rawashdeh et al., (2008) chose to increase the available sodium hydroxide so that it is always in excess, a $\frac{n_{CO_2}}{n_{NaOH}}$ ratio of 0.4 was used.

The first endpoint illustrates the point at which all excess unreacted sodium hydroxide is neutralised and converts any sodium carbonate to sodium bicarbonate (Equation 3.5). The second endpoint, indicated by methyl orange, shows the point at which sodium bicarbonate is converted to sodium chloride, carbon dioxide and water (Equation 3.6).

$$Na_2CO_{3(aq)} + HCl_{(aq)} \leftrightarrow NaCl_{(aq)} + NaHCO_{3(aq)} \quad (3.5)$$

$$NaHCO_{3(aq)} + HCl_{(aq)} \leftrightarrow NaCl_{(aq)} + CO_{2(g)} + H_2O_{(l)} \quad (3.6)$$

The concentration of carbon dioxide that was absorbed into the sodium hydroxide can be easily determined from Equation 3.7 (Zhang et al., 2009):

$$C_{CO_2,Out} = \frac{V_{HCl}\, C_{HCl}}{\dot{V}_L\, t} \quad (3.7)$$

Where $C_{CO_2,Out}$ is the concentration of carbon dioxide that was absorbed in the reactor product, V_{HCl} is the volume of hydrochloric acid titrated which has a concentration of C_{HCl}, $\dot{V}_L$ is the volumetric flow rate of the liquid and finally t is the duration of the experiment. The validation experiments were run for 20 min and with a hydrochloric acid concentration of 0.01 mol·L^{-1}. The liquid-side mass transfer coefficient may then be calculated using Equation 3.8.

$$K_L = \frac{\dot{V}_L}{b\, L} \ln\left(\frac{C^*}{C^* - C_{CO_2,Out}}\right) \quad (3.8)$$

Where, K_L is the overall liquid side mass transfer coefficient, b is the width of a microchannel, L is the length of the reaction plate (66.4 mm) and C^* is the saturated concentration of carbon dioxide in sodium hydroxide.

3.3 Present work: falling film microreactor experiments

3.3.1 Experimental equipment

The FFMR used in the present work is the FFMR-Standard which is purchasable from the Institut für Mikrotechnik Mainz GmbH and is constructed out of 316Ti stainless steel. The FFMR-Standard has an integrated heat exchanger with a copper heating/cooling plate and may be operated with three different reaction plates, namely a 64 channel 200 × 300 μm, a 32 channel 300 × 600 μm and a 16 channel 300 × 1200 μm reaction plate. All experiments were conducted on the 32 channel 300 × 600 μm reaction plate. This reaction plate was chosen as it provided the advantages of high interfacial areas (which increases as the number of microchannels increases) while avoiding too narrow channel widths in which channel blockages can easily occur.

The FFMR equipment was commissioned for the first time in this study and provided an efficient medium for multi-phase reactions due to its high rates of heat and mass transfer. The reactor also

offered a very convenient advantage in that was it easily installed, requiring only a few additional units. In summary, the FFMR experimental set-up includes reactant gas cylinders, the FFMR-Standard (as described above), a cooling water bath, feed pump, withdrawal pump and 3 product and feed vessels. What follows is a more detailed description of the experimental equipment.

The process starts at the introduction of the gases to the system. The gas cylinders (hexafluoropropene (for the HME system), hexafluoropropene oxide (for the MTFMP system), carbon dioxide (for validation experiments) and nitrogen) were all fitted with pressure regulators and set to a discharge pressure of 2 bar. At any time in an experiment there was at most two gases being used simultaneously, there was thus a need for only 2 precision rotameters which were calibrated for each gas using a 50 mL BFM. Gases then passed to a mixing point before being sent to the reactor. A 3-way ball valve (Swagelok, 316, PTFE) was installed before the reactor inlet in order to allow for gas flow to be directed towards the BFM during calibration of roatmeters. Directing gas flow towards the reactor meant that the gas was met with another valve, a 2-way ball valve (Swagelok, 316 SS, AFS) which may either close the reactor off or allow gas to continue to flow. This valve (at the base of the reactor, valve D in Photograph 3.4) prevents liquid from entering the gas line during flooding of the reactor. The gas then passed over the reaction plate and exited through the top of the reaction plate where it was vented (as can be seen in Figure 3.2).

Gases were fed to the base of the reactor to operate it in counter-current mode, i.e. liquid flowing vertically down the reaction plate and gas flowing vertically up the reaction plate. This flow arrangement was chosen so that a high driving force for mass transfer was achieved over the whole reaction plate. A total gas flow rate of 90 $mL \cdot min^{-1}$ was used for all experiments as this was close to the upper limit of what was capable in the system and ensured that sufficient reactant gas was available for reaction allowing for a feasible residence time of the gas in the reactor.

All gas lines which contained either hexafluoropropene or hexafluoropropene oxide were made of perfluroalkoxy alkane (PFA) tubing which is typically used to handle chemically aggressive compounds.

The liquid reactant (potassium methoxide) for each experiment was prepared and then placed in a 1 L glass feed vessel which was fed to the reactor via a HPLC (High performance liquid chromatography) Series II, Scientific Systems, Inc. pump. Liquid was withdrawn from the reactor using a Heidolph Pumpdrive 5201 peristaltic pump because it was capable of operating without liquid in the process line, which occured during experiments when liquid was withdrawn at a rate

greater than it was introduced into the reactor (thus causing dry slugs to form in the liquid exit line).

Liquid withdrawn from the reactor then passed through a 3-way ball valve (Swagelok, 316, PTFE) which allowed the now processed fluid to be directed to one of two 500 mL product vessels. One product vessel was used during flooding and steady-state operations of each experiment while the second product vessel was used to collect product once a run had been started.

The integrated heat exchanger was used to affect the temperature of the reaction plate (in essence, the reaction temperature), this was done by circulating water from a water bath at the desired reaction temperature. The temperature of the water in the water bath was allowed to circulate through the reactor prior to each run to ensure that the reactor would reach the necessary temperature. An assumption was made that the reaction temperature was at the same temperature of the circulated cooling water due to the high rates of heat transfer intrinsic to a FFMR. A temperature probe would allow for the reaction temperature to be directly measured but this was unfeasible as the reactor is a sealed unit and the presence of any foreign devices would disturb the hydrodynamics of the system.

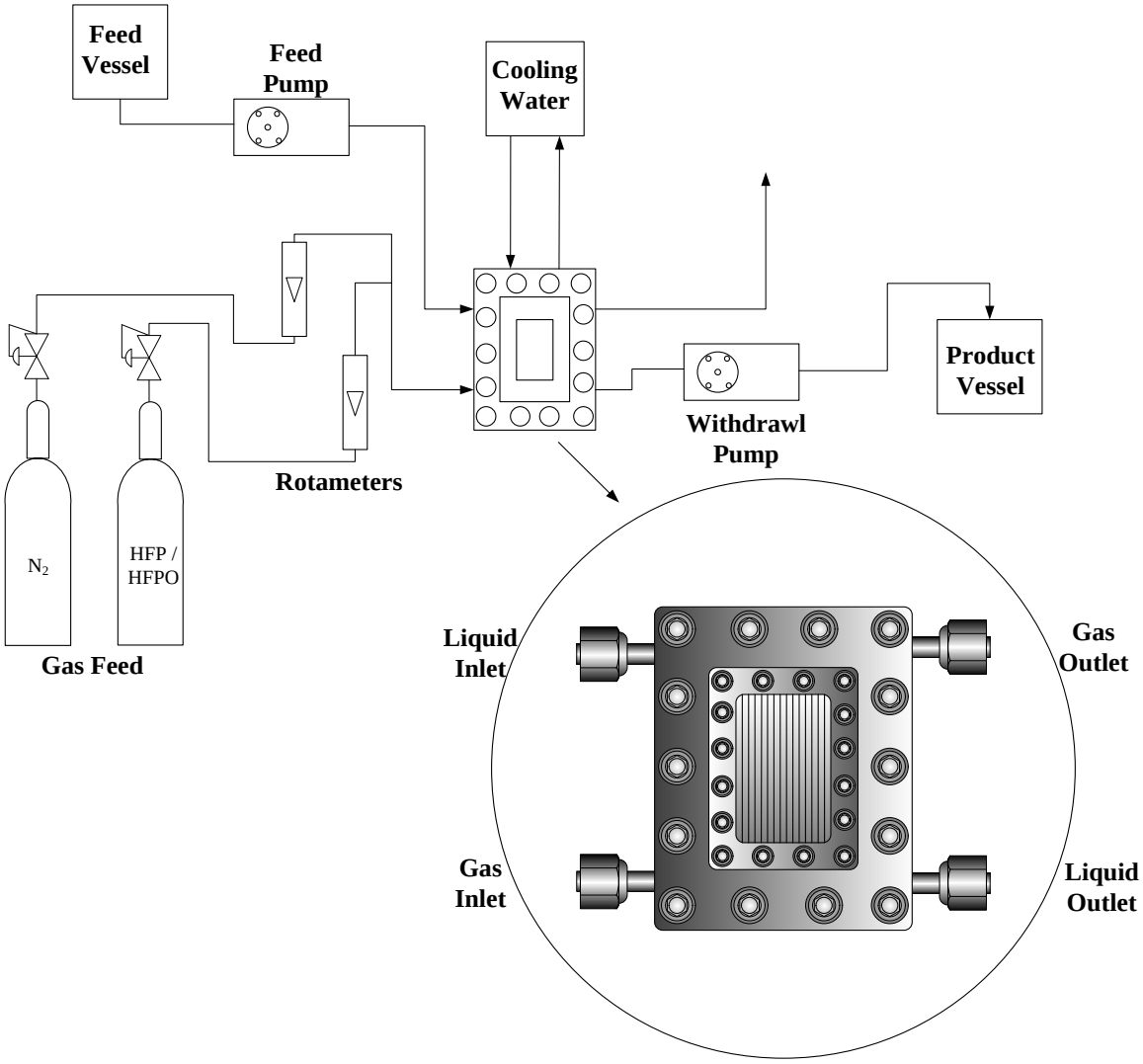

Figure 3.2: Schematic of fully commissioned Falling film microreactor experimental set-up.

3.3.2 Experimental procedure and materials

The synthesis of HME using a FFMR involves the same reaction mechanism as with the glass reactor but provides a more efficient medium for contacting the valid phases, the chemicals used are thus the same as mention in Section 3.1.2. For the MTFMP system, hexafluoropropene oxide with an experimentally determined purity of 99.5 % was sourced from the NECSA.

A. Feed preparation

500 mL of potassium methoxide was prepared for each experimental run. 500 mL of methanol was measured using a graduated cylinder, to which potassium hydroxide pellets were added in order to obtain the required feed concentration. The required mass of catalyst was weighed on an Adventurer™ Ohaus Corp. mass balance. The weighed catalyst was then added to the methanol which was placed on a heating pad with a magnetic stirrer and vigorously mixed for 10 min to

ensure that all the potassium hydroxide pellets had dissolved. The percentage uncertainty in the reported concentration of potassium hydroxide was 0.04 %.

B. Reactor start-up

The start-up procedure for the FFMR is of utmost importance to ensure that the reactor operates efficiently. One hour prior to conducting experiments the cooling water bath was set at the desired reaction temperature. Once the cooling water reached the desired reaction temperature it was allowed to circulate through the reactor for 15 min before starting an experimental run. This allowed for thermal equilibrium to be achieved on the reaction plate. 15 min of cooling water circulation was sufficient due to the high rate of heat transfer experienced in the FFMR.

After ensuring that the cooling water and reaction plate were at the requisite temperatures, the reactor was flooded with the liquid feed solution. Flooding of the reactor guaranteed that the reaction plate had a completely wetted surface which maximised the interfacial contact area between the gas and liquid phases. Flooding of the reactor was achieved by closing the liquid outlet valve (valve A – Photograph 3.3) and allowing the liquid feed to build-up within the reactor, at the liquid flow rate of that particular experiment, until the reaction plate cavity was completely filled (as seen through the sight window in Photograph 3.3). The liquid feed rate was set on the HPLC Series II liquid feed pump. The Heidolph Pumpdrive 5201 peristaltic withdrawal pump was then set to 80 rpm and switched on while simultaneously opening valve A thus allowing liquid to be withdrawn and sent to product vessel 1 (as indicated by the position of valve B – Photograph 3.4). 80 rpm resulted in a withdrawal rate that far exceeded the liquid feed rate ensuring that liquid did not build-up in the reactor during experiments.

C. Experimental procedure

Before each experiment was conducted the temperature of the cooling water was checked to make sure that it was at the required reaction temperature. Checks were also made to ensure that the liquid outlet line (valve A) was open and the HPLC feed pump (unit G – Photograph 3.4) as well as the peristaltic withdrawal pump (unit H – Photograph 3.4) were both switched on and were at the correct flow rates directing liquid flow into product vessel 1. The start position of the outlet gas valve (valve C – Photograph 3.4) was set to vent while the inlet gas valve directed gas to the BFM (valve D – Photograph 3.4).

a. The first step of every experiment was setting of the gas flow rates.
    i. The hexafluoropropene or hexafluoropropene oxide and nitrogen flow rates were set using rotameters E and F, respectively (Photograph 3.4). Hexafluoropropene

and nitrogen were used for the HME system while hexafluoropropene oxide and nitrogen were used for the MTFMP system. The rotameters were calibrated using a BFM with average absolute relative deviation uncertainties of 2.32 %, 3.07 % and 4.87 % for the nitrogen, hexafluoropropene and hexafluoropropene oxide rotameters, respectively.

ii. Once the flow rates of the gas had been set, valve D was opened thereby directing the reactant gas to the reactor. The reactant gas passed counter-currently over the reaction plate and unreacted gas was vented to the atmosphere through valve C.

b. The system was then run at the desired operating conditions for 5 min in order to ensure that steady-state conditions were achieved.

c. Once steady-state conditions were achieved valve B was turned to redirect product flow from product vessel 1 to product vessel 2 and a stop watch was simultaneously started. The reactor was run for 30 min allowing ample time for HME product to accrue.

d. At the 30 min mark the reaction was stopped by:

i. First switching off the HPLC feed pump and closing valve D. The rotameters were then closed (rotameters E and F).

ii. The withdrawal pump was run for 1 min after the feed of liquid was to remove all product in the equipment lines.

iii. Product vessel 2 was weighed before and after the experiment was conducted so that the mass of crude product could be easily determined.

iv. A sample of the crude product was taken by drawing out approximately 1 mL of crude through a micropore filter (Millipore Millex-GV 0.22 µm filter) to remove any solid particles entrained in the liquid. The sample vial was cleaned and weighed prior to use. Samples were stored in a refrigerator until analysis was conducted. Analysis was conducted using a Shimadzu 2010 Gas Chromatograph and Shimadzu QP 2010 Plus Quadropole Gas Chromatograph – Mass Spectroscopy. Details regarding the analytical techniques used are discussed in more detail in Section 3.5 and 3.6.

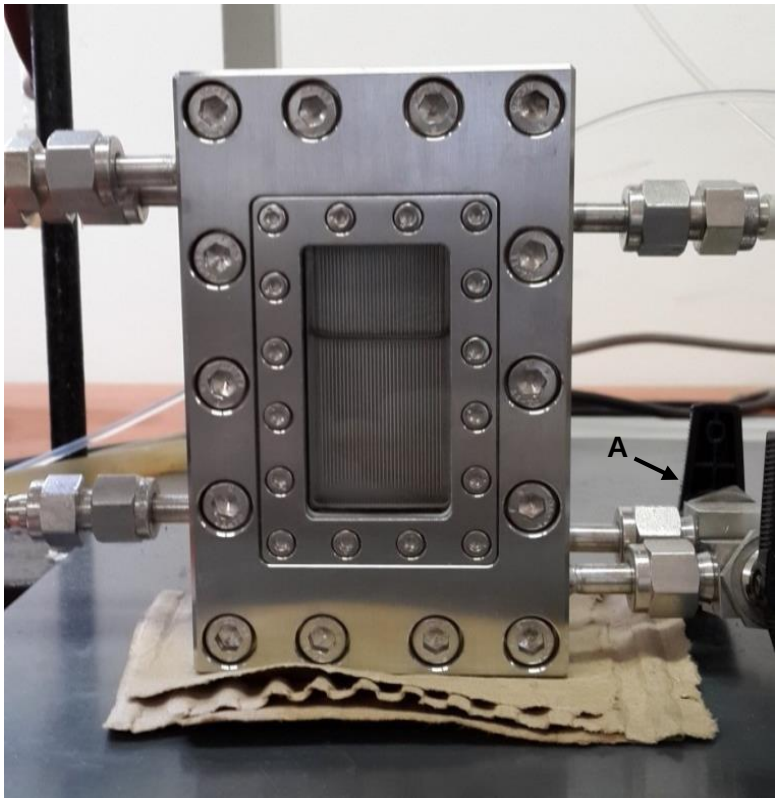

Photograph 3.3: Falling film microreactor while being flooded with potassium methoxide solution 1,1,2,3,3,3-hexafluoropropyl methyl ether synthesis.

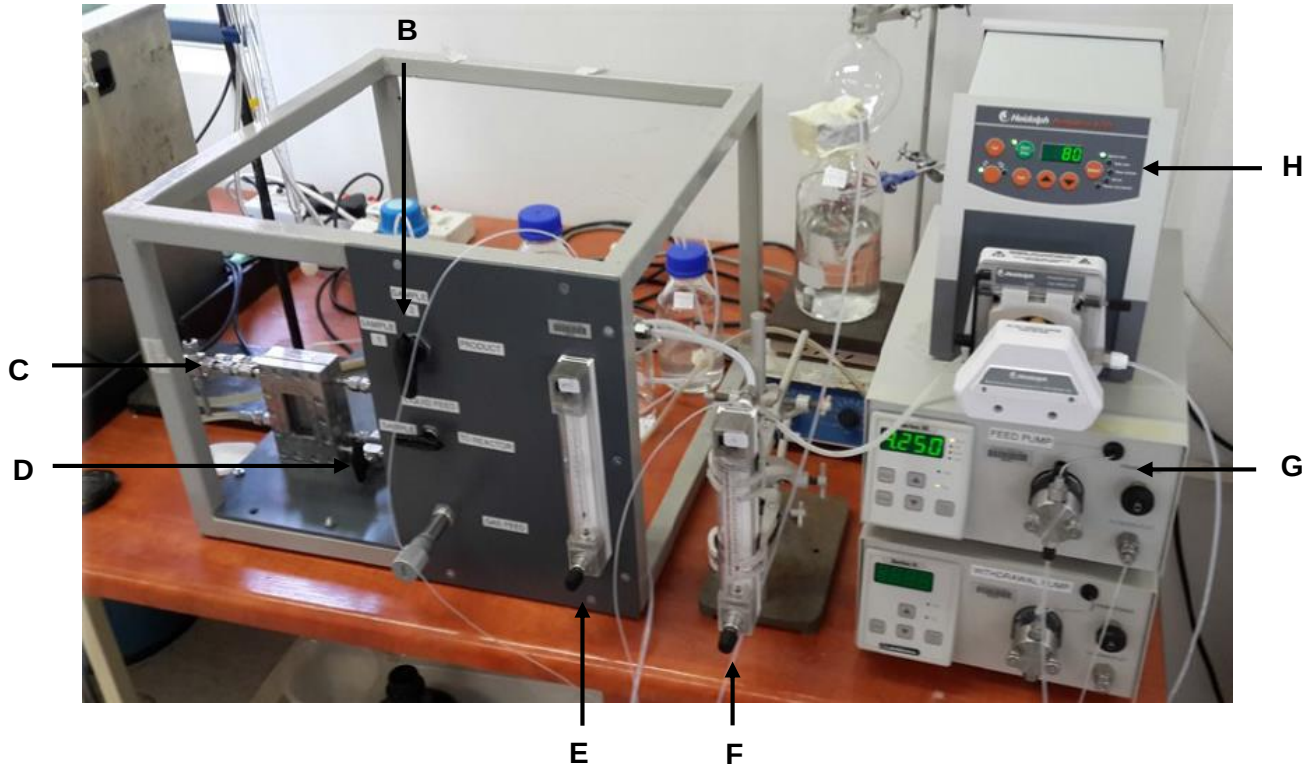

Photograph 3.4: Falling film microreactor experimental set-up used for the synthesis of 1,1,2,3,3,3-hexafluoropropyl methyl ether and methyl-2,3,3,3-tetrafluoro-2-methoxypropionate.

3.3.3 Experimental design

An important aim of the present work was to ascertain the effect of varying operating conditions on the yield of the target compounds of each system of interest. 4 operating conditions were chosen to be varied, these were: reactant gas mole fraction in feed (average absolute relative percentage deviation of 3.85 %), catalyst concentration (i.e. potassium hydroxide concentration) (average percentage uncertainty of 0.04 %), reaction temperature (average percentage uncertainty of 5.26 %) and liquid flow rate. A range of investigation was then chosen for each operating condition and each factor was chosen to be investigated at 5 levels within this range (i.e. the $-\alpha$, -1, 0, +1 and $+\alpha$ levels), this lead to a total of 1024 experiments for a full factorial design. However, a full factorial design was not feasible as it would require a large amount of time and resources, thus a central composite design (as outlined in Section 2.6) was chosen.

It was most desirable to investigate the widest range of operating conditions while still obtaining valuable interaction data and limiting the required number of experimental runs. These criteria necessitated the use of a circumscribed Box-Wilson central composite design with 4 factors and 5 levels. Choosing to replicate the centrepoint conditions 6 times dictated that a total of 30 experimental runs were required and the permutations of which may be seen in Table 3.3.Each level represented in Table 3.3 indicates a specific level of the operating parameter of interest. The levels of the operating parameters for both the HME and MTFMP systems were chosen based on previous work as well as conditions achievable by the available equipment. Tables 3.4 and 3.5 show the various levels of the operating parameters investigated for the HME and MTFMP systems, respectively.

The temperature range used was benchmarked based on previous work by of Rendall et al. (1958) and Il'in et al. (2004) – the temperature range for the HME system was shifted to lower temperatures based on findings from preliminary investigations. The temperatures were shifted such that literature temperatures (of approximately 20 ^{o}C) still remained in the investigative space (Il'in et al., 2004, Rendall, 1958). Hexafluoropropene and hexafluoropropene oxide mole fractions were chosen to try and span a large portion of the whole range mole fraction range. The catalyst concentration was varied from 0.25 to 0.61 $mol \cdot L^{-1}$ for the HME system and from 0.15 to 0.65 $mol \cdot L^{-1}$ for the MTFMP system. These ranges were guided by findings from the preliminary investigations which indicated that yields of the desired products were found to be favored at low to moderate catalyst concentrations – in literature, a catalyst concentration of 1 $mol \cdot L^{-1}$ was used. Finally, the liquid flow rate for both systems were varied from 0.50 to 5.50 $ml \cdot min^{-1}$ which spanned more than 80% of the full range of the feed HPLC pump.

Table 3.3: Permutations of experimental conditions required for a 4 factor circumscribed Box-Wilson central composite design. 0, ±1 and ±α indicates centrepoint, factorial and axial operating conditions, respectively.

Run Number	Manipulated variables			
	Feed gas mole fraction	Catalyst concentration	Reaction temperature	Liquid flow rate
1	-1	-1	-1	-1
2	-1	-1	-1	1
3	1	-1	-1	-1
4	1	-1	-1	1
5	-1	1	-1	-1
6	-1	1	-1	1
7	1	1	-1	-1
8	1	1	-1	1
9	-1	-1	1	-1
10	-1	-1	1	1
11	1	-1	1	-1
12	1	-1	1	1
13	-1	1	1	-1
14	-1	1	1	1
15	1	1	1	-1
16	1	1	1	1
17	0	0	-α	0
18	0	0	α	0
19	0	-α	0	0
20	0	α	0	0
21	-α	0	0	0
22	α	0	0	0
23	0	0	0	-α
24	0	0	0	α
25	0	0	0	0
26	0	0	0	0
27	0	0	0	0
28	0	0	0	0
29	0	0	0	0
30	0	0	0	0

Table 3.4: Levels of operating conditions to be investigated in 4 factor circumscribed central composite design for 1,1,2,3,3,3-hexafluoropropyl methyl ether system. 0, ±1 and ±α indicates centrepoint, factorial and axial operating conditions, respectively.

	Levels				
Factors	-α	-1	0	+1	+α
Hexafluoropropene mole fraction	0.17	0.34	0.52	0.70	0.88
Catalyst concentration ($mol \cdot L^{-1}$)	0.25	0.34	0.43	0.52	0.61
Reaction temperature (^oC)	2.0	7.0	12.0	17.0	22.0
Liquid flow rate ($ml \cdot min^{-1}$)	0.50	1.75	3.00	4.25	5.50

Table 3.5: Levels of operating conditions to be investigated in 4 factor circumscribed central composite design for methyl-2,3,3,3-tetrafluoro-2-methoxypropionate system. 0, ±1 and ±α indicates centrepoint, factorial and axial operating conditions, respectively.

	Levels				
Factors	-α	-1	0	+1	+α
Hexafluoropropene oxide mole fraction	0.16	0.33	0.50	0.67	0.84
Catalyst concentration ($mol \cdot L^{-1}$)	0.15	0.28	0.40	0.53	0.65
Reaction temperature (^oC)	30.0	32.5	35.0	37.5	40.0
Liquid flow rate ($ml \cdot min^{-1}$)	0.50	1.75	3.00	4.25	5.50

3.4 Quantitative analysis using gas chromatography

Qualitative analyses of gas and liquid reaction reagents and products were conducted using gas chromatography and mass spectroscopy. Quantitative analyses of products were conducted using gas chromatography which is the most widely used analytical technique in the world for analysing gas and liquid mixtures (Raal and Mühlbauer, 1998, Snow and McNair, 1992).

In order to conduct accurate analyses using gas chromatography a suitable column and detector is required to successfully separate and analyse injected samples. Successful gas chromatography analyses begin with column selection and this is based on four main criteria viz., the stationary phase, column inner diameter, film thickness and column length.

The stationary phase within the column is the basis upon which separation between various components is made as different compounds interact differently with the stationary phase and thus have varying retention times. Correct selection of a stationary phase will allow for distinctive separation between the species of interest.

The column inner diameter is chosen to find a compromise between the separation efficiency and the sample capacity of the column. A thinner column will increase the separation efficiency of the analysis but lowers the sample capacity that may be injected into the gas chromatograph.

The third criteria that needs to be evaluated is the required film thickness of the stationary phase, decreasing the film thickness may lead to sharper resolved peaks, reduce bleeding of the stationary phase out of the column as well as increase the maximum column temperature.

Lastly, the length of the column needs to be chosen based on the needs of the investigated system. Chemical systems which have components that are vastly dissimilar may require a short column (15 m) whereas systems which have compounds of similar chemical behaviour may require columns of up to 60 m in order to obtain a better peak resolution. Column length may also be varied to obtain a desired analysis time (McNair and Miller, 2011).

In addition to column selection, a suitable detector is also required which meets the sensitivity, detectivity and cost requirements of the investigation. The most common detector which is used to analyse a large variety of species and can detect concentrations as small as 50 ppb is a flame-ionization detector (FID). The FID is highly sensitive, has a high detectivity and is relatively inexpensive and, for the aforementioned characteristics was selected for this study.

Gas chromatography may be used for quantitative analyses of samples using five different methods, viz., area normalization, area normalization with response factors, external standards, internal standards and the standard addition method.

3.4.1 Area normalization

Area normalization is the simplest quantification technique and is based on the assumption that the area percent of a particular peak may be approximately equal to the weight percent of that species. Thus the mass percentage of component i may be calculated using Equation 3.9 below:

$$\text{Mass percent} \cong \text{area percent} = \left[\frac{A_i}{\sum_j (A_j)}\right] \times 100\% \tag{3.9}$$

The area normalization technique may be employed when the following assumptions hold true; the detector has the same sensitivity to all the analytes in the sample and that all components present in the injected sample have been clearly and accurately resolved by the gas chromatograph (McNair and Miller, 2011).

3.4.2 Area normalization with response factor

This method is used to negate the effect of varied sensitivities of species with the detector by use of a response factor, F_i. When using this quantification technique a calibration plot will need to be generated for the gas chromatograph used This may be done by preparing mixtures of the standard and analytes by weight and analysing the respective areas obtained after being chromatographed (A_s and A_x). The standard is given an arbitrary relative response factor, such as 1.00, and the relative response factor of the unknown sample may then be determined by Equation 3.10. $\frac{w_x}{w_s}$ is the mass ratio of target compound to standard and is obtained from the prepared mixtures used in the calibration. The standard chosen may also be one of the peaks already in the injected sample (McNair and Miller, 2011).

$$\mathrm{F_x} = \mathrm{F_s} \times \left(\frac{\mathrm{A_s}}{\mathrm{A_x}}\right) \times \left(\frac{\mathrm{w_x}}{\mathrm{w_s}}\right) \tag{3.10}$$

The mass percentage of a target compound may then be determined as in the area normalization technique with the response factor being included in the numerator of Equation 3.9 as can be seen in Equation 3.11 below (McNair and Miller, 2011):

$$\text{Mass percent} \cong \text{area percent} = \left[\frac{\mathrm{A_i \cdot F_i}}{\sum_{\mathrm{j}}(\mathrm{A_j})}\right] \times 100\% \tag{3.11}$$

3.4.3 External standard

The external standard is one of the more commonly employed quantification techniques and is a graphical method which may be performed using software that relies on the use of calibration curves to determine the concentration of analyte in a sample (Harvey, 2000, McNair and Miller, 2011).

The external standard method is so named because it requires that the standards be prepared and analysed separately from the samples of interest in the experiment. The calibration curves may be generated by two principles means, namely, single-point and multiple-point external standard calibrations. A single-point calibration requires that only one standard be prepared with a known concentration of the standard. The slope of the curve, k, may then be determined by Equation 3.12 (Harvey, 2000, McNair and Miller, 2011).

$$\mathrm{k} = \frac{\mathrm{S_{stand}}}{\mathrm{C_S}} \tag{3.12}$$

Once k has been determined, the concentration of the analyte in the injected sample may be determined by the response, S_{stand}, (either the height or area of the analyte peak).

The second means of calibration is via a multiple-point calibration which requires that multiple standards of varied concentrations be prepared. A calibration curve may then be plotted where the response of the standard is a function of the concentration of standard for each sample. There are usually two possible calibration curves that result, viz., a linear and non-linear normal calibration (Figure 3.3).

A straight line normal calibration is the most desirable and allows for the gradient of the calibration curve to be quantified by a single factor which may be used to determine the concentration of standard for a given response. For a curved line normal calibration plot the gradient is a function of the concentration of standard which requires that an equation be used to describe the non-linear relationship (Harvey, 2000).

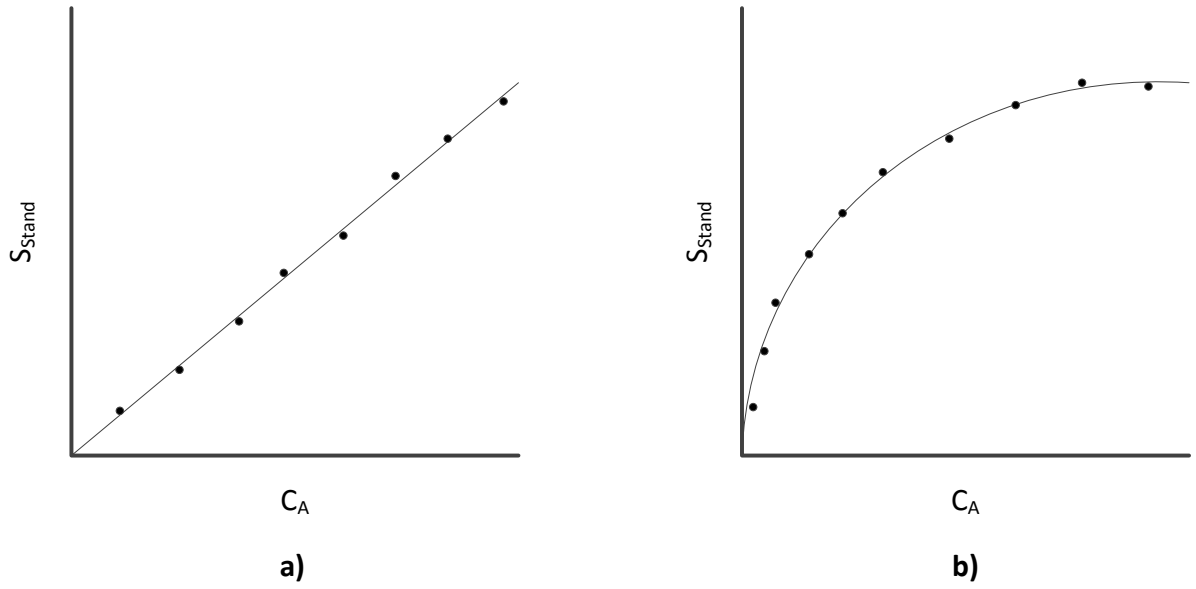

Figure 3.3: Illustrative examples of **a)** linear line and **b)** non-linear line normal calibration plots for an external standard quantification method (Harvey, 2000).

Harvey (2000) recommends that a multiple point calibration be conducted wherever possible as it provides more accurate results and may clearly show if the system behaves linearly or non-linearly as the concentration of standard is increased. It is also of vital importance that the volume injected for every sample during the calibration procedure be exactly the same. Thus, McNair and Miller (2011) recommend that manual injection apparatus be avoided and that an auto-injection system be used to ensure repeatability.

3.4.4 Method of standard additions

The standard addition method allows the unknown concentration of analyte in a sample to be determined by either a single point or a multiple point calibration. The procedure for a single point calibration is as follows; a volume V_A of unknown concentration C_A is diluted to a final volume V_F. A second solution is then made by adding the exact same volume of analyte (V_A) with an unknown concentration (C_A) to a beaker and adding a volume of a standard (V_{Stand}) of a known concentration (C_{Stand}) and then again diluting the mixture to the final volume (V_F). The two aliquots (i.e. the aliquot containing only the diluted analyte and the aliquot containing the analyte which was doped with a standard) are then analysed and yield responses S_A and S_{Spiked} for the analyte peak, respectively. The relationship between the respective responses and the concentration of analyte may be described by Equations 3.13 and 3.14, respectively.

$$S_A = k \cdot C_A \cdot \frac{V_A}{V_F} \tag{3.13}$$

$$S_{Doped} = k \cdot \left(C_A \cdot \frac{V_A}{V_F} + C_{Stand} \cdot \frac{V_{Stand}}{V_F} \right) \tag{3.14}$$

Equation 3.15 results by the elimination of the proportionality constant k and indicates the relationship between S_A and S_{Spiked}:

$$\frac{S_A}{C_A \cdot \frac{V_A}{V_F}} = \frac{S_{Doped}}{\left(C_A \cdot \frac{V_A}{V_F} + C_{Stand} \cdot \frac{V_{Stand}}{V_F} \right)} \tag{3.15}$$

For a multiple point calibration a series of doped solutions are made which all have the same volume of analyte (V_A) at an unknown concentration (C_A) and varied amounts standard in each doped mixture. The calibration plot may then be constructed by plotting the signal response of the doped mixtures versus a suitable measurement of the amount of standard added i.e. either volume (V_{Stand}) (Figure 3.4a) or concentration (C_{Stand}) (Figure 3.4b). The calibration depicts the relationship shown in Equation 3.14 and thus, if written in the form of a straight-line (Equation 3.16), it can be seen that the concentration of analyte may be determined by calculating the y-intercept or the absolute value of the x-intercept as follows;

$$Y = y\ \text{intercept} + \text{slope} \times X$$

$$S_{Doped} = \frac{k \cdot C_A \cdot V_A}{V_F} + \frac{k \cdot C_{Stand}}{V_F} \times V_{Stand} \tag{3.16}$$

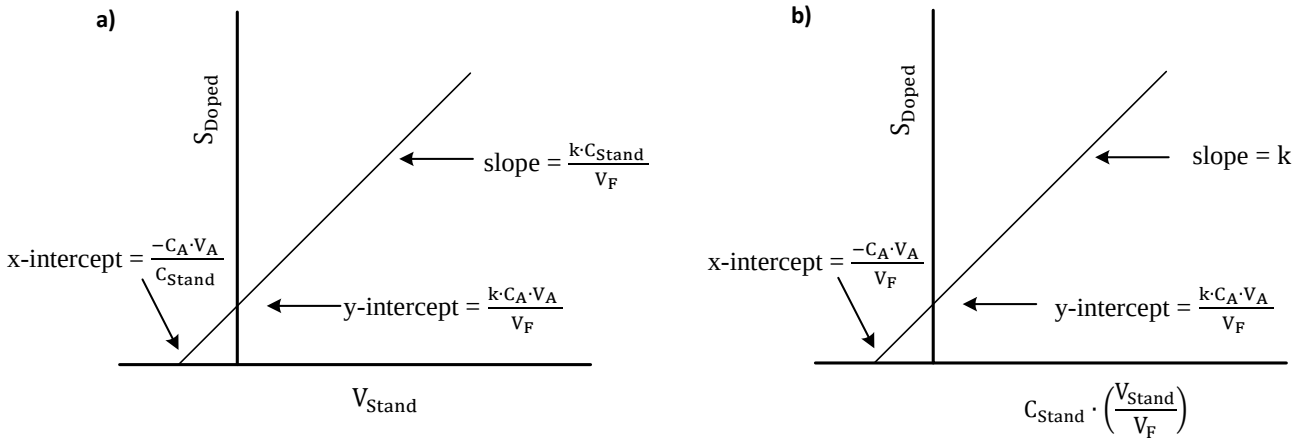

Figure 3.4 : Illustrative examples of a multiple point calibration plot generated for method of standard additions. In **a)** signal response is plotted as a function of volume of standard and in **b)** signal response is plotted as a function of concentration.

3.4.5 Internal standard

Previously mentioned quantification techniques rely on the calibration procedure to be reproducible and precise (i.e. sensitivity to volume of injected samples or final diluted volumes). In situations where the reproducibility of the calibration cannot be guaranteed, the precision of the calibration may be compromised. It is, however, still possible to obtain an accurate standardization by referencing the analyte peak to another species in the injected sample, this species is called the internal standard. This is possible due to the fact that all samples experience the same conditions when injected into the gas chromatograph which negates the effect of any lack in reproducibility of the calibration procedure (Harvey, 2000, McNair and Miller, 2011).

The internal standard chosen needs to meet the following criteria in order to be an effective standard (McNair and Miller, 2011):

- It should elute near the species of interest
- The internal standard peak should be clearly discernible
- It should be chemically similar to the species of interest while ensuring that it is chemically inert with all other species present
- It should be of a high purity

The relationship between the responses observed in a chromatograph and the amount of analyte or internal standard may be seen in Equations 3.17 and 3.18 respectively:

$$S_A = k_A \times M_A \tag{3.17}$$

$$S_{IS} = k_{IS} \times M_{IS} \tag{3.18}$$

Proportionality constants k_A and k_{IS} indicate the sensitivity of the analyte and internal standard to the detector respectively. Taking the ratio of the responses yields Equation 3.19.

$$\frac{S_A}{S_{IS}} = \frac{k_A}{k_{IS}} \times \frac{M_A}{M_{IS}} \tag{3.19}$$

Using the area of the respective peaks to quantify the responses and defining the ratio of the proportionality constants as $K_{A,IS}$ (relative response factor), Equation 3.19 may be expressed as:

$$\frac{A_A}{A_{IS}} = K_{A,IS} \times \frac{M_A}{M_{IS}} \tag{3.20}$$

In order to determine the relative response factor a calibration curve needs to be generated showing the relationship between the analyte and internal standard responses with the detector. This is done by preparing samples with known amounts of internal standard and analyte and observing the ratio between their respective responses on the resulting chromatograph. A calibration plot similar to Figure 3.5 results from the obtained data.

Figure 3.5 shows the relationship described by Equation 3.20, thus the slope of the calibration plot is simply equal to the relative response factor of the analyte and internal standard. The amount of analyte (M_A) in future samples to be analysed may be determined by adding a known mass of internal standard (M_{IS}) to the injected sample then observing the ratio between the respective responses in the chromatograph (Equation 3.21).

$$M_A = \frac{M_{IS}}{K_{A,IS}} \times \frac{A_A}{A_{IS}} \tag{3.21}$$

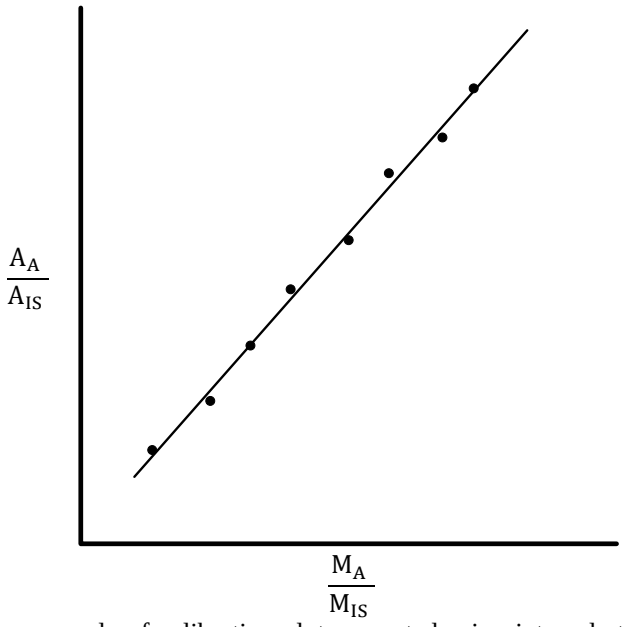

Figure 3.5: Illustrative example of calibration plot generated using internal standard gas chromatography quantification method (McNair and Miller, 2011).

3.5 Calibrations

3.5.1 Rotameter calibration

The rotameters are integral to ensure that the concentration and flow rates are accurately set and controlled throughout the experimental procedure. The rotameters were calibrated using a 50 mL BFM in order to determine the range of possible flow rates and quantify the uncertainty of flow rate measurements.

Rotameter calibrations were conducted for each of the gases in use during experimentation viz., carbon dioxide, nitrogen, hexafluoropropene and hexafluoropropene oxide. Calibrations were conducted by setting rotameter readings and recording the time taken for a bubble to be displaced by 50 mL in the BFM. Subsequently, this allowed the determination of a volumetric flow rate. This procedure was repeated three times to improve the precision and consistency of the calibration. The resultant calibration plots can be found in Appendix A as well as the corresponding uncertainties.

3.6 Analytical techniques

Qualitative analyses of gas and liquid reaction reagents and products were conducted using gas chromatography and mass spectroscopy. Quantitative analyses of products was conducted using gas chromatography which is the most commonly used technique for analysing gas and liquid mixtures (Raal and Mühlbauer, 1998).

All gas chromatography analyses were conducted on a Shimadzu 2010 GC using a Restek® capillary column (30 m × 0.25 mm) coated with in a 0.25μm layer of polyethylene glycol with helium as the carrier gas. Gas chromatography-mass spectroscopy was used for qualitative analysis of product samples and analysed on a Shimadzu QP 2010 Plus Quadropole GCMS which was equipped with a Zebron® capillary column (30 m × 0.25 mm) coated with in a 0.25μm layer of ZB-5MS Phenomenex®.

The temperature program used is integral to the quality and sharpness of the separation achieved in gas chromatograph, the temperature program developed for the analytes started at 30 °C with a hold time of 4 min. A heating rate of 30 $^{o}C \cdot min^{-1}$ was applied until a temperature of 250 °C was reached and then held for a further 5 min, this resulted in a total run time of 16 min. The same temperature program was used for gas chromatography-mass spectroscopy analyses.

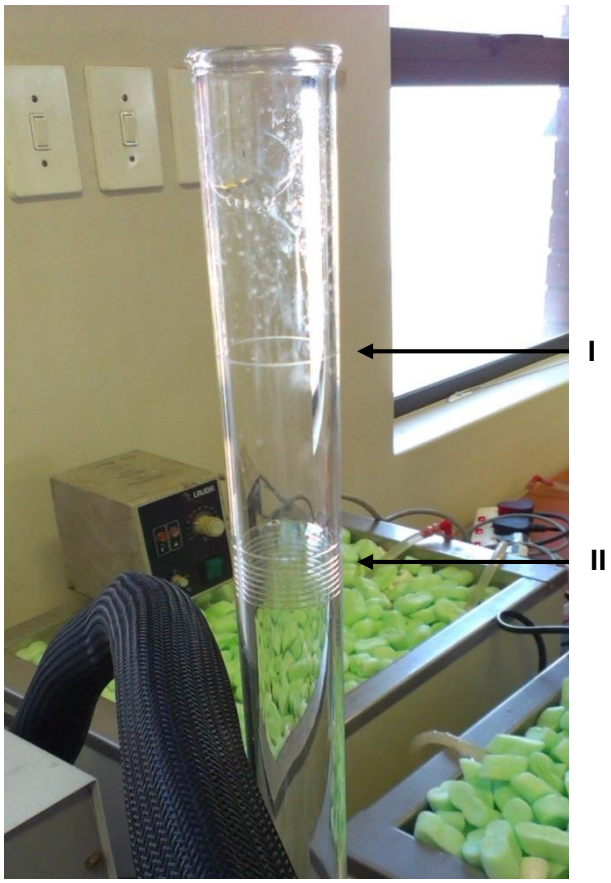

Photograph 3.5: Bubble flow meter used for rotameter calibration. **I** is the 50 mL final volume of the bubble flow meter while **II** indicates the position of the bubble front.

3.6.1 Gas chromatography calibration

There are various techniques that may be adopted to quantify the amount of analyte in a sample. The most precise and reliable means of quantification is the internal standard method (discussed further in Section 3.4.5). As with most standardisation techniques; the precision of the technique is only as good as the calibration used thus an accurate calibration increases the reliability of the results (Raal and Mühlbauer, 1998). The analytes of interest in this study were HME and MTFMP, thus a calibration plot describing the relationship between the internal standard and the analytes were required.

The first step when undertaking an internal standard calibration is to identify a suitable internal standard that satisfy the criteria outlined in Section 3.4.5. Three suitable internal standards were identified which were relatively cheap and easily available, these were acetone, 2-butanol and propanol. Propanol was chosen as the internal standard as it eluted close to the analytes of interest and was well resolved from other peaks in the injected sample. Propanol with an experimentally confirmed purity of 99% was purchased from Merck KGaA.

The calibration procedure involved the preparation of 5 samples each with 1 mL of analyte and an internal standard volume of 0.2, 0.4, 0.6, 0.8 and 1 mL, respectively. The masses of the samples were accurately measured before and after the addition of each of the volumes so that the masses of each addition were known. These samples were then injected into the gas chromatograph with a constant injection volume of 0.5 μL. This procedure was repeated three times to improve the precision and consistency of the calibration.

4

CHAPTER FOUR

4. MODEL DEVELOPMENT

4.1 Model overview

The second principle aim of this study was the development and identification of suitable kinetic models which adequately represent the systems of interest. The model was developed from first principles and programmed in the MATLAB® environment (version R2012b, The MathWorks, Inc.). The MATLAB® script files are provided in Appendix E.

Figure 4.1 shows the algorithm used to identify a suitable kinetic model for the HME system. The algorithm shows three main concentric levels. The outermost level was a constrained optimisation into which a permutation of initial kinetic parameter guesses was passed. The MATLAB® function `lsqnonlin` was used to carry out the constrained optimisation. The second level was a reactor model which was responsible for computing the hydrodynamics and thermophysical properties of the system. The third level integration solver used the MATLAB function `ode15s` to solve the system of ODEs representing the component material balances outlined in Section 4.2. The ODE solver was a variable order solver and used either backward differentiation formulas or numerical differentiation formulas to solve the set of ODEs. The set of ODEs which were solved are the resultant equivalents of the PDEs by the Method-of-Lines numerical methods.

The model was initialized by providing initial guesses for the unknown kinetic parameters to the constrained optimiser. The MATLAB® function `lsqnonlin` is typically used to solve nonlinear data regression problems with the option to impose constraints on the fitting parameters. This solver can solve complex problems using the Levenberg-Marquardt Optimisation algorithm and the Trust-Region-Reflective optimisation algorithm. Each of these algorithms have limitations in that the Levenberg-Marquardt Optimisation algorithm cannot handle bound constraints and the Trust-Region-Reflective optimisation algorithm requires that the number of equations be greater than the number of fitting parameters. It was for this reason that the Trust-Region-Reflective optimisation algorithm was used (Marquardt, 1963, Morini and Porcelli, 2012).

The constrained optimiser then passed the kinetic parameter guesses to a reactor model which was responsible for computing the hydrodynamics and thermophysical properties of the system. These properties were necessary to accurately describe the liquid phase behaviour and reaction progression. One of the principle inputs to the reactor model is the size of the grid space over which the MOL is defined. The grid size is an input to the momentum balance which calculates the stead-state velocity profile in the microchannel of the reactor. The reactions of the system were described in the reaction model which included the relevant material balances that were solved simultaneously with the corresponding boundary conditions.

Overall, the goal of the kinetic model was to obtain kinetic parameters by least squares regression of outlet product concentrations obtained from experiments to model target concentration predictions. The quality of the fit was quantified using the following summed relative-square-error objective function:

$$\mathrm{E} = \sum \left(\frac{\mathrm{C_i^{EXP}} - \mathrm{C_i^{Pred}}}{\mathrm{C_i^{EXP}}} \right)^2 \tag{4.1}$$

Where E is the summed relative-square-error, C_i^{EXP} is the concentration of species i in the product as observed in experiments and C_i^{Pred} is the concentration of species i in the product as predicted by the kinetic model. The final kinetic parameters are chosen based on the permutation which reduced summed relative-square-error to its global minimum.

Figure 4.2 shows the algorithm used to identify a suitable kinetic model for the MTFMP system. The algorithm differs from that of the HME system as it incorporates the use of a three factor circumscribed central composite design in conjunction with response surface methodology, to identify the most optimal permutation of initial kinetic parameter guesses to minimise the model objective function. Surface response methodology allowed for the visual triangulation of the set of input parameters that resulted in the global minimum of the summed relative-square-error. This technique was not practical with the HME system as the HME system had a significantly greater number of fitting parameters (eight versus three for the MTFMP system, this is discussed further in Section 4.4).

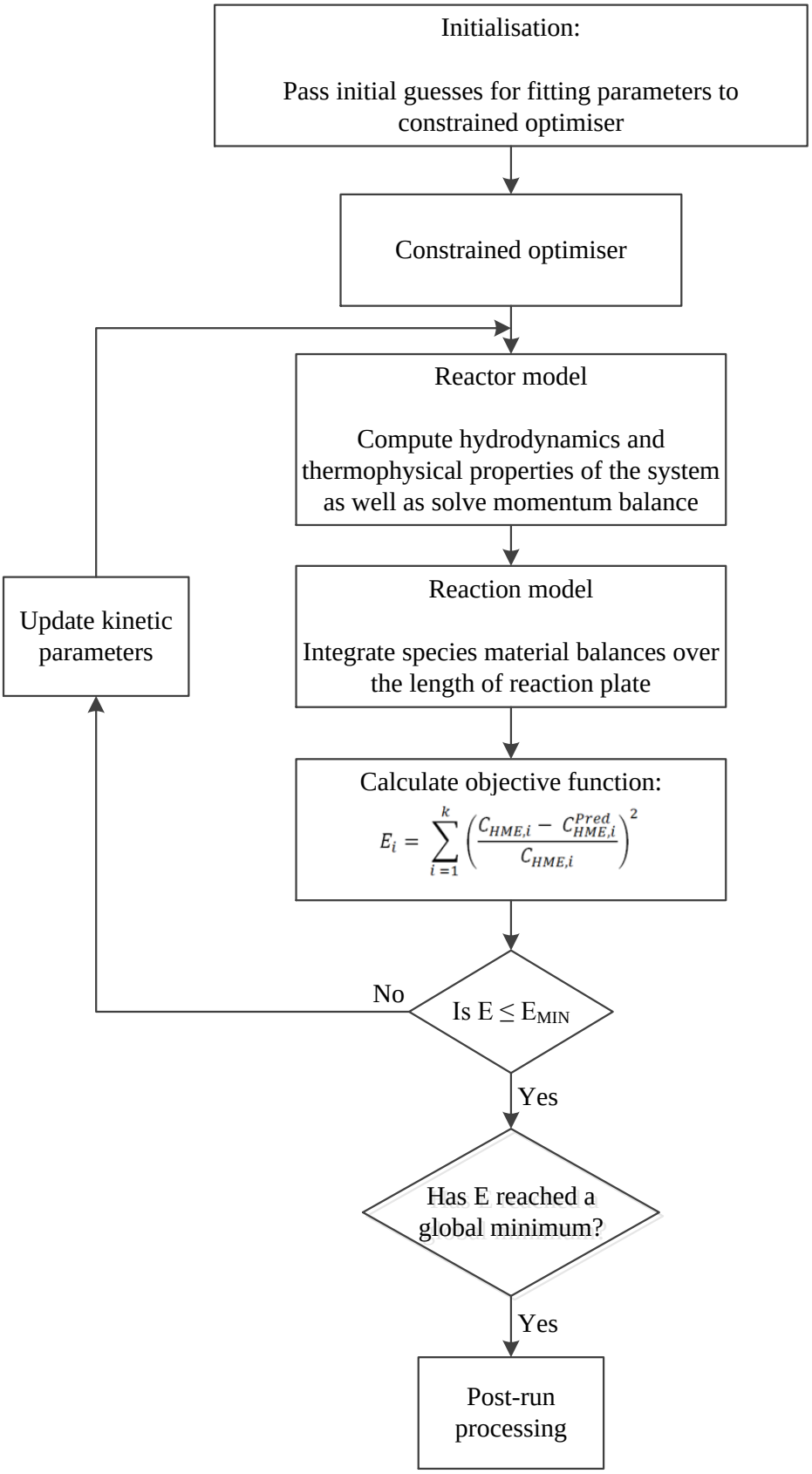

Figure 4.1: A flow diagram of the computational algorithm for kinetic model identification for 1,1,2,3,3,3-hexafluoropropyl methyl ether synthesis.

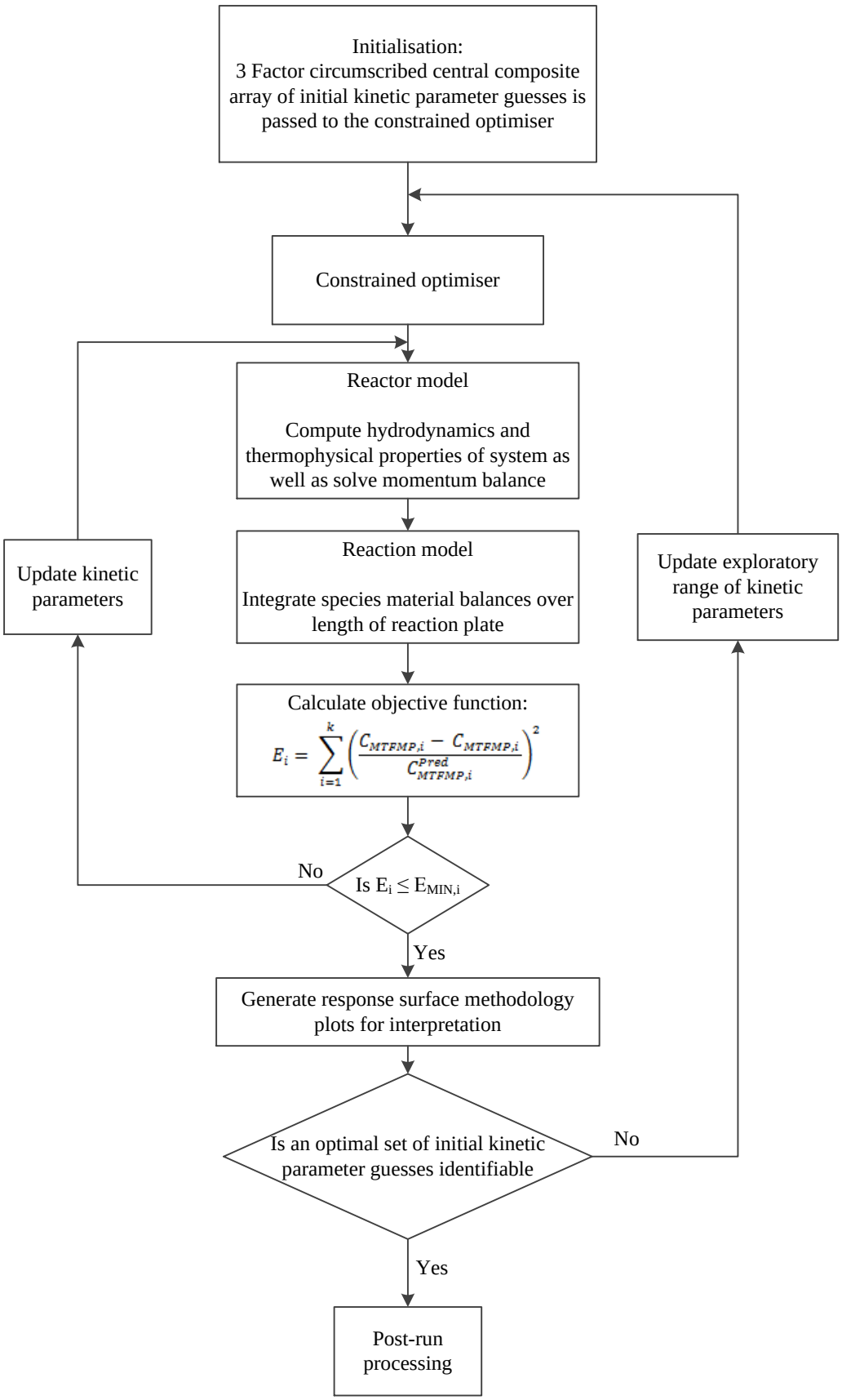

Figure 4.2: A flow diagram of the computational algorithm for kinetic model identification for methyl-2,3,3,3-tetrafluoro-2-methoxypropionate synthesis.

4.2 Reaction model

4.2.1 HME system

The reaction mechanism detailing the synthesis of HME by the contacting of hexafluoropropene gas with methanol and dissolved potassium hydroxide salt is shown in Figure 2.1 (Section 2.2.2). In order to best describe this reaction network in the reaction model the system was described by the following five reaction scheme in Figure 4.3. The following reactions were deduced after careful consideration of the HME reaction mechanism proposed by Il'in et al., 2004:

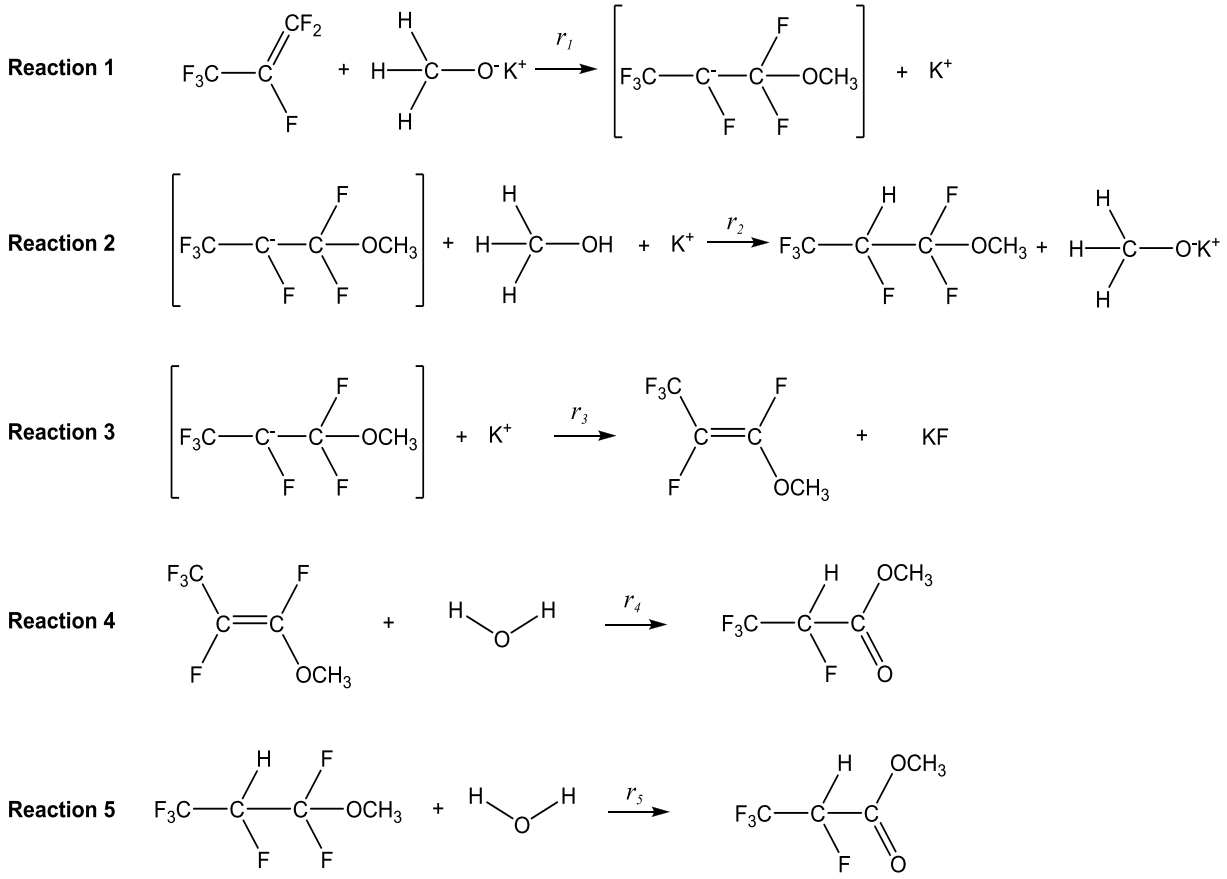

Figure 4.3: The five reaction sequence representing the 1,1,2,3,3,3-hexafluoropropyl methyl ether (HME) reaction mechanism used in the HME reaction model. **Reaction 1**, reaction of hexafluoropropene and potassium methoxide to produce reaction intermediate and a potassium ion. **Reaction 2**, reaction of intermediate and methanol to produce desired product HME and methanol ion. **Reaction 3**, intermediate reacting with free potassium ions to produce 1,2,3,3,3-pentafluoro-1-methoxyprop-1-ene and potassium fluoride (alkenyl ether). **Reaction 4**, reaction of alkenyl ether in the presence of water to produce secondary by-product, methyl 2,3,3,3-tetrafluoropropionate (alkyl tetrafluoropropionate). **Reaction 5**, reaction of HME in the presence of water to produce secondary by-product, alkyl tetrafluoropropionate.

Reaction 1 involves the reaction of hexafluoropropene (HFP) in the liquid phase and potassium methoxide ($CH_3O^-K^+$). The loosely formed oxygen-potassium bond gives way to allow the methoxy anion to attack the sterically unhindered carbon from the carbon-carbon double bond in

the hexafluoropropene molecule. The result is the formation of a reaction intermediate anion ($CF_3C^-FCF_2OCH_3$) and a dissociated potassium cation.

The intermediate then undergoes two transitions; firstly (Reaction 2), addition of the freely available methanol initiates proton transfer to stabilise the secondary carbon of the intermediate resulting in the desired major product (HME) and a methoxy anion. The second transition undergone by the intermediate is shown in Reaction 3. This step incorporates the potassium cation made free in Reaction 1 resulting in the formation of the first of two by-products, an alkenyl ether (1,2,3,3,3-pentafluoro-1-methoxyprop-1-ene).

In the presence of water there are two additional reaction steps; firstly, the alkenyl ether is hydrolysed according to Reaction 4 to obtain the second by-product, an alkyl tetrafluoropropionate (methyl 2,3,3,3-tetrafluoropropionate). Secondly, HME is hydrolysed according to Reaction 5 to also produce methyl 2,3,3,3-tetrafluoropropionate.

The next step to formulating the reaction model, after appropriately representing the reactive system in terms of individual reactions, was defining the reaction rates.

$$r_1 = k_1 C_{HFP,L} C_{CH_3O^-K^+} \tag{4.2}$$

$$r_2 = k_2 C_{CF_3C^-FCF_2OCH_3} \tag{4.3}$$

$$r_3 = k_3 C_{CF_3C^-FCF_2OCH_3} \tag{4.4}$$

$$r_4 = k_4 C_{CF_3CFCFOCH_3} C_{H_2O} \tag{4.5}$$

$$r_5 = k_5 C_{HME} C_{H_2O} \tag{4.6}$$

It is important to note that all reactions were considered to be elementary and irreversible. Equations 4.2 and 4.3 deviate from the elementary narrative of Reaction 2 and 3 (Figure 4.3) as they do not incorporate the concentrations of methanol and potassium into their reaction rate expressions respectively.

The dependence of Equation 4.3 on the concentration of methanol is negated due to the excess of available methanol in the system, the concentration of methanol in the liquid phase was thus assumed to be constant and incorporated into the rate constant k_2. The dependence of Equation

4.4 on the concentration of potassium cations is also negated as potassium is assumed to be freely available in solution.

Representing the concentration of the intermediate at any point in the reactor poses some difficulty due to the pseudo presence of the intermediate being produced and consumed at high rates according to Reactions 1 to 3 (Figure 4.3). The concentration of the intermediate is thus very low but finite, and the net rate of change in concentration is zero. To navigate this problem a commonly adopted approach is use of the quasi steady-state approximation to express the concentration of an active centre, in this instance, the reaction intermediate (Roberts, 2009).

The quasi steady-state approximation estimates the net rate of production or consumption of the active centre to be zero as the net rate of formation and disappearance is approximately equal (Equation 4.). Thus there exists a finite concentration of the intermediate at all times to allow for the formation of HME and methyl 1,2,3,3,3-pentafluoro-1-methoxyprop-1-ene (according to Reactions 2 and 3).

$$R_{\text{Active centre}} = 0 \tag{4.7}$$

Applying the quasi steady-state approximation (Equation 4.7), the concentration of the intermediate may be represented as a function of other components in the system, i.e.:

$$R_{CF_3C^-FCF_2OCH_3} = r_1 - r_2 - r_3 = 0 \tag{4.8}$$

Substituting the definitions for the reaction rates (Equations 4.2 to 4.6) and solving for the concentration of the reaction intermediate, we get:

$$C_{CF_3C^-FCF_2OCH_3} = \frac{k_1 C_{HFP,L} C_{CH_3O^-K^+}}{k_2 + k_3} \tag{4.9}$$

The net rates of production or consumption of species were then defined. The species of concern are HME, HFP in the liquid phase, 1,2,3,3,3-pentafluoro-1-methoxyprop-1-ene (B), methyl 2,3,3,3-tetrafluoropropionate (C), potassium fluoride, potassium methoxide and water.

$$R_{HME} = r_2 - r_5 = k_2 \cdot \frac{k_1 C_{HFP,L} C_{CH_3O^-K^+}}{k_2 + k_3} - k_5 C_{HME} \tag{4.10}$$

$$R_{HFP,L} = -r_1 = -k_1 C_{HFP,L} C_{CH_3O^-K^+} \tag{4.11}$$

$$R_B = r_3 - r_4 = k_3 \cdot \frac{k_1 C_{HFP,L} C_{CH_3O^-K^+}}{k_2 + k_3} - k_4 C_B C_{H_2O} \quad (4.12)$$

$$R_C = r_4 + r_5 = k_4 C_B C_{H_2O} + k_5 C_{HME} C_{H_2O} \quad (4.13)$$

$$R_{KF} = r_3 = k_3 \cdot \frac{k_1 C_{HFP,L} C_{CH_3O^-K^+}}{k_2 + k_3} \quad (4.14)$$

$$R_{CH_3O^-K^+} = -r_3 = -k_3 \cdot \frac{k_1 C_{HFP,L} C_{CH_3O^-K^+}}{k_2 + k_3} \quad (4.15)$$

$$R_{H_2O} = -r_4 - r_5 = -k_4 C_B C_{H_2O} - k_5 C_{HME} C_{H_2O} \quad (4.16)$$

Having fully defined the reactive network for the HME system the appropriate material balances may be constructed according to Equation 2.18. In differential form and considering a variation in only one spatial dimension (i.e. across the length of the reaction plate) for species concentrations in each microchannel, the governing material balances were:

$$\frac{\partial C_{HME}}{\partial t} = -\mathbf{v} D_{HME,l} \frac{\partial C_{HME}}{\partial z} + \left(\frac{\partial^2 C_{HME}}{\partial x^2} + \frac{\partial^2 C_{HME}}{\partial y^2} \right) + k_2 \cdot \frac{k_1 C_{HFP,L} C_{CH_3O^-K^+}}{k_2 + k_3} - k_5 C_{HME} \quad (4.17)$$

$$\frac{\partial C_{HFP,L}}{\partial t} = -\mathbf{v} D_{HFP,l} \frac{\partial C_{HFP,L}}{\partial z} + \left(\frac{\partial^2 C_{HFP,L}}{\partial x^2} + \frac{\partial^2 C_{HFP,L}}{\partial y^2} \right) - k_1 C_{HFP,L} C_{CH_3O^-K^+} \quad (4.18)$$

$$\frac{\partial C_B}{\partial t} = -\mathbf{v} D_{B,l} \frac{dC_B}{dz} + \left(\frac{\partial^2 C_B}{\partial x^2} + \frac{\partial^2 C_B}{\partial y^2} \right) + k_3 \cdot \frac{k_1 C_{HFP,L} C_{CH_3O^-K^+}}{k_2 + k_3} - k_4 C_B C_{H_2O} \quad (4.19)$$

$$\frac{\partial C_C}{\partial t} = -\mathbf{v} D_{C,l} \frac{\partial C_C}{\partial z} + \left(\frac{\partial^2 C_C}{\partial x^2} + \frac{\partial^2 C_C}{\partial y^2} \right) + k_4 C_B C_{H_2O} + k_5 C_{HME} C_{H_2O} \quad (4.20)$$

$$\frac{\partial C_{KF}}{\partial t} = -\mathbf{v} D_{KF,l} \frac{\partial C_{KF}}{\partial z} + \left(\frac{\partial^2 C_{KF}}{\partial x^2} + \frac{\partial^2 C_{KF}}{\partial y^2} \right) + k_3 \cdot \frac{k_1 C_{HFP,L} C_{CH_3O^-K^+}}{k_2 + k_3} \quad (4.21)$$

$$\frac{\partial C_{CH_3O^-K^+}}{\partial t} = -\mathbf{v} D_{CH_3O^-K^+,l} \frac{\partial C_{CH_3O^-K^+}}{\partial z} + \left(\frac{\partial^2 C_{CH_3O^-K^+}}{\partial x^2} + \frac{\partial^2 C_{CH_3O^-K^+}}{\partial y^2} \right) - k_3 \cdot \frac{k_1 C_{HFP,L} C_{CH_3O^-K^+}}{k_2 + k_3} \quad (4.22)$$

$$\frac{\partial C_{H_2O}}{\partial t} = -\mathbf{v} D_{H_2O,l} \frac{\partial C_{H_2O}}{\partial z} + \left(\frac{\partial^2 C_{H_2O}}{\partial x^2} + \frac{\partial^2 C_{H_2O}}{\partial y^2} \right) - k_4 C_B C_{H_2O} - k_5 C_{HME} C_{H_2O} \quad (4.23)$$

4.2.2 MTFMP system

MTFMP was conveniently synthesized by the reaction of hexafluoropropene oxide and potassium methoxide (as outlined in Figure 2.4, Section 2.3.2, Lousenberg and Shoichet, 1997).

The mechanism leading to the production of the desired product was considered to be a two-step reaction sequence as outlined in Figure 4.4 below.

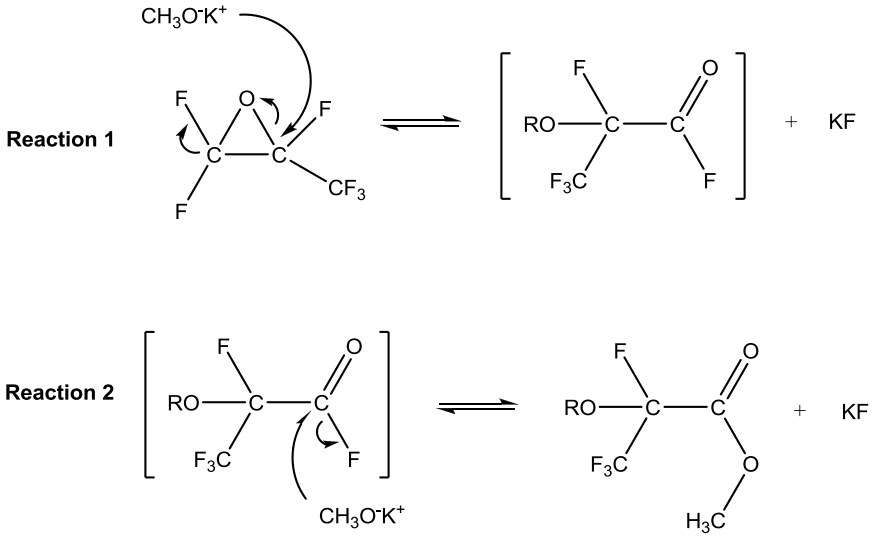

Figure 4.4: Two-step reaction sequence representing methyl-2,3,3,3-tetrafluoro-2-methoxypropionate (MTFMP) reaction mechanism used in MTFMP reaction model. **Reaction 1**, addition of methoxide anion to hexafluoropropene oxide to form an acid fluoride intermediate and potassium fluoride. **Reaction 2**, defluoronation of acid fluoride intermediate to produce desired product, MTFMP and potassium fluoride.

Reaction 1, illustrates the addition of a methoxide anion to the secondary carbon of hexafluoropropene oxide (HFPO). This addition forces ring opening at the central carbon due to the presence of the trifluoromethyl group (CF_3) drawing in electrons. Elimination of a peripheral fluoride yields an acid fluoride intermediate ($COFCFCF_3OCH_3$) and potassium fluoride.

Reaction 2, is initiated by the addition of another methoxide anion to the acid fluoride intermediate which emits a fluoride from the intermediate to obtain the desired major product, MTFMP and potassium fluoride (Lousenberg and Shoichet, 1997).

Following the methodology outlined for formulating the HME reaction model, the next step is definition of the reaction rates.

$$r_1 = k_1 C_{HFPO,L} C_{CH_3O^-K^+} \tag{4.24}$$

$$r_2 = k_2 C_{COFCFCF_3OCH_3} C_{CH_3O^-K^+} \quad (4.25)$$

Reactions 1 and 2 were considered to be irreversible. The quasi steady-state approximation may again be applied according to Equation 4.7 to the reaction intermediate (acid fluoride). Calculating the net rate of production or consumption of acid fluoride and equating to zero. The following equation is obtained:

$$R_{COFCFCF_3OCH_3} = r_1 - r_2 = 0 \quad (4.26)$$

Substituting the definitions for the reaction rates (Equations 4.24 and 4.25) and solving for the concentration of the reaction intermediate, the following equation results:

$$C_{COFCFCF_3OCH_3} = \frac{k_1 C_{HFPO,L}}{k_2} \quad (4.27)$$

Combining Equations 4.26 and 4.27:

$$r_2 = k_2 C_{HFPO,L} C_{CH_3O^-K^+} \quad (4.28)$$

Which is exactly equal to r_1, thus the rate of Reaction 1 is identical to Reaction 2. The net rates of production or consumption may now be defined for the species of interest. For the MTFMP system these were potassium methoxide, hexafluoropropene oxide, potassium fluoride and MTFMP.

$$R_{CH_3O^-K^+} = -r_1 - r_2 = -2 \cdot r_1 = -2 \cdot k_1 C_{HFPO,L} C_{CH_3O^-K^+} \quad (4.29)$$

$$R_{HFPO,L} = -r_1 = -k_1 C_{HFPO,L} C_{CH_3O^-K^+} \quad (4.30)$$

$$R_{KF} = r_1 + r_2 = 2 \cdot r_1 = 2 \cdot k_1 C_{HFPO,L} C_{CH_3O^-K^+} \quad (4.31)$$

$$R_{MTFMP} = r_2 = r_1 = k_1 C_{HFPO,L} C_{CH_3O^-K^+} \quad (4.32)$$

The system of equations was now fully defined and was used to draw up suitable material balances according to Equation 2.18. In differential form and considering a 1-dimensional variation (i.e. across the length of the reaction plate) of species' concentrations in each microchannel, the governing material balances were:

$$\frac{\partial C_{CH_3O^-K^+}}{\partial t} = -\mathbf{v}D_{CH_3O^-K^+,l}\frac{\partial C_{CH_3O^-K^+}}{\partial z} + \left(\frac{\partial^2 C_{CH_3O^-K^+}}{\partial x^2} + \frac{\partial^2 C_{CH_3O^-K^+}}{\partial y^2}\right) - 2 \cdot k_1 C_{HFPO,L} C_{CH_3O^-K^+} \quad (4.33)$$

$$\frac{\partial C_{HFPO,L}}{\partial t} = -\mathbf{v}D_{HFPO,l}\frac{\partial C_{HFPO,L}}{\partial z} + \left(\frac{\partial^2 C_{HFPO,L}}{\partial x^2} + \frac{\partial^2 C_{HFPO,L}}{\partial y^2}\right) - k_1 C_{HFPO,L} C_{CH_3O^-K^+} \quad (4.34)$$

$$\frac{\partial C_{KF}}{\partial t} = -\mathbf{v}D_{KF,l}\frac{\partial C_{KF}}{\partial z} + \left(\frac{\partial^2 C_{KF}}{\partial x^2} + \frac{\partial^2 C_{KF}}{\partial y^2}\right) + 2 \cdot k_1 C_{HFPO,L} C_{CH_3O^-K^+} \quad (4.35)$$

$$\frac{\partial C_{MTFMP}}{\partial t} = -\mathbf{v}D_{MTFMP,l}\frac{\partial C_{MTFMP}}{\partial z} + \left(\frac{\partial^2 C_{MTFMP}}{\partial x^2} + \frac{\partial^2 C_{MTFMP}}{\partial y^2}\right) + k_1 C_{HFPO,L} C_{CH_3O^-K^+} \quad (4.36)$$

4.3 Initial and Boundary conditions

As mentioned in Section 2.8.3 the simulations in this study are of the pseudo initial value 3-D nature, they thus need both initial and boundary conditions. From Section 4.2 it can be seen that one initial condition and five boundary conditions are required for each material balance.

4.3.1 HME system

A. Initial conditions

At time zero the only species present in the fully wetted microchannel was potassium methoxide ions and water equal to the concentration of the catalyst in the inlet feedstock, all other species were defined as zero. This is due to the equal amount of water created from the dissolution of potassium hydroxide in the feed methanol.

B. Boundary conditions

Material balances are second order in terms of the *x* component which dictates that 2 boundary conditions are required per species. The commonly used no-slip condition was employed which dictates that fluid in contact with the channels walls are immobile and thus there is no concentration gradient at *x* boundaries (Al-Rawashdeh et al., 2008, Schiesser and Griffiths, 2009).

Similarly, all material balances are second order in the *y* direction which also requires 2 boundary conditions. The no-slip condition was again applied to the fluid in contact with the base of the reactor channel. For dissolved HFP in the liquid phase however, the concentration at the boundary in contact with the gaseous phase was assumed to have a concentration equal to the saturated concentration of HFP in methanol. For the other species it was assumed that the concentration gradient at the interface was zero as per similar studies by Zanfir, et al. (2005).

Finally, in the *z* direction all species except potassium methoxide were assumed to have zero concentration at the top of the microchannel. Potassium methoxide concentration at the top of the microchannel is equal to that of the feedstock.

4.3.2 MTFMP system

A. Initial Conditions

At time zero the only species present in the fully wetted microchannel was potassium methoxide ions equal to the concentration of the catalyst in the inlet feedstock, all other species were defined as zero.

B. Boundary Conditions

As with the HME system a condition of no-slip was applied at the channel walls in the *x* direction which meant that the concentration gradient was zero for all species. Similarly, for the *y* direction a condition of no-slip was enforced at the boundary at the bottom of the reactor channel. At the upper *y* boundary no concentration gradient was assumed except for hexafluoropropene oxide which was assumed to have a concentration equal to the saturated concentration of hexafluoropropene oxide in methanol.

Finally, in the *z* direction all species except potassium methoxide were assumed to have zero concentration at the top of the microchannel. Potassium methoxide concentration at the top of the microchannel is equal to that of the feedstock as with the HME system.

4.4 Variables of interest

The objective of the kinetic model was to identify suitable kinetic parameters to adequately describe the behaviour of the reactive systems; this was achieved through least squares non-linear regression. The previously unknown kinetic parameters (or fitting parameters) were obtained by minimisation of the objective function seen in Equation 4.1.

4.4.1 HME system

The HME system incorporates five reactions (Figure 4.3, Section 4.3.1), all with unknown kinetic rate constants and activation energies. The number of fitting parameters were thus eleven (a kinetic rate constant k_i, an activation energy $E_{A,i}$ for each of the five reactions and a Sechenov coefficient).

Determination of kinetic parameters such as rate constants and activation energies often cause problems in parameter estimation studies due to the large difference in magnitudes between the two variables as well as their strong non-linear relationship. A commonly adopted means of alleviating this problem is to apply a simple internal scaling technique known as *temperature centreing*. In this method the reaction rate expression is re-parameterised around some reference temperature T_0 (Wojciechowski and Rice, 2003). The Arrhenius form of the rate expression is rewritten as:

$$\mathrm{k_i} = \mathrm{k_{i,0}}\ \exp\left(-\frac{\mathrm{E_{A,i}}}{\mathrm{R}}\left(\frac{1}{\mathrm{T}} - \frac{1}{\mathrm{T_0}}\right)\right) \tag{4.37}$$

Where

$$\mathrm{k_{i,0}} = \mathrm{A_i}\ \exp\left(-\frac{\mathrm{E_{A,i}}}{\mathrm{R\,T_0}}\right) \tag{4.38}$$

In Equation 4.38 $k_{i,0}$ is the reference kinetic rate constant evaluated at temperature T_0 and A_i is the pre-exponential factor of reaction i. The parameters which were thus regressed for were the activation energy and rate constant at the reference temperature ($k_{i,0}$). In order to reduce the number of fitting parameters an assumption was made to equate the rate of hydrolysis of HME and methyl 1,2,3,3,3-pentafluoro-1-methoxyprop-1-ene, thus Reactions 4 and 5 (Figure 4.3, Section 4.3.1) have equivalent kinetic rate constants and activation energies. This assumption was based on the fact that the structurally similar reagents both undergo hydrolysis by nucleophilic attack on the tertiary carbon of HME and methyl 1,2,3,3,3-pentafluoro-1-methoxyprop-1-ene.

Additionally, the Sechenov coefficient was found to have little effect on the solubility of hexafluoropropene oxide and was thus omitted from the computational algorithm. The number of fitting parameters was then reduced to eight from the original eleven.

4.4.2 MTFMP system

The MTFMP system is less complex, incorporating just two reactions (Figure 4.4, Section 4.3.2) with unknown kinetic constants and activation energies. Use of the quasi steady-state approximation resulted in the rate of Reaction 2 being equivalent to that of Reaction 1 (Figure 4.4, Section 4.3.2). Thus the number of fitting parameters for the MTFMP system was three (a rate constant at the reference temperature $k_{i,0}$, an activation energy $E_{A,i}$ for Reaction 1 and a Sechenov coefficient).

5

CHAPTER FIVE

5. RESULTS AND DISCUSSION

5.1 Preliminary investigations: Semi-batch gas-liquid stirred tank reactor

The principle aim of the preliminary investigations was to validate the reaction system presented in literature; this was carried out by contacting gaseous hexafluoropropene with methanol in the presence of potassium hydroxide using a 2 L semi-batch gas-liquid stirred tank reactor. The secondary aim was to ascertain whether HME could be successfully synthesized in the falling film microreactor. These investigations also provided a basis for the selection of an appropriate operating envelope for the experiments conducted using the FFMR.

The equipment was successfully commissioned with calibrations conducted on the precision gas rotameters and reactor PT100 temperature probe. These calibrations are presented in Appendix A. Samples obtained from the experiments were analysed using the internal standard method on a gas chromatograph. An integral aspect of the internal standard quantification method was the development of a reliable and precise calibration plot indicating the relationship between the mass and area ratios of HME and the internal standard. *n*-Propanol was confirmed as a suitable internal standard and was used to carry out quantitative analysis on all product samples. The calibration plot generated is shown in Figure B.1 (Appendix B) and resulted in a response factor of 3.1208 (with an average absolute relative deviation percentage of 2.83 %), the calibration equation used to quantify product samples was thus:

$$\frac{M_{Unknown}}{M_{IS}} = 3.1208 \times \frac{A_{Unknown}}{A_{IS}} \tag{5.1}$$

Il'in et al. (2004) indicated that the reaction system is likely to produce two additional products, the presence of these additional species was seen in the product chromatograms and their presence confirmed by gas chromatography-mass spectroscopy. In order to quantify these species, they were assumed to interact with the gas chromatograph detector in the same way that HME does. Thus they were assigned the same relative response factor as that of HME, which was then used

to quantify the amounts of the alkenyl ether and the alkyl tetrafluoropropionate. This assumption was based on the structural similarity between HME and the by-products and was used to infer the concentrations of by-products qualitatively rather than quantitatively.

Table 5.1 shows the results of preliminary investigations as dictated by a three factor circumscribed central composite experimental design. HME was successfully identified and synthesised with an experimental yield which ranged from 19.21 to 53.32% with respect to hexafluoropropene gas introduced into the system. The yields of the by-products were also quantified and the yield of alkenyl ether was found to vary between 0.07 and 1.03% while alkyl tetrafluoropropionate varied from 2.42 to 5.10%. The repeatability of the experimental apparatus was evaluated by the centrepoint experiments and these results show a standard deviation of 7.50% yield in HME, which is significantly high and is mainly due to the transient nature of the reactor as well as the difficulty of maintaining uniform bubbling from the gas sparger. Bubble size and bubble intensity from the gas sparger were noted to vary during each run thus reducing or elevating the availability of hexafluoropropene in the liquid phase for reaction, in turn contributing to the variability of the HME yield.

The investigation also revealed that the system was highly exothermic, the reaction rate was fast and produced negligible amounts of solid. The latter of these findings was the most significant as it deems the FFMR a suitable apparatus in which to carry out the reaction in a continuous mode. The presence of a significant amount of precipitate would have blocked reactor channels thus disturbing the liquid film and reducing the effective interfacial area for gas-liquid mass transfer.

Upon analysis of the effect of the reaction conditions on the yield of HME it was found that the yield was favoured at higher reaction temperatures, high hexafluoropropene concentrations and low to moderate potassium hydroxide concentrations. The increased yield at lower reaction temperatures may be due to the favourable equilibrium position of the reaction as well as, possibly, lower activation energy of the desired reaction (Figure 2.4 – Reaction products **II**) as opposed to that of the undesired reactions (Figure 2.4 – Reaction products **III** and **IV**). Higher concentrations of hexafluoropropene allowed for more of the limiting reactant available for conversion to the desired product. The greater yields of HME observed at lower concentrations of potassium hydroxide (a catalyst to the reaction) initially seemed counter intuitive, but the reason for this behavioural trend can be explained by a phenomenon known as *salting-out*. The salting-out effect is when the solubility of a gas in a liquid is decreased by the presence of a salt in the liquid phase (Tiepel and Gubbins, 1973), thus the greater the concentration of potassium hydroxide in methanol, the lower the driving force for mass transfer of hexafluoropropene into the liquid phase and hence the lower the reaction rate.

Table 5.1: Results of experiments conducted on semi-batch gas-liquid stirred tank reactor during preliminary investigations for the synthesis of 1,1,2,3,3,3-hexafluoropropyl methyl ether.

Exp. No.	Hexafluoropropene mole fraction[a]	KOH concentration, $mol \cdot L^{-1}$	Temperature, °C	Moles of hexafluoropropyl methyl ether produced	Product yield[b], %		
					Hexafluoropropyl methyl ether	Alkenyl ether	Alkyl tetrafluoropropionate
1	0.74	0.71	25.0	0.799 ± 0.0044	49.76 ± 1.60	0.59 ± 0.43	3.19 ± 0.27
2	0.74	0.71	15.0	0.849 ± 0.0040	53.32 ± 1.69	0.23 ± 0.96	3.24 ± 0.78
3	0.74	0.48	25.0	0.658 ± 0.0023	40.58 ± 1.30	0.07 ± 1.71	3.64 ± 0.23
4	0.74	0.48	15.0	0.786 ± 0.0025	48.78 ± 1.56	0.07 ± 1.93	4.15 ± 0.49
5	0.49	0.71	25.0	0.312 ± 0.0023	29.46 ± 1.41	1.03 ± 0.13	3.23 ± 0.33
6	0.49	0.71	15.0	0.360 ± 0.0023	33.62 ± 1.62	0.59 ± 0.23	2.63 ± 0.59
7	0.49	0.48	25.0	0.441 ± 0.0025	41.00 ± 1.98	0.16 ± 0.86	3.53 ± 0.53
8	0.49	0.48	15.0	0.492 ± 0.0024	46.08 ± 2.20	0.13 ± 1.03	4.29 ± 0.15
9	0.41	0.60	20.0	0.302 ± 0.0023	35.02 ± 1.98	0.69 ± 0.19	3.10 ± 0.37
10	0.83	0.60	20.0	0.727 ± 0.0025	41.07 ± 1.16	0.18 ± 0.75	3.64 ± 0.64
11	0.62	0.40	20.0	0.604 ± 0.0022	45.50 ± 1.73	0.03 ± 0.43	3.76 ± 0.19
12	0.62	0.80	20.0	0.367 ± 0.0022	26.99 ± 1.06	0.13 ± 0.92	2.42 ± 0.38
13	0.62	0.60	12.0	0.526 ± 0.0021	39.80 ± 1.51	0.08 ± 1.43	3.21 ± 0.29
14	0.62	0.60	28.0	0.482 ± 0.0024	36.48 ± 1.38	0.24 ± 0.56	3.37 ± 0.63
15	0.62	0.60	20.0	0.560 ± 0.0025	41.68 ± 1.61	0.17 ± 0.80	3.93 ± 0.16
16	0.62	0.60	20.0	0.440 ± 0.0025	32.64 ± 1.27	0.07 ± 1.84	2.72 ± 0.37
17	0.62	0.60	20.0	0.393 ± 0.0025	28.11 ± 1.14	0.27 ± 0.54	2.77 ± 0.31
18	0.62	0.60	20.0	0.255 ± 0.0019	19.21 ± 0.74	0.69 ± 0.29	3.83 ± 0.57
19	0.62	0.60	20.0	0.440 ± 0.0024	33.11 ± 1.26	0.22 ± 1.07	5.10 ± 0.32
20	0.62	0.60	20.0	0.332 ± 0.0017	24.95 ± 0.95	0.44 ± 1.29	4.63 ± 0.23

[a] Hexafluoropropene diluted with inert nitrogen gas.
[b] Yield of products are defined as mole of product divided by moles of hexafluoropropene introduced into the reactor over duration of reaction.

The suitability of the reaction system for a FFMR was a crucial finding as Rendall et al. (1958) and Il'in et al. (2004) suggested synthesizing HME in a semi-batch process, whereas using a FFMR allows for continuous production of HME. Continuous processes offer various advantages over batch processes, such as being safer, production at constant quality, easier to operate and generally more amenable scale-up.

5.2 Falling film microreactor equipment validation

Validation studies on the FFMR were carried out by observing the absorption of carbon dioxide into sodium hydroxide. Sodium hydroxide was passed through the reactor at flow rates of 3, 4 and 5 mL·min^{-1} and a carbon dioxide at flow rates of 50 and 80 mL·min^{-1}. Figure 5.1 shows the results of the experiments as well as comparison with literature data produced by Zhang et al., (2009).

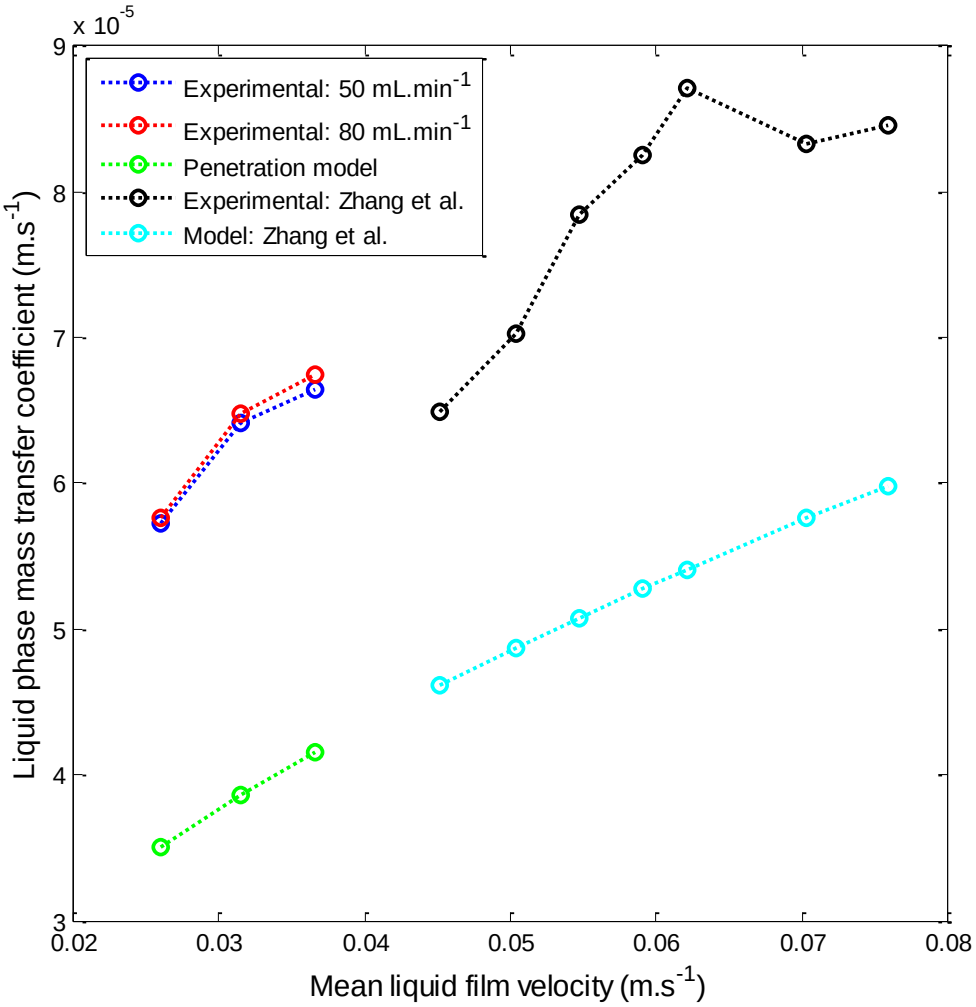

Figure 5.1: Results of validation studies as well as literature results by Zhang et al., (2009) observing the absorption of carbon dioxide into sodium hydroxide solution using a falling film microreactor with a 32 channel 300 × 600 μm reaction plate.

From Figure 5.1 it can be seen that the experimentally determined mass transfer coefficient was found to be up to three time greater than that predicted by the penetration model as well as the experimental and model results presented by Zhang et al., (2009). Exact mean liquid fluid velocities could not be replicated in this study due to practical limitations on the reactor as well as the HPLC Series II feed pump. The enhanced mass transfer observed may be due to an increase in the specific interfacial areas of the installed apparatus which result from the formation of ripples on the surface of each microchannel.

The greater mass transfer coefficients observed in the experimental set-up do not hinder mass transfer and in fact improve the yields of reactions. Thus the equipment was deemed to operate satisfactorily and ready to conduct experiments.

5.3 Falling film microreactor experiments

5.3.1 HME system

A. Steady-state investigation

In order to allow comparison of the results from the semi-batch gas-liquid stirred tank reactor and the FFMR it was decided to carry out the experiment for a period of 30 min for the FFMR, the FFMR would thus operate for 30 min at steady-state conditions. The first step to conducting experiments on the FFMR was to thus determine how long the process required before attaining steady-state conditions.

For FFMRs, the time to reach steady-state conditions is usually longer than the residence time of the liquid within the vessel (Smith et al., 2001). The exact time at which steady-state conditions are achieved differ based on the reaction conditions, reactor geometry as well as the flow regime within the microchannels, and since the production of HME using a FFMR has not been attempted before, the time at which steady-state is achieved was unknown. A single experiment was thus conducted with samples taken periodically (every 3 min over 21 min) in order to observe how the yield of HME varied with time. Observing the transient behaviour of the reactor allowed for the determination of the point at which the product stream attained a uniform concentration of HME. Figure 5.2 shows the results of the steady-state test. Note that the dashed line does not indicate a model prediction of the percentage yield of HME but was instead used to illustrate the trend of the experimental data.

The experimental conditions for the steady-state test were a reaction temperature of 17.0 °C, a potassium hydroxide concentration of 0.52 mol·L^{-1}, a hexafluoropropene mole fraction of 0.34

and a liquid volumetric flow rate of 1.75 mL·min^{-1}. The calibration plots for the rotameters of the FFMR experimental set-up are provided in Appendix A. From the results of these experiments a lead time of 5 min was appropriated at the start of each experiment in order to ensure that the reactor reached steady-state conditions.

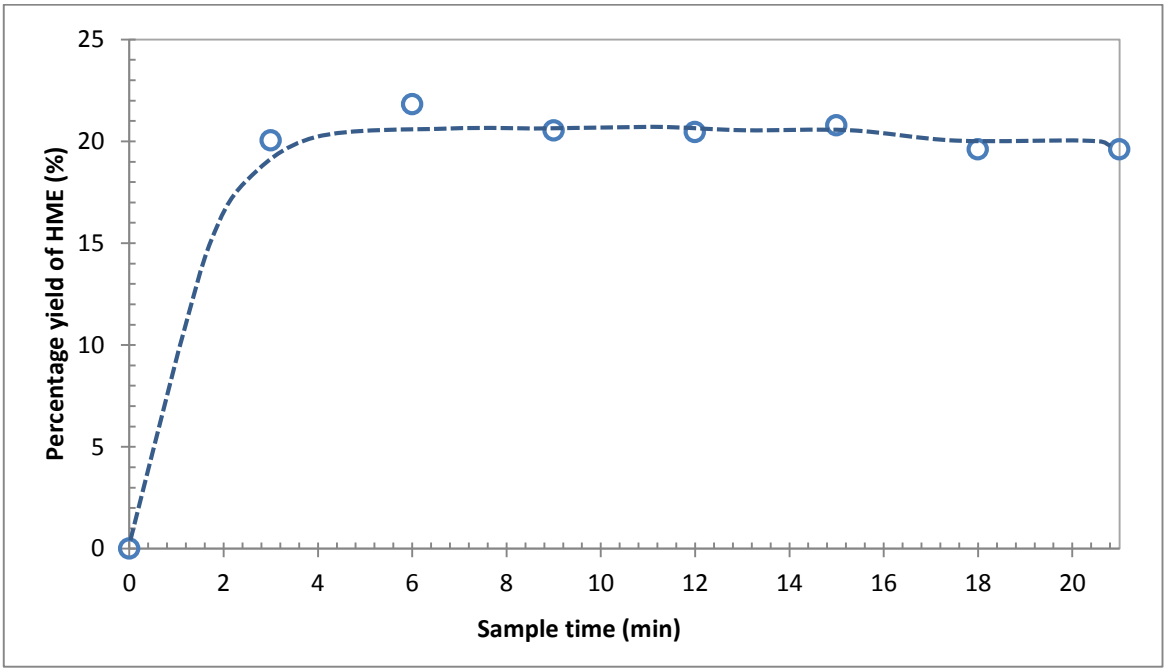

Figure 5.2: Results of transient experiments used to determine point at which steady-state conditions are observed for the 1,1,2,3,3,3-hexafluoropropyl methyl ether system. Experiment was conducted at a reaction temperature of 17 °C, a potassium hydroxide concentration of 0.52 mol·L^{-1}, a hexafluoropropene mole fraction of 0.34 and a liquid volumetric flow rate of 1.75 mL·min^{-1}. Dashed line indicates trend of experimental data.

B. Central composite design investigations

Once the appropriate stabilisation period for the FFMR was identified, experiments were conducted according to the experimental design shown in Table 3.1 (Section 3.1.3). Operation of the FFMR was noticeably simpler than that of the glass reactor as the system required less handling of material as well as was easier to clean and prepare for consecutive experiments. As confirmed by preliminary investigations, negligible salt formation meant that there was no blocking of the reactor microchannels during all experimental runs.

Table 5.2 shows the results of experiments conducted on the FFMR for the HME system. HME was successfully synthesized using the reactor and was noted to appear in the reactor product at yields between 11.60 and 71.47%. The presence of the by-products was also identified in the reactor product at yields between 0.11 and 6.99% for the alkenyl ether and 0.75 and 6.24% for the alkyl tetrafluoropropionate. The repeatability of the experimental equipment was assessed by

repeating the centrepoint experiments 6 times, the centrepoints were found to have a standard deviation of 3.04% with respect to the yield of HME. This was found to be satisfactory and indicated improved repeatability as compared with the glass reactor experiments.

Results show that greater yields were observed on the FFMR when compared with the glass reactor which was as expected. The results also show that greater yields were obtained at high mole fractions of hexafluoropropene in the feed reactant gas and lower concentrations of potassium hydroxide in the liquid feed. The greatest yields were also achievable at high liquid flow rates due to the fast rate of reaction in the reactor.

Table 5.2: Results of experiments conducted on a falling film microreactor for the 1,1,2,3,3,3-hexafluoropropyl methyl ether system.

Exp. No.	Hexafluoropropene mole fraction	KOH concentration, $mol \cdot L^{-1}$	Temperature, °C	Liquid flow rate $mL \cdot min^{-1}$	Moles of hexafluoropropyl methyl ether produced[a]	Product yield, %		
						Hexafluoropropyl methyl ether	Alkenyl ether	Alkyl tetrafluoropropionate
1	0.34	0.34	7.0	1.75	$0.126 \pm 7.74\times10^{-5}$	11.60 ± 0.30	0.32 ± 0.25	1.10 ± 0.27
2	0.34	0.34	7.0	4.27	$0.216 \pm 2.49\times10^{-4}$	48.32 ± 1.05	3.91 ± 0.76	4.22 ± 0.77
3	0.70	0.34	7.0	1.75	$0.858 \pm 1.33\times10^{-4}$	38.88 ± 0.36	2.15 ± 0.20	4.00 ± 0.20
4	0.70	0.34	7.0	4.27	$0.518 \pm 3.16\times10^{-4}$	56.93 ± 0.62	6.99 ± 0.46	5.06 ± 0.47
5	0.34	0.52	7.0	1.75	$0.359 \pm 9.70\times10^{-5}$	33.12 ± 0.61	2.21 ± 0.28	3.59 ± 0.29
6	0.34	0.52	7.0	4.27	$0.178 \pm 1.81\times10^{-4}$	39.78 ± 0.82	2.82 ± 0.55	3.26 ± 0.57
7	0.70	0.52	7.0	1.75	$0.621 \pm 1.62\times10^{-4}$	42.21 ± 0.71	0.11 ± 0.23	3.70 ± 0.25
8	0.70	0.52	7.0	4.27	$0.433 \pm 8.76\times10^{-5}$	71.47 ± 0.22	0.65 ± 0.12	6.24 ± 0.13
9	0.34	0.34	17.0	1.75	$0.465 \pm 1.00\times10^{-4}$	42.94 ± 0.77	3.58 ± 0.31	3.47 ± 0.31
10	0.34	0.34	17.0	4.27	$0.222 \pm 2.04\times10^{-4}$	49.85 ± 1.00	1.48 ± 0.63	3.79 ± 0.63
11	0.70	0.34	17.0	1.75	$0.892 \pm 8.39\times10^{-5}$	40.38 ± 0.35	3.01 ± 0.12	3.78 ± 0.13
12	0.70	0.34	17.0	4.27	$0.476 \pm 2.22\times10^{-4}$	52.36 ± 0.52	1.60 ± 0.33	4.58 ± 0.34
13	0.34	0.52	17.0	1.75	$0.324 \pm 8.53\times10^{-5}$	29.90 ± 0.55	1.04 ± 0.25	2.95 ± 0.27
14	0.34	0.52	17.0	4.27	$0.167 \pm 2.08\times10^{-4}$	37.48 ± 0.84	1.73 ± 0.61	3.64 ± 0.62
15	0.70	0.52	17.0	1.75	$0.826 \pm 7.56\times10^{-5}$	37.41 ± 0.32	2.44 ± 0.11	3.18 ± 0.11
16	0.70	0.52	17.0	4.27	$0.426 \pm 2.26\times10^{-4}$	46.88 ± 0.49	2.91 ± 0.33	3.92 ± 0.34
17	0.52	0.43	2.0	3.00	$0.591 \pm 1.20\times10^{-4}$	61.53 ± 0.71	5.10 ± 0.24	5.12 ± 0.25
18	0.52	0.43	22.0	3.00	$0.497 \pm 2.77\times10^{-4}$	51.76 ± 0.75	3.28 ± 0.55	3.76 ± 0.56
19	0.52	0.25	12.0	3.00	$0.512 \pm 1.41\times10^{-4}$	53.30 ± 0.64	5.39 ± 0.27	4.52 ± 0.27
20	0.52	0.61	12.0	3.00	$0.429 \pm 9.43\times10^{-5}$	44.73 ± 0.52	2.58 ± 0.18	3.74 ± 0.18
21	0.17	0.43	12.0	3.00	$0.106 \pm 1.45\times10^{-4}$	34.91 ± 1.48	1.88 ± 1.00	3.26 ± 1.00
22	0.88	0.43	12.0	3.00	$0.997 \pm 1.18\times10^{-4}$	61.67 ± 0.42	5.39 ± 0.14	5.51 ± 0.14
23	0.52	0.43	12.0	0.50	$1.639 \pm 2.20\times10^{-5}$	28.45 ± 0.32	2.84 ± 0.05	0.75 ± 0.04
24	0.52	0.43	12.0	5.50	$0.289 \pm 2.39\times10^{-4}$	55.13 ± 0.74	1.87 ± 0.46	4.30 ± 0.46
25	0.52	0.43	12.0	3.00	$0.499 \pm 1.11\times10^{-4}$	51.98 ± 0.61	3.37 ± 0.21	4.68 ± 0.22
26	0.52	0.43	12.0	3.00	$0.355 \pm 4.80\times10^{-5}$	55.40 ± 0.63	0.44 ± 0.18	4.70 ± 0.19
27	0.52	0.43	12.0	3.00	$0.571 \pm 1.41\times10^{-4}$	59.44 ± 0.70	5.12 ± 0.28	4.98 ± 0.29
28	0.52	0.43	12.0	3.00	$0.514 \pm 1.07\times10^{-4}$	53.55 ± 0.62	3.30 ± 0.21	4.63 ± 0.21
29	0.52	0.43	12.0	3.00	$0.653 \pm 1.77\times10^{-4}$	55.13 ± 0.66	2.74 ± 0.28	5.95 ± 0.35
30	0.52	0.43	12.0	3.00	$0.570 \pm 9.71\times10^{-5}$	59.36 ± 0.68	3.80 ± 0.19	5.04 ± 0.20

[a] Based on processing 1.5 L of potassium methoxide solution in multiple parallel reactors within 30 min.

5.3.2 MTFMP system

A. Steady-state investigation

The MTFMP system (similar to the HME system) also required the calculation of the point at which steady-state was achieved. A single experiment was conducted over 20 min with a 5 min sampling interval so that the transient behaviour of the reactor could be understood. The experiment was conducted at a reaction temperature of 32.5 °C, a potassium hydroxide concentration of 0.37 mol·L^{-1}, a hexafluoropropene oxide mole fraction of 0.33 and a total liquid volumetric flow rate of 1.75 mL·min^{-1}. The calibration plots for the rotameters of the FFMR experimental set-up are provided in Appendix A.

Figure 5.3 shows the results of these experiments, and it can be seen that steady-state conditions were achieved within the first 5 min of operation. A lead time of 5 min was thus appropriated at the start of each experiment to ensure that the reactor operated at steady-state conditions. The dashed line in Figure 5.3 was used to illustrate the trend of the experimental data.

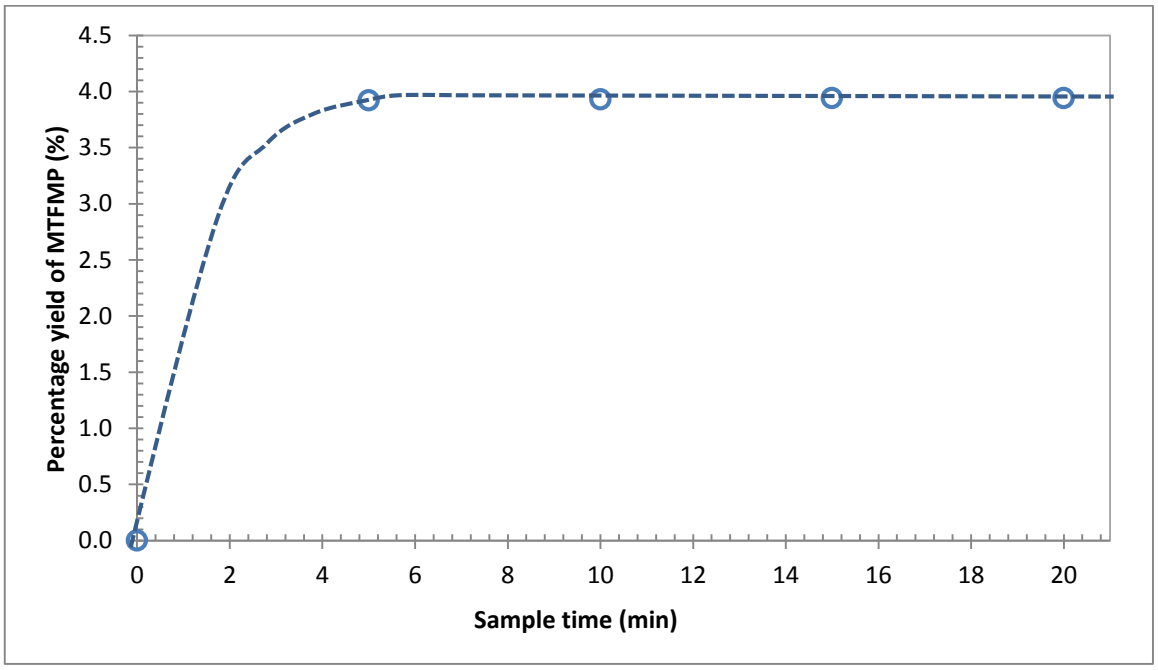

Figure 5.3: Results of transient experiments used to determine point at which steady-state conditions are observed for the methyl-2,3,3,3-tetrafluoro-2-methoxypropionate system. Experiment was conducted at a reaction temperature of 32.5 °C, a potassium hydroxide concentration of 0.37 mol·L^{-1}, a hexafluoropropene oxide mole fraction of 0.33 and a liquid volumetric flow rate of 1.75 mL·min^{-1}. Dashed line indicates trend of experimental data.

B. Choice of alkali salt

Lousenberg and Shoichet (1997) indicated that a suitable alkali salt to use in the synthesis of TFVEs (and their precursors) was sodium hydroxide. Sodium hydroxide however posed some problems when being used to synthesize MTFMP on a FFMR. Sodium hydroxide was sparingly soluble in methanol, thus the concentration of the salt in the feed solution to the reactor was maintained at low levels (below 0.1 $mol \cdot L^{-1}$). The low levels of the salt then reduced the extent to which the reaction could progress as the sodium hydroxide was now a limiting reagent.

Additionally, according to the reaction mechanism outlined in Figure 4.4 (Section 4.3.2), it can be seen that for every mole of MTFMP 2 moles of alkali fluoride are produced. If sodium hydroxide is used the alkali fluoride formed is sodium fluoride. Sodium fluoride is sparingly soluble in methanol. The low solubility of sodium fluoride in methanol led to the formation of solid precipitate in the reactor. The solid would then build up on the reaction plate and in the liquid flow lines causing blockages and reducing the efficacy of the microstructured reaction plate (Photograph 5.1). It was, therefore, not viable to use sodium hydroxide as an alkali salt for the synthesis of MTFMP.

a) **b)**

Photograph 5.1: Evidence of salt build up on reaction plate **a)** and blockage of liquid outlet and viewing window **b)** when using sodium hydroxide as alkali salt in the synthesis of methyl-2,3,3,3-tetrafluoro-2-methoxypropionate.

Attempts were made in order to improve operation by further decreasing the concentration of the salt in the feed as well as increasing reaction temperature (thus improving the solubility of species in solution) but the salt build-up persisted.

The purpose of the alkali salt was to facilitate the addition of the alkoxide to the hexafluoropropene oxide to form the reaction intermediate. The salt, therefore, does not affect the identity of the final product and an alternative salt could be used. Potassium hydroxide has shown

to be a suitable alkali salt as was seen in the HME system and was thus used as a substitute for sodium hydroxide. Using potassium hydroxide as a catalyst, all further experiments were conducted without inhibiting amounts of salt build-up on the reaction plate or pipeline blockages forming. This allowed the central composite design experiments to be completed as per Table 3.3 (Section 3.3.3). Slight solid potassium fluoride build-up was, however, noted at mole fractions greater than 0.67 of hexafluoropropene oxide in the feed gas.

C. Central composite design investigations

MTFMP was successfully synthesized and identified using gas chromatography-mass spectroscopy. MTFMP was quantified using gas chromatography and the internal standard quantification technique. The calibration plot generated for the internal standard technique is provided in Appendix B and the following equation was used to quantify the major product:

$$\frac{M_{MTFMP}}{M_{IS}} = 4.6595 \times \frac{A_{MTFMP}}{A_{IS}} \quad (5.2)$$

Table 5.3 shows the results of the central composite design experiments conducted on the FFMR for the synthesis of MTFMP. 30 experiments were conducted on the FFMR for the synthesis of MTFMP where the yield of the target compound was found to vary from zero to 23.62%. The reason for low yields in some of the experiments was due to the combination of low mole fraction of hexafluoropropene oxide in the gas feed and low liquid residence time in the reactor (high liquid flow rate). The low mole fraction of hexafluoropropene oxide in the gas reduced the concentration driving force that allowed for transfer of the reactant gas into the liquid phase thus directly reducing the amount of MTFMP formed. The high liquid flow rate resulted in a liquid residence time which was too low to allow for quantifiable amounts of MTFMP to be formed.

MTFMP production was found to be favoured at low liquid flow rates, this observation was due to the slow nature of the reaction requiring longer reaction periods in order to facilitate the production of MTFMP.

The yield of MTFMP was favoured at high mole fractions of hexafluoropropene oxide but it is important to note that operating the FFMR at mole fractions greater than 0.67 resulted in the build-up of salt on the reaction plate and the liquid flow lines. This salt build-up was not inhibiting but required additional cleaning of the FFMR after a series of experiments.

The yield and mole fraction of MTFMP was found to be higher at moderate concentrations of potassium hydroxide in the liquid phase. This may be due to the balance between having

sufficient potassium ions to drive the reaction (according to the reaction mechanism outlined in Figure 4.4) and avoiding inhibiting the transfer of hexafluoropropene oxide to the liquid phase by the salting-out effect.

Lastly, the yield and number of moles of MTFMP were favoured at low temperatures. There exists a practical limit on the lowest temperature that can be employed as the solubility of potassium hydroxide and potassium fluoride decreases with temperature as was noted experimentally.

Considering these trends, the yield of MTFMP was found to be favoured at a liquid flow rate of between 3.00 and 3.50 $mL \cdot min^{-1}$, a hexafluoropropene oxide mole fraction of ~0.60, a potassium hydroxide concentration of ~0.35 $mol \cdot L^{-1}$ and a reaction temperature of ~30.0 °C.

Overall more operational problems were associated with the MTFMP system than the HME system and in order to avoid these problems the experiments were constrained to a narrow operating region as outlined above. Considering the low yields of MTFMP seen in Table 5.3 and the low number of moles of the target compound in the product it can be seen the FFMR-Standard with a 32 channel 300 × 600 μm reaction plate is not the most appropriate apparatus for MTFMP synthesis.

In order to improve both the yields and concentration of MTFMP in the product stream, the residence time of the liquid in the reactor may be increased. This is certainly a limitation to the MTFMP system as the FFMR offers liquid residence times of only a few seconds. A possible solution may be the use of smart interface reaction plates as well as longer reaction plates. Smart interface reaction plates were recently developed by the Institut für Mikrotechnik Mainz GmbH to enhance mass transfer as well as structure fluid flow to increase liquid residence time on the reaction plate (Ziegenbalg et al., 2010).

Use of a batch reactor with effective gas sparging would also serve as a suitable medium for MTFMP system, this option is made more viable by the low dependency of the reaction on reaction temperature, thus reducing the need for stringent temperature control.

Table 5.3: Results of experiments conducted on a falling film microreactor for the methyl-2,3,3,3-tetrafluoro-2-methoxypropionate system.

Exp. No.	Hexafluoropropene mole fraction	KOH concentration, $mol \cdot L^{-1}$	Temperature, °C	Liquid flow rate, $mL \cdot min^{-1}$	Moles of MTFMP produced	Product yield, %
						MTFMP
1	0.33	0.28	32.5	1.75	0.002	9.19 ± 0.25
2	0.33	0.28	32.5	4.27	0.000	Not observed
3	0.67	0.28	32.5	1.75	0.005	9.94 ± 0.47
4	0.67	0.28	32.5	4.27	0.008	15.80 ± 0.72
5	0.33	0.53	32.5	1.75	0.001	3.04 ± 1.13
6	0.33	0.53	32.5	4.27	0.000	Not observed
7	0.67	0.53	32.5	1.75	0.005	10.24 ± 0.89
8	0.67	0.53	32.5	4.27	0.012	23.62 ± 0.26
9	0.33	0.28	37.5	1.75	0.002	9.48 ± 0.91
10	0.33	0.28	37.5	4.27	0.000	Not observed
11	0.67	0.28	37.5	1.75	0.003	6.78 ± 0.52
12	0.67	0.28	37.5	4.27	0.008	15.71 ± 0.65
13	0.33	0.53	37.5	1.75	0.001	3.10 ± 0.82
14	0.33	0.53	37.5	4.27	0.000	Not observed
15	0.67	0.53	37.5	1.75	0.006	11.79 ± 0.42
16	0.67	0.53	37.5	4.27	0.011	21.95 ± 0.60
17	0.50	0.40	30.0	3.00	0.006	17.48 ± 1.01
18	0.50	0.40	40.0	3.00	0.004	11.88 ± 0.94
19	0.50	0.15	35.0	3.00	0.004	9.71 ± 0.85
20	0.50	0.65	35.0	3.00	0.006	16.11 ± 0.75
21	0.16	0.40	35.0	3.00	0.000	1.73 ± 0.20
22	0.84	0.40	35.0	3.00	0.007	11.79 ± 0.58
23	0.50	0.40	35.0	0.50	0.001	2.63 ± 0.46
24	0.50	0.40	35.0	5.50	0.001	3.96 ± 2.57
25	0.50	0.40	35.0	3.00	0.005	14.09 ± 0.82
26	0.50	0.40	35.0	3.00	0.006	15.90 ± 0.85
27	0.50	0.40	35.0	3.00	0.005	14.07 ± 0.93
28	0.50	0.40	35.0	3.00	0.006	15.37 ± 0.90
29	0.50	0.40	35.0	3.00	0.006	16.66 ± 0.90
30	0.50	0.40	35.0	3.00	0.006	15.18 ± 0.91

5.4 Kinetic models

After successfully conducting all experiments on a FFMR and analysing the product samples the experimental results presented in Section 5.3 (Table 5.2 and 5.3) were used to identify suitable kinetic models and previously unknown kinetic parameters for the systems of interest. These parameters were obtained by least squares regression of experimental and predicted concentrations of reaction products from the experiments. The predicted concentrations were calculated from models developed according to Chapter 4 and implemented through the algorithms shown in Figure 4.1 for the HME system and Figure 4.2 for the MTFMP system. All models developed were formulated and implemented using MATLAB® (version R2012b, The MathWorks, Inc.).

What follows is a discussion of the results of the kinetic models (parameter identification), their capabilities, limitations and validity. An important aspect when establishing models is to correctly find the balance between usability, complexity and accuracy and this was of particular importance in this study as there is still room to expand the capabilities of the models.

5.4.1 Momentum Balance

The first step in the solution of the governing equations for both the HME and the MTFMP system was the solution of the momentum balance which defined the steady-state liquid velocity profile in each channel. The momentum balance (Equation 2.26) is dependent on *x* and *y* position within the reactor microchannel as well as the solvent viscosity and density.

Since both viscosity and density were temperature dependent as well as the velocity profile being dependent on the volumetric flow rate per channel – each set of experimental conditions resulted in different profiles being formed. Figure 5.4 shows the velocity profile at a centre-point temperature of 285 K and a total liquid volumetric flow rate of 3 $mL.min^{-1}$.

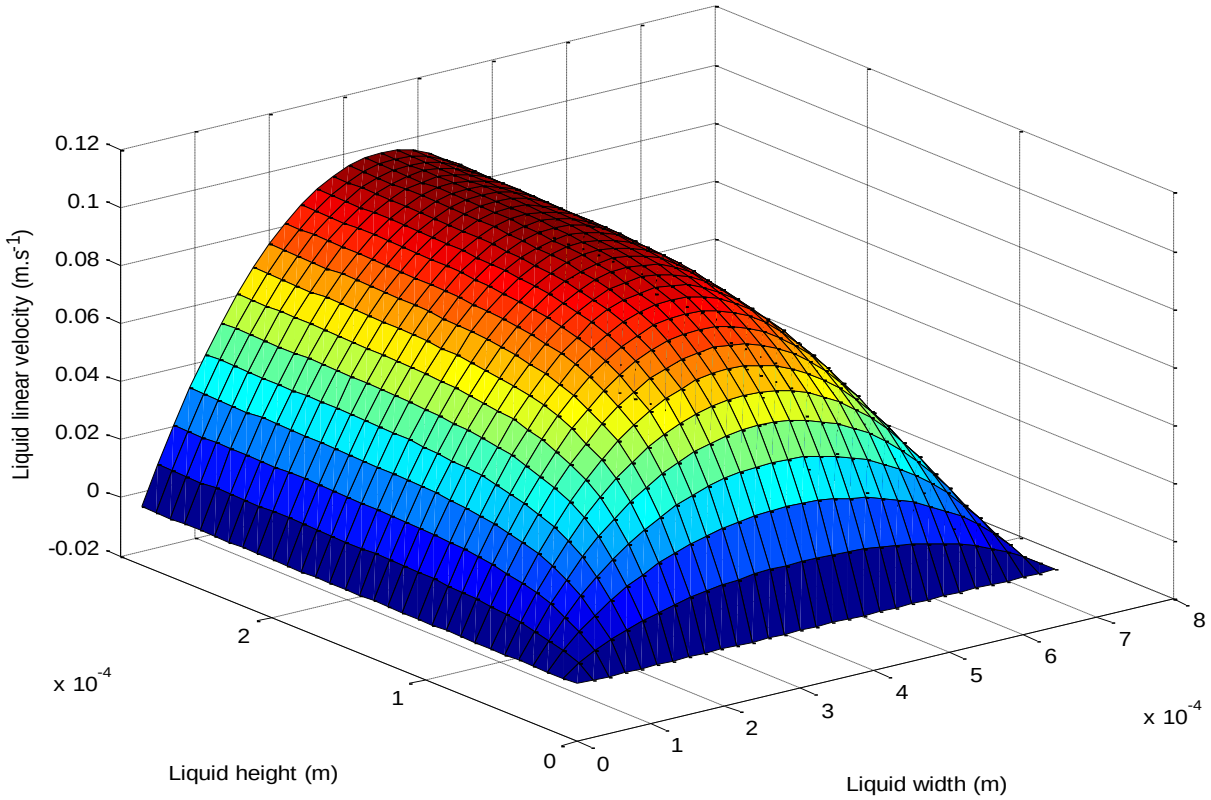

Figure 5.4: Liquid linear velocity profile within a single microchannel at a reaction temperature of 285 K and a total reactor liquid volumetric flowrate of 3 mL.min^{-1}.

5.4.2 HME system

A kinetic model for the synthesis of HME using a FFMR-Standard and a 32 channel 300 × 600 μm reaction plate was successfully developed in the MATLAB® environment. The model was then used to identify a suitable kinetic model for the reactive system as well as the associated kinetic parameters.

After the development of the generalised material balances for the system it can be seen that an important parameter is the Henry's Law constant which was computed as outlined in Section 4.2.2 and then fit to the Valentiner equation in order to increase the usability of the parameter in the model.

A. Henry's Law constant

There is a general lack of thermochemical and thermophysical properties for HME, this extends to vapour-liquid equilibrium data for a HME and methanol system. As a result, Aspen Plus® (version 8.0, Aspen Technology, Inc.) was used to simulate the vapour-liquid equilibrium behaviour of the system (Figure 5.5). An "Ideal" property method was selected in Aspen Plus® (version 8.0, Aspen Technology, Inc.) to describe the vapour-liquid equilibrium behaviour which assumes ideal liquid phase behaviour (a liquid phase activity coefficient equal to 1) and an ideal gas phase (by the ideal

gas law). Ideal conditions were adopted to describe liquid and gas behaviour due to the absence of experimental data and interaction parameters for a suitable equation of state model for the system.

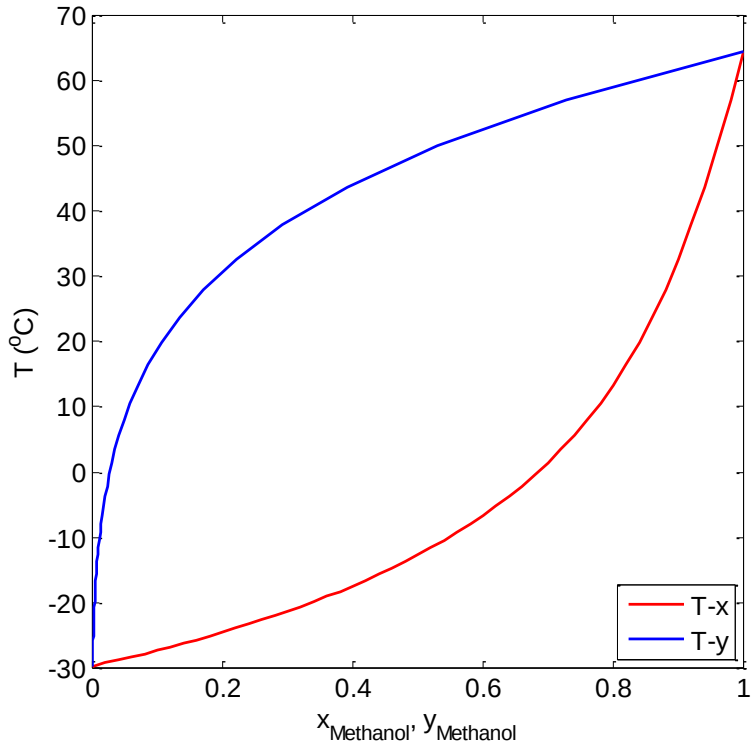

Figure 5.5: Vapour-liquid equilibrium data for methanol and hexafluoropropene system at 1.01 bar. Data simulated using Aspen Plus® (version 8.0, Aspen Technology, Inc.) assuming an ideal liquid and vapour phase.

The simulated vapour-liquid equilibrium data was then translated to H_i^{CC} as outlined in Section 4.2.2 and fitted to the Valentiner equation by least squares regression in the MATLAB® environment (version R2012b, The MathWorks, Inc.). The resulting fit is shown in Figure 5.6 with the corresponding fitting parameters shown in Table 5.4.

Table 5.4: Constants of Valentiner equation[a] for hexafluoropropene in methanol at a pressure of 1.01 bar.

Constants	a, dimensionless	b, K	c, K^{-1}
Value	63.48	-6155.30	-6.29

[a] $\ln H_i^{CC} = a + \frac{b}{T} + c \ln T$, (Takenouchi et al., 2001)

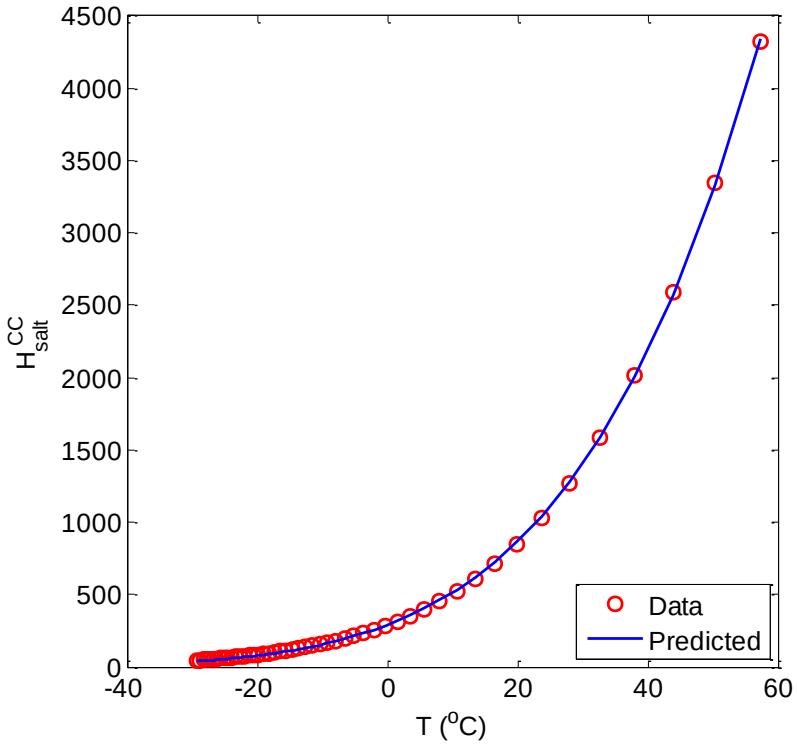

Figure 5.6: Plot of calculated (O) and regressed (—) dimensionless concentration based Henry's Law constants according to the Valentiner equation for methanol and hexafluoropropene system (Takenouchi et al., 2001).

After the Henry's Law constant was presented in a more usable form in the Valentiner equation various physical parameters of the system such as viscosity, density and diffusivities were calculated in the reactor model. These parameters were estimated using correlations found in Green (2008), use of these correlations can be seen in Appendix D. Physical parameters calculated were used to compute the hydrodynamics of the system thereafter, the generalised material balances were solved simultaneously in the reaction model.

B. Simple single reaction model

Early on in the investigative process it was apparent that the by-products accounted for a relatively small percentage of the final product composition (usually less than 5 to 8% - as seen in Tables 5.1 and 5.2) and so a model was developed that considered only the reaction to form HME from potassium methoxide and hexafluoropropene. The proposed scheme is shown in Figure 5.7.

The proposed scheme assumed that the formation of the by-products was negligible and thus the only reaction was that to produce HME. This single reaction was also assumed to be forward and irreversible. The addition of the proton was sourced from the freely available methanol and was thus assumed to be in abundance.

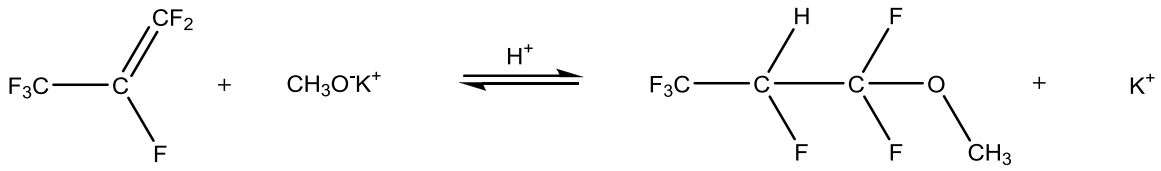

Figure 5.7: Simple reaction mechanism proposed for the preliminary 1,1,2,3,3,3-hexafluoropropyl methyl ether kinetic model.

The concentration of HME in the product was chosen as the response variable to be regressed for instead of the yield of the major product due to the fact that the outlet concentration was in fact the variable that was output by the generalised material balances. Thus any accumulation of error or distortion was avoided.

The results of each simulation were compared using a parity plot. A parity plot is an easy means of evaluating the fit of a model by comparing predicted values of a response and either actual or reference values of the same response. The quality of the fit at a point is judged by the distance between that point and the $y = x$ line (marked in blue – Figure 5.8). Points at which the fit is poor are thus easily noticeable from this plot.

Figure 5.8 shows the resulting parity plot of the single reaction system, corresponding residual deviation plot as well as absolute relative deviation plot. The model did not show a very good representation of experimental results over the whole range of observed concentrations (Average absolute relative deviation percentage of 31.55 %). It was seen that the model tended to under estimate the outlet concentration of HME at higher observed concentrations of HME (above 500 $mol \cdot m^{-3}$). This model was not optimised but was investigated in order to obtain a better understanding of the system.

This representation of the HME system was limited in that it did not account for the presence of any of the other species in the system (such as the reaction intermediate, alkenyl ether or alkyl tetrafluoropropionate), for this reason it lacked robustness.

The reaction mechanism used in the final model was more elaborate and provided a more accurate representation of the solution chemistry by relaxing some of the major assumptions made in this simplified model.

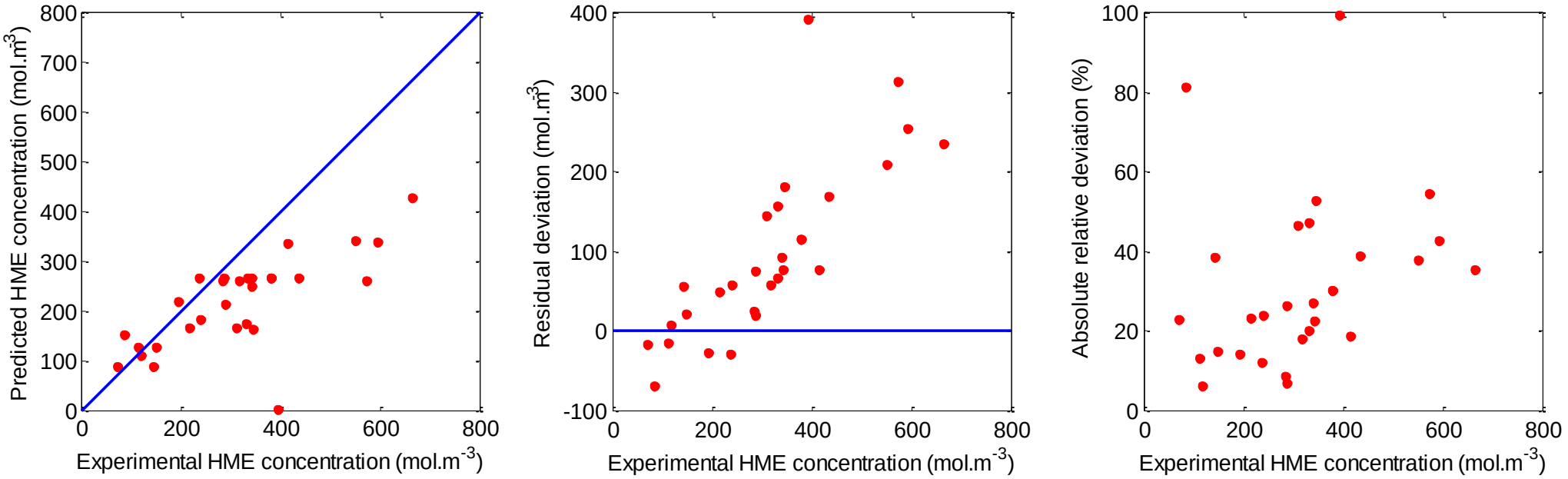

Figure 5.8: Left - parity plot showing a comparison of predicted outlet concentration of 1,1,2,3,3,3-hexafluoropropyl methyl ether (HME) versus experimentally obtained concentrations of HME a simple single reaction mechanism. Middle – residual deviation plot defined as difference between experimental and predicted concentrations of HME. Right – absolute relative deviation plot versus experimentally observed HME concentrations. Initial guesses for kinetic model were reference kinetic rate constant of 1.0×10^{-4} $m^3.mol^{-1}.s^{-1}$, activation energy of 30.0 $kJ.mol^{-1}$ and Sechenov coefficient of 1.0 $L.mol^{-1}$. Average absolute relative deviation percentage of 31.55 %.

C. Objective function definition

The first assumption that was relaxed in the final reaction mechanism proposed for the HME system was that the presence of the by-products was negligible. This assumption required amending the reaction mechanism. The reaction mechanism seen in Figure 4.3 (Section 4.3.1) was developed to incorporate the presence of the by-products into the model. This mechanism consists of 5 main reactions which gave a more comprehensive representation of the system.

Incorporating the presence of the by-products meant that there were now 3 response variables (i.e. HME, alkenyl ether and alkyl tetrafluoropropionate outlet concentrations) which needed to be incorporated into the objective function (Equation 4.1); this was done by calculating the summed square error for each species and summing the three values. There was, however, a problem with doing this, since there was a large difference between the magnitudes of the concentrations of the various product species and the objective function was susceptible to becoming biased towards the contribution of HME (which was numerically larger).

A similar problem was encountered when dealing with the large differences in magnitude between the rate constants and the activation energies and this was dealt with by adopting internal scaling methods such as the temperature centreing method. Similarly, an artificial scaling method was applied to the objective function in the HME model (Wojciechowski and Rice, 2003). Usually, weighting factors that are adopted are found in literature and are well-accepted for a specific system. The synthesis of HME is not a very well-studied system and thus weighting factors are not available, so a new set of weighting factors was defined. The weighting factor $\lambda_{j,HME}$ was defined as the average concentration of HME in the centrepoint experiments divided by the average concentration of product j in its centrepoint experiments.

$$\lambda_{\mathrm{j,HME}} = \frac{\overline{\mathrm{C}}_{\mathrm{HME,Centrepoints}}}{\overline{\mathrm{C}}_{\mathrm{j,Centrepoints}}} \tag{5.3}$$

The objective function for the system was thus:

$$\mathrm{E} = \sum_{j=1}^{3} \lambda_{\mathrm{j,HME}}^{2} \cdot \sum_{i=1}^{N} \left(\frac{\mathrm{C_i^{EXP}} - \mathrm{C_i^{Pred}}}{\mathrm{C_i^{EXP}}} \right)^2 \tag{5.4}$$

Where the 3 terms in the outer summation refer to each of the 3 species that constitute the objective function i.e. HME, alkenyl ether and alkyl tetrafluoropropionate. Note also that the weighting factor has been squared; this is due to the fact that the weighting applies to each relative

error and thus lies within the second summation's bracket. Table 5.5 shows the weighting factor used for each of the product species.

Table 5.5: Weighting factors[a] used for product species in 1,1,2,3,3,3-hexafluoropropyl methyl ether kinetic model.

Species	Hexafluoropropyl methyl ether	Alkenyl ether	Alkyl tetrafluoropropionate
Average concentration over centrepoints ($mol \cdot m^{-3}$)	351.27	20.10	31.22
Weighting factor	1.00	17.47	11.25

[a]Weighting factor for a species was calculated by dividing average concentration of 1,1,2,3,3,3-hexafluoropropyl methyl ether in centrepoint runs by the average concentration of the corresponding species in centrepoint runs.

D. Kinetic model results

After the objective function was established the reaction rates were defined and incorporated into 7 generalised material balances for all the relevant species in the model. The reaction rates were defined as per the reaction mechanism outlined in Section 4.2.1. This mechanism was formulated given the information in the works of both Il'in, et al. (2004) and Rendall, et al. (1958). The published mechanisms were then isolated into 5 reaction steps which fully defines the system. The final set of balances were Equations 4.40 to 4.46 (Section 4.3.1) and required kinetic parameters (i.e. reference kinetic rate constants and activation energies) before the outlet concentrations of species could be calculated. These parameters were unknown and were thus the fitting parameters of the model. Initial guesses for each of these eight parameters were fed in at the start of the kinetic model and these can be seen in Table 5.6.

Table 5.6: Initial guesses passed into1,1,2,3,3,3-hexafluoropropyl methyl ether kinetic model.

Units of $k_{i,o}$	Reaction 1, $m^3 \cdot mol^{-1} \cdot s^{-1}$	Reaction 2, s^{-1}	Reaction 3, s^{-1}	Reaction 4 & 5, $m^3 \cdot mol^{-1} \cdot s^{-1}$
$k_{i,o}$	1.000×10^{-2}	1.000×10^{-1}	5.000×10^{-3}	1.500×10^{-4}
$E_{A,i}$ ($kJ.mol^{-1}$)	30.000	80.000	11.000	8.000

The initial guesses established in Table 5.6 were found to lie close to the minimum of the function and were thus deemed suitable starting points for the kinetic model. A RSM analysis, like that carried out for the MTFMP system (Section 5.4.2 C), was not possible for the HME system due to the large number of variables. Trying to analyse the interaction between 8 variables graphically would have resulted in 28 surface plots which would have been difficult to translate into usable trends.

Figure 5.9, 5.10 and 5.11 shows the results of the kinetic model. The corresponding parity, residual deviation and absolute relative deviation plots are shown for each of the species in the system. The residual deviation was calculated by finding the difference between experimental and predicted values of the outlet concentration of the corresponding species. The absolute relative deviation was calculated by finding the absolute value of the deviation between predicted and experimental concentrations and dividing by the corresponding experimental concentration.

The HME model did not perform satisfactorily when compared to experimental concentrations. The model also performed less agreeably for the alkenyl ether and alkyl tetrafluoropropionate species. The model predicted outlet concentrations of HME reasonably well for a small portion of the experimentally observed range but tended to provide less agreement at higher observed concentrations as seen by the corresponding residual deviation plot. The average absolute relative deviation percentage of the model was found to be 34.12 % which is marginally worse than the simplified HME kinetic model presented in Section 5.4.1 B.

The model did not perform well when predicting the concentration of alkenyl ether over the experimentally observed range with an average absolute relative deviation percentage of 53.64 %. The model under-predicted the concentration of alkenyl ether in the reactor outlet at the majority of the experimental data points with a greater discrepancy between the two values seen at higher observed concentrations of alkenyl ether.

The model fits a small percentage of the data well for the alkyl tetrafluoropropionate outlet concentrations with the rest of the data being under-predicted by the model as shown by an average absolute relative deviation percentage of 50.27 %. Deviations again tend to increase at higher observed concentrations of the alkyl tetrafluoropropionate.

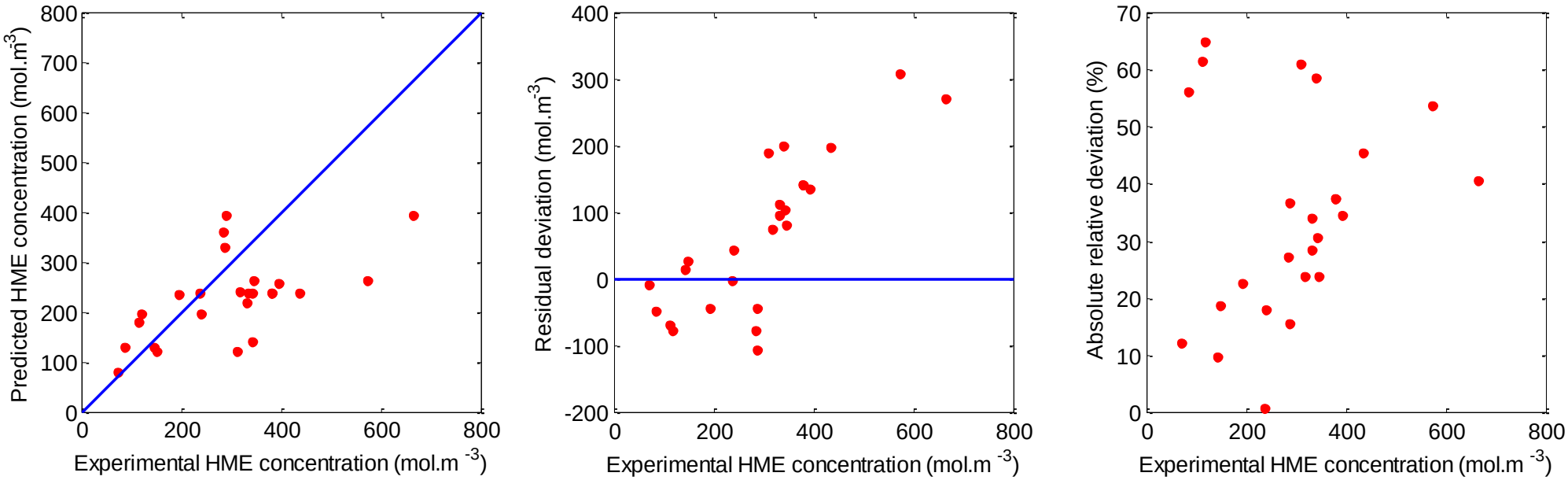

Figure 5.9: Left - parity plot showing a comparison of predicted outlet concentration of 1,1,2,3,3,3-hexafluoropropyl methyl ether (HME) versus experimentally obtained concentrations of HME. Middle – residual deviation plot defined as difference between experimental and predicted concentrations of HME. Right – absolute relative deviation plot versus experimentally observed HME concentrations. Average absolute relative deviation percentage of 34.12 %.

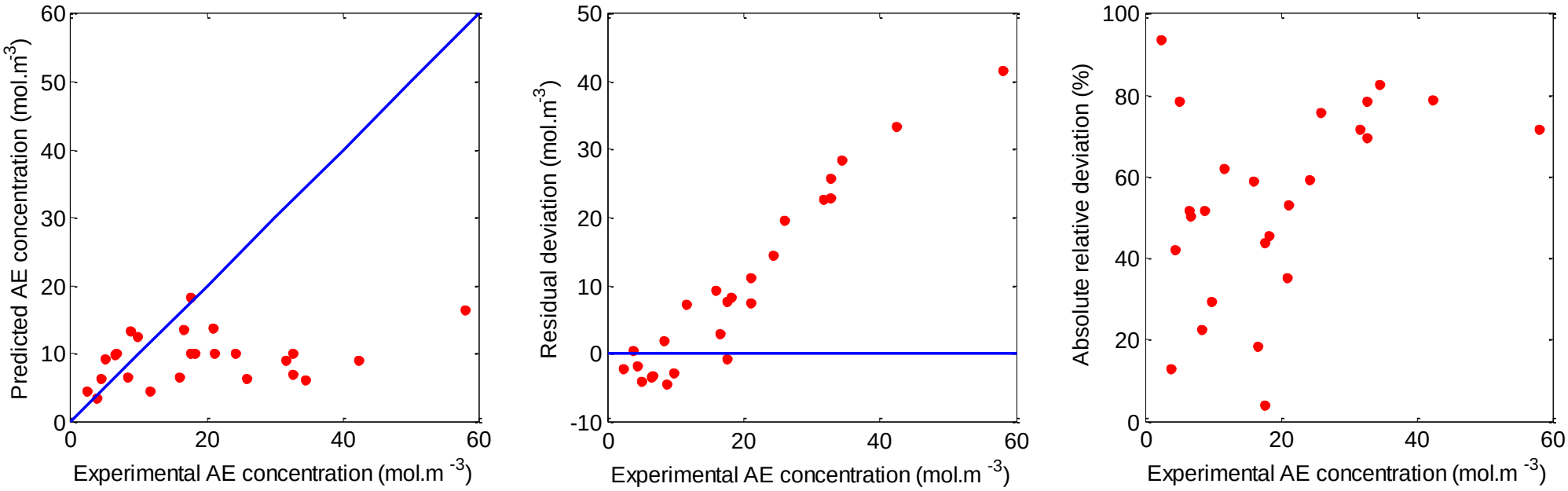

Figure 5.10: Left - parity plot showing a comparison of predicted outlet concentration of alkenyl ether (AE) versus experimentally obtained concentrations of AE. Middle – residual deviation plot defined as difference between experimental and predicted concentrations of AE. Right – absolute relative deviation plot versus experimentally observed AE concentrations. Average absolute relative deviation percentage of 53.64 %.

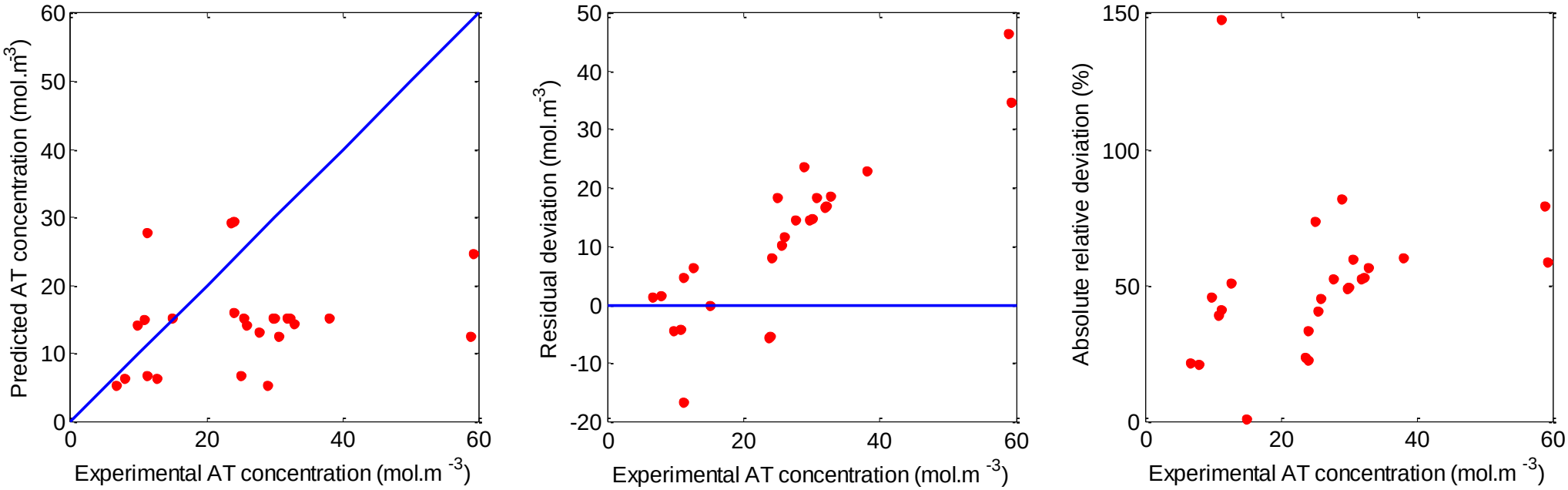

Figure 5.11: Left - parity plot showing a comparison of predicted outlet concentration of alkyl tetrafluoropropionate (AT) versus experimentally obtained concentrations of AT. Middle – residual deviation plot defined as difference between experimental and predicted concentrations of AT. Right – absolute relative deviation plot versus experimentally observed AT concentrations. Average absolute relative deviation percentage of 50.27 %.

Finally, Table 5.7 shows the kinetic parameter results of the model. Due to the inaccuracies of the kinetic model 95% confidence limits on the regressed parameters were found to be unsatisfactory, varying by an order of magnitude. Possible contributors to this variance may be the scatter in the experimental data and small sample set (30 experimental runs).

Table 5.7: Kinetic parameter results of kinetic model for 1,1,2,3,3,3-hexafluoropropyl methyl ether system.

Units of $k_{i,o}$	Reaction 1, $m^3 \cdot mol^{-1} \cdot s^{-1}$	Reaction 2, s^{-1}	Reaction 3, s^{-1}	Reaction 4 & 5, $m^3 \cdot mol^{-1} \cdot s^{-1}$
$k_{i,o}$	1.054×10^{-2}	1.461×10^{-1}	5.615×10^{-3}	1.574×10^{-4}
$E_{A,i}$ ($kJ.mol^{-1}$)	34.502	80.999	10.851	8.047

5.4.3 MTFMP system

A kinetic model for the synthesis of MTFMP using a FFMR-Standard and a 32 channel 300 × 600 μm reaction plate was successfully developed in the MATLAB® environment. The model was then used to identify a suitable kinetic model for the reactive system as well as the associated kinetic parameters.

A similar procedure was followed as was for the HME system in that the first step after formulating the relevant generalised material balances was computation of the required thermophysical properties of the components in the system. The first of which was the Henry's Law constant for the system which was calculated as outlined in Section 4.2.2 and then fitted to the Valentiner equation.

A. Henry's Law constant

Experimental vapour-liquid equilibrium data was not available for the methanol and hexafluoropropene oxide system. Consequently, Aspen Plus® (version 8.0, Aspen Technology, Inc.) was once again used to simulate the vapour-liquid equilibrium behaviour of the system (Figure 5.12). An "Ideal" property method was selected in Aspen Plus® (version 8.0, Aspen Technology, Inc.) to describe the vapour-liquid equilibrium behaviour which assumes ideal liquid phase behaviour (a liquid phase activity coefficient equal to 1) and an ideal gas phase (by the ideal gas law). Ideal conditions were adopted to describe liquid and gas behaviour due to the absence of experimental data and interaction parameters for a suitable equation of state model.

Continuing with the process followed for the HME system, the vapour-liquid equilibrium data was translated to corresponding H_i^{CC} values and fit to the Valentiner equation by least squares regression in the MATLAB® environment (version R2012b, The MathWorks, Inc.). The resulting fit is shown in Figure 5.13 with the corresponding fitting parameters shown in Table 5.8.

Physical parameters of the system such as viscosity, density and diffusivities were then estimated using empirical correlations found in Green (2008) (refer to Appendix D for examples of their use) and the generalised balances for the MTFMP system were then solved simultaneously in the reaction model.

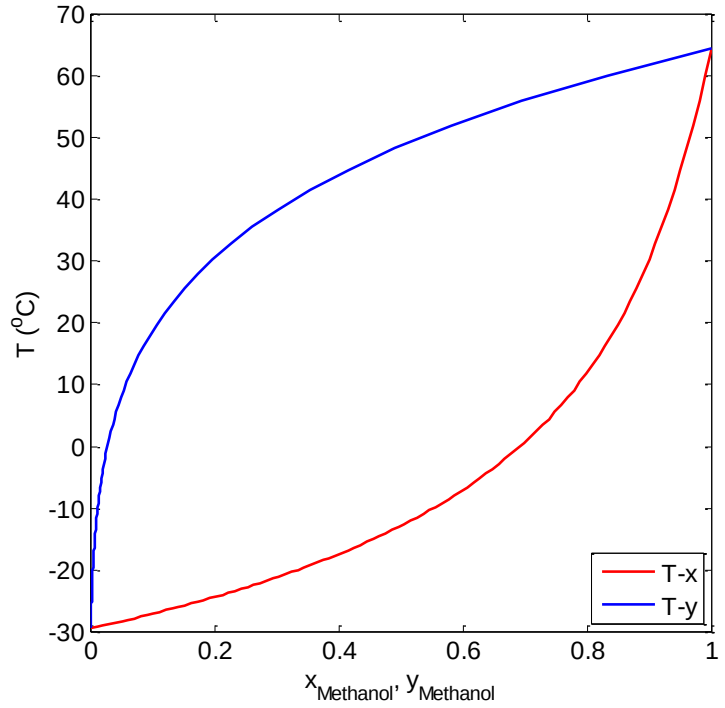

Figure 5.12: Vapour-liquid equilibrium data for methanol and hexafluoropropene oxide system at 1.01 bar. Data simulated using Aspen Plus® (version 8.0, Aspen Technology, Inc.) assuming an ideal liquid and vapour phase.

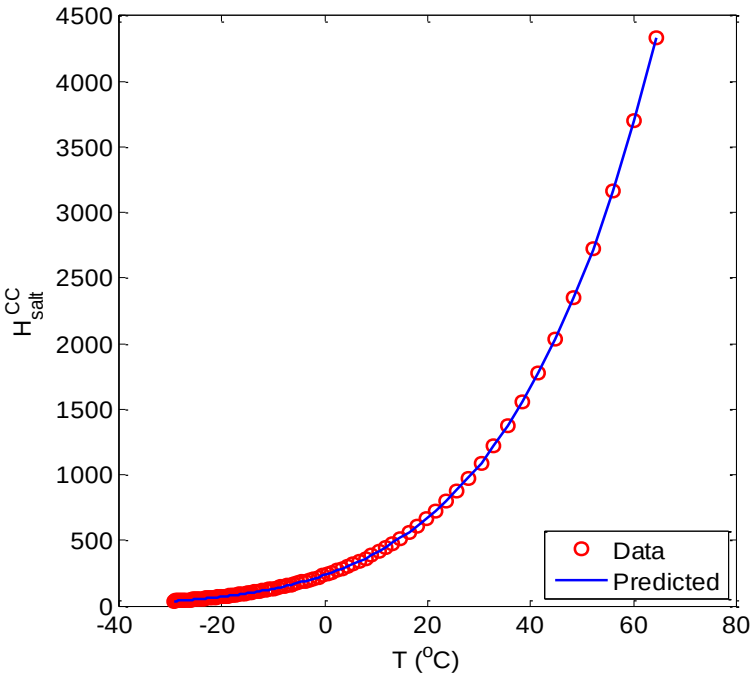

Figure 5.13: Plot of calculated (**O**) and regressed (**—**) dimensionless concentration based Henry's Law constants according to the Valentiner equation for methanol and hexafluoropropene oxide system (Takenouchi et al., 2001).

Table 5.8: Constants of Valentiner equation for hexafluoropropene oxide in methanol at a pressure of 1.01 bar.

Constants	a, dimensionless	b, K	c, K^{-1}
Value	30.20	-4590.30	-1.41

[a] $\ln H_i^{CC} = a + \frac{b}{T} + c \ln T$, (Takenouchi et al., 2001)

B. Effect of reaction order

Applying the quasi steady-state approximation to the MTFMP reaction mechanism indicated that the rate of the second reaction was exactly equal to that of the first reaction in Section 4.2.2. Thus, for every mole of MTFMP formed, two moles of potassium methoxide is consumed. Overall, the formation of MTFMP may be second order in terms of potassium methoxide. Following this finding, a choice was made to observe the effect of changing the order of Reaction 1 with respect to the concentration of potassium methoxide; this is simply done by changing the exponent of $C_{CH_3O^-K^+}$ in:

$$r_1 = k_1 C_{HFPO,L} C_{CH_3O^-K^+} \tag{5.5}$$

In order to observe the effect of reaction order, the kinetic model was run with initial guesses for the reference kinetic rate constant at 5×10^{-5} $m^3 \cdot mol^{-1} \cdot s^{-1}$, the activation energy at 60 $kJ \cdot mol^{-1}$ and a Sechenov coefficient of 0.500 $L \cdot mol^{-1}$ and the subsequent results were compared.

Figure 5.14 and 5.15 shows the parity, residual and absolute relative deviation plots for the kinetic model when a first order and second order reaction was prescribed, respectively. From these graphs it can be seen that the second order description of the reaction mechanism results in a better parity plot as characterized by the concentrated spread of data points about the $y = x$ line. The first order representation under-predicts the outlet concentration of MTFMP at observed concentrations above 70 $mol \cdot m^{-3}$ (Figure 5.14). This was evident in the corresponding residual and absolute relative deviation plot that showed a systematic trend which was an increase in the magnitude of the deviation at greater observed concentrations and an average absolute relative deviation of 66.31 %. The second order representation showed a greater scatter in the residual deviation which is more desirable as it indicates an absence of a systematic error. The absolute relative deviation plot also shows decreased absolute relative deviations (average absolute relative deviation of 54.53 % which is lower than the first order model). From the results shown in Figures 5.14 and 5.15 it was decided that a second order representation of the MTFMP reaction mechanism was a better narrative of the observed data.

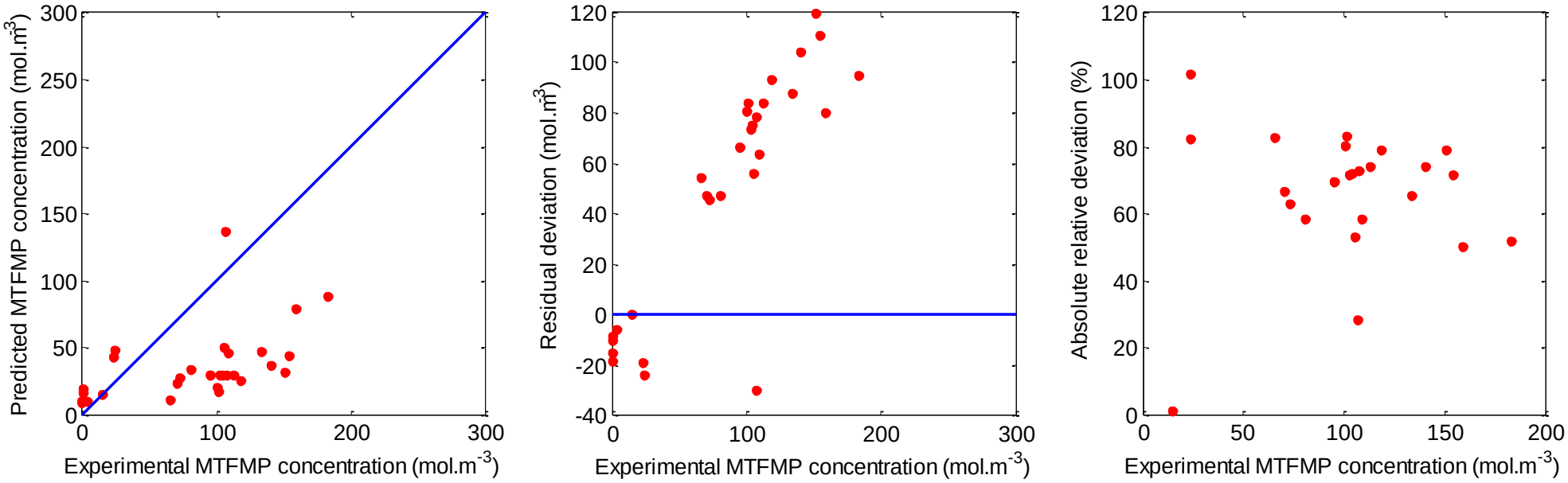

Figure 5.14: Left - parity plot showing a comparison of predicted outlet concentration of methyl-2,3,3,3-tetrafluoro-2-methoxypropionate (MTFMP) versus experimentally obtained concentrations of MTFMP when considering the reaction as first order. Middle – residual deviation plot defined as difference between experimental and predicted concentrations of MTFMP. Right – absolute relative deviation plot versus experimentally observed MTFMP concentrations. Average absolute relative deviation percentage of 66.31 %.

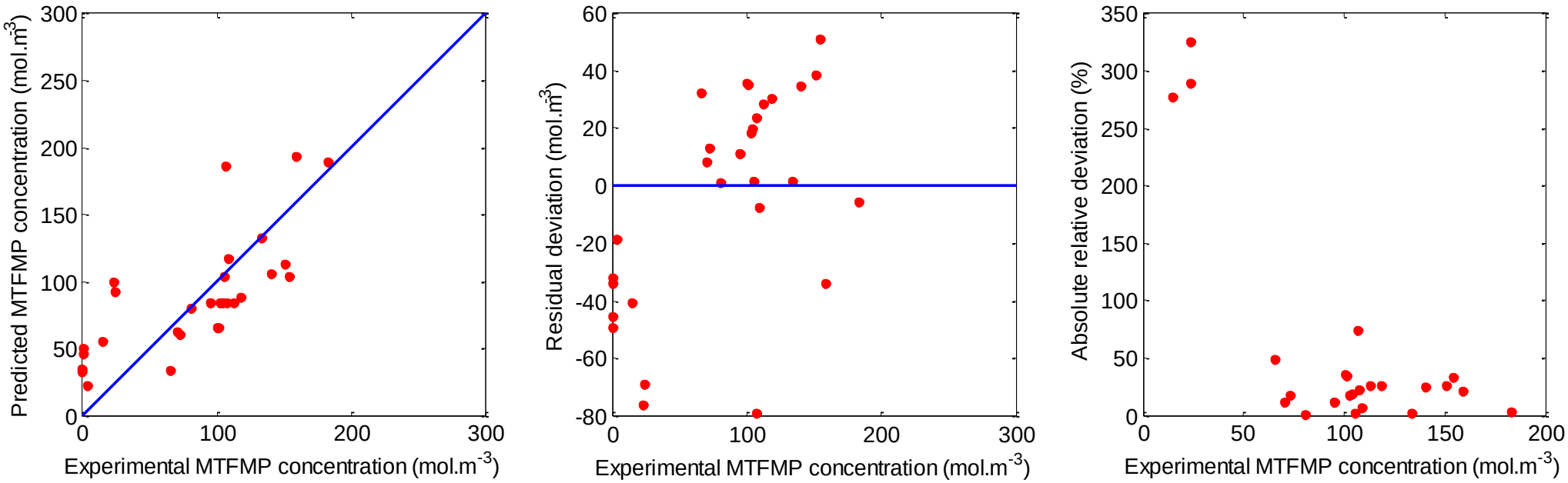

Figure 5.15: Left - parity plot showing a comparison of predicted outlet concentration of methyl-2,3,3,3-tetrafluoro-2-methoxypropionate (MTFMP) versus experimentally obtained concentrations of MTFMP when considering the reaction as second order. Middle – residual deviation plot defined as difference between experimental and predicted concentrations of MTFMP. Right – absolute relative deviation plot versus experimentally observed MTFMP concentrations. Average absolute relative deviation percentage of 54.53 %.

C. Kinetic model results

The kinetic model did not provide a very good fit of experimental data with an average absolute relative deviation percentage of 170.00 % over all 30 data points, as can be seen in Figure 5.16. The absolute relative deviation plot shows that this average may be skewed by numerically larger deviations at low experimentally observed concentrations which are in excess of 500 %. In the absence of absolute relative deviations, below MTFMP concentrations of 50 $mol \cdot m^{-3}$, the average absolute relative deviation percentage was 17.80 %. The model showed good congruency with experimental data at observed concentrations between 75 and 200 $mol \cdot m^{-3}$. Conversely, the model tended to over-estimate the concentration of MTFMP in the outlet at observed concentrations below 50 $mol \cdot m^{-3}$ which contributed to the negative deviations seen in the deviation plot of Figure 5.16. As with the HME kinetic model, 95% confidence limits on the regressed parameters were found to be unsatisfactory, also varying by an order of magnitude. The motivation for which has previously been detailed in Section 5.4.2 D.

Table 5.9: Kinetic parameter results of kinetic model for methyl-2,3,3,3-tetrafluoro-2-methoxypropionate system.

Reference kinetic rate constant, $m^3 \cdot mol^{-1} \cdot s^{-1} \times 10^4$	Activation energy, $kJ \cdot mol^{-1}$	Sechenov coefficient, $L \cdot mol^{-1}$	Relative summed square error
1.2892	40.0	0.8012	1.700

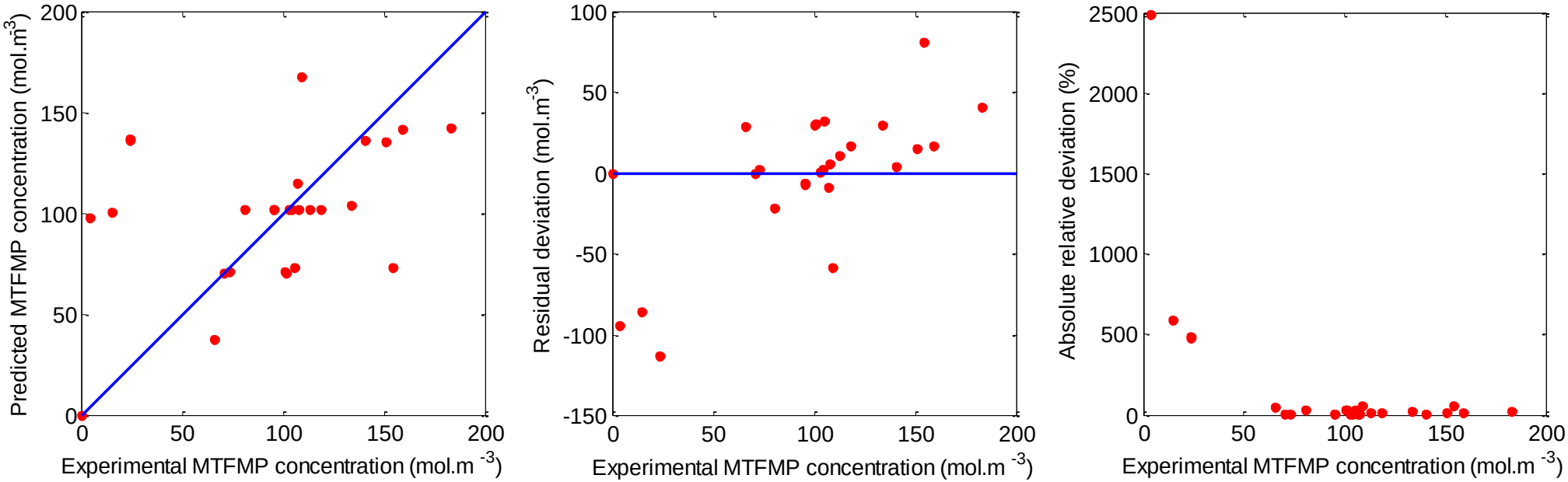

Figure 5.16: Left - parity plot showing a comparison of predicted outlet concentration of methyl-2,3,3,3-tetrafluoro-2-methoxypropionate (MTFMP) versus experimentally obtained concentrations of MTFMP. Middle – residual deviation plot defined as difference between experimental and predicted concentrations of MTFMP. Right – absolute relative deviation plot versus experimentally observed MTFMP concentrations. Initial guesses for kinetic model were reference kinetic rate constant of 1.2892×10^{-4} $m^3\cdot mol^{-1}\cdot s^{-1}$, activation energy of 40.0 $kJ\cdot mol^{-1}$ and Sechenov coefficient of 0.8012 $L\cdot mol^{-1}$. Average absolute relative deviation percentage of 170.00 %. Average absolute relative deviation percentage of 17.80 % at experimental MTFMP results greater than 50 $mol.m^{-3}$.

6

CHAPTER SIX

6. CONCLUSIONS & RECOMMENDATIONS

6.1 Conclusions

The objectives of this study were in line with the principle objectives of the Fluorochemical Expansion Initiative i.e. the development of local fluorochemical technologies and products. This study focused on the processing of fluorspar derivatives in the form of hexafluoropropene and hexafluoropropene oxide, considerations of the reaction chemistry and identification of kinetic models for the processes.

6.1.1 Organofluorine synthesis

A. Equipment validation

Experimental equipment was validated by observing the absorption of carbon dioxide in a sodium hydroxide solution. Results showed mass transfer coefficients greater than similar experiments conducted by Zhang et al., (2009). Increased rates of mass transfer were postulated to be due to the formation of ripples on the microchannel which increased the interfacial area between the valid phases. Enhanced mass transfer was deemed to be beneficial to the study and thus the equipment was declared fit to conduct experiments.

B. HME synthesis

Considering first the synthesis of HME, preliminary investigations were conducted on a semi-batch gas-liquid stirred tank reactor where hexafluoropropene gas was bubbled through 1.5 L of methanol and dissolved amounts of potassium hydroxide for 30 min. There were 3 reaction variables of interest in the preliminary investigations and these were hexafluoropropene mole fraction in the feed, potassium hydroxide concentration and reaction temperature. A 3 factor central composite design was used to conduct these experiments over a hexafluoropropene mole fraction range of 0.41 to 0.83, a catalyst concentration range of 0.40 to 0.80 $\mathrm{mol \cdot L^{-1}}$ and a reaction temperature range of 12.0 to 28.0 ^{0}C. HME and the associated by-products were successfully synthesised in the glass reactor and were qualitatively analysed using gas

chromatography-mass spectroscopy and quantitatively analysed using gas chromatography and the internal standard quantification technique. Experimental yields of HME ranged from 19.21 to 53.32% with respect to the moles of hexafluoropropene gas introduced into the system over the reaction period. The yields of the by-products were also quantified and the yield of alkenyl ether was found to vary between 0.07 and 1.03% while alkyl tetrafluoropropionate varied from 2.42 to 5.10%.

The preliminary investigations also provided two very important findings and these were, firstly, that negligible amounts of solid precipitate was formed at all reaction conditions which permitted the use of a FFMR for the system and secondly, the trends observed in experimental results allowed for a more appropriate operating envelope to be established for the FFMR experiments.

An additional observation from experiments conducted on the glass reactor was that temperature control was inefficient for a highly exothermic reaction such as that of the HME system. A sharp temperature increase was noted over the first 5 min of all experiments and this may decrease the selectivity of the reaction when attempting to target an optimum operating region.

Experiments were then conducted on a FFMR which offers greater rates of heat and mass transfer allowing for more stringent reaction temperature control and enhanced reaction rates. It was desirable to operate at steady-state conditions for all experiments and this was found to be achieved within the first 5 min of reactor start-up. The reactor was operated counter-currently in order to make use of a high concentration driving force over the length of the reaction plate. There were 4 reaction variables of interest in the FFMR experiments and these were hexafluoropropene mole fraction in the feed, potassium hydroxide concentration, reaction temperature and liquid flowrate. The ranges investigated for these parameters were between 0.17 and 0.88, 0.25 and 0.61 $mol \cdot L^{-1}$, 2.0 to 22.0 ^{0}C and 0.50 to 5.50 $mL \cdot min^{-1}$ for the hexafluoropropene mole fraction in the feed gas, potassium hydroxide concentration, reaction temperature and liquid flowrate respectively. A 4 factor circumscribed central composite design was used to dictate the number of experiments as well as the combination of reaction conditions. The amounts of HME as well as the by-products were again quantified using gas chromatography and the internal standard method to give yields of HME of between 11.60 and 68.00%. The by-products appeared in the reactor product at yields between 0.11 and 6.99% for the alkenyl ether and 0.75 and 6.24% for the alkyl tetrafluoropropionate.

The FFMR presented an easier method of synthesising HME via a continuous process, this allowed for easier processing and handling of materials pre- and post-experimentation. The favourable characteristics of the FFMR allowed for stringent reaction temperature control which

aided repeatability of experiments as well as greater yields being observed in comparison to the glass reactor results.

C. MTFMP system

MTFMP was similarly synthesized using a FFMR by passing hexafluoropropene oxide gas over a methanol liquid solution with a dissolved alkali salt. Literature dictated that sodium hydroxide be a suitable salt for the reaction but this to created blockages of microchannels as well as liquid exit lines. Potassium hydroxide was used instead. The alternate salt proved to be a viable replacement as MTFMP was successfully synthesized. The identification and quantification of the MTFMP product used gas chromatography-mass spectroscopy and gas chromatography, respectively.

There were 4 reaction variables of interest in the MTFMP system and these were hexafluoropropene oxide mole fraction in the feed, potassium hydroxide concentration, reaction temperature and liquid flowrate. The ranges investigated for these parameters were between 0.16 and 0.84, 0.15 and 0.65 $mol \cdot L^{-1}$, 30.0 to 40.0 ^{0}C and 0.50 to 5.50 $mL \cdot min^{-1}$ for the hexafluoropropene oxide mole fraction in the feed gas, potassium hydroxide concentration, reaction temperature and liquid flowrate, respectively. A steady-state study was once again conducted and it was found that the system reached steady-state within the first 5 min of operation. Yields of MTFMP ranged from 0.00 to 23.62%. The low yields observed were due to a combination of high liquid flowrate (which resulted in a low liquid residence time) and low mole fractions of hexafluoropropene oxide in the gas (meaning insufficient reactant gas to drive the production of MTFMP). Overall, considering the difficulties experienced with the system as well as the low yields obtained, it was concluded that a FFMR may not be the most appropriate means of synthesising MTFMP.

6.1.2 Kinetic model and parameter identification

A secondary objective of this study was to use the experimental results obtained from the FFMR for both the systems and model the reactor from fundamental principles, in order to identify a suitable kinetic model as well as previously unknown kinetic parameters.

A. HME system

A set of generalised material balances were developed from fundamental principles. Both a simple and a more complex description of the HME reaction mechanism were investigated. The simple reaction mechanism description provided little insight into the interaction of the various species thus the more elaborate description of the solution chemistry was opted for. This novel reaction mechanism broke the reaction network into 5 reactions which were assumed to be

forward and irreversible. There was no available literature on the kinetics of the 5 reactions and the required rate constants and activation energies were solved for by least square non-linear regression MATLAB® environment (version R2012b, The MathWorks, Inc.). The temperature centreing internal scaling method was employed for both the HME and MTFMP systems which meant that the reference kinetic rate constant, and not the reaction rate constant, was found by regression of experimental data. A similar scaling method was also applied to the objective function in the form of artificial weighting factors. The system was found to be very weakly affected by the presence of salt in the liquid phase thus the Sechenov coefficient was eliminated to reduce the number of fitting parameters from 9 to 8 for the system.

The kinetic model was eventually solved and results showed that the model performed satisfactorily for HME in solution but did not perform as well for alkenyl ether and alkyl tetrafluoropropionate in solution.

B. MTFMP system

A set of generalised material balances was developed from fundamental principles assuming. The reaction mechanism for the synthesis of MTFMP was broken down into a two-step reaction sequence. Each step was found to have equivalent rates after employing the steady-state approximation to the pseudo present reaction intermediate. The generalised system of material balances was then solved simultaneously in the MATLAB® environment (version R2012b, The MathWorks, Inc.) with the unknown variables (fitting parameters) being regressed for in the model.

In order to ascertain the combination of initial guesses which would result in the lowest summed square error being observed a RSM analysis was conducted on the regression. The analysis revealed that the kinetic model was sensitive to the second order response of reference kinetic rate constant and the interaction between reference kinetic rate constant and Sechenov coefficient, it was also invariable to the value of the activation energy. An initial guess of 40.0 $kJ \cdot mol^{-1}$, 1.6×10^{-4} $m^3 \cdot mol^{-1} \cdot s^{-1}$ and 0.800 $L \cdot mol^{-1}$ was used for the activation energy, reference kinetic rate constant and Sechenov coefficient, respectively. It was also found that a better representation of the system was observed when the mechanism was considered to be second order with respect to the concentration of potassium methoxide. The final values of the kinetic parameters were 40.0 $kJ \cdot mol^{-1}$, 1.2892×10^{-4} $m^3 \cdot mol^{-1} \cdot s^{-1}$ and 0.8012 $L \cdot mol^{-1}$ with an average absolute relative deviation of 41.04 %.

6.2 Recommendations

A. HME system

The HME showed promising results when synthesised on the FFMR, making use of the various advantages of the reactor. HME is also a valuable fluorochemical and research into the development of a continuous industrial scale process may be a very lucrative and profitable venture. This is certainly possible with the wide variety of FFMRs available as well as the ease of scale up of the process.

One source of error with regards to the kinetic model lies in the fact that experimental vapour-liquid equilibrium data was not available for systems and the use of experimental data will improve the accuracy of the predicted Henry's Law constants.

B. MTFMP system

Although potassium hydroxide was used as an alkali salt to catalyse the MTFMP reaction a viable alternative may be found in the use of pure sodium instead of sodium hydroxide. This may allow for a decrease in the amount of salt formation as well as increase the yield of the reaction, ultimately making the synthesis of MTFMP, using a FFMR, a viable initiative. This process may then serve as the initial stages in the synthesis of TFVEs which can then be used as monomers and comonomers to produce high value fluoroplastics.

C. General

For experimental data that exhibit some noise the experimental data may be passed through an appropriate filter in order to reduce the noise but by still keeping the integrity of the data. One such filter is the Savitzky-Golay filter (Savitzky and Golay, 1964). The smoothening of experimental data may lead to more definitive trends allowing easier fitting and kinetic parameter identification.

The kinetic model fits in this study were found to have large absolute relative percentage error this may be due to the fact that multiple local minima exist and the global minima can be located by optimizing the initial guesses. This was possible for the MTFMP system but not for the HME system due to the large number of fitting parameters. Future work can focus on shifting reaction conditions so that the reaction mechanism can be dominantly described by fewer reactions which will require fewer fitting parameters and increase the accuracy of the resultant fit.

REFERENCES

Al-Rawashdeh, M. M., Hessel, V., Löb, P., Mevissen, K. & Schönfeld, F. 2008. Pseudo 3-D simulation of a falling film microreactor based on realistic channel and film profiles. *Chemical Engineering Science,* 63**,** 5149-5159.

Antony, J. 2003. *Design of experiments for engineers and scientists*, Butterworth-Heinemann.

Astarita, G. 1967. *Mass transfer with chemical reaction,* New York, Elsevier.

Auffhammer, M., Morzuch, B. J. & Stranlund, J. K. 2005. Production of chlorofluorocarbons in anticipation of the Montreal Protocol. *Environmental and Resource Economics,* 30**,** 377-391.

Baldascini, H., Ganzeveld, K. J., Janssen, D. B. & Beenackers, A. 2001. Effect of mass transfer limitations on the enzymatic kinetic resolution of epoxides in a two-liquid-phase system. *Biotechnology and bioengineering,* 73**,** 44-54.

Banks, R. E., Smart, B. E. & Tatlow, J. 1994. *Organofluorine chemistry: principles and commercial applications*, Springer.

Berty, J. M. 1999. *Experiments in catalytic reaction engineering*, Elsevier.

Bide, T. 2011. Fluorspar.

Bird, R. B., Stewart, W. E. & Lightfoot, E. N. 2007. *Transport phenomena,* John Wiley & Sons.

Box, G. E. & Hunter, J. S. 1957. Multi-factor experimental designs for exploring response surfaces. *The Annals of Mathematical Statistics***,** 195-241.

Box, G. E. & Wilson, K. 1951. On the experimental attainment of optimum conditions. *Journal of the Royal Statistical Society. Series B (Methodological),* 13**,** 1-45.

Chen, G., Yue, J. & Yuan, Q. 2008. Gas-liquid microreaction technology: recent developments and future challenges. *Chinese Journal of Chemical Engineering,* 16**,** 663-669.

Danckwerts, P. 1970. Gas–liquid reactions. McGraw-Hill, New York.

Darby, R. 2001. *Chemical engineering fluid mechanics*, CRC PressI Llc.

Degaleesan, S., Dudukovic, M. & Pan, Y. 2001. Experimental study of gas-induced liquid-flow structures in bubble columns. *AIChE journal,* 47**,** 1913-1931.

Dixon, S. 1959. *Chemical compounds and process for their preparation*.

Ebnesajjad, S. 2011. Introduction to Fluoropolymers. Elsevier: Amsterdam.

Finger, G. C., Risser, H. & Bradbury, J. 1960. *Illinois Fluorspar*, Division of the Illinois State Geological Survey.

Fritz, C. G., Moore Jr, E. P. & Selman, S. 1963. *Fluorinated vinyl ethers and their preperation*

Froment, G. F., Bischoff, K. B. & De Wilde, J. 1990. *Chemical reactor analysis and design*, Wiley New York.

Green, D. W. 2008. *Perry's chemical engineers' handbook*, McGraw-hill New York.

Gunawan, R., Ma, D. L., Fujiwara, M. & Braatz, R. D. 2002. Identification of kinetic parameters in multidimensional crystallization processes. *International Journal of Modern Physics B,* 16**,** 367-374.

Haas, P. M. 1992. Banning chlorofluorocarbons: epistemic community efforts to protect stratospheric ozone. *International organization*, 46**,** 187-224.

Harvey, D. 2000. *Modern analytical chemistry,* McGraw-Hill New York.

Henley, E. J., Seader, J. D. & Roper, D. K. 2011. *Separation process principles*, Wiley.

Hessel, V., Ehrfeld, W., Herweck, T., Haverkamp, V., Löwe, H., Schiewe, J., Wille, C., Kern, T. & Lutz, N. Gas/liquid microreactors: hydrodynamics and mass transfer.

Proceedings of the 4th International Conference on Microreaction Technology, 2000. 174-186.
Holland, F. & Bragg, R. 1995. *Fluid Flow for Chemical and Process Engineers*, Butterworth-Heinemann.
Il'in, A., Bakhmutov, Y. L., Ivanova, L., Furin, G., Tolstikova, T. & Sukhinin, V. 2004. Synthesis and use of partially fluorinated dialkyl ethers derived from hexafluoropropylene. *Russian journal of applied chemistry,* 77**,** 98-101.
Inoue, T., Schmidt, M. A. & Jensen, K. F. 2007. Microfabricated multiphase reactors for the direct synthesis of hydrogen peroxide from hydrogen and oxygen. *Industrial & engineering chemistry research,* 46**,** 1153-1160.
Istadi, I. & Amin, N. a. S. 2007. Modelling and optimization of catalytic–dielectric barrier discharge plasma reactor for methane and carbon dioxide conversion using hybrid artificial neural network—genetic algorithm technique. *Chemical engineering science,* 62**,** 6568-6581.
Jähnisch, K., Baerns, M., Hessel, V., Ehrfeld, W., Haverkamp, V., Löwe, H., Wille, C. & Guber, A. 2000. Direct fluorination of toluene using elemental fluorine in gas/liquid microreactors. *Journal of Fluorine Chemistry,* 105**,** 117-128.
Kantarci, N., Borak, F. & Ulgen, K. O. 2005. Bubble column reactors. *Process Biochemistry,* 40**,** 2263-2283.
Kirsch, P. 2004. Modern Fluoroorganic Chemistry, 2004. *Fluorine in Organic Chemistry*.
Lazić, Ž. R. 2004. *Design and Analysis of Experiments: Section 2.3,* Wiley Online Library.
Lousenberg, R. D. & Shoichet, M. S. 1997. Synthesis of trifluorovinyl ethers incorporating functionalized hydrocarbon ether groups: Insight into the mechanism of trifluorovinyl ether formation from trimethylsilyl 2-alkoxy-2, 3, 3, 3-tetrafluoropropionates. *The Journal of Organic Chemistry,* 62**,** 7844-7849.
Marquardt, D. W. 1963. An algorithm for least-squares estimation of nonlinear parameters. *Journal of the Society for Industrial & Applied Mathematics,* 11**,** 431-441.
Mcnair, H. M. & Miller, J. M. 2011. *Basic gas chromatography*, John Wiley & Sons.
Meyers, R. A. & Meyers, R. A. 2004. *Handbook of petroleum refining processes*, McGraw-Hill New York.
Midgley Jr, T. & Henne, A. L. 1930. Organic Fluorides as Refrigerants1. *Industrial & Engineering Chemistry,* 22**,** 542-545.
Molina, C. T. & Bouallou, C. 2012. Relationship between pH and carbonation ratio to measure CO2 capture efficiency by NH3 solvent. *Chemical Engineering Transactions,* 29**,** 421-426.
Molina, C. T. & Bouallou, C. 2013. Kinetics Study and Simulation of CO2 Absorption into Mixed Aqueous Solutions of Methyldiethanolamine and Diethanolamine. *Chemical Engineering Transactions,* 35**,** 319-314.
Montgomery, D. C. 2008. *Design and analysis of experiments*, John Wiley & Sons.
Morini, B. & Porcelli, M. 2012. TRESNEI, a Matlab trust-region solver for systems of nonlinear equalities and inequalities. *Computational Optimization and Applications,* 51**,** 27-49.
Nauman, E. B. 2008. *Chemical reactor design, optimization, and scaleup*, John Wiley & Sons.
Okazoe, T. 2009. Overview on the history of organofluorine chemistry from the viewpoint of material industry. *Proceedings of the Japan Academy. Series B, Physical and biological sciences,* 85**,** 276.
Pelchem. 2011. *Fluorochemical Expansion Initiative* [Online]. Available: http://www.pelchem.com/FEI.html [Accessed 21 January 2014].

Petrov, V. A. 2009. *Fluorinated heterocyclic compounds: synthesis, chemistry, and applications*, John Wiley & Sons.
Raal, J. & MüHlbauer, A. 1998. Phase equilibria—measurement and computation. *Taylor & Fraccis, London***,** 302-309.
Rendall, J. L. 1958. Fluorinated carbon compounds. Google Patents.
Rice, R. G. & Do, D. D. 2012. *Applied mathematics and modeling for chemical engineers*, John Wiley & Sons.
Roberson, J. & Crowe, C. 1985. *Engineering fluid mechanics*, Houghton Mifflin Company.
Roberts, G. W. 2009. *Chemical reactions and chemical reactors*, John Wiley & Sons Hoboken, NJ.
Ruckenstein, E. & Shulgin, I. 2002. Salting-out or-in by fluctuation theory. *Industrial & engineering chemistry research,* 41**,** 4674-4680.
Savitzky, A. & Golay, M. J. 1964. Smoothing and differentiation of data by simplified least squares procedures. *Analytical chemistry,* 36**,** 1627-1639.
Schiesser, W. E. & Griffiths, G. W. 2009. *A compendium of partial differential equation models: method of lines analysis with Matlab*, Cambridge University Press.
Schumpe, A. & Grund, G. 1986. The gas disengagement technique for studying gas holdup structure in bubble columns. *The Canadian Journal of Chemical Engineering,* 64**,** 891-896.
Sematech, N. 2006. Engineering statistics handbook. NIST SEMATECH.
Shampine, L. F. 1994. *Numerical solution of ordinary differential equations*, CRC Press.
Simandl, G. J. 2009. World fluorspar resources, market and deposit examples from British Columbia, Canada. *British Columbia Geological Survey, Information Circular,* 2009-4.
Smith, J., Van Ness, H. & Abbott, M. 2001. Chemical engineering thermodynamics. *McGraw-Hill, NY*.
Snow, N. & Mcnair, H. 1992. A numerical simulation of temperature-programmed gas chromatography. *Journal of chromatographic science,* 30**,** 271-275.
Sobieszuk, P. & Pohorecki, R. 2010. Gas-side mass transfer coefficients in a falling film microreactor. *Chemical Engineering and Processing: Process Intensification,* 49**,** 820-824.
Souza, A. S., Dos Santos, W. N. & Ferreira, S. L. 2005. Application of Box–Behnken design in the optimisation of an on-line pre-concentration system using knotted reactor for cadmium determination by flame atomic absorption spectrometry. *Spectrochimica Acta Part B: Atomic Spectroscopy,* 60**,** 737-742.
Spraul, B. K., Suresh, S., Jin, J. & Smith, D. W. 2006. Synthesis and electronic factors in thermal cyclodimerization of functionalized aromatic trifluorovinyl ethers. *Journal of the American Chemical Society,* 128**,** 7055-7064.
Suli, E. 2010. Numerical solution of ordinary differential equations. Oxford.
Survey, U. S. G. 2013. Mineral commodity summaries 2013. *U.S. Geological Survey*.
Takenouchi, M., Kato, R. & Nishiumi, H. 2001. Henry's law constant measurements of CCl2F2, CHClF2, CH2F2, C2ClF5, C2HF5, CH2FCF3, and CH3CHF2 in methanol, ethanol, and 2-propanol. *Journal of Chemical & Engineering Data,* 46**,** 746-749.
Teng, H. 2012. Overview of the Development of the Fluoropolymer Industry. *Applied Sciences,* 2**,** 496-512.
Tiepel, E. W. & Gubbins, K. E. 1973. Thermodynamic properties of gases dissolved in electrolyte solutions. *Industrial & Engineering Chemistry Fundamentals,* 12**,** 18-25.
Tsai, W.-T. 2005. An overview of environmental hazards and exposure risk of hydrofluorocarbons (HFCs). *Chemosphere,* 61**,** 1539-1547.

Vankayala, B. K., Löb, P., Hessel, V., Menges, G., Hofmann, C., Metzke, D., Krtschil, U. & Kost, H.-J. 2007. Scale-up of process intensifying falling film microreactors to pilot production scale. *International Journal of Chemical Reactor Engineering,* 5.

Velders, G. J., Andersen, S. O., Daniel, J. S., Fahey, D. W. & Mcfarland, M. 2007. The importance of the Montreal Protocol in protecting climate. *Proceedings of the National Academy of Sciences,* 104**,** 4814-4819.

Wojciechowski, B. & Rice, N. 2003. *Experimental methods in kinetic studies*, Elsevier.

Wouwer, A. V., Saucez, P. & Vilas, C. 2014. *Simulation of ODE/PDE Models with MATLAB, OCTAVE and SCILAB*, Springer.

Yeong, K. K., Gavriilidis, A., Zapf, R. & Hessel, V. 2003. Catalyst preparation and deactivation issues for nitrobenzene hydrogenation in a microstructured falling film reactor. *Catalysis Today,* 81**,** 641-651.

Yue, J., Chen, G., Yuan, Q., Luo, L. & Gonthier, Y. 2007. Hydrodynamics and mass transfer characteristics in gas–liquid flow through a rectangular microchannel. *Chemical Engineering Science,* 62**,** 2096-2108.

Zanfir, M., Gavriilidis, A., Wille, C. & Hessel, V. 2005. Carbon dioxide absorption in a falling film microstructured reactor: experiments and modeling. *Industrial & engineering chemistry research,* 44**,** 1742-1751.

Zhang, H., Chen, G., Yue, J. & Yuan, Q. 2009. Hydrodynamics and mass transfer of gas–liquid flow in a falling film microreactor. *AIChE journal,* 55**,** 1110-1120.

Ziegenbalg, D., Löb, P., Al-Rawashdeh, M. M., Kralisch, D., Hessel, V. & Schönfeld, F. 2010. Use of 'smart interfaces' to improve the liquid-sided mass transport in a falling film microreactor. *Chemical Engineering Science,* 65**,** 3557-3566.

APPENDICES

APPENDIX A: INSTRUMENT CALIBRATION RESULTS

A. Glass reactor instrument calibrations

Table A.1: Glass reactor nitrogen gas precision rotameter calibration data. Calibration conducted using a 200 mL bubble flow meter.

Rotameter reading	Run 1, min	Run 2, min	Run 3, min
0.2	36.0	36.0	35.6
0.4	20.5	20.4	21.0
0.6	15.5	15.8	15.4
0.8	12.0	11.7	11.8
1.0	9.9	10.1	9.6
1.2	8.2	8.5	8.2
1.4	7.3	7.3	7.5
1.6	6.3	6.3	6.3
1.8	5.7	5.6	5.6
2.0	5.3	5.4	5.2

Table A.2: Glass reactor hexafluoropropene gas precision rotameter calibration data. Calibration conducted using a 200 mL bubble flow meter.

Rotameter reading	Run 1, min	Run 2, min	Run 3, min
15	0.371	0.366	0.371
30	0.275	0.270	0.270
45	0.215	0.214	0.213
60	0.181	0.176	0.180
75	0.155	0.154	0.156
90	0.139	0.139	0.139
105	0.128	0.128	0.129
120	0.111	0.114	0.116
135	0.109	0.105	0.107
150	0.099	0.098	0.095

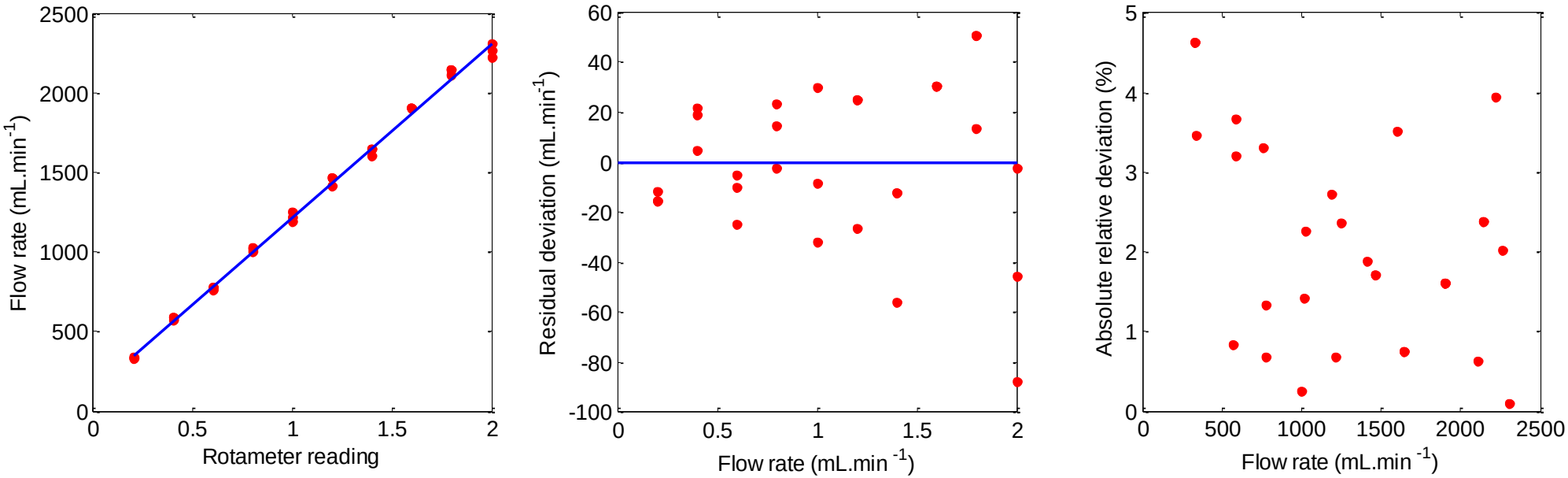

Figure A.1: Left – calibration plot of nitrogen gas precision rotameter used for the glass reactor experimental set-up. Middle – residual deviation plot defined as difference between observed and predicted flow rates of nitrogen gas. Right – Absolute relative deviation percentage versus nitrogen gas volumetric flow rate. Calibration equation was $y = 1089.5x + 130.84$, linear regression presented with a R^2 value of 0.9976. Average absolute relative deviation percentage was 2.07 %.

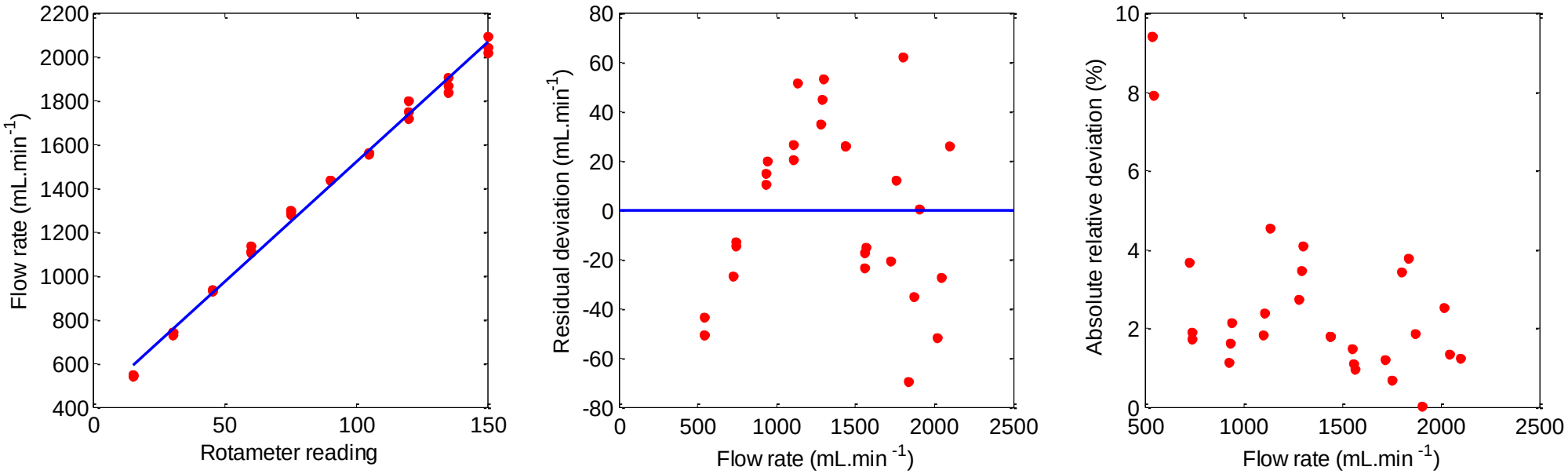

Figure A.2: Left – calibration plot of hexafluoropropene gas precision rotameter used for the glass reactor experimental set-up. Middle – residual deviation plot defined as difference between observed and predicted flow rates of hexafluoropropene gas. Right – Absolute relative deviation percentage versus hexafluoropropene gas volumetric flow rate. Calibration equation was $y = 10.980 + 424.6444$, linear regression presented with a R^2 value of 0.9946. Average absolute relative deviation percentage was 2.78 %.

Table A. 3: Raw data of temperature calibration carried out on a WIKA CTH 6500 display and CTB 9100 thermostated oil bath for gas-liquid glass reactor experimental equipment.

Standard temperature (°C)	Instrument display temperature (°C)
10	10.3
10	9.8
20	19.7
20	20.3
30	30.2
30	30.3
40	39.9
40	39.9

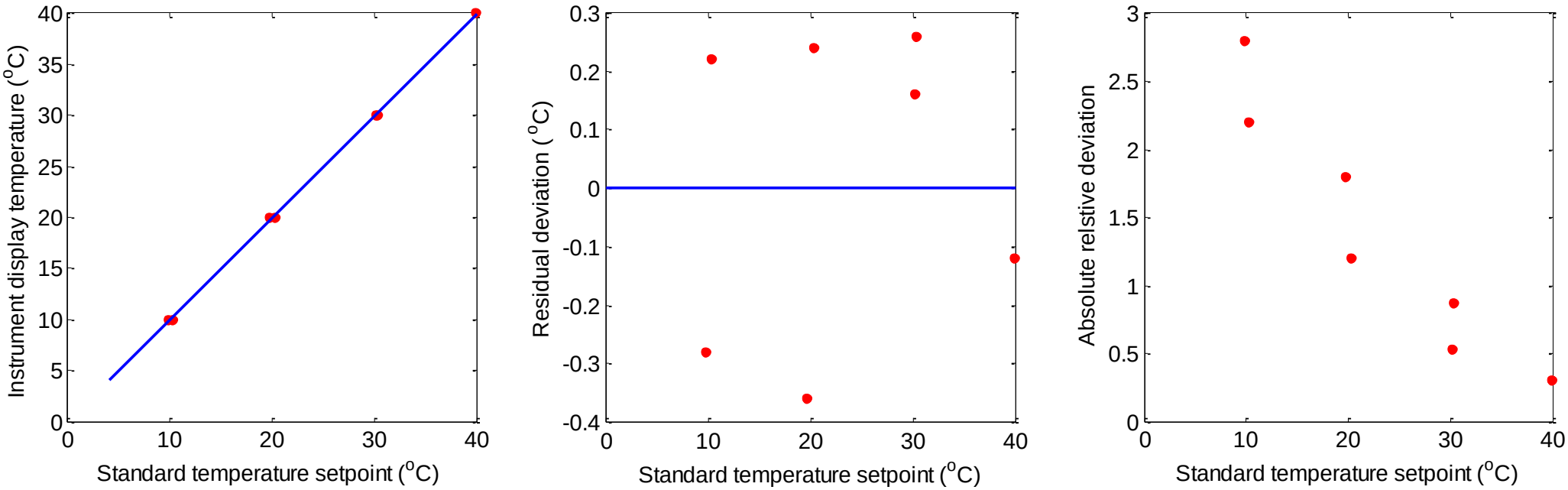

Figure A. 3: Left – calibration plot of PT 100 temperature probe used for the glass reactor experimental set-up. Middle – residual deviation plot defined as difference standard temperature bath and instrument display temperature. Right – Absolute relative deviation percentage versus standard temperature bath. Calibration equation was $y = 0.100 + 0.9980$, linear regression presented with a R^2 value of 0.9996. Average absolute relative deviation percentage was 1.25 %.

B. Falling film microreactor instrument calibrations

Table A.4: Falling film microreactor nitrogen gas precision rotameter calibration data. Calibration conducted using a 50 mL bubble flow meter.

Rotameter reading	Run 1, min	Run 2, min	Run 3, min
15	0.598	0.604	0.585
30	0.284	0.289	0.289
45	0.201	0.205	0.204
60	0.148	0.147	0.146
75	0.122	0.122	0.121

Table A.5: Falling film microreactor hexafluoropropene gas precision rotameter calibration data. Calibration conducted using a 50 mL bubble flow meter.

Rotameter reading	Run 1, min	Run 2, min	Run 3, min
15	0.531	0.543	0.529
30	0.265	0.266	0.267
45	0.187	0.188	0.188
60	0.145	0.146	0.148
75	0.120	0.119	0.120

Table A.6: Falling film microreactor hexafluoropropene oxide gas precision rotameter calibration data. Calibration conducted using a 50 mL bubble flow meter.

Rotameter reading	Run 1, min	Run 2, min	Run 3, min
15	0.488	0.492	0.494
30	0.249	0.252	0.250
45	0.179	0.180	0.181
60	0.144	0.148	0.147
75	0.122	0.121	0.122

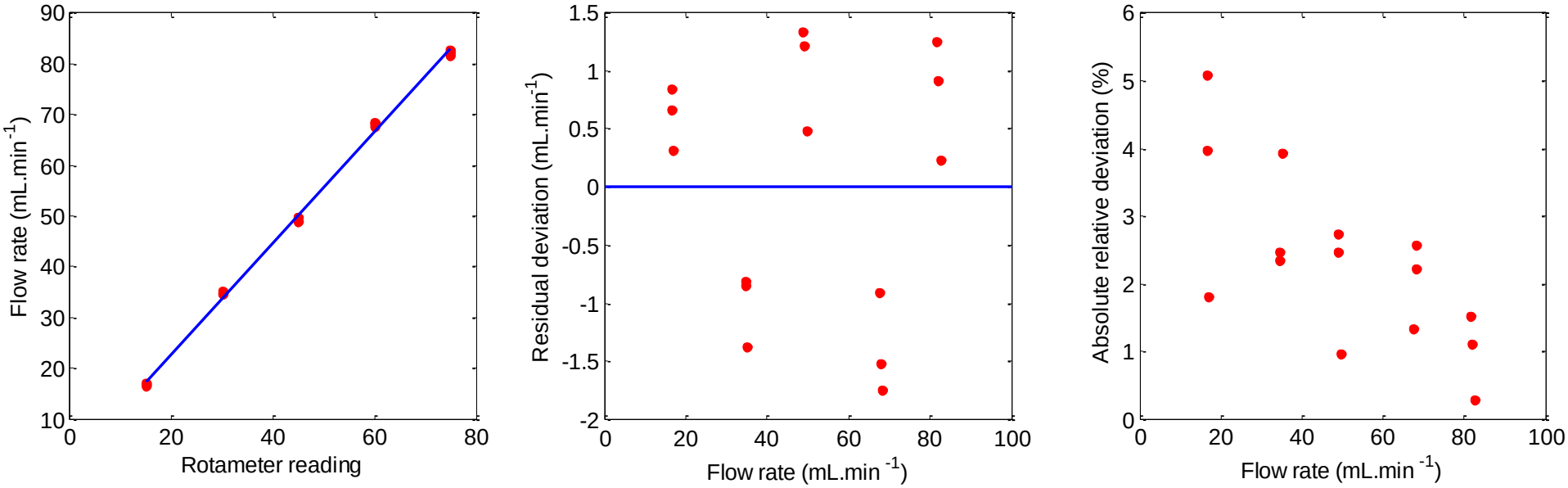

Figure A.4: Left – calibration plot of nitrogen gas precision rotameter used for the falling film microreactor experimental set-up. Middle – residual deviation plot defined as difference between observed and predicted flow rates of nitrogen gas. Right – Absolute relative deviation percentage versus nitrogen gas volumetric flow rate. Calibration equation was $y = 1.0932x + 0.9938$, linear regression presented with a R^2 value of 0.9979. Average absolute relative deviation percentage was 2.32 %.

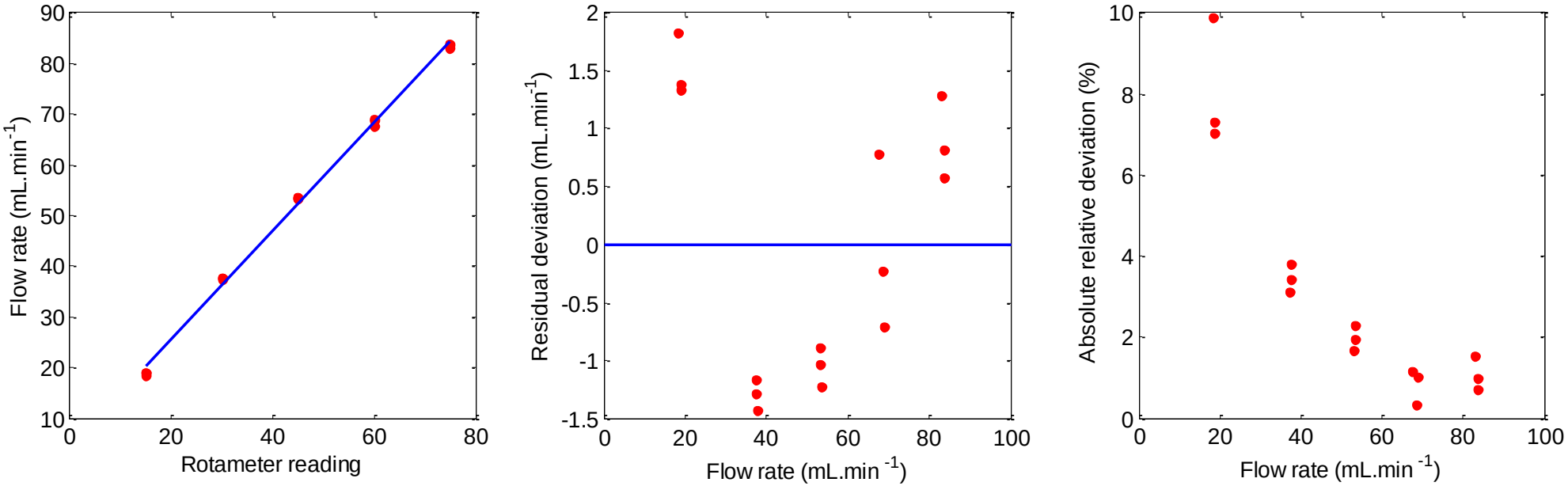

Figure A.5: Left – calibration plot of hexafluoropropene gas precision rotameter used for the falling film microreactor experimental set-up. Middle – residual deviation plot defined as difference between observed and predicted flow rates of hexafluoropropene gas. Right – Absolute relative deviation percentage versus hexafluoropropene gas volumetric flow rate. Calibration equation was $y = 1.0692x + 4.1864$, linear regression presented with a R^2 value of 0.9975. Average absolute relative deviation percentage was 3.07 %.

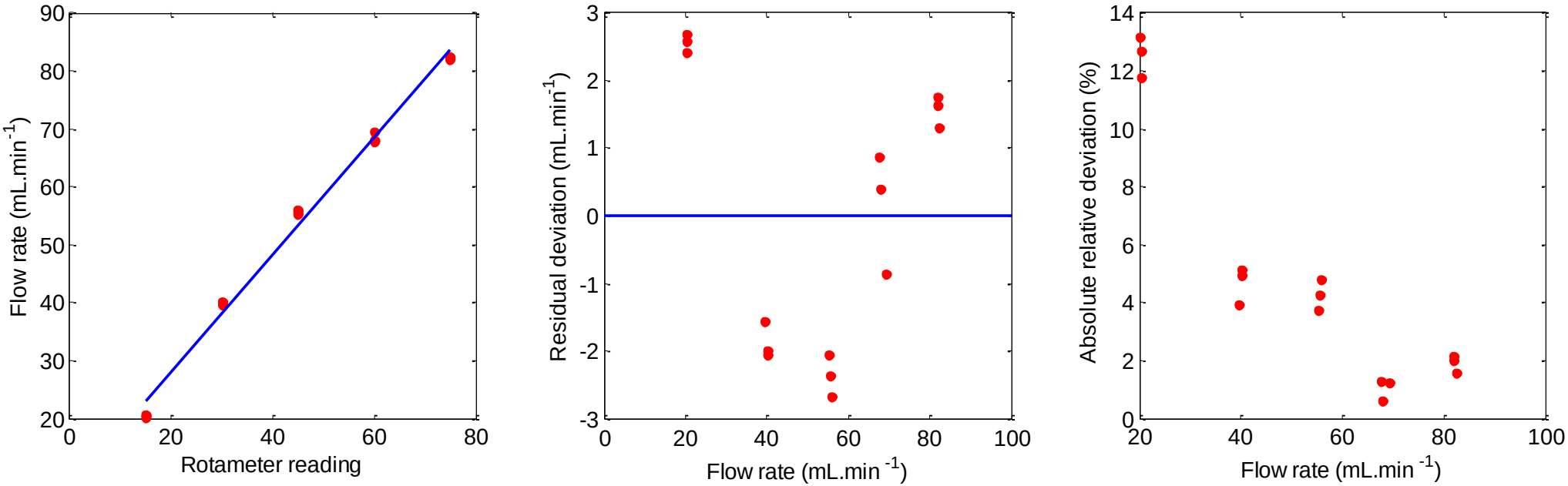

Figure A.6: Left – calibration plot of hexafluoropropene oxide gas precision rotameter used for the falling film microreactor experimental set-up. Middle – residual deviation plot defined as difference between observed and predicted flow rates of hexafluoropropene oxide gas. Right – Absolute relative deviation percentage versus hexafluoropropene oxide gas volumetric flow rate. Calibration equation was $y = 1.0135x + 7.6911$, linear regression presented with a R^2 value of 0.9920. Average absolute relative deviation percentage was 4.87 %.

APPENDIX B: GAS CHROMATOGRAPHY CALIBRATION PLOTS

Table B.1: Raw 1,1,2,3,3,3-hexafluoropropyl methyl ether (HME) gas chromatograph calibration data for the internal standard (IS) quantification method. *n*-Propanol was used as the internal standard.

Sample mass ratio $\left(\frac{M_{HME}}{M_{IS}}\right)$	Observed area ratios $\left(\frac{A_{HME}}{A_{IS}}\right)$		
	Run 1	Run 2	Run 3
15.064	0.018	4.897	0.019
7.861	0.034	2.555	0.034
5.209	0.048	1.790	0.048
3.941	0.067	1.282	0.067
3.193	0.087	0.995	0.086

Table B.2: Raw methyl-2,3,3,3-tetrafluoro-2-methoxypropionate (MTFMP) gas chromatograph calibration data for the internal standard (IS) quantification method. *n*-Propanol was used as the internal standard.

Sample mass ratio $\left(\frac{M_{MTFMP}}{M_{IS}}\right)$	Observed area ratios $\left(\frac{A_{MTFMP}}{A_{IS}}\right)$		
	Run 1	Run 2	Run 3
0.279	0.0617	0.0606	0.0607
0.209	0.0442	0.0447	0.0443
0.103	0.0217	0.0213	0.0216
0.135	0.0282	0.0278	0.0281
0.016	0.0028	0.0026	0.0027

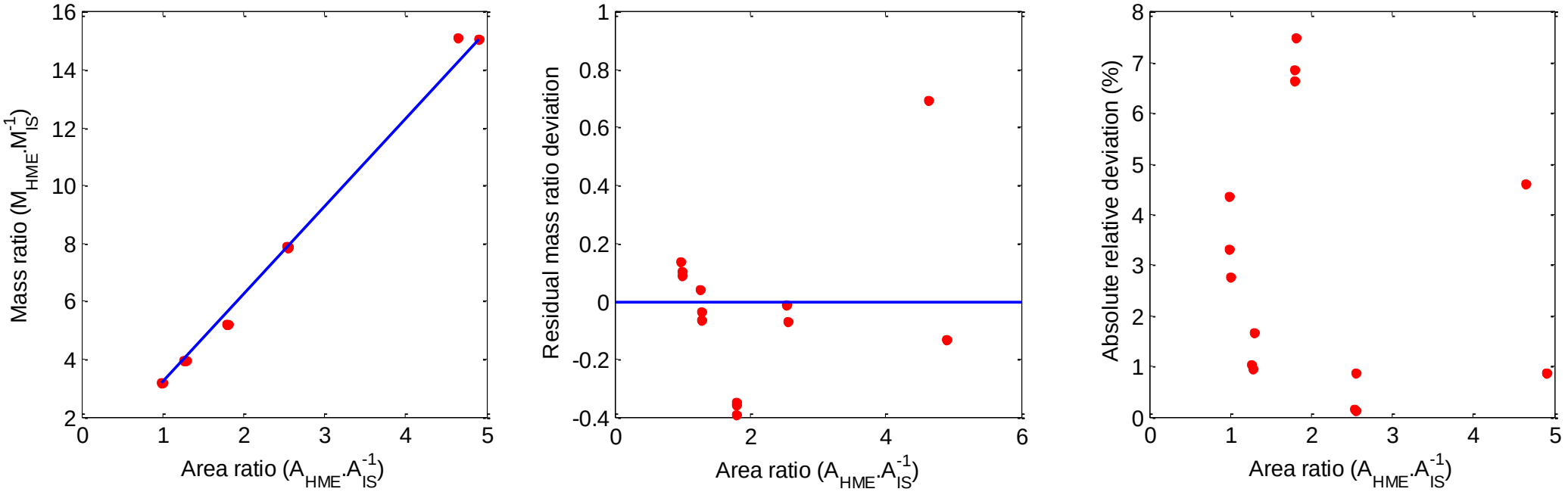

Figure B.1: Left - 1,1,2,3,3,3-hexafluoropropyl methyl ether (HME) gas chromatograph calibration plot for the internal standard quantification (IS) method on a Shimadzu 2010 GC using a Restek® capillary column (30 m × 0.25 mm) coated with in a 0.25μm layer of polyethylene glycol with helium as the carrier gas. Middle – residual deviation plot defined as difference between observed and predicted mass ratios of HME to internal standard. Right – absolute relative percentage deviation plot versus HME and IS area ratio. Calibration equation was $y = 3.1028x$, linear regression presented with a R^2 value of 0.9965. Average absolute relative deviation percentage was 2.83 %.

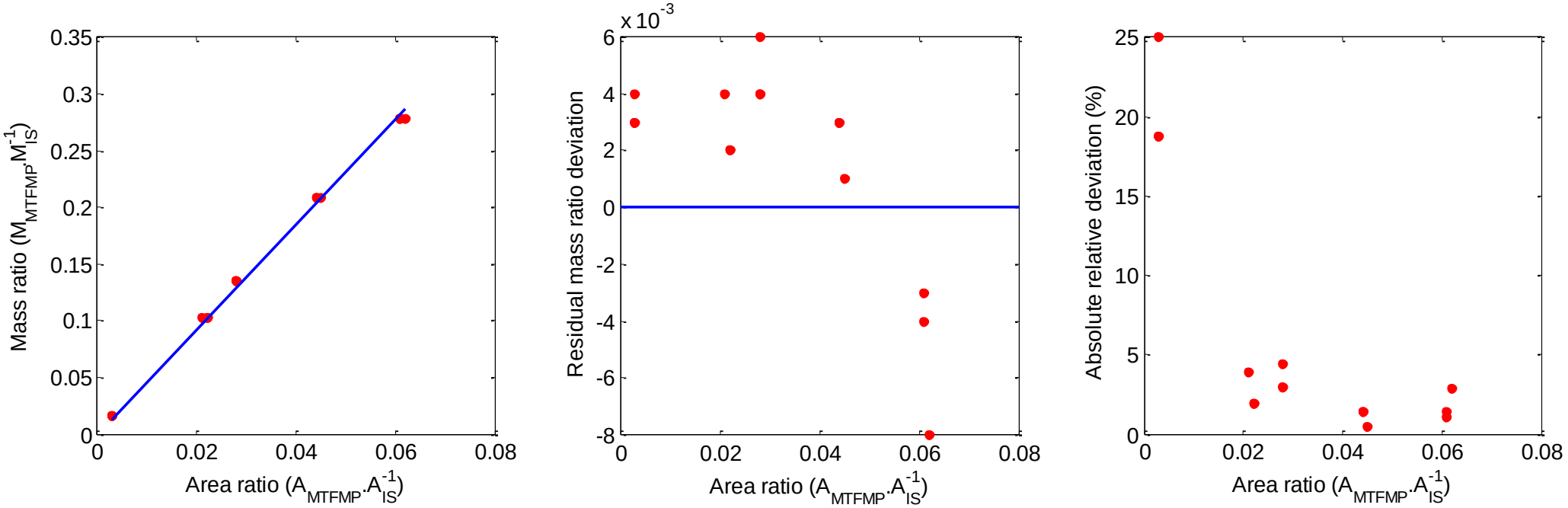

Figure B.2: Left - methyl-2,3,3,3-tetrafluoro-2-methoxypropionate (MTFMP) gas chromatograph calibration plot for the internal standard (IS) quantification method on a Shimadzu 2010 GC using a Restek® capillary column (30 m × 0.25 mm) coated with in a 0.25μm layer of polyethylene glycol with helium as the carrier gas. Middle – residual deviation plot defined as difference between observed and predicted mass ratios of MTFMP to internal standard. Right – absolute relative deviation versus MTFMP and IS area ratio. Calibration equation was $y = 4.6595x$, linear regression presented with a R^2 value of 0.9981. Average absolute relative deviation percentage was 5.96 %.

APPENDIX C: RAW DATA

A. Preliminary experiments

Table C.1: Gas-chromatograph raw data for preliminary experiments on semi-batch gas-liquid stirred tank reactor for the for 1,1,2,3,3,3-hexafluoropropyl methyl ether.

Peak	Exp.	Methanol	HME	AE	IS	AT	Exp.	Methanol	HME	AE	IS	AT
Retention time (min)	1	1.687	1.788	1.863	2.648	4.825	11	1.756	1.849	1.972	2.635	4.721
Area		30791260	2187233	22886.7	62825516	122476.4		33187126	2318326	1230.6	43059325	168550.4
Retention time (min)	2	1.736	1.846	1.922	2.688	4.87	12	1.759	1.848	1.924	2.638	4.718
Area		23381626	2397549	9401.3	58375715	128290.6		34577721	1382301	5774.5	41671095	106517.9
Retention time (min)	3	1.752	1.845	1.918	2.638	4.719	13	1.752	1.837	1.912	2.644	4.715
Area		35853510	2481284	3954.2	45474791	192621.7		37497624	2262419	4301.2	45762361	160886.8
Retention time (min)	4	1.747	1.84	1.913	2.625	4.716	14	1.753	1.844	1.928	2.638	4.715
Area		35007550	2682710	3633.6	43704242	198805.5		34601665	1692113	10136.5	43721577	138236.8
Retention time (min)	5	1.742	1.842	1.916	2.609	4.712	15	1.727	1.817	1.892	2.609	4.7
Area		36196887	1138576	35456.7	43520502	110126.1		35445073	1971266	7143.7	44491550	161416.5
Retention time (min)	6	1.765	1.847	1.922	2.638	4.718	16	1.74	1.844	1.92	2.601	4.706
Area		41288017	1267618	19505.3	42940190	86544.1		28734413	1281436	2462.4	37597565	92671.8
Retention time (min)	7	1.76	1.849	1.923	2.643	4.718	17	1.752	1.842	1.917	2.639	4.713
Area		34586030	1448695	5114	42663106	107981.4		36628777	1386176	11071.4	45504012	114063.2
Retention time (min)	8	1.765	1.848	1.923	2.651	4.722	18	1.727	1.821	1.938	2.67	4.839
Area		39851960	1844951	4678.4	45764987	150071.6		32769871	1569309	27761.9	61332653	151955.9
Retention time (min)	9	1.756	1.848	1.924	2.628	4.714	19	1.773	1.836	1.91	2.379	4.843
Area		35966736	1083800	19444.3	43791746	85936.9		53687111	2566569	141835.7	974303	184541.3
Retention time (min)	10	1.75	1.842	1.917	2.623	4.717	20	1.755	1.836	1.911	2.519	4.841
Area		34640547	2454041	9623.9	42642346	191787.1		43201080	1858437	89960.1	21599554	148849.6

Table C.2: Extended results for 1,1,2,3,3,3-hexafluoropropyl methyl ether (HME) preliminary experiments on semi-batch gas-liquid stirred tank reactor, HME analysis.

Exp. No.	Crude mass in sample (g)	IS mass in sample (g)	HME mass in sample(g)	HME mass fraction in sample	Total mass of reactor crude (g)	Mass HME in crude (g)	Moles HME	Volumetric flow rate HFP ($m^3 \cdot s^{-1} \times 10^5$)	Moles HFP	Yield %
1	0.740	0.766	0.083	0.112	1301.10	145.486	0.799 ± 0.0044	2.168	1.596	49.76 ± 1.60
2	0.837	0.783	0.100	0.119	1296.44	154.553	0.849 ± 0.0040	2.168	1.596	53.32 ± 1.69
3	0.854	0.471	0.080	0.093	1282.79	119.778	0.658 ± 0.0023	2.168	1.596	40.58 ± 1.30
4	0.857	0.475	0.090	0.106	1355.76	143.12	0.786 ± 0.0025	2.168	1.596	48.78 ± 1.56
5	0.849	0.480	0.039	0.046	1236.31	56.739	0.312 ± 0.0023	1.442	1.061	29.46 ± 1.41
6	0.822	0.475	0.044	0.053	1237.70	65.511	0.360 ± 0.0023	1.442	1.061	33.62 ± 1.62
7	0.811	0.484	0.051	0.063	1277.25	80.312	0.441 ± 0.0025	1.442	1.061	41.00 ± 1.98
8	0.832	0.473	0.059	0.071	1258.95	89.526	0.492 ± 0.0024	1.442	1.061	46.08 ± 2.20
9	0.831	0.479	0.037	0.044	1242.99	55.019	0.302 ± 0.0023	1.194	0.879	35.02 ± 1.98
10	0.844	0.470	0.084	0.099	1331.31	132.382	0.727 ± 0.0025	2.416	1.778	41.07 ± 1.16
11	0.833	0.489	0.082	0.098	1121.74	110.006	0.604 ± 0.0022	1.805	1.329	45.50 ± 1.73
12	0.827	0.465	0.048	0.058	1153.19	66.737	0.367 ± 0.0022	1.805	1.329	26.99 ± 1.06
13	0.828	0.471	0.072	0.087	1098.06	95.815	0.526 ± 0.0021	1.805	1.329	39.80 ± 1.51
14	0.834	0.484	0.058	0.070	1257.95	87.666	0.482 ± 0.0024	1.805	1.329	36.48 ± 1.38
15	0.823	0.477	0.066	0.080	1279.69	101.964	0.560 ± 0.0025	1.805	1.329	41.68 ± 1.61
16	0.831	0.478	0.051	0.061	1315.23	80.005	0.440 ± 0.0025	1.805	1.329	32.64 ± 1.27
17	0.827	0.490	0.046	0.056	1278.31	71.590	0.393 ± 0.0025	1.805	1.329	28.11 ± 1.14
18	0.921	0.487	0.039	0.042	1106.06	46.455	0.255 ± 0.0019	1.805	1.329	19.21 ± 0.74
19	0.839	0.479	0.052	0.062	1291.43	80.068	0.440 ± 0.0024	1.805	1.329	33.11 ± 1.26
20	0.977	0.489	0.058	0.059	1022.63	60.335	0.332 ± 0.0017	1.805	1.329	24.95 ± 0.95

Table C.3: Extended results for 1,1,2,3,3,3-hexafluoropropyl methyl ether (HME) preliminary experiments on semi-batch gas-liquid stirred tank reactor, alkenyl ether (AE) analysis.

Exp. No.	Crude mass in sample (g)	IS mass in sample (g)	AE mass in sample (g)	AE mass fraction in sample	Total mass of reactor crude (g)	Mass AE in crude (g)	Moles AE	Volumetric flow rate HFP ($m^3 \cdot s^{-1} \times 10^5$)	Moles HFP	Yield %
1	0.740	0.766	0.00087	0.00117	1301.1	1.522	0.009	2.168	1.596	0.59 ± 0.43
2	0.837	0.783	0.00039	0.00047	1296.44	0.606	0.004	2.168	1.596	0.23 ± 0.96
3	0.854	0.471	0.00013	0.00015	1282.79	0.191	0.001	2.168	1.596	0.07 ± 1.71
4	0.857	0.475	0.00012	0.00014	1355.76	0.194	0.001	2.168	1.596	0.07 ± 1.93
5	0.849	0.480	0.00121	0.00143	1236.31	1.767	0.011	1.442	1.061	1.03 ± 0.13
6	0.822	0.475	0.00067	0.00081	1237.7	1.008	0.006	1.442	1.061	0.59 ± 0.23
7	0.811	0.484	0.00018	0.00022	1277.25	0.284	0.002	1.442	1.061	0.16 ± 0.86
8	0.832	0.473	0.00015	0.00018	1258.95	0.227	0.001	1.442	1.061	0.13 ± 1.03
9	0.831	0.479	0.00066	0.00079	1242.99	0.987	0.006	1.194	0.879	0.69 ± 0.19
10	0.844	0.470	0.00033	0.00039	1331.31	0.519	0.003	2.416	1.778	0.18 ± 0.75
11	0.833	0.489	0.00004	0.00005	1121.74	0.058	0.000	1.805	1.329	0.03 ± 0.43
12	0.827	0.465	0.00020	0.00024	1153.19	0.279	0.002	1.805	1.329	0.13 ± 0.92
13	0.828	0.471	0.00014	0.00017	1098.06	0.182	0.001	1.805	1.329	0.08 ± 1.43
14	0.834	0.484	0.00035	0.00042	1257.95	0.525	0.003	1.805	1.329	0.24 ± 0.56
15	0.823	0.477	0.00024	0.00029	1279.69	0.370	0.002	1.805	1.329	0.17 ± 0.80
16	0.831	0.478	0.00010	0.00012	1315.23	0.154	0.001	1.805	1.329	0.07 ± 1.84
17	0.827	0.490	0.00037	0.00045	1278.31	0.572	0.004	1.805	1.329	0.27 ± 0.54
18	0.921	0.487	0.00068	0.00074	1106.06	1.485	0.009	1.805	1.329	0.69 ± 0.29
19	0.839	0.479	0.00018	0.00021	1291.43	0.474	0.003	1.805	1.329	0.22 ± 1.07
20	0.977	0.489	0.00015	0.00016	1022.63	0.947	0.006	1.805	1.329	0.44 ± 1.29

Table C.4: Extended results for 1,1,2,3,3,3-hexafluoropropyl methyl ether (HME) preliminary experiments on semi-batch gas-liquid stirred tank reactor, alkyl tetrafluoropropionate (AT) analysis.

Exp. No.	Crude mass in sample (g)	IS mass in sample (g)	AT mass in sample (g)	AT mass fraction in sample	Total mass of reactor crude (g)	Mass AT in crude (g)	Moles AT	Volumetric flow rate HFP ($m^3 \cdot s^{-1} \times 10^5$)	Moles HFP	Yield %
1	0.740	0.766	0.005	0.006	1301.100	8.147	0.051	2.168	1.596	3.19 ± 0.27
2	0.837	0.783	0.005	0.006	1296.440	8.270	0.052	2.168	1.596	3.24 ± 0.78
3	0.854	0.471	0.006	0.007	1282.790	9.298	0.058	2.168	1.596	3.64 ± 0.23
4	0.857	0.475	0.007	0.008	1355.760	10.606	0.066	2.168	1.596	4.15 ± 0.49
5	0.849	0.480	0.004	0.004	1236.310	5.488	0.034	1.442	1.061	3.23 ± 0.33
6	0.822	0.475	0.003	0.004	1237.700	4.473	0.028	1.442	1.061	2.63 ± 0.59
7	0.811	0.484	0.004	0.005	1277.250	5.986	0.037	1.442	1.061	3.53 ± 0.53
8	0.832	0.473	0.005	0.006	1258.950	7.282	0.046	1.442	1.061	4.29 ± 0.15
9	0.831	0.479	0.003	0.004	1242.990	4.363	0.027	1.194	0.879	3.10 ± 0.37
10	0.844	0.470	0.007	0.008	1331.310	10.346	0.065	2.416	1.778	3.64 ± 0.64
11	0.833	0.489	0.006	0.007	1121.740	7.998	0.050	1.805	1.329	3.76 ± 0.19
12	0.827	0.465	0.004	0.004	1153.190	5.143	0.032	1.805	1.329	2.42 ± 0.38
13	0.828	0.471	0.005	0.006	1098.060	6.814	0.043	1.805	1.329	3.21 ± 0.29
14	0.834	0.484	0.005	0.006	1257.950	7.162	0.045	1.805	1.329	3.37 ± 0.63
15	0.823	0.477	0.005	0.007	1279.690	8.349	0.052	1.805	1.329	3.93 ± 0.16
16	0.831	0.478	0.004	0.004	1315.230	5.786	0.036	1.805	1.329	2.72 ± 0.37
17	0.827	0.490	0.004	0.005	1278.310	5.891	0.037	1.805	1.329	2.77 ± 0.31
18	0.921	0.487	0.007	0.007	1106.060	8.142	0.051	1.805	1.329	3.83 ± 0.57
19	0.839	0.479	0.007	0.008	1291.430	10.842	0.068	1.805	1.329	5.10 ± 0.32
20	0.977	0.489	0.009	0.010	1022.630	9.843	0.062	1.805	1.329	4.63 ± 0.23

B. FFMR experiments

Table C.5: Gas-chromatograph raw data for central composite design experiments on the falling film micro reactor for the 1,1,2,3,3,3-hexafluoropropyl methyl ether system.

Peak	Exp.	Methanol	HME	AE	IS	AT	Exp.	Methanol	HME	AE	IS	AT
Retention time (min)	1	1.673	1.794	1.908	2.736	4.678	16	1.72	1.802	1.876	2.647	4.679
Area		21293996.3	869239.2	21312.3	91060869.1	72168.6		42014194	1776040.7	98011.1	58150447	130400.2
Retention time (min)	2	1.776	1.846	1.967	2.704	4.712	17	1.771	1.846	1.92	2.622	4.711
Area		49844591.4	843401.6	60816.5	61369356.2	64758.3		46101651.7	2241694.1	165510.6	39646601	163862.9
Retention time (min)	3	1.731	1.839	1.914	2.717	4.712	18	1.748	1.845	1.92	2.741	4.71
Area		30197238.3	3128922.4	154090.6	70605718.4	283055.5		32136517.5	1487109	83803.1	71768546	95087.4
Retention time (min)	4	1.724	1.827	1.903	2.643	4.691	19	1.765	1.845	1.92	2.648	4.712
Area		29680879.7	1422856.8	155495.1	52764606.4	111192.2		43601434.4	2039559.9	183435.7	46912208	151937.6
Retention time (min)	5	1.756	1.839	1.913	2.647	4.697	20	1.775	1.848	1.922	2.633	4.712
Area		40714566.6	1283328.9	76147.2	50257327.9	122171		48402053.9	2298137.9	117901.8	42445449	169156.8
Retention time (min)	6	1.758	1.833	1.909	2.635	4.693	21	1.774	1.845	1.921	2.68	4.709
Area		45623541.7	726639.5	45927	46787149.3	52382		48550022.8	432309.1	20763.2	55403613	35498.6
Retention time (min)	7	1.761	1.839	1.912	2.64	4.711	22	1.761	1.845	1.918	2.601	4.716
Area		45731932.8	3719685	257594.4	48187840.8	399379.3		42227503.8	3881094.5	301873.2	37747871	304608.9
Retention time (min)	8	1.761	1.838	1.912	2.653	4.701	23	1.757	1.848	1.919	2.625	4.705
Area		46390396.9	2084437.1	114602.7	52222868.4	144579.4		38581694.5	6796454.6	602873.3	43999914	157387.1
Retention time (min)	9	1.755	1.845	1.92	2.712	4.711	24	1.751	1.84	1.917	2.6	4.703
Area		36594410.5	1998944	148549.3	64442036.9	141880.1		40054499.1	1027974.1	31076.5	38957539	70530
Retention time (min)	10	1.774	1.846	1.921	2.657	4.714	25	1.77	1.846	1.921	2.616	4.707
Area		46998705.8	849626	22497.3	48394794.3	56839.3		46068482.6	2092604.9	37190.4	39748622	165785.4
Retention time (min)	11	1.72	1.802	1.876	2.647	4.679	26	1.769	1.845	1.919	2.619	4.708
Area		42014194	1776040.7	98011.1	58150446.9	130400.2		45420818.1	1805675.3	123093.9	40498884	169682.2
Retention time (min)	12	1.771	1.846	1.92	2.622	4.711	27	1.682	1.757	1.83	2.557	4.658
Area		46101651.7	2241694.1	165510.6	39646600.8	163862.9		45694862.8	2129188.9	163079.8	45693588	156960.1
Retention time (min)	13	1.748	1.845	1.92	2.741	4.71	28	1.732	1.817	1.892	2.563	4.685
Area		32136517.5	1487109	83803.1	71768546.2	95087.4		39114151	1993585.3	109297.4	35034881	151658.8
Retention time (min)	14	1.765	1.845	1.92	2.648	4.712	29	1.746	1.845	1.921	2.607	4.702
Area		43601434.4	2039559.9	183435.7	46912208.4	151937.6		40824035.9	1940662.7	69702	45095598	149234.2
Retention time (min)	15	1.775	1.848	1.922	2.633	4.712	30	1.762	1.828	1.901	2.601	4.706
Area		48402053.9	2298137.9	117901.8	42445449.1	169156.8		55193550.9	2703052.1	154049.5	39335672	201576.6

Table C.6: Extended results for 1,1,2,3,3,3-hexafluoropropyl methyl ether (HME) central composite design experiments on falling film microreactor, HME analysis.

Exp. No.	Crude mass in sample (g)	IS mass in sample (g)	HME mass in sample (g)	HME mass fraction in sample	Total mass of reactor crude (g)	Mass HME in crude (g)	Moles HME	Volumetric flow rate HFP ($m^3 \cdot s^{-1} \times 10^6$)	Moles HFP	HME Concentration ($mol \cdot m^{-3}$)	Yield %
1	0.953	0.557	0.016	0.017	46.265	0.801	$0.126 \pm 7.74\times10^{-5}$	0.515	0.038	83.83	11.60 ± 0.30
2	0.731	0.518	0.022	0.030	110.398	3.336	$0.216 \pm 2.49\times10^{-4}$	0.515	0.038	143.76	48.32 ± 1.05
3	0.798	0.683	0.094	0.118	46.456	5.468	$0.858 \pm 1.33\times10^{-4}$	1.050	0.077	572.29	38.88 ± 0.36
4	0.769	0.605	0.051	0.066	121.662	8.009	$0.518 \pm 3.16\times10^{-4}$	1.050	0.077	345.12	56.93 ± 0.62
5	0.910	0.563	0.045	0.049	46.643	2.286	$0.359 \pm 9.70\times10^{-5}$	0.515	0.038	239.28	33.12 ± 0.61
6	1.021	0.500	0.024	0.024	116.373	2.746	$0.178 \pm 1.81\times10^{-4}$	0.515	0.038	118.35	39.78 ± 0.82
7	1.067	0.519	0.124	0.116	98.509	11.476	$0.621 \pm 1.62\times10^{-4}$	1.050	0.077	414.29	42.21 ± 0.71
8	0.954	0.504	0.062	0.065	50.157	3.282	$0.433 \pm 8.76\times10^{-5}$	1.050	0.077	288.81	71.47 ± 0.22
9	0.864	0.536	0.052	0.060	49.647	2.964	$0.465 \pm 1.00\times10^{-4}$	0.515	0.038	310.24	42.94 ± 0.77
10	0.894	0.507	0.028	0.031	111.395	3.441	$0.222 \pm 2.04\times10^{-4}$	0.515	0.038	148.30	49.85 ± 1.00
11	0.960	0.502	0.113	0.118	48.047	5.680	$0.892 \pm 8.39\times10^{-5}$	1.050	0.077	594.43	40.38 ± 0.35
12	0.947	0.558	0.060	0.063	116.107	7.365	$0.476 \pm 2.22\times10^{-4}$	1.050	0.077	317.37	52.36 ± 0.52
13	0.950	0.593	0.046	0.049	42.266	2.064	$0.324 \pm 8.53\times10^{-5}$	0.515	0.038	216.04	29.90 ± 0.55
14	0.872	0.474	0.019	0.022	116.113	2.587	$0.167 \pm 2.08\times10^{-4}$	0.515	0.038	111.50	37.48 ± 0.84
15	1.007	0.484	0.114	0.113	46.372	5.263	$0.826 \pm 7.56\times10^{-5}$	1.050	0.077	550.78	37.41 ± 0.32
16	0.851	0.489	0.046	0.054	121.106	6.595	$0.426 \pm 2.26\times10^{-4}$	1.050	0.077	284.20	46.88 ± 0.49
17	1.062	0.452	0.079	0.075	86.407	6.452	$0.591 \pm 1.20\times10^{-4}$	0.783	0.058	393.89	61.53 ± 0.71
18	0.706	0.708	0.046	0.064	84.174	5.427	$0.497 \pm 2.77\times10^{-4}$	0.783	0.058	331.33	51.76 ± 0.75
19	0.956	0.482	0.065	0.068	82.165	5.588	$0.512 \pm 1.41\times10^{-4}$	0.783	0.058	341.17	53.30 ± 0.64
20	1.096	0.356	0.060	0.055	85.941	4.690	$0.429 \pm 9.43\times10^{-5}$	0.783	0.058	286.30	44.73 ± 0.52
21	0.954	0.565	0.014	0.014	80.883	1.160	$0.106 \pm 1.45\times10^{-4}$	0.248	0.018	70.80	34.91 ± 1.48
22	1.151	0.437	0.139	0.121	89.847	10.882	$0.997 \pm 1.18\times10^{-4}$	1.317	0.097	664.37	61.67 ± 0.42
23	1.191	0.424	0.203	0.171	17.484	2.983	$1.639 \pm 2.20\times10^{-5}$	0.783	0.058	1092.74	28.45 ± 0.32
24	1.022	0.482	0.039	0.039	149.696	5.780	$0.289 \pm 2.39\times10^{-4}$	0.783	0.058	192.48	55.13 ± 0.74
25	1.053	0.418	0.068	0.065	84.044	5.450	$0.499 \pm 1.11\times10^{-4}$	0.783	0.058	332.71	51.98 ± 0.61
26	1.097	0.290	0.078	0.071	55.530	3.873	$0.355 \pm 4.80\times10^{-5}$	0.783	0.038	236.43	55.40 ± 0.63
27	1.039	0.506	0.073	0.070	88.517	6.233	$0.571 \pm 1.41\times10^{-4}$	0.783	0.058	380.51	59.44 ± 0.70
28	1.112	0.402	0.071	0.064	87.964	5.615	$0.514 \pm 1.07\times10^{-4}$	0.783	0.058	342.77	53.55 ± 0.62
29	0.950	0.487	0.065	0.068	104.157	7.130	$0.653 \pm 1.77\times10^{-4}$	0.783	0.071	435.26	55.13 ± 0.66
30	1.106	0.378	0.081	0.073	85.405	6.224	$0.570 \pm 9.71\times10^{-5}$	0.783	0.058	379.95	59.36 ± 0.68

Table C.7: Extended results for 1,1,2,3,3,3-hexafluoropropyl methyl ether (HME) central composite design experiments on falling film microreactor, alkenyl ether (AE) analysis.

Exp. No.	Crude mass in sample (g)	IS mass in sample (g)	AE mass in sample (g)	AE mass fraction in sample	Total mass of reactor crude (g)	Mass AE in crude (g)	Moles AE	Volumetric flow rate HFP ($m^3 \cdot s^{-1} \times 10^6$)	Moles HFP	AE Concentration ($mol \cdot m^{-3}$)	Yield %	Reynolds Number	Flow Regime
1	0.953	0.557	0	0	46.265	0.02	0.0001	0.515	0.038	0.32	0.32 ± 0.25	6.30	Laminar
2	0.731	0.518	0.002	0.002	110.398	0.241	0.0015	0.515	0.038	3.91	3.91 ± 0.76	15.30	Laminar
3	0.798	0.683	0.005	0.006	46.456	0.269	0.0017	1.05	0.077	2.15	2.15 ± 0.20	6.30	Laminar
4	0.769	0.605	0.006	0.007	121.662	0.875	0.0054	1.05	0.077	6.99	6.99 ± 0.46	15.30	Laminar
5	0.91	0.563	0.003	0.003	46.643	0.136	0.0008	0.515	0.038	2.21	2.21 ± 0.28	6.30	Laminar
6	1.021	0.5	0.002	0.001	116.373	0.174	0.0011	0.515	0.038	2.82	2.82 ± 0.55	15.30	Laminar
7	1.067	0.519	0.009	0.008	98.509	0.795	0.0049	1.05	0.077	6.35	0.11 ± 0.23	6.30	Laminar
8	0.954	0.504	0.003	0.004	50.157	0.18	0.0011	1.05	0.077	1.44	0.65 ± 0.12	15.30	Laminar
9	0.864	0.536	0.004	0.004	49.647	0.22	0.0014	0.515	0.038	3.58	3.58 ± 0.31	7.30	Laminar
10	0.894	0.507	0.001	0.001	111.395	0.091	0.0006	0.515	0.038	1.48	1.48 ± 0.63	17.74	Laminar
11	0.96	0.502	0.008	0.008	48.047	0.377	0.0023	1.05	0.077	3.01	3.01 ± 0.12	7.30	Laminar
12	0.947	0.558	0.002	0.002	116.107	0.2	0.0012	1.05	0.077	1.6	1.60 ± 0.33	17.74	Laminar
13	0.95	0.593	0.001	0.002	42.266	0.064	0.0004	0.515	0.038	1.04	1.04 ± 0.25	7.30	Laminar
14	0.872	0.474	0.001	0.001	116.113	0.106	0.0007	0.515	0.038	1.73	1.73 ± 0.61	17.74	Laminar
15	1.007	0.484	0.007	0.007	46.372	0.306	0.0019	1.05	0.077	2.44	2.44 ± 0.11	7.30	Laminar
16	0.851	0.489	0.003	0.003	121.106	0.364	0.0023	1.05	0.077	2.91	2.91 ± 0.33	17.74	Laminar
17	1.062	0.452	0.006	0.006	86.407	0.476	0.0029	0.783	0.058	5.1	5.10 ± 0.24	9.98	Laminar
18	0.706	0.708	0.003	0.004	84.174	0.306	0.0019	0.783	0.058	3.28	3.28 ± 0.55	13.42	Laminar
19	0.956	0.482	0.006	0.006	82.165	0.503	0.0031	0.783	0.058	5.39	5.39 ± 0.27	11.65	Laminar
20	1.096	0.356	0.003	0.003	85.941	0.241	0.0015	0.783	0.058	2.58	2.58 ± 0.18	11.65	Laminar
21	0.954	0.565	0.001	0.001	80.883	0.056	0.0003	0.248	0.018	1.88	1.88 ± 1.00	11.65	Laminar
22	1.151	0.437	0.011	0.009	89.847	0.846	0.0052	1.317	0.097	5.39	5.39 ± 0.14	11.65	Laminar
23	1.191	0.424	0.018	0.015	17.484	0.265	0.0016	0.783	0.058	2.84	2.84 ± 0.05	1.94	Laminar
24	1.022	0.482	0.001	0.001	149.696	0.175	0.0011	0.783	0.058	1.87	1.87 ± 0.46	21.35	Laminar
25	1.053	0.418	0.001	0.001	84.044	0.097	0.0006	0.783	0.058	1.04	3.37 ± 0.21	11.65	Laminar
26	1.106	0.383	0.004	0.003	55.53	0.266	0.0016	0.783	0.058	2.85	0.44 ± 0.18	11.65	Laminar
27	1.039	0.506	0.006	0.005	88.517	0.477	0.003	0.783	0.058	5.12	5.12 ± 0.28	11.65	Laminar
28	1.112	0.402	0.004	0.004	87.964	0.308	0.0019	0.783	0.058	3.3	3.30 ± 0.21	11.65	Laminar
29	0.95	0.487	0.002	0.002	104.157	0.256	0.0016	0.783	0.071	2.22	2.74 ± 0.28	11.65	Laminar
30	1.106	0.378	0.005	0.004	85.405	0.355	0.0022	0.783	0.058	3.8	3.80 ± 0.19	11.65	Laminar

Table C.8: Extended results for 1,1,2,3,3,3-hexafluoropropyl methyl ether (HME) central composite design experiments on falling film microreactor, alkyl tetrafluoropropionate (AT) analysis.

Exp. No.	Crude mass in sample (g)	IS mass in sample (g)	AT mass in sample(g)	AT mass fraction in sample	Total mass of reactor crude (g)	Mass AT in crude (g)	Moles AT	Volumetric flow rate HFP ($m^3 \cdot s^{-1} \times 10^6$)	Moles HFP	AT Concentration ($mol \cdot m^{-3}$)	Yield %	Reynolds Number	Flow Regime
1	0.953	0.557	0.001	0.001	46.265	0.067	0.0004	0.515	0.038	0.32	1.10 ± 0.27	8.96	Laminar
2	0.731	0.518	0.002	0.002	110.398	0.256	0.0016	0.515	0.038	3.91	4.22 ± 0.77	21.77	Laminar
3	0.798	0.683	0.009	0.011	46.456	0.495	0.0031	1.05	0.077	2.15	4.00 ± 0.20	8.96	Laminar
4	0.769	0.605	0.004	0.005	121.662	0.626	0.0039	1.05	0.077	6.99	5.06 ± 0.47	21.77	Laminar
5	0.91	0.563	0.004	0.005	46.643	0.218	0.0014	0.515	0.038	2.21	3.59 ± 0.29	8.96	Laminar
6	1.021	0.5	0.002	0.002	116.373	0.198	0.0012	0.515	0.038	2.82	3.26 ± 0.57	21.77	Laminar
7	1.067	0.519	0.013	0.013	98.509	1.232	0.0077	1.05	0.077	6.35	3.70 ± 0.25	8.96	Laminar
8	0.954	0.504	0.004	0.005	50.157	0.228	0.0014	1.05	0.077	1.44	6.24 ± 0.13	21.77	Laminar
9	0.864	0.536	0.004	0.004	49.647	0.21	0.0013	0.515	0.038	3.58	3.47 ± 0.31	9.53	Laminar
10	0.894	0.507	0.002	0.002	111.395	0.23	0.0014	0.515	0.038	1.48	3.79 ± 0.63	23.13	Laminar
11	0.96	0.502	0.009	0.01	48.047	0.467	0.0029	1.05	0.077	3.01	3.78 ± 0.13	9.53	Laminar
12	0.947	0.558	0.005	0.005	116.107	0.566	0.0035	1.05	0.077	1.6	4.58 ± 0.34	23.13	Laminar
13	0.95	0.593	0.004	0.004	42.266	0.179	0.0011	0.515	0.038	1.04	2.95 ± 0.27	9.53	Laminar
14	0.872	0.474	0.002	0.002	116.113	0.221	0.0014	0.515	0.038	1.73	3.64 ± 0.62	23.13	Laminar
15	1.007	0.484	0.009	0.008	46.372	0.393	0.0025	1.05	0.077	2.44	3.18 ± 0.11	9.53	Laminar
16	0.851	0.489	0.003	0.004	121.106	0.484	0.003	1.05	0.077	2.91	3.92 ± 0.34	23.13	Laminar
17	1.062	0.452	0.006	0.005	86.407	0.472	0.003	0.783	0.058	5.1	5.12 ± 0.25	14.90	Laminar
18	0.706	0.708	0.003	0.004	84.174	0.347	0.0022	0.783	0.058	3.28	3.76 ± 0.56	16.82	Laminar
19	0.956	0.482	0.005	0.005	82.165	0.416	0.0026	0.783	0.058	5.39	4.52 ± 0.27	15.85	Laminar
20	1.096	0.356	0.004	0.004	85.941	0.345	0.0022	0.783	0.058	2.58	3.74 ± 0.18	15.85	Laminar
21	0.954	0.565	0.001	0.001	80.883	0.095	0.0006	0.248	0.018	1.88	3.26 ± 1.00	15.85	Laminar
22	1.151	0.437	0.011	0.01	89.847	0.854	0.0053	1.317	0.097	5.39	5.51 ± 0.14	15.85	Laminar
23	1.191	0.424	0.005	0.004	17.484	0.069	0.0004	0.783	0.058	2.84	0.75 ± 0.04	2.64	Laminar
24	1.022	0.482	0.003	0.003	149.696	0.397	0.0025	0.783	0.058	1.87	4.30 ± 0.46	29.05	Laminar
25	1.053	0.418	0.005	0.005	84.044	0.432	0.0027	0.783	0.058	1.04	4.68 ± 0.22	15.85	Laminar
26	1.106	0.383	0.005	0.005	55.53	0.367	0.0023	0.783	0.058	2.85	4.70 ± 0.19	15.85	Laminar
27	1.039	0.506	0.005	0.005	88.517	0.459	0.0029	0.783	0.058	5.12	4.98 ± 0.29	15.85	Laminar
28	1.112	0.402	0.005	0.005	87.964	0.427	0.0027	0.783	0.058	3.3	4.63 ± 0.21	15.85	Laminar
29	0.95	0.487	0.005	0.005	104.157	0.548	0.0034	0.783	0.058	2.22	5.95 ± 0.35	15.85	Laminar
30	1.106	0.378	0.006	0.005	85.405	0.464	0.0029	0.783	0.058	3.8	5.04 ± 0.20	15.85	Laminar

Table C.9: Gas-chromatograph raw data for central composite design experiments on the falling film micro reactor for the for methyl-2,3,3,3-tetrafluoro-2-methoxypropionate.

Peak	Exp.	Methanol	HME	AE	Exp.	Methanol	HME	AE
Retention time (min)	1	2.591	4.313	4.869	16	2.768	4.785	5.185
Area		56057731.6	22036816.2	298913.6		52776958	36510174	574849.5
Retention time (min)	2	3.471	5.513	0	17	3.436	5.405	5.735
Area		58621825.1	23782869.6	0		48926379	32951522	421455.4
Retention time (min)	3	3.436	5.547	5.943	18	3.435	5.409	5.737
Area		44708845.6	32148594	589544.3		46334476	33657442	340048.4
Retention time (min)	4	3.484	5.521	5.94	19	3.436	5.363	5.729
Area		58588331.3	24288711.2	385031.5		52018305	20999332	299099.5
Retention time (min)	5	3.436	5.503	5.92	20	3.459	5.421	5.737
Area		52037698.7	21754454.5	100044.4		55710776	37043166	452073.1
Retention time (min)	6	3.618	5.531	6.169	21	3.446	5.369	6.263
Area		97353119.3	73629160.2	7188.9		50356402	22695428	14525.3
Retention time (min)	7	3.487	5.402	5.754	22	3.459	5.383	5.743
Area		59267524.8	29392786.4	785907.1		51931838	26211787	651408.2
Retention time (min)	8	3.492	5.4	5.755	23	3.457	5.429	5.731
Area		59726464.1	28467469.2	655791		52231019	35443274	486878.6
Retention time (min)	9	3.451	5.368	5.738	24	3.491	5.389	5.737
Area		57134313.4	21712714.5	353485.1		59376763	27090719	77999.6
Retention time (min)	10	3.408	5.377	0	25	3.464	5.405	5.739
Area		58094226.7	30723532.7	0		55072422	30898773	444322.1
Retention time (min)	11	3.457	5.41	5.746	26	3.487	5.405	5.742
Area		49521481.2	30717845.7	476762.3		62963776	33674550	533082.1
Retention time (min)	12	3.496	5.395	5.753	27	3.498	5.416	5.746
Area		61047697.3	28963277.9	492520.4		62986743	35014334	530027.3
Retention time (min)	13	3.705	5.476	5.754	28	3.433	5.398	5.739
Area		139702508.1	42380825.1	283243.1		46441617	32539808	399332.8
Retention time (min)	14	3.337	5.312	5.861	29	3.474	5.415	5.746
Area		18404020.5	6865606.5	325.1		56269182	35678507	476006.6
Retention time (min)	15	3.458	5.398	5.751	30	3.473	5.394	5.742
Area		49252033.4	26844369.5	627879.4		55820662	28381899	452507.2

Table C.10: Extended results for methyl-2,3,3,3-tetrafluoro-2-methoxypropionate (MTFMP) central composite design experiments on falling film microreactor, MTFMP analysis.

Exp. No.	Crude mass in sample (g)	IS mass in sample (g)	MTFMP mass in sample(g)	MTFMP mass fraction in sample	Total mass of reactor crude (g)	Mass MTFMP in crude (g)	Moles MTFMP	Volumetric flow rate HFPO ($m^3 \cdot s^{-1} \times 10^6$)	Moles HFPO	MTFMP Concentration ($mol \cdot m^{-3}$)	Yield %
1	0.977	0.226	0.014	0.015	29.200	0.426	0.002	0.497	0.024	63.99	9.19 ± 0.25
2	1.053	0.241	0.000	0.000	70.630	0.000	0.000	0.497	0.024	0.00	Not observed
3	0.935	0.367	0.031	0.034	27.710	0.931	0.005	1.004	0.049	139.87	9.94 ± 0.47
4	0.899	0.256	0.019	0.021	70.460	1.479	0.008	1.004	0.049	91.55	15.80 ± 0.72
5	1.087	0.243	0.005	0.005	29.440	0.141	0.001	0.497	0.024	21.19	3.04 ± 1.13
6	0.951	0.355	0.000	0.000	71.100	0.012	0.000	0.497	0.024	0.75	Not observed
7	1.037	0.266	0.033	0.032	30.060	0.958	0.005	1.004	0.049	144.05	10.24 ± 0.89
8	0.994	0.281	0.030	0.030	72.970	2.212	0.012	1.004	0.049	136.88	23.62 ± 0.26
9	1.038	0.220	0.017	0.016	27.380	0.439	0.002	0.497	0.024	66.00	9.48 ± 0.91
10	0.996	0.317	0.000	0.000	70.720	0.000	0.000	0.497	0.024	0.00	Not observed
11	1.058	0.332	0.024	0.023	27.950	0.635	0.003	1.004	0.049	95.44	6.78 ± 0.52
12	0.977	0.268	0.021	0.022	67.590	1.471	0.008	1.004	0.049	91.02	15.71 ± 0.65
13	0.998	0.155	0.005	0.005	29.730	0.143	0.001	0.497	0.024	21.56	3.10 ± 0.82
14	1.080	0.211	0.000	0.000	70.250	0.003	0.000	0.497	0.024	0.19	Not observed
15	0.966	0.323	0.035	0.036	30.290	1.103	0.006	1.004	0.049	165.83	11.79 ± 0.42
16	0.953	0.369	0.027	0.028	72.270	2.055	0.011	1.004	0.049	127.18	21.95 ± 0.60
17	0.926	0.358	0.021	0.023	53.080	1.223	0.006	0.750	0.037	107.26	17.48 ± 1.01
18	0.935	0.384	0.018	0.019	43.030	0.831	0.004	0.750	0.037	72.88	11.88 ± 0.94
19	1.073	0.223	0.015	0.014	49.320	0.679	0.004	0.750	0.037	59.57	9.71 ± 0.85
20	0.917	0.358	0.020	0.022	50.820	1.127	0.006	0.750	0.037	98.81	16.11 ± 0.75
21	0.966	0.256	0.001	0.001	49.500	0.039	0.000	0.243	0.012	3.43	1.73 ± 0.20
22	0.987	0.269	0.031	0.032	43.840	1.383	0.007	1.257	0.062	121.25	11.79 ± 0.58
23	0.973	0.317	0.020	0.021	8.830	0.184	0.001	0.750	0.037	96.74	2.63 ± 0.46
24	1.103	0.282	0.004	0.003	80.790	0.277	0.001	0.750	0.037	13.25	3.96 ± 2.57
25	1.001	0.304	0.020	0.020	48.430	0.986	0.005	0.750	0.037	86.47	14.09 ± 0.82
26	0.911	0.284	0.021	0.023	48.460	1.112	0.006	0.750	0.037	97.52	15.90 ± 0.85
27	1.039	0.301	0.021	0.020	48.110	0.985	0.005	0.750	0.037	86.34	14.07 ± 0.93
28	0.913	0.352	0.020	0.022	48.720	1.075	0.006	0.750	0.037	94.28	15.37 ± 0.90
29	0.939	0.367	0.023	0.024	48.000	1.166	0.006	0.750	0.037	102.19	16.66 ± 0.90
30	0.934	0.280	0.021	0.022	47.630	1.062	0.006	0.750	0.037	93.11	15.18 ± 0.91

APPENDIX D: SAMPLE CALCULATIONS

A. Yield computation

The internal standard quantification technique was used to determine the mass of HME, alkenyl ether and alkyl tetrafluoropropionate in the reaction product, execution of this technique require that Equation 5.1 be rearranged and the $M_{Unknown}$ being solved for. For example, if the unknown was HME then applying this technique to Experiment number 1 of the HME central composite design experiments for the FFMR:

M_{crude}	M_{IS}	Area ratio$\left(\frac{A_{HME}}{A_{IS}}\right)$	M_{Total}
0.953	0.557	0.01	46.275

$$M_{Unknown} = 3.1208 \times \frac{A_{Unknown}}{A_{IS}} \times M_{IS} = 3.1208 \times 0.010 \times 0.557 = 0.016\ g \quad \text{D.1}$$

Then the mass fraction of the HME layer in the crude sample is:

$$x_{HME} = \frac{M_{HME}}{M_{Crude}} = \frac{0.016}{0.953} = 0.017 \quad \text{D.2}$$

Thus the mass of HME in the reactor vessel, where M_{Total} is the total mass of the reactor contents:

$$M_{HME,Total} = x_{HME} \cdot M_{Total} \quad \text{D.3}$$

$$= (0.012) \cdot (46.275)$$

$$= 0.801\ g$$

Number of moles of HME produced:

$$n_{HME} = \frac{M_{HME}}{MM_{HME}} = \frac{0.801}{182.06} = 0.004\ mol \quad \text{D.4}$$

Number of moles of HFP introduced into reactor at reactor conditions:

$$n_{HFP} = \frac{P \cdot \dot{V}}{R \cdot T} \cdot t = \frac{(101325) \cdot (0.515 \times 10^{-6})}{(8.314) \cdot (25+273.15)} \cdot 30 = 0.038\ mol \quad \text{D.4}$$

$$\% \text{ Yield} = \frac{0.004}{0.038} \cdot 100 = 11.60\ \%$$

B. Physical parameters

Various physical parameters were required in the kinetic model, a convenient means of estimating these parameters lies in the use of empirical correlations available in the open literature.

Viscosity:

The kinematic viscosity of methanol was required to calculate the mean velocity of the liquid film (Equation 2.5) as well as its diffusivity, this may be obtained by simply dividing the dynamic viscosity of a fluid by its mass density. The viscosity of methanol was estimated using the following correlation:

$$\mu = \exp\left(-25.317 + \frac{1789.2}{T} 2.069 \ln(T)\right) \qquad \text{D.5}$$

For example, at a temperature of 300 K, μ is found to be 5.25×10^{-4} Pa·s. At the same temperature the density of methanol is 770.467 kg·m^{-3} and the kinematic viscosity is:

$$\nu = \frac{\mu}{\rho} = \frac{5.25\times10^{-4}}{770.467} = 6.82 \times 10^{-7}\ \text{m}^2 \cdot \text{s}^{-1} \qquad \text{D.6}$$

Diffusivity:

Diffusivities of species where necessary at various points in the model, the diffusivity of hexafluoropropene in the liquid phase under dilute conditions was estimated by using the method of Wilke and Chang (1955) as seen in Equation D.7 below (Green, 2008):

$$D_{HFP,b} = 1.1728 \times 10^{-16} \frac{T(\chi_{Meth} \cdot M_{Methanol})}{\mu_{Methanol} \cdot \hat{V}_{HFP}^{0.6}} \qquad \text{D.7}$$

Where χ_{Meth} is the association parameter which is equal to 1.9 for methanol, $M_{Methanol}$ is the molar mass of methanol, $\mu_{Methanol}$ is the viscosity of methanol and $\hat{V}_{HFP}$ is the specific volume of hexafluoropropene and is 0.0432 L·mol^{-1}.

The second type of diffusivity which was required was that of potassium methoxide. Potassium methoxide behaves as an electrolyte in solution and thus its diffusivity was calculated using the Nernst-Haskell equation for binary electrolyte mixtures (Henley et al., 2011).

$$D_{Meth,b} = \frac{RT}{F^2}\frac{\left|\frac{1}{n_+}\right| + \left|\frac{1}{n_-}\right|}{\frac{1}{\lambda_+^0} + \frac{1}{\lambda_-^0}} \quad \text{D.8}$$

F is Faraday's constant 96485.34 A·s·mol^{-1}, $n_\pm$ is the valance charge of the cation and anion respectively and $\lambda_\pm^0$ is the limiting ionic conductance of the dissolved species. For a potassium methoxide solution in methanol at 298 K λ_+^0 is 73.5 A·cm^{-2} and λ_-^0 is 197.6 A·cm^{-2}. For ionic conductances other than at 298 K a temperature correction factor is needed (TCF), which may be calculated using Equation D.9.

$$TCF = \frac{T}{334 \cdot \mu_{Methanol}} \quad \text{D.9}$$

C. Uncertainty calculations

The uncertainty of a reported value is essential to ascertain the validity of experimental results, in the present study there were 2 fundamental laws of uncertainty that were applied. The first involved the calculation of uncertainty on values for which the same measurement was repeatedly taken, the uncertainty on that measurement was calculated using the following equation:

$$u_i = \frac{\sigma}{\sqrt{N_{rp}}} \quad \text{D.10}$$

Where u_i is the standard uncertainty, σ is the standard deviation of the replicate data points and N_{rp} is the number of replicate data points. Using the hexafluoropropene precision rotameter as an example, the standard deviation of the times measured at a rotameter reading of 15 (Table A.4) was 0.272 mL·min^{-1}, the number of replicate readings was 3 and thus the standard uncertainty of that result was:

$$u_i = \frac{0.272}{\sqrt{3}} = 0.157 \text{ mL} \cdot \text{min}^{-1}$$

The uncertainty of the entire calibration was then calculated by finding the square root of the sum-of-squares, i.e. again looking at the results of Table A.4:

Rotameter reading	Run 1, min	Run 2, min	Run 3, min	u_i, mL·min^{-1}	$(u_i)^2$ mL^2·min^{-2}	$\sqrt{\sum (u_i)^2}$ mL·min^{-1}
15	0.531	0.543	0.529	0.157	0.0246	
30	0.265	0.266	0.267	0.075	0.0056	
45	0.187	0.188	0.188	0.096	0.0093	0.521
60	0.145	0.146	0.148	0.436	0.1897	
75	0.120	0.119	0.120	0.205	0.0419	

The uncertainty on the calibration was thus determined to be 0.521 mL·min^{-1}.

The second law that was utilised was the *law of propagation of uncertainty*, this was used to evaluate the combined uncertainty of a value. This uncertainty comes from when two values (each with their associated uncertainties) are combined (by addition, subtraction, multiplication, etc.). Equation D.11 was used to calculate the combined effect of uncertainty. For example, the mass of a sample vial was measured m_a and the mass of the same vial plus crude product was also measured m_b, subtracting m_a from m_b gives the mass of crude, m_c. Knowing that the mass balance used for the measurement of these masses has a standard uncertainty of ± 0.001 g, the fractional uncertainty of m_a and m_b is found by dividing the standard uncertainty by the value of the measurement. These fractional uncertainties are then combined by the law of propagation of uncertainty in order to obtain the fractional uncertainty on m_c as follows:

$$\frac{u_c}{m_c} = \sqrt{\left(\frac{u_a}{m_a}\right)^2 + \left(\frac{u_b}{m_b}\right)^2} \qquad \text{D.11}$$

This procedure was followed incorporating all the various factors of uncertainty to obtain the standard uncertainties seen in Tables 5.1, 5.2 and 5.3.

APPENDIX E: MATLAB® SCRIPTS

E.1 HME system

E.1.1 Henry's law constants regression

a) Main file

```
%Kuveshan Padayachee
%Valentiner Equation regression code - Main for HME System
%MSc
%Main file used for the regression of desired parameters

clear all
clc

global T H henry

%=========================================================================
T =[243800
244272
244757
245254
245765
246289
246829
247384
247956
248545
249153
249780
250427
251096
251789
252506
253249
254021
```

```
254822
255656
256524
257429
258374
259363
260399
261486
262629
263833
265105
266450
267876
269394
271013
272745
274604
276607
278774
281127
283694
286508
289605
293031
296836
301075
305805
311077
316924
323345
330296];

T = T/1000;
%=========================================================================
H=[45.98
47.49
49.09
50.77
52.56
```

54.45
56.47
58.60
60.88
63.31
65.90
68.68
71.65
74.85
78.29
82.01
86.02
90.38
95.11
100.27
105.91
112.10
118.91
126.43
134.77
144.06
154.44
166.12
179.32
194.31
211.46
231.21
254.12
280.90
312.49
350.13
395.43
450.58
518.59
603.55
711.24
849.71
1030.34
1269.07

```
1587.80
2015.46
2587.91
3345.30
4326.57];

%=========================================================================


initial = [30 -3315 3.2];
[parameters error] = fminearch(@ParaRegress, initial)

disp(parameters)

a = parameters(1);
b = parameters(2);
c = parameters(3);
Henry = exp(a + b./T+ c.*log(T));                %Fitting to the Valentiner Equation

%=========================================================================

figure1 = figure;
axes1 = axes('Parent',figure1,'PlotBoxAspectRatio',[1 1 1],'FontSize',14);
box(axes1,'on');
hold(axes1,'all');

T = T - 273.15;

plot(T,H,'ro','MarkerSize',8,'LineWidth',2)
hold on
plot(T,Henry,'LineWidth',2)
xlabel('T (^{o}C)', 'FontSize', 14);
ylabel('H^ ^{CC}_{salt}')
legend('Data','Predicted','Location','SouthEast');
axis square
%=========================================================================
```

b) Regression

```
%Kuveshan Padayachee
%Valentiner Equation regression code - Function File
%Main file used for the regression of desired parameters

function err = ParaRegress(w)

global T H henry

a = w(1);                       %Extractin the passed variables to be used.
b = w(2);
c = w(3);

for i =1 :length(T)
    henry(i) = exp(a + b/T(i) + c*log(T(i)));
end

error=0;
for i = 1:length(T)
    deviation(i) = abs(henry(i) - H(i))^2;
    error = error + deviation(i);
end

err = error^2;
```

E.1.2 Kinetic model files

a) Constrained optimisation

```
%Kuveshan Padayachee
%HME FFMR reactor modelling
%MSC
%Main file used for the regression of desired parameters
%Round 2

%=========================================================================
clear all
clc
tic
global  XHME XAE XAT XHMEPred XAEPred XATPred nx ny nz HMEerror AEerror ATerror

initial = [1.0535   14.6054 5.6145  15.7436 3.4502  8.0999  10.8514 0.8047]; %Results of 8 iter with compounded
error term
%Defining the space.
    nx = 5;
    ny = 5;
    nz = 5;

lb = [0 0 0 0 0 0 0 0];                                          %lower bounds of fitting parameters
ub = [1e2 1e2 1e8 1e2 1e2 1e2 1e2 1e2];                          %upper bounds of fitting parameters

options = optimset('MaxIter',20);

[parameters] = lsqnonlin(@MatBalance_Main, initial,lb,ub, options);

%-------------------------------------------------------------------------
%   HME Plots
% Create figure

toc
figure1 = figure;

% Create subplot
```

```
subplot1 = subplot(3,2,1,'Parent',figure1,'PlotBoxAspectRatio',[1 1 1],...
    'FontSize',12);
box(subplot1,'on');
hold(subplot1,'all');

line = 0:10:1000;

subplot(3,2,1)
plot(XHME(1:25),XHMEPred,'MarkerFaceColor',[1 0 0],'Marker','o','Color',[1 0 0], 'MarkerSize', 5, 'LineStyle',
'none');
hold on
plot(line,line, 'LineWidth',2)
xlabel('Experimental HME concentration (mol.m ^{-3})', 'FontSize',12)
ylabel('Predicted HME concentration (mol.m^{-3})', 'FontSize',12)
axis square

%Residual plot

%  Create subplot
subplot2 = subplot(3,2,2,'Parent',figure1,'PlotBoxAspectRatio',[1 1 1],...
    'FontSize',12);
box(subplot2,'on');
hold(subplot2,'all');

subplot(3,2,2)
E = XHME(1:25) - XHMEPred;
base = [0 0];
basex = [0 1000];
% figure(2)
plot(XHME(1:25), E, 'MarkerFaceColor',[1 0 0],'Marker','o','Color',[1 0 0], 'MarkerSize', 5, 'LineStyle', 'none')
hold on
plot(basex,base,'LineWidth',2)
xlabel('Experimental HME concentration (mol.m ^{-3})', 'FontSize',12)
ylabel('Residual deviation (mol.m ^{-3})', 'FontSize',12)
axis square
%--------------------------------------------------------------------------
%   AE Plots
% Create subplot
```

```
subplot3 = subplot(3,2,3,'Parent',figure1,'PlotBoxAspectRatio',[1 1 1],...
    'FontSize',12);
box(subplot3,'on');
hold(subplot3,'all');

line = 0:10:100;

subplot(3,2,3)
plot(XAE(1:25),XAEPred,'MarkerFaceColor',[1 0 0],'Marker','o','Color',[1 0 0], 'MarkerSize', 5, 'LineStyle',
'none');
hold on
plot(line,line, 'LineWidth',2)
xlabel('Experimental AE concentration (mol.m ^{-3})', 'FontSize',12)
ylabel('Predicted AE concentration (mol.m^{-3})', 'FontSize',12)
axis square

%Residual plot

%  Create subplot
subplot4 = subplot(3,2,4,'Parent',figure1,'PlotBoxAspectRatio',[1 1 1],...
    'FontSize',12);
box(subplot4,'on');
hold(subplot4,'all');

subplot(3,2,4)
E = XAE(1:25) - XAEPred;
base = [0 0];
basex = [0 100];
% figure(2)
plot(XAE(1:25), E, 'MarkerFaceColor',[1 0 0],'Marker','o','Color',[1 0 0], 'MarkerSize', 5, 'LineStyle', 'none')
hold on
plot(basex,base,'LineWidth',2)
xlabel('Experimental AE concentration (mol.m ^{-3})', 'FontSize',12)
ylabel('Residual deviation (mol.m ^{-3})', 'FontSize',12)
axis square
%--------------------------------------------------------------------------
%   AT Plots
% Create subplot
```

```
subplot5 = subplot(3,2,1,'Parent',figure1,'PlotBoxAspectRatio',[1 1 1],...
    'FontSize',12);
box(subplot5,'on');
hold(subplot5,'all');

line = 0:10:60;

subplot(3,2,5)
plot(XAT(1:25),XATPred,'MarkerFaceColor',[1 0 0],'Marker','o','Color',[1 0 0], 'MarkerSize', 5, 'LineStyle',
'none');
hold on
plot(line,line, 'LineWidth',2)
xlabel('Experimental AT concentration (mol.m ^{-3})', 'FontSize',12)
ylabel('Predicted AT concentration (mol.m^{-3})', 'FontSize',12)
axis square

%Residual plot

%  Create subplot
subplot6 = subplot(3,2,6,'Parent',figure1,'PlotBoxAspectRatio',[1 1 1],...
    'FontSize',12);
box(subplot6,'on');
hold(subplot6,'all');

subplot(3,2,6)
E = XAT(1:25) - XATPred;
base = [0 0];
basex = [0 60];
% figure(2)
plot(XAT(1:25), E, 'MarkerFaceColor',[1 0 0],'Marker','o','Color',[1 0 0], 'MarkerSize', 5, 'LineStyle', 'none')
hold on
plot(basex,base,'LineWidth',2)
xlabel('Experimental AT concentration (mol.m ^{-3})', 'FontSize',12)
ylabel('Residual deviation (mol.m ^{-3})', 'FontSize',12)
axis square

parameters
ABC = [XHME XHMEPred XAE XAEPred XAT XATPred]
```

b) Reactor model

```
function error = MatBalance_Main(parameters)
%MOL Material Balance for HME system
%Main

global nx ny nz b delta z xx yy zz DHFP DHME DB DC DH20 DMeth DKF XX YY ZZ Nspecies cHFPliqSat cMeth0 k dx dy dz uz
XHME XAE XAT XHMEPred XAEPred XATPred HMEerror AEerror ATerror

    %=========================================================================
    %=========================================================================
        data = [280.150 0.340   0.340   1.750
    280.150 0.340   0.340   4.250
    280.150 0.340   0.700   1.750
    280.150 0.340   0.700   4.250
    280.150 0.520   0.340   1.750
    280.150 0.520   0.340   4.250
    280.150 0.520   0.700   4.250
    290.150 0.340   0.340   1.750
    290.150 0.340   0.340   4.250
    290.150 0.340   0.700   4.250
    290.150 0.520   0.340   4.250
    290.150 0.520   0.700   4.250
    275.150 0.430   0.520   3.000
    295.150 0.430   0.520   3.000
    285.150 0.250   0.520   3.000
    285.150 0.610   0.520   3.000
    285.150 0.430   0.170   3.000
    285.150 0.430   0.880   3.000
    285.150 0.430   0.520   5.500
    285.150 0.430   0.520   3.000
    285.150 0.430   0.520   3.000
    285.150 0.430   0.520   3.000
    285.150 0.430   0.520   3.000
    285.150 0.430   0.520   3.000
    285.150 0.430   0.520   3.000];
    % units [T catconc HFPfrac liqflowrate] = [K mol/L frac mL/min]

        XHME =[83.80
```

```
143.80
572.30
345.10
239.30
118.40
288.80
310.20
148.30
317.40
111.50
284.20
393.90
331.30
341.20
286.30
70.80
664.40
192.50
332.70
236.40
380.50
342.80
435.30
380.00];

XAE = [2.30
11.70
31.70
42.40
15.90
8.40
8.70
25.90
4.40
9.70
5.10
17.60
32.70
21.00
```

```
34.50
16.50
3.80
58.00
6.50
6.60
18.20
32.70
21.10
17.60
24.30];

XAT = [7.90
12.60
58.90
30.70
25.90
9.70
11.20
25.00
11.30
27.70
10.80
23.70
32.80
24.10
28.90
24.00
6.60
59.30
15.00
30.00
25.50
31.90
29.70
38.10
32.20];
%=========================================================================
```

```
for ijk=1:25
    tic
%Inputs-----------------------------------------------------------------------
T = data(ijk,1);                %Temp in K
HFPMolFrac = data(ijk,3);       %Mole fraction of HFP in the gas phase
n = 32;                         %Number of channels
Fl = data(ijk,4)/(1e6*60)/n;    %m3/sec
cMeth0 = data(ijk,2);           %mol/L
R = 8.314;

%=========================================================================
k10 = parameters(1)*1e-2;
k20 = parameters(2)*1e-2;
k30 = parameters(3)*1e-3;
k40 = parameters(4)*1e-5;
k50 = parameters(4)*1e-5;

Ea1 = parameters(5)*1e4;
Ea2 = parameters(6)*1e4;
Ea3 = parameters(7)*1e4;
Ea4 = parameters(8)*1e4;
Ea5 = parameters(8)*1e4;

k1 = k10 * exp(-1*Ea1/(R) * (1/T - 1/285.15));        %Arrhenius expression for reaction rate constant
k2 = k20 * exp(-1*Ea2/(R) * (1/T - 1/285.15));
k3 = k30 * exp(-1*Ea3/(R) * (1/T - 1/285.15));
k4 = k40 * exp(-1*Ea4/(R) * (1/T - 1/285.15));
k5 = k50 * exp(-1*Ea5/(R) * (1/T - 1/285.15));
k = [k1 k2 k3 k4 k5];
%-------------------------------------------------------------------------

mu = exp(-25.317 + 1789.2/T + 2.069*log(T));        %Perrys 2-430 (Pa.s)
rho = 770.467;                                      %Perrys 2-116 = denisty of methanol at 97% purity
nu = mu/rho;                                        %Calculting kinematic viscosity
MM = 32.04;                                         %Molar mass of methanol
S = 1.9;
b = 641*10^-6;                                      %Width of a microchannel (m)
z = 0.0664;                                         %Channel length (m)
g = 9.81;                                           %Acceleration due to gravity(m/s^2)
```

```
    delta = (3 * Fl * nu/(b*g))^(1/3);                  %Film thickness (m)
    jL = g * delta^2/(3*nu);
    Re = 4*delta*jL/nu;

    %=========================================================================
    dimensions = [nx ny T Fl];
    uz = main(dimensions);
    %=========================================================================
    %Calculating diffusivities of all components
    %Wilke-Chang
    %1. HFP
    VHFP = (1462.58/166.02 * 1000/(100^3))^(-1);           %1 / ([Kg/m3] / molar mass[Kg/Kmol] / 10^3 [dm3] * 1000
[mol/Kmol]) = [cm3/mol]
    DHFP = (7.4e-8 * T * sqrt(S * MM)/(mu/0.001 * VHFP^0.6))/(100)^2;

    %2. HME
    VHME = (1419/182.07 * 1000/(100^3))^(-1);
    DHME = (7.4e-8 * T * sqrt(S * MM)/(mu/0.001 * VHME^0.6))/(100)^2;

    %3. Alkenyl ether
    VB = (1362.75/162.06 * 1000/(100^3))^(-1);           %1 / ([Kg/m3] / molar mass[Kg/Kmol] / 10^3 [dm3] * 1000
[mol/Kmol]) = [cm3/mol]
    DB = (7.4e-8 * T * sqrt(S * MM)/(mu/0.001 * VB^0.6))/(100)^2;

    %4. H2O
    theta=4.5;
    VH20 = (1000/18.02 * 1000/(100^3))^(-1);           %1 / ([Kg/m3] / molar mass[Kg/Kmol] / 10^3 [dm3] * 1000
[mol/Kmol]) = [cm3/mol]
    DH20 = (7.4e-8 * T * sqrt(S * MM)/(mu/0.001 * (theta*VH20)^0.6))/(100)^2;

    %5. Alkyl Tetrafluoropropionate
    VC = (1399.45/144.0 * 1000/(100^3))^(-1);           %1 / ([Kg/m3] / molar mass[Kg/Kmol] / 10^3 [dm3] * 1000
[mol/Kmol]) = [cm3/mol]
    DC = (7.4e-8 * T * sqrt(S * MM)/(mu/0.001 * VC^0.6))/(100)^2;

    %Nernst-Heskell
    F = 96485.34;                                       %Faraday's constant
    lamdaK = 73.52;                                     %Limiting ionic conductance for K+
```

```
    lamdaMeth = 197.6;                                  %Limiting ionic conductance for Meth-
    lamdaF = 55.32;                                     %Limiting ionic conductance for F-

    %6. KF
    DKF = (R*T/F^2) * (1)/((1/lamdaK) + (1/lamdaMeth))/(100)^2;

    %7. Methoxide
    DMeth = (R*T/F^2) * (1)/((1/lamdaK) + (1/lamdaF))/(100)^2;
    %=========================================================================

    Sc = mu/(rho * DHFP);
    cl = 300 * 10^(-6);
    kL = DHFP/cl*(0.0145*Re^(0.69)*Sc^(0.57));          %Hydrodynamics and mass transfer journal
    a = 20000;                                          %Specific area (m2/m3)
    kLa = kL * a;
    Ks = 0;                                             %Set Sechenov coeff to 0

    aa = 63.4792;                                       %Regressed parameters to determine corrected Henry's Law
constant from Valentiner EQuation
    bb = -6.1553e+03;
    cc = -6.2873;
    Hpc = exp(aa + bb/T + cc*log(T));                   %Valentiner equation to calculate corrected Henry's Law
constant
    Hcc = Hpc/(R*T);
    Hsalt = Hcc*exp(Ks * cMeth0*1000/1000);                 %Corrected Henry's Law constant
    HFPgas = 101325*HFPMolFrac/(R*T);
    cHFPliqSat = HFPgas/Hsalt;                          %Saturated concentration of HFP in Methanol

    trange = linspace(0, 1800, 3);
    Nspecies = 7;
    Ntime = length(trange);
    %=========================================================================
    %          [ 1     2      3  4  5  6  7]
    %initial = [HFPl CH3O-K+ HME B KF H2O C]
    %going to extebd the intial value matrix for all 7 species (as specified
    %for above) - this means that we will have 7 11*11*11 matrices next to each
    %other so will have a 11*77*11 matrix
```

```
    %Important to note here that all species need 1 initial condition and 5 boundary conditions (2 for x, 2 for y
and 1 for z) so now for the initial conditions:

    %initial conditions - unique for each species
    u0 = zeros(nx,ny*Nspecies,nz);
    %HFPliq - initial condition is that its zero everywhere
    %Methoxide - initial condition is that the inlet concentration is the concentration everywhere
    u0(:,[(ny+1):(2*ny)],:) = cMeth0;
    %HME - initial condition is that its zero everywhere
    %B - initial condition is that its zero everywhere(Alkenyl Ether)
    %KF - initial condition is that its zero everywhere
    %H20 - initial condition is that its zero everywhere
    u0(:,[((5*ny)+1):(6*ny)],:) = cMeth0;
    %C - initial condition is that its zero everywhere (Alkyl tetrafluoropropionate)

    [xx,yy,zz] = size(u0);
    elements = xx*yy*zz;

    C0 = reshape(u0,1,elements);
    options=odeset('NonNegative', [1:(nx*Nspecies*ny*nz)]);
    [t,Conc] = ode15s(@MatBalance_Funct,trange,C0,options);

    dv = dx*dy*dz;

    SteadyState = Conc(end,:);
    SteadyState = reshape(SteadyState,XX,YY,ZZ);

    SteadyStateMoles = SteadyState(:,:,nz)*dv;

    for i=1:Nspecies
    MolesOut(i) = sum(sum(SteadyStateMoles(:,[(((i-1)*ny)+1):(i*ny)],:)));
    end

    SliceVolume = nx*ny*dv;
    ConcOut(ijk,:) = MolesOut/SliceVolume*1000;
    toc
    end
```

```
    XHMEPred = ConcOut([1:25],3);
    XAEPred = ConcOut([1:25],4);
    XATPred = ConcOut([1:25],7);

    HMEerror = ((XHMEPred-XHME(1:25))./XHME(1:25));
    AEerror = ((XAEPred-XAE(1:25))./XAE(1:25));
    ATerror = ((XATPred-XAT(1:25))./XAT(1:25));

    WeightingFactor = [1 17.47 11.25];
    WeightingFactor = WeightingFactor.^2;
    error = [WeightingFactor(1)*HMEerror; WeightingFactor(2)*AEerror; WeightingFactor(3)*ATerror];
end
```

c) Reaction model

```
%MOL PDE for Material Balance
function Cout = MatBalance_Funct(h,C0)

global nx ny nz b delta z xx yy zz DHFP DHME DB DC DH20 DMeth DKF XX YY ZZ Nspecies cHFPliqSat cMeth0 k dx dy dz uz

C = reshape(C0,xx,yy,zz);
%          [ 1     2      3     4     5     6     7]
%          [1-11 12-22  23-33 34-44 45-55 56-66 67-77
%initial = [HFPl CH3O-K+ HME    B     KF   H2O    C]

%=========================================================================
%Boundary conditions in the x direction [In general no gradient at each wall in x direction]
%1. HFPliq
dCdxx(1,[((0*ny)+1):(1*ny)],:) = 0;     %No concentration gradient a tthe first side wall
dCdxx(nx,[((0*ny)+1):(1*ny)],:) = 0;    %No concentration gradient at the end side wall
%2. Methoxide
dCdxx(1,[((1*ny)+1):(2*ny)],:) = 0;     %No concentration gradient a tthe first side wall
dCdxx(nx,[((1*ny)+1):(2*ny)],:) = 0;    %No concentration gradient at the end side wall
%3. HME
dCdxx(1,[((2*ny)+1):(3*ny)],:) = 0;     %No concentration gradient a tthe first side wall
dCdxx(nx,[((2*ny)+1):(3*ny)],:) = 0;    %No concentration gradient at the end side wall
%4. B (Alkenyl Ether)
dCdxx(1,[((3*ny)+1):(4*ny)],:) = 0;     %No concentration gradient a tthe first side wall
dCdxx(nx,[((3*ny)+1):(4*ny)],:) = 0;    %No concentration gradient at the end side wall
%5. KF
dCdxx(1,[((4*ny)+1):(5*ny)],:) = 0;     %No concentration gradient a tthe first side wall
dCdxx(nx,[((4*ny)+1):(5*ny)],:) = 0;    %No concentration gradient at the end side wall
%6. H20
dCdxx(1,[((5*ny)+1):(6*ny)],:) = 0;     %Noconcentration gradient a tthe first side wall
dCdxx(nx,[((5*ny)+1):(6*ny)],:) = 0;    % No concentration gradient at the end side wall
%7. C (Alkyl Tetrafluoropropionate)
dCdxx(1,[((6*ny)+1):(7*ny)],:) = 0;     %No concentration gradient a tthe first side wall
dCdxx(nx,[((6*ny)+1):(7*ny)],:) = 0;    %No concentration gradient at the end side wall
%-------------------------------------------------------------------------

%-------------------------------------------------------------------------
%Boundary conditions in the y direction
```

```
%1. HFPliq
dCdyy(:,(0*ny+1),:) = 0;                %No concentration gradient at the first side wall
C(:,(1*ny),:) = cHFPliqSat/1000;             %Concentration at surface in contact with the gas is a constant =
Saturated conc of HFPliq in methanol
%2. Methoxide
dCdyy(:,(1*ny+1),:) = 0;                %No concentration gradient at the first side wall
dCdyy(:,(2*ny),:) = 0;                  %No concentration gradient at surface in contact with the gas
%3. HME
dCdyy(:,(2*ny+1),:) = 0;                %No concentration gradient at the first side wall
dCdyy(:,(3*ny),:) = 0;                  %No concentration gradient at surface in contact with the gas
%4. B (Alkenyl Ether)
dCdyy(:,(3*ny+1),:) = 0;                %No concentration gradient at the first side wall
dCdyy(:,(4*ny),:) = 0;                  %No concentration gradient at surface in contact with the gas
%5. KF
dCdyy(:,(4*ny+1),:) = 0;                %No concentration gradient at the first side wall
dCdyy(:,(5*ny),:) = 0;                  %No concentration gradient at surface in contact with the gas
%6. H20
dCdyy(:,(5*ny+1),:) = 0;                %No concentration gradient at the first side wall
dCdyy(:,(6*ny),:) = 0;                  %No concentration gradient at surface in contact with the gas
%7. C (Alkyl Tetrafluoropropionate)
dCdyy(:,(6*ny+1),:) = 0;                %No concentration gradient at the first side wall
dCdyy(:,(7*ny),:) = 0;                  %No concentration gradient at surface in contact with the gas
%-------------------------------------------------------------------------

%-------------------------------------------------------------------------
%Boundary conditions in the z direction
%1. HFPliq
C(:,[((0*ny)+1):(1*ny)],1) = 0;         %Inlet concentration is zero
%2. Methoxide
C(:,[((1*ny)+1):(2*ny)],1) = cMeth0;    %Inlet concentration is constant at the inlet concentration of Methoxide
%3. HME
C(:,[((2*ny)+1):(3*ny)],1) = 0;         %Inlet concentration is zero
%4. B (Alkenyl Ether)
C(:,[((3*ny)+1):(4*ny)],1) = 0;         %Inlet concentration is zero
%5. KF
C(:,[((4*ny)+1):(5*ny)],1) = 0;         %Inlet concentration is zero
%6. H20
C(:,[((5*ny)+1):(6*ny)],1) = cMeth0;         %Inlet concentration is zero
%7. C (Alkyl Tetrafluoropropionate)
```

```
C(:,[((6*ny)+1):(7*ny)],1) = 0;          %Inlet concentration is zero
%=========================================================================


%=========================================================================
%Second derivative in the x direction
dx2 = (delta/(nx-1))^2;
dx = (delta/(nx-1));
dCdxx = zeros(nx,ny*Nspecies,nz);
for i = 1:nx
    if(i==1) dCdxx(i,:,:) = 2*(C(i+1,:,:) - C(i,:,:))/dx2;
    elseif(i==nx) dCxx(i,:,:) = 2*(C(i-1,:,:) - C(i,:,:))/dx2;
    else dCdxx(i,:,:) = (C(i+1,:,:) - 2*C(i,:,:) + C(i-1,:,:))/dx2;
    end
end

%Second derivative in the y direction
dy2 = (b/(ny-1))^2;
dy = (b/(ny-1));
dCdyy = zeros(nx,ny*Nspecies,nz);
for i = 1:ny
    if(i==1) dCdyy(:,i,:) = 2*(C(:,i+1,:) - C(:,i,:))/dy2;
    elseif(i==ny) dCyy(:,ny,:) = 2*(C(:,i-1,:) - C(:,i,:))/dy2;
    else dCdyy(:,i,:) = (C(:,i+1,:) - 2*C(:,i,:) + C(:,i-1,:))/dy2;
    end
end

%First derivative in the z direction
dz = (z/(nz-1));
dCdz = zeros(nx,ny*Nspecies,nz);
for i = 1:nz
    if(i==1) dCdz(:,:,i) = (C(:,:,i+1) - C(:,:,i))/dz;
    elseif(i==nz) dCdz(:,:,nz) = (C(:,:,i) - C(:,:,i-1))/dz;
    else dCdz(:,:,i) = (C(:,:,i+1) - C(:,:,i-1))/(2*dz);
    end
end
%=========================================================================
```

```
%=========================================================================
%Boundary conditions in the x direction [In general no gradient at each wall in x direction]
%1. HFPliq
dCdxx(1,[((0*ny)+1):(1*ny)],:) = 0;      %No concentration gradient a tthe first side wall
dCdxx(nx,[((0*ny)+1):(1*ny)],:) = 0;     %No concentration gradient at the end side wall
%2. Methoxide
dCdxx(1,[((1*ny)+1):(2*ny)],:) = 0;      %No concentration gradient a tthe first side wall
dCdxx(nx,[((1*ny)+1):(2*ny)],:) = 0;     %No concentration gradient at the end side wall
%3. HME
dCdxx(1,[((2*ny)+1):(3*ny)],:) = 0;      %No concentration gradient a tthe first side wall
dCdxx(nx,[((2*ny)+1):(3*ny)],:) = 0;     %No concentration gradient at the end side wall
%4. B (Alkenyl Ether)
dCdxx(1,[((3*ny)+1):(4*ny)],:) = 0;      %No concentration gradient a tthe first side wall
dCdxx(nx,[((3*ny)+1):(4*ny)],:) = 0;     %No concentration gradient at the end side wall
%5. KF
dCdxx(1,[((4*ny)+1):(5*ny)],:) = 0;      %No concentration gradient a tthe first side wall
dCdxx(nx,[((4*ny)+1):(5*ny)],:) = 0;     %No concentration gradient at the end side wall
%6. H20
dCdxx(1,[((5*ny)+1):(6*ny)],:) = 0;      %Noconcentration gradient a tthe first side wall
dCdxx(nx,[((5*ny)+1):(6*ny)],:) = 0;     % No concentration gradient at the end side wall
%7. C (Alkyl Tetrafluoropropionate)
dCdxx(1,[((6*ny)+1):(7*ny)],:) = 0;      %No concentration gradient a tthe first side wall
dCdxx(nx,[((6*ny)+1):(7*ny)],:) = 0;     %No concentration gradient at the end side wall
%-------------------------------------------------------------------------

%-------------------------------------------------------------------------
%Boundary conditions in the y direction
%1. HFPliq
dCdyy(:,(0*ny+1),:) = 0;                 %No concentration gradient at the first side wall
C(:,(1*ny),:) = cHFPliqSat/1000;              %Concentration at surface in contact with the gas is a constant =
Saturated conc of HFPliq in methanol
%2. Methoxide
dCdyy(:,(1*ny+1),:) = 0;                 %No concentration gradient at the first side wall
dCdyy(:,(2*ny),:) = 0;                   %No concentration gradient at surface in contact with the gas
%3. HME
dCdyy(:,(2*ny+1),:) = 0;                 %No concentration gradient at the first side wall
dCdyy(:,(3*ny),:) = 0;                   %No concentration gradient at surface in contact with the gas
%4. B (Alkenyl Ether)
dCdyy(:,(3*ny+1),:) = 0;                 %No concentration gradient at the first side wall
```

```
dCdyy(:,(4*ny),:) = 0;                  %No concentration gradient at surface in contact with the gas
%5. KF
dCdyy(:,(4*ny+1),:) = 0;                %No concentration gradient at the first side wall
dCdyy(:,(5*ny),:) = 0;                  %No concentration gradient at surface in contact with the gas
%6. H20
dCdyy(:,(5*ny+1),:) = 0;                %No concentration gradient at the first side wall
dCdyy(:,(6*ny),:) = 0;                  %No concentration gradient at surface in contact with the gas
%7. C (Alkyl Tetrafluoropropionate)
dCdyy(:,(6*ny+1),:) = 0;                %No concentration gradient at the first side wall
dCdyy(:,(7*ny),:) = 0;                  %No concentration gradient at surface in contact with the gas
%-------------------------------------------------------------------------

%-------------------------------------------------------------------------
%Boundary conditions in the z direction
%1. HFPliq
C(:,[((0*ny)+1):(1*ny)],1) = 0;         %Inlet concentration is zero
%2. Methoxide
C(:,[((1*ny)+1):(2*ny)],1) = cMeth0;    %Inlet concentration is constant at the inlet concentration of Methoxide
%3. HME
C(:,[((2*ny)+1):(3*ny)],1) = 0;         %Inlet concentration is zero
%4. B (Alkenyl Ether)
C(:,[((3*ny)+1):(4*ny)],1) = 0;         %Inlet concentration is zero
%5. KF
C(:,[((4*ny)+1):(5*ny)],1) = 0;         %Inlet concentration is zero
%6. H20
C(:,[((5*ny)+1):(6*ny)],1) = cMeth0;    %Inlet concentration is zero
%7. C (Alkyl Tetrafluoropropionate)
C(:,[((6*ny)+1):(7*ny)],1) = 0;         %Inlet concentration is zero
%=========================================================================

%We have:
%1. Inlet conditions that define the concentration of all 7 species at all points in the reactor channel
%2. We have boundary conditions for the derivatives as well as where the concentration of species are known as
constants
%3. The derivatives are then calculated
%4. Now need to create a grid of the material balances for all the species

%=========================================================================
%Need to incorporate the velocity profile into the derivative in the z direction
```

```
for i = 1:Nspecies
    for j=1:nz
        dCdzuz(:,[(((i-1)*ny)+1):(i*ny)],j) = dCdz(:,[(((i-1)*ny)+1):(i*ny)],j).*uz;
    end
end
%=========================================================================
%-------------------------------------------------------------------------
%Reaction Rates
k1 = k(1); k2 = k(2); k3 = k(3); k4 = k(4); k5 = k(5);
%1. HFPliq
rHFP = k1.*C(:,[((0*ny)+1):(1*ny)],:).*C(:,[((1*ny)+1):(2*ny)],:);
%3. Meth
rMeth = k3.*k1.*C(:,[((0*ny)+1):(1*ny)],:).*C(:,[((1*ny)+1):(2*ny)],:)./(k2 + k3);
%3. HME
rHME = (k2.*k1.*C(:,[((0*ny)+1):(1*ny)],:).*C(:,[((1*ny)+1):(2*ny)],:))./(k2 + k3) - k5.*C(:,[((2*ny)+1):(3*ny)],:);
%4. B (Alkenyl Ether)
rB = (k3.*k1.*C(:,[((0*ny)+1):(1*ny)],:).*C(:,[((1*ny)+1):(2*ny)],:))./(k2 + k3) -
k4.*C(:,[((3*ny)+1):(4*ny)],:).*C(:,[((5*ny)+1):(6*ny)],:);
%5. KF
rKF = rMeth;
%6. H2O
rH2O = k4.*C(:,[((3*ny)+1):(4*ny)],:).*C(:,[((5*ny)+1):(6*ny)],:) +
k5.*C(:,[((2*ny)+1):(3*ny)],:).*C(:,[((5*ny)+1):(6*ny)],:);
%7. C (Alkyl tetrafluoropropionate)
rC = rH2O;
%=========================================================================
%Liquid Phase Balances
%1. HFPliq
dcHFPdt(:,:,:) = DHFP*(dCdxx(:,[((0*ny)+1):(1*ny)],:) + dCdyy(:,[((0*ny)+1):(1*ny)],:)) -
dCdzuz(:,[((0*ny)+1):(1*ny)],:) - rHFP;
%2. Methoxide
dcMethdt(:,:,:) = DMeth*(dCdxx(:,[((1*ny)+1):(2*ny)],:) + dCdyy(:,[((1*ny)+1):(2*ny)],:)) -
dCdzuz(:,[((1*ny)+1):(2*ny)],:) - rMeth;
%3. HME
dcHMEdt(:,:,:) = DHME*(dCdxx(:,[((2*ny)+1):(3*ny)],:) + dCdyy(:,[((2*ny)+1):(3*ny)],:)) -
dCdzuz(:,[((2*ny)+1):(3*ny)],:) + rHME;
%4. B (Alkenyl Ether)
dcBdt(:,:,:) = DB*(dCdxx(:,[((3*ny)+1):(4*ny)],:) + dCdyy(:,[((3*ny)+1):(4*ny)],:)) -
dCdzuz(:,[((3*ny)+1):(4*ny)],:) + rB;
```

```
%5. KF
dcKFdt(:,:,:) = DKF*(dCdxx(:,[((4*ny)+1):(5*ny)],:) + dCdyy(:,[((4*ny)+1):(5*ny)],:)) -
dCdzuz(:,[((4*ny)+1):(5*ny)],:) + rKF;
%6. H20
dcH2Odt(:,:,:) = DH20*(dCdxx(:,[((5*ny)+1):(6*ny)],:) + dCdyy(:,[((5*ny)+1):(6*ny)],:)) -
dCdzuz(:,[((5*ny)+1):(6*ny)],:) - rH2O;
%7. C (Alkyl Tetrafluoropropionate)
dcCdt(:,:,:) = DC*(dCdxx(:,[((6*ny)+1):(7*ny)],:) + dCdyy(:,[((6*ny)+1):(7*ny)],:)) -
dCdzuz(:,[((6*ny)+1):(7*ny)],:) + rC;
%-------------------------------------------------------------------------

Conc = [dcHFPdt dcMethdt dcHMEdt dcBdt dcKFdt dcH2Odt dcCdt];

[XX,YY,ZZ] = size(Conc);
Cout = reshape(Conc,1,(XX*YY*ZZ))';
end
```

E.2 MTFMP system

E.2.1 Henry's law constants regression

a) Main file

```
%Kuveshan Padayachee
%Valentiner Equation regression code - Main for MTFMP system
%MSc
%Main file used for the regression of desired parameters

clear all
clc

global T H henry

%=========================================================================
T =[243.842
244.074
244.308
244.545
244.785
245.029
245.275
245.525
245.778
246.035
246.295
246.558
246.825
247.096
247.371
247.650
247.932
248.219
248.510
248.806
249.106
```

249.410
249.720
250.034
250.354
250.678
251.008
251.344
251.685
252.032
252.385
252.744
253.110
253.482
253.86113
254.24744
254.64109
255.04235
255.45149
255.86878
256.29453
256.72905
257.17267
257.62574
258.089
258.562
259.045
259.540
260.046
260.565
261.096
261.639
262.197
262.769
263.356
263.958
264.577
265.213
265.867
266.541

```
267.234
267.948
268.685
269.445
270.230
271.042
271.881
272.750
273.650
274.584
275.554
276.562
277.610
278.703
279.842
281.031
282.275
283.577
284.941
286.375
287.881
289.468
291.142
292.911
294.782
296.766
298.872
301.111
303.494
306.034
308.744
311.635
314.720
318.010
321.513
325.234
329.174
333.328
337.685];
```

```
%=========================================================================
H=[38.03
38.65
39.28
39.93
40.60
41.29
41.99
42.72
43.46
44.23
45.02
45.84
46.68
47.54
48.43
49.35
50.30
51.28
52.29
53.33
54.40
55.52
56.67
57.86
59.09
60.37
61.69
63.06
64.48
65.95
67.48
69.07
70.72
72.44
74.22
76.08
78.02
```

80.04
82.14
84.34
86.63
89.03
91.54
94.17
96.92
99.80
102.83
106.01
109.36
112.88
116.59
120.50
124.63
128.99
133.61
138.50
143.68
149.19
155.05
161.29
167.95
175.06
182.67
190.83
199.58
209.00
219.15
230.12
241.99
254.86
268.86
284.11
300.79
319.06
339.14
361.28

```
385.76
412.93
443.19
477.01
514.97
557.74
606.15
661.20
724.09
796.28
879.58
976.19
1088.82
1220.81
1376.24
1560.12
1778.58
2038.98
2350.12
2722.31
3167.37
3698.48
4329.85
];

%=========================================================================


initial = [30 -3315 3.2];
[parameters error] = fminearch(@ParaRegress, initial)

disp(parameters)

a = parameters(1);
b = parameters(2);
c = parameters(3);
Henry = exp(a + b./T+ c.*log(T));               %Fitting to the Valentiner Equation
```

```
%==========================================================================
figure1 = figure;
axes1 = axes('Parent',figure1,'PlotBoxAspectRatio',[1 1 1],'FontSize',14);
box(axes1,'on');
hold(axes1,'all');

T = T - 273.15;

plot(T,H,'ro','MarkerSize',8,'LineWidth',2)
hold on
plot(T,Henry,'LineWidth',2)
xlabel('T (^{o}C)', 'FontSize', 14);
ylabel('H^ ^{CC}_{salt}')
legend('Data','Predicted','Location','SouthEast');
axis square
%==========================================================================
```

b) Regression

```
%Kuveshan Padayachee
%Valentiner Equation regression code - Function File
%Main file used for the regression of desired parameters

function err = ParaRegress(w)

global T H henry

a = w(1);                       %Extracting the passed variables to be used.
b = w(2);
c = w(3);

for i =1 :length(T)
    henry(i) = exp(a + b/T(i) + c*log(T(i)));
end

error=0;
for i = 1:length(T)
    deviation(i) = abs(henry(i) - H(i))^2;
    error = error + deviation(i);
end

err = error^2;
```

E.2.2 Kinetic model files

a) Constrained optimisation

```
%Kuveshan Padayachee
%MTFMP FFMR reactor modelling
%MSC
%Main file used for the regression of desired parameters
%Round 2

%=========================================================================
clear all
clc
tic
global  XData XMTFMPPred nx ny nz MTFMPerror

initial = [1.2892    4.0000    0.8012]; %5 iter results
    %Defining the space.
    nx = 5;
    ny = 5;
    nz = 5;

lb = [0 0 0];                                           %lower bounds of fitting parameters
ub = [1e5 1e2 5];                                       %upper bounds of fitting parameters

options = optimset('MaxIter',4);
[parameters] = lsqnonlin(@MatBalance_Main_MTFMP, initial,lb,ub, options);

%-------------------------------------------------------------------------
% Create figure

toc

AbsRelDev = mean(abs(XData - XMTFMPPred)./XData * 100);

%-------------------------------------------------------------------------
% Create figure
figure1 = figure;
```

```
% Create subplot
subplot1 = subplot(1,2,1,'Parent',figure1,'PlotBoxAspectRatio',[1 1 1],...
'FontSize',12);
box(subplot1,'on');
hold(subplot1,'all');
line = 0:10:300;
subplot(1,2,1)
plot(XData,XMTFMPPred,'MarkerFaceColor',[1 0 0],'Marker','o','Color',[1 0 0], 'MarkerSize', 5, 'LineStyle', 'none');

hold on
plot(line,line, 'LineWidth',2)
xlabel('Experimental MTFMP concentration (mol.m ^{-3})', 'FontSize',12)
ylabel('Predicted MTFMP concentration (mol.m^{-3})', 'FontSize',12)
axis square
%Residual plot
% Create subplot
subplot2 = subplot(1,2,2,'Parent',figure1,'PlotBoxAspectRatio',[1 1 1],...
'FontSize',12);
box(subplot2,'on');
hold(subplot2,'all');
subplot(1,2,2)
E = XData - XMTFMPPred;
base = [0 0];
basex = [0 300];
% figure(2)
plot(XData, E, 'MarkerFaceColor',[1 0 0],'Marker','o','Color',[1 0 0], 'MarkerSize', 5, 'LineStyle', 'none')
hold on
plot(basex,base,'LineWidth',2)
xlabel('Experimental MTFMP concentration (mol.m ^{-3})', 'FontSize',12)
ylabel('Residual deviation (mol.m ^{-3})', 'FontSize',12)
axis square
%--------------------------------------------------------------------------
%==========================================================================
```

b) Reactor model

```
function MTFMPerror = MatBalance_Main_MTFMP(parameters)
%MOL Material Balance for MTFP system
%Main

global nx ny nz b delta z xx yy zz XX YY ZZ Nspecies cHFPOliqSat cMeth0 k1 dx dy dz uz DHFPO DMTFMP DKF DMeth alpha
beta XMTFMPPred MTFMPerror XData

    %=========================================================================
    %=========================================================================
        data = [305.65  0.28    0.33    1.75
305.65  0.28    0.67    1.75
305.65  0.28    0.67    4.25
305.65  0.53    0.33    1.75
305.65  0.53    0.67    1.75
305.65  0.53    0.67    4.25
310.65  0.28    0.33    1.75
310.65  0.28    0.67    1.75
310.65  0.28    0.67    4.25
310.65  0.53    0.33    1.75
310.65  0.53    0.67    1.75
310.65  0.53    0.67    4.25
303.15  0.40    0.50    3
313.15  0.40    0.50    3
308.15  0.15    0.50    3
308.15  0.65    0.50    3
308.15  0.40    0.16    3
308.15  0.40    0.8380  3
308.15  0.40    0.50    0.5
308.15  0.40    0.50    5.5
308.15  0.40    0.50    3
308.15  0.40    0.50    3
308.15  0.40    0.50    3
308.15  0.40    0.50    3
308.15  0.40    0.50    3
308.15  0.40    0.50    3];

%units [T catconc HFPOfrac liqflowrate] = [K mol/L frac mL/min]
```

```
XData = [70.69
154.49
101.13
23.41
159.12
151.19
72.91
105.42
100.54
23.81
183.17
140.48
118.47
80.51
65.79
109.14
3.79
133.93
106.85
14.63
95.51
107.71
95.36
104.13
112.88
102.85];

alpha = 2;
beta = 1;
    for ijk=1:26

    %Inputs-----------------------------------------------------------------
    T = data(ijk,1);              %Temp in K
    HFPOMolFrac = data(ijk,3);    %Mole fraction of HFP in the gas phase
    n = 32;                       %Number of channels
    Fl = data(ijk,4)/(1e6*60)/n;  %m3/sec
    cMeth0 = data(ijk,2);         %mol/L
    R = 8.314;
```

```
    k0 = parameters(1)*1e-3;
    Ea = -1*parameters(2)*1e4;
%     k1 = (parameters(1)*(1e-4)) * (exp(-1*parameters(2)*1e5)/(R) * (1/T - 1/285.15));        %Arrhenius expression
for reaction rate constant
        k1 = k0 * (exp(Ea/(R) * (1/T - 1/285.15)));        %Arrhenius expression for reaction rate constant
    %-------------------------------------------------------------------------

    mu = exp(-25.317 + 1789.2/T + 2.069*log(T));        %Perrys 2-430 (Pa.s)
    rho = 770.467;                                      %Perrys 2-116 = denisty of methanol at 97% purity
    nu = mu/rho;                                        %Calculting kinematic viscosity
    MM = 32.04;                                         %Molar mass of methanol
    S = 1.9;
    b = 641*10^-6;                                      %Width of a microchannel (m)
    z = 0.0664;                                         %Channel length (m)
    g = 9.81;                                           %Acceleration due to gravity(m/s^2)
    delta = (3 * Fl * nu/(b*g))^(1/3);                  %Film thickness (m)
    jL = g * delta^2/(3*nu);
    Re = 4*delta*jL/nu;
    %-------------------------------------------------------------------------
%Velocity profile defined
    dimensions = [nx ny T Fl];
    uz = main(dimensions);
    %-------------------------------------------------------------------------
    %Calculating diffusivities of all components
    %Wilke-Chang
    %1. HFPO
    VHFPO = ((1462.58/166.02)*1000/100^3)^(-1); %1 / ([Kg/m3] / molar mass[Kg/Kmol] / 10^3 [dm3] * 1000 [mol/Kmol])
= [dm3/mol]
    DHFPO = (7.4e-8 * T * sqrt(S * MM)/(mu/0.001 * VHFPO^0.6))/(100)^2;

    %2. MTFMP
    VMTFMP = (1331/175.06 * 1000/(100^3))^(-1);
    DMTFMP = (7.4e-8 * T * sqrt(S * MM)/(mu/0.001 * VMTFMP^0.6))/(100)^2;

    %Nernst-Heskell
    F = 96485.34;                                       %Faraday's constant
    lamdaK = 73.52;                                     %Limiting ionic conductance for K+
    lamdaMeth = 197.6;                                  %Limiting ionic conductance for Meth-
    lamdaF = 55.32;                                     %Limiting ionic conductance for F-
```

```
    %3. KF
    DKF = (R*T/F^2) * (1)/((1/lamdaK) + (1/lamdaMeth))/(100)^2;

    %4. Methoxide
    DMeth = (R*T/F^2) * (1)/((1/lamdaK) + (1/lamdaF))/(100)^2;
    %=========================================================================

    Sc = mu/(rho * DHFPO);
    cl = 300 * 10^(-6);
    kL = DHFPO/cl*(0.0145*Re^(0.69)*Sc^(0.57));          %Hydrodynamics and mass transfer journal
    a = 20000;                                          %Specific area (m2/m3)
    kLa = kL * a;
    Ks = parameters(3);
    aa = 30.1976; %Regressed parameters to determine corrected Henry's Law constant from Valentiner Equation
    bb = -4.5903e+03;
    cc = -1.4135;
    Hpc = exp(aa + bb/T + cc*log(T));                   %Valentiner equation to calculate corrected Henry's Law
constant
    Hcc = Hpc/(R*T);
    Hsalt = Hcc*exp(Ks * cMeth0*1000/1000);                %Corrected Henry's Law constant
    HFPOgas = 101325*HFPOMolFrac/(R*T);
    cHFPOliqSat = HFPOgas/Hsalt;                          %Saturated concentration of HFP in Methanol

    trange = linspace(0, 1800, 3);
    Nspecies = 4;
    Ntime = length(trange);
    %=============================================================================
    %          [ 1      2      3      4]
    %initial = [HFPOl MTFMP   KF    CH3O-K+]
    %going to extebd the intial value matrix for all 4 species (as specified
    %for above) - this means that we will have 7 11*11*11 matrices next to each
    %other so will have a 11*77*11 matrix

    %Important to note here that all species need 1 initial condition and 5 boundary conditions (2 for x, 2 for y
and 1 for z) so now for the initial conditions:

    %initial conditions - unique for each species
```

```
    u0 = zeros(nx,ny*Nspecies,nz);
    %1. HFPO
    %2. MTFMP
    %3. KF
    %4. Methoxide
    u0(:,[((3*ny)+1):(4*ny)],:) = cMeth0;


    [xx,yy,zz] = size(u0);
    elements = xx*yy*zz;

    C0 = reshape(u0,1,elements);
    options=odeset('NonNegative', [1:(nx*Nspecies*ny*nz)]);
    [t,Conc] = ode15s(@MatBalance_Funct_MTFMP,trange,C0,options);

    dv = dx*dy*dz;

    SteadyState = Conc(end,:);
    SteadyState = reshape(SteadyState,XX,YY,ZZ);

    SteadyStateMoles = SteadyState(:,:,nz)*dv;

    for i=1:Nspecies
    MolesOut(i) = sum(sum(SteadyStateMoles(:,[(((i-1)*ny)+1):(i*ny)],:)));
    end

    SliceVolume = nx*ny*dv;
    ConcOut(ijk,:) = MolesOut/SliceVolume*1000;

    end
      toc
    XMTFMPPred = ConcOut(:,2);
    MTFMPerror = (((XMTFMPPred-XData))./XData)*100;

AA = [XData XMTFMPPred]
end
```

c) Reaction model

```
%MOL PDE for Material Balance - MTFP system
function Cout = MatBalance_Funct_MTFMP(h,C0)

global nx ny nz b delta z xx yy zz DHFPO DMeth DKF DMTFMP XX YY ZZ Nspecies cHFPOliqSat cMeth0 k1 dx dy dz uz alpha
beta C dCdxx

C = reshape(C0,xx,yy,zz);
%          [ 1          2          3     4  ]
%          [1-11      12-22     23-33 34-44]
%Initial = [HFPOliq   MTFMP      KF    Meth]

%=========================================================================
%Boundary conditions in the x direction [In general no gradient at each wall in x direction]
%1. HFPOliq
dCdxx(1,[((0*ny)+1):(1*ny)],:) = 0;     %No concentration gradient a tthe first side wall
dCdxx(nx,[((0*ny)+1):(1*ny)],:) = 0;    %No concentration gradient at the end side wall
%2. MTFMP
dCdxx(1,[((1*ny)+1):(2*ny)],:) = 0;     %No concentration gradient a tthe first side wall
dCdxx(nx,[((1*ny)+1):(2*ny)],:) = 0;    %No concentration gradient at the end side wall
%3. KF
dCdxx(1,[((2*ny)+1):(3*ny)],:) = 0;     %No concentration gradient a tthe first side wall
dCdxx(nx,[((2*ny)+1):(3*ny)],:) = 0;    %No concentration gradient at the end side wall
%4. Meth
dCdxx(1,[((3*ny)+1):(4*ny)],:) = 0;     %No concentration gradient a tthe first side wall
dCdxx(nx,[((3*ny)+1):(4*ny)],:) = 0;    %No concentration gradient at the end side wall
%-------------------------------------------------------------------------

%-------------------------------------------------------------------------
%Boundary conditions in the y direction
%1. HFPOliq
dCdyy(:,(0*ny+1),:) = 0;                %No concentration gradient at the first side wall
C(:,(1*ny),:) = cHFPOliqSat;             %Concentration at surface in contact with the gas is a constant = Saturated
conc of HFPliq in methanol
%2. MTFMP
dCdyy(:,(1*ny+1),:) = 0;                %No concentration gradient at the first side wall
dCdyy(:,(2*ny),:) = 0;                  %No concentration gradient at surface in contact with the gas
%3. KF
```

```
dCdyy(:,(2*ny+1),:) = 0;                %No concentration gradient at the first side wall
dCdyy(:,(3*ny),:) = 0;                  %No concentration gradient at surface in contact with the gas
%4. Meth
dCdyy(:,(3*ny+1),:) = 0;                %No concentration gradient at the first side wall
dCdyy(:,(4*ny),:) = 0;                  %No concentration gradient at surface in contact with the gas
%-------------------------------------------------------------------------

%-------------------------------------------------------------------------
%Boundary conditions in the z direction
%1. HFPOliq
C(:,[((0*ny)+1):(1*ny)],1) = 0;         %Inlet concentration is zero
%2. MTFMP
C(:,[((1*ny)+1):(2*ny)],1) = 0;    %Inlet concentration is constant at the inlet concentration of Methoxide
%3. KF
C(:,[((2*ny)+1):(3*ny)],1) = 0;         %Inlet concentration is zero
%4. Meth
C(:,[((3*ny)+1):(4*ny)],1) = cMeth0;         %Inlet concentration is zero
%=========================================================================



%=========================================================================
%Second derivative in the x direction
dx2 = (delta/(nx-1))^2;
dx = (delta/(nx-1));
dCdxx = zeros(nx,ny*Nspecies,nz);
for i = 1:nx
    if(i==1) dCdxx(i,:,:) = 2*(C(i+1,:,:) - C(i,:,:))/dx2;
    elseif(i==nx) dCxx(i,:,:) = 2*(C(i-1,:,:) - C(i,:,:))/dx2;
    else dCdxx(i,:,:) = (C(i+1,:,:) - 2*C(i,:,:) + C(i-1,:,:))/dx2;
    end
end

%Second derivative in the y direction
dy2 = (b/(ny-1))^2;
dy = (b/(ny-1));
dCdyy = zeros(nx,ny*Nspecies,nz);
for i = 1:ny
    if(i==1) dCdyy(:,i,:) = 2*(C(:,i+1,:) - C(:,i,:))/dy2;
    elseif(i==ny) dCyy(:,ny,:) = 2*(C(:,i-1,:) - C(:,i,:))/dy2;
```

```
    else dCdyy(:,i,:) = (C(:,i+1,:) - 2*C(:,i,:) + C(:,i-1,:))/dy2;
    end
end

%First derivative in the z direction
dz = (z/(nz-1));
dCdz = zeros(nx,ny*Nspecies,nz);
for i = 1:nz
    if(i==1) dCdz(:,:,i) = (C(:,:,i+1) - C(:,:,i))/dz;
    elseif(i==nz) dCdz(:,:,nz) = (C(:,:,i) - C(:,:,i-1))/dz;
    else dCdz(:,:,i) = (C(:,:,i+1) - C(:,:,i-1))/(2*dz);
    end
end
%=========================================================================

%=========================================================================
%Boundary conditions in the x direction [In general no gradient at each wall in x direction]
%1. HFPOliq
dCdxx(1,[((0*ny)+1):(1*ny)],:) = 0;      %No concentration gradient a tthe first side wall
dCdxx(nx,[((0*ny)+1):(1*ny)],:) = 0;     %No concentration gradient at the end side wall
%2. MTFMP
dCdxx(1,[((1*ny)+1):(2*ny)],:) = 0;      %No concentration gradient a tthe first side wall
dCdxx(nx,[((1*ny)+1):(2*ny)],:) = 0;     %No concentration gradient at the end side wall
%3. KF
dCdxx(1,[((2*ny)+1):(3*ny)],:) = 0;      %No concentration gradient a tthe first side wall
dCdxx(nx,[((2*ny)+1):(3*ny)],:) = 0;     %No concentration gradient at the end side wall
%4. Meth
dCdxx(1,[((3*ny)+1):(4*ny)],:) = 0;      %No concentration gradient a tthe first side wall
dCdxx(nx,[((3*ny)+1):(4*ny)],:) = 0;     %No concentration gradient at the end side wall
%-------------------------------------------------------------------------

%-------------------------------------------------------------------------
%Boundary conditions in the y direction
%1. HFPOliq
dCdyy(:,(0*ny+1),:) = 0;                 %No concentration gradient at the first side wall
C(:,(1*ny),:) = cHFPOliqSat;              %Concentration at surface in contact with the gas is a constant = Saturated
conc of HFPliq in methanol
%2. MTFMP
dCdyy(:,(1*ny+1),:) = 0;                 %No concentration gradient at the first side wall
```

```
dCdyy(:,(2*ny),:) = 0;                  %No concentration gradient at surface in contact with the gas
%3. KF
dCdyy(:,(2*ny+1),:) = 0;                %No concentration gradient at the first side wall
dCdyy(:,(3*ny),:) = 0;                  %No concentration gradient at surface in contact with the gas
%4. Meth
dCdyy(:,(3*ny+1),:) = 0;                %No concentration gradient at the first side wall
dCdyy(:,(4*ny),:) = 0;                  %No concentration gradient at surface in contact with the gas
%-------------------------------------------------------------------------

%-------------------------------------------------------------------------
%Boundary conditions in the z direction
%1. HFPOliq
C(:,[((0*ny)+1):(1*ny)],1) = 0;         %Inlet concentration is zero
%2. MTFMP
C(:,[((1*ny)+1):(2*ny)],1) = 0;    %Inlet concentration is constant at the inlet concentration of Methoxide
%3. KF
C(:,[((2*ny)+1):(3*ny)],1) = 0;         %Inlet concentration is zero
%4. Meth
C(:,[((3*ny)+1):(4*ny)],1) = cMeth0;         %Inlet concentration is zero
%=========================================================================

%We have:
%1. Inlet conditions that define the concentration of all 4 species at all points in the reactor channel
%2. We have boundary conditions for the derivatives as well as where the concentration of species are known as
constants
%3. The derivatives are then calculated
%4. Now need to create a grid of the material balances for all the species

%=========================================================================
%Need to incorporate the velocity profile into the derivative in the z direction
for i = 1:Nspecies
    for j=1:nz
        dCdzuz(:,[(((i-1)*ny)+1):(i*ny)],j) = dCdz(:,[(((i-1)*ny)+1):(i*ny)],j).*uz;
    end
end
%=========================================================================

%-------------------------------------------------------------------------
%Reaction Rates
```

```
r = k1*C(:,[((3*ny)+1):(4*ny)],:).^(alpha).*C(:,[((0*ny)+1):(1*ny)],:).^(beta);

%=========================================================================
%Liquid Phase Balances
%1. HFPOliq
dcHFPOdt(:,:,:) = DHFPO*(dCdxx(:,[((0*ny)+1):(1*ny)],:) + dCdyy(:,[((0*ny)+1):(1*ny)],:)) -
dCdzuz(:,[((0*ny)+1):(1*ny)],:) - r;
%2. MTFMP
dcMTFMPdt(:,:,:) = DMTFMP*(dCdxx(:,[((1*ny)+1):(2*ny)],:) + dCdyy(:,[((1*ny)+1):(2*ny)],:)) -
dCdzuz(:,[((1*ny)+1):(2*ny)],:) + r;
%3. KF
dcKFdt(:,:,:) = DKF*(dCdxx(:,[((2*ny)+1):(3*ny)],:) + dCdyy(:,[((2*ny)+1):(3*ny)],:)) -
dCdzuz(:,[((2*ny)+1):(3*ny)],:) + 2*r;
%4. Meth
dcMethdt(:,:,:) = DMeth*(dCdxx(:,[((3*ny)+1):(4*ny)],:) + dCdyy(:,[((3*ny)+1):(4*ny)],:)) -
dCdzuz(:,[((3*ny)+1):(4*ny)],:) - 2*r;
%-------------------------------------------------------------------------

Conc = [dcHFPOdt dcMTFMPdt dcKFdt dcMethdt];

[XX,YY,ZZ] = size(Conc);
Cout = reshape(Conc,1,(XX*YY*ZZ))';

end
```

E.2.3 Response surface methodology files

a) Interaction between activation energy and reference kinetic rate constant

```
close all
clear all
clc

X=[1.900000 75.000  0.7000  142.5000    1.3300  52.5000 3.6100  5625.0000   0.4900
1.900000    75.000  0.3000  142.5000    0.5700  22.5000 3.6100  5625.0000   0.0900
1.900000    45.000  0.7000  85.5000 1.3300  31.5000 3.6100  2025.0000   0.4900
1.900000    45.000  0.3000  85.5000 0.5700  13.5000 3.6100  2025.0000   0.0900
1.100000    75.000  0.7000  82.5000 0.7700  52.5000 1.2100  5625.0000   0.4900
1.100000    75.000  0.3000  82.5000 0.3300  22.5000 1.2100  5625.0000   0.0900
1.100000    45.000  0.7000  49.5000 0.7700  31.5000 1.2100  2025.0000   0.4900
1.100000    45.000  0.3000  49.5000 0.3300  13.5000 1.2100  2025.0000   0.0900
0.828000    60.000  0.5000  49.6800 0.4140  30.0000 0.6856  3600.0000   0.2500
2.172000    60.000  0.5000  130.3200    1.0860  30.0000 4.7176  3600.0000   0.2500
1.500000    34.800  0.5000  52.2000 0.7500  17.4000 2.2500  1211.0400   0.2500
1.500000    85.200  0.5000  127.8000    0.7500  42.6000 2.2500  7259.0400   0.2500
1.500000    60.000  0.1640  90.0000 0.2460  9.8400  2.2500  3600.0000   0.0269
1.500000    60.000  0.8360  90.0000 1.2540  50.1600 2.2500  3600.0000   0.6989
1.500000    60.000  0.5000  90.0000 0.7500  30.0000 2.2500  3600.0000   0.2500
1.500000    60.000  0.5000  90.0000 0.7500  30.0000 2.2500  3600.0000   0.2500
1.500000    60.000  0.5000  90.0000 0.7500  30.0000 2.2500  3600.0000   0.2500
1.500000    60.000  0.5000  90.0000 0.7500  30.0000 2.2500  3600.0000   0.2500
1.500000    60.000  0.5000  90.0000 0.7500  30.0000 2.2500  3600.0000   0.2500
1.500000    60.000  0.5000  90.0000 0.7500  30.0000 2.2500  3600.0000   0.2500];


X1 = [ones(size(X,1),1) X(:,1:9)]; % Adding a row of ones to the beginning of the matrix

PreExp=X(:,1);
ActEnergy=X(:,2);
Sechenov=X(:,3);

ypred=ones(20,1);

y=[7.4079
```

```
    7.9737
    7.3604
    7.9284
    7.5561
    7.4533
    7.5018
    7.4101
    7.9946
    7.9482
    7.3561
    7.4153
    7.8095
    7.2378
    7.3749
    7.3749
    7.3749
    7.3749
    7.3749
    7.3749];


stats=regstats(y,X);

beta=stats.beta

for index=1:20
    ypred(index,1)= beta(1)+ beta(2)*PreExp(index) + beta(3)*ActEnergy(index) + beta(4)*Sechenov(index)...
    + beta(5)*(PreExp(index))*(ActEnergy(index)) + beta(6)*(PreExp(index))*(Sechenov(index)) +
beta(7)*(ActEnergy(index))*(Sechenov(index))...
    + beta(8)*(PreExp(index))^2 + beta(9)*(ActEnergy(index))^2 +beta(10)*(Sechenov(index))^2;
end

R = stats.rsquare

f = stats.fstat;

fprintf('\n')
fprintf('Regression ANOVA');
```

```
fprintf('\n\n')

fprintf('%6s','Source');
fprintf('%10s','df','SS','MS','F','P');
fprintf('\n')

fprintf('%6s','Regr');
fprintf('%10.4f',f.dfr,f.ssr,f.ssr/f.dfr,f.f,f.pval);
fprintf('\n')

fprintf('%6s','Resid');
fprintf('%10.4f',f.dfe,f.sse,f.sse/f.dfe);
fprintf('\n')

fprintf('%6s','Total');
fprintf('%10.4f',f.dfe+f.dfr,f.sse+f.ssr);
fprintf('\n')



t = stats.tstat;
CoeffTable = dataset({t.beta,'Coef'},{t.se,'StdErr'}, ...
                     {t.t,'tStat'},{t.pval,'pVal'})


FZ=40;
F=linspace(min(X(:,1)),max(X(:,1)),FZ)';

MZ=40;
M=linspace(min(X(:,2)),max(X(:,2)),MZ);

FM=repmat(F,[1,MZ]);
MM=repmat(M,[FZ,1]);

TM=zeros(FZ,MZ);

for a=1:FZ;
```

```
    for g=1:MZ;
        TM(a,g)=0.5;
    end
end

%The model to predict the response variable
YD=beta(1)+ beta(2).*FM + beta(3).*MM + beta(4).*TM + beta(5).*(FM).*(MM) + beta(6).*(FM).*(TM) +
beta(7).*(MM).*(TM) + beta(8).*(FM).^2 + beta(9).*(MM).^2 +beta(10).*(TM).^2;

%to make any values that are negative, zero
for d=1:40;
    for e=1:40;
        YD_new(d,e)=YD(d,e);

        if YD(d,e)<0
            YD_new(d,e)= YD(d,e);
        end
    end
end



surf(MM,FM,YD_new);
set(gca,'Xcolor',[0 0 0],'Ycolor',[0 0 0],'Zcolor',[0 0 0],'FontName','Arial','FontSize',16);
colorbar('FontName','Arial','FontSize',22,'Xcolor',[0 0 0],'Ycolor',[0 0 0],'location','eastoutside')

axis square
shading faceted
colormap jet
view(225,30)
xlabel('Activation energy (kJ.mol^{-1})','FontName','Arial','FontSize',14,'FontWeight','normal','Color',[0 0 0])
ylabel('Reference kinetic rate constant (m^{3}.mol^{-1}.s^{-1} ×10^{-
5})','FontName','Arial','FontSize',14,'FontWeight','normal','Color',[0 0 0])
zlabel('Summed relative square error','FontName','Arial','FontSize',14,'FontWeight','normal','Color',[0 0 0])

%-----------------------------------------

figure(2)
```

```
[C,h]=contour(MM,FM,YD);
clabel(C,h,'FontName','Arial','FontSize',20,'LabelSpacing',200,'Color',[0 0 0]);
set(gca,'Xcolor',[0 0 0],'Ycolor',[0 0 0],'FontName','Arial','FontSize',16,'LineWidth',0.5);
set(h,'LineWidth',2);

axis square
shading interp
colormap jet
xlabel('Mass KOH','FontName','Arial','FontSize',22,'FontWeight','normal','Color',[0 0 0])
ylabel('HFP Flow rate (mL/s)','Arial','FontSize',22)
```

b) Interaction between activation energy and Sechenov coefficient

```
close all
clear all
clc

X=[1.900000 75.000  0.7000  142.5000    1.3300  52.5000 3.6100  5625.0000   0.4900
1.900000    75.000  0.3000  142.5000    0.5700  22.5000 3.6100  5625.0000   0.0900
1.900000    45.000  0.7000  85.5000 1.3300  31.5000 3.6100  2025.0000   0.4900
1.900000    45.000  0.3000  85.5000 0.5700  13.5000 3.6100  2025.0000   0.0900
1.100000    75.000  0.7000  82.5000 0.7700  52.5000 1.2100  5625.0000   0.4900
1.100000    75.000  0.3000  82.5000 0.3300  22.5000 1.2100  5625.0000   0.0900
1.100000    45.000  0.7000  49.5000 0.7700  31.5000 1.2100  2025.0000   0.4900
1.100000    45.000  0.3000  49.5000 0.3300  13.5000 1.2100  2025.0000   0.0900
0.828000    60.000  0.5000  49.6800 0.4140  30.0000 0.6856  3600.0000   0.2500
2.172000    60.000  0.5000  130.3200    1.0860  30.0000 4.7176  3600.0000   0.2500
1.500000    34.800  0.5000  52.2000 0.7500  17.4000 2.2500  1211.0400   0.2500
1.500000    85.200  0.5000  127.8000    0.7500  42.6000 2.2500  7259.0400   0.2500
1.500000    60.000  0.1640  90.0000 0.2460  9.8400  2.2500  3600.0000   0.0269
1.500000    60.000  0.8360  90.0000 1.2540  50.1600 2.2500  3600.0000   0.6989
1.500000    60.000  0.5000  90.0000 0.7500  30.0000 2.2500  3600.0000   0.2500
1.500000    60.000  0.5000  90.0000 0.7500  30.0000 2.2500  3600.0000   0.2500
1.500000    60.000  0.5000  90.0000 0.7500  30.0000 2.2500  3600.0000   0.2500
1.500000    60.000  0.5000  90.0000 0.7500  30.0000 2.2500  3600.0000   0.2500
1.500000    60.000  0.5000  90.0000 0.7500  30.0000 2.2500  3600.0000   0.2500
1.500000    60.000  0.5000  90.0000 0.7500  30.0000 2.2500  3600.0000   0.2500];


X1 = [ones(size(X,1),1) X(:,1:9)]; % Adding a row of ones to the beginning of the matrix

PreExp=X(:,1);
ActEnergy=X(:,2);
Sechenov=X(:,3);

ypred=ones(20,1);

y=[7.4079
    7.9737
```

```
    7.3604
    7.9284
    7.5561
    7.4533
    7.5018
    7.4101
    7.9946
    7.9482
    7.3561
    7.4153
    7.8095
    7.2378
    7.3749
    7.3749
    7.3749
    7.3749
    7.3749
    7.3749];



stats=regstats(y,X);

beta=stats.beta

for index=1:20
    ypred(index,1)= beta(1)+ beta(2)*PreExp(index) + beta(3)*ActEnergy(index) + beta(4)*Sechenov(index)...
    + beta(5)*(PreExp(index))*(ActEnergy(index)) + beta(6)*(PreExp(index))*(Sechenov(index)) +
beta(7)*(ActEnergy(index))*(Sechenov(index))...
    + beta(8)*(PreExp(index))^2 + beta(9)*(ActEnergy(index))^2 +beta(10)*(Sechenov(index))^2;
end

R = stats.rsquare

f = stats.fstat;

fprintf('\n')
fprintf('Regression ANOVA');
```

```
fprintf('\n\n')

fprintf('%6s','Source');
fprintf('%10s','df','SS','MS','F','P');
fprintf('\n')

fprintf('%6s','Regr');
fprintf('%10.4f',f.dfr,f.ssr,f.ssr/f.dfr,f.f,f.pval);
fprintf('\n')

fprintf('%6s','Resid');
fprintf('%10.4f',f.dfe,f.sse,f.sse/f.dfe);
fprintf('\n')

fprintf('%6s','Total');
fprintf('%10.4f',f.dfe+f.dfr,f.sse+f.ssr);
fprintf('\n')



t = stats.tstat;
CoeffTable = dataset({t.beta,'Coef'},{t.se,'StdErr'}, ...
                     {t.t,'tStat'},{t.pval,'pVal'})



TZ=20;
T=linspace(min(X(:,3)),max(X(:,3)),TZ)';

MZ=20;
M=linspace(min(X(:,2)),max(X(:,2)),MZ);

TM=repmat(T,[1,MZ]);
MM=repmat(M,[TZ,1]);

FM=zeros(TZ,MZ);
```

```
for a=1:TZ;
    for g=1:MZ;
        FM(a,g)= 1.5;
    end
end

%The model to predict the response variable
YD=beta(1)+ beta(2).*FM + beta(3).*MM + beta(4).*TM + beta(5).*(FM).*(MM) + beta(6).*(FM).*(TM) +
beta(7).*(MM).*(TM) + beta(8).*(FM).^2 + beta(9).*(MM).^2 +beta(10).*(TM).^2;
%to make any values that are negative, zero
for d=1:20;
    for e=1:20;
        YD_new(d,e)=YD(d,e);

        if YD(d,e)<0
            YD_new(d,e)=0;
        end
    end
end

surf(MM,TM,YD_new);
set(gca,'Xcolor',[0 0 0],'Ycolor',[0 0 0],'Zcolor',[0 0 0],'FontName','Arial','FontSize',16);
colorbar('FontName','Arial','FontSize',22,'Xcolor',[0 0 0],'Ycolor',[0 0 0],'location','eastoutside')

axis square
shading faceted
colormap jet
view(-135,30)
xlabel('Ea','FontName','Arial','FontSize',22,'FontWeight','normal','Color',[0 0 0])
ylabel('Ks','FontName','Arial','FontSize',22,'FontWeight','normal','Color',[0 0 0])
zlabel('Relative error','FontName','Arial','FontSize',22,'FontWeight','normal','Color',[0 0 0])

%-----------------------------------------

figure(2)

[C,h]=contour(MM,TM,YD);
clabel(C,h,'FontName','Arial','FontSize',20,'LabelSpacing',200,'Color',[0 0 0]);
```

```
set(gca,'Xcolor',[0 0 0],'Ycolor',[0 0 0],'FontName','Arial','FontSize',16,'LineWidth',0.5);
set(h,'LineWidth',2);

axis square
shading interp
colormap jet
xlabel('Mass KOH','FontName','Arial','FontSize',22,'FontWeight','normal','Color',[0 0 0])
ylabel('Temperature /K','FontName','Arial','FontSize',22,'FontWeight','normal','Color',[0 0 0])

figure(3)
line = 7:1:9;
% Create figure
figure1 = figure(3);

% Create axes
axes1 = axes('Parent',figure1,'PlotBoxAspectRatio',[1 1 1],'FontSize',22);
box(axes1,'on');
hold(axes1,'all');
plot(y,ypred,'MarkerFaceColor',[1 0 0],'Marker','o','Color',[1 0 0], 'MarkerSize', 12,'LineStyle','none');
hold on
plot(line,line, 'LineWidth',4)
xlabel('Observed relative summed square error', 'FontSize',22)
ylabel('Predicted relative summed square error', 'FontSize',22)
axis square

B=zeros(3,3);

B(1,1)=(beta(8));
B(1,2)=(beta(5))/2;
B(1,3)=(beta(6))/2;
B(2,1)=(beta(5))/2;
B(2,2)=(beta(9));
B(2,3)=(beta(7))/2;
B(3,1)=(beta(6))/2;
B(3,2)=(beta(7))/2;
B(3,3)=(beta(10));

b=[beta(2); beta(3); beta(4)];
```

```
D=B^-1;

X0=-0.5*D*b;

X0T=X0';

Y0=beta(1)+0.5*X0T*b
```

c) Interaction between Reference kinetic rate constant and Sechenov coefficient

```
close all
clear all
clc

X=[1.900000 75.000  0.7000  142.5000    1.3300  52.5000 3.6100  5625.0000   0.4900
1.900000    75.000  0.3000  142.5000    0.5700  22.5000 3.6100  5625.0000   0.0900
1.900000    45.000  0.7000  85.5000 1.3300  31.5000 3.6100  2025.0000   0.4900
1.900000    45.000  0.3000  85.5000 0.5700  13.5000 3.6100  2025.0000   0.0900
1.100000    75.000  0.7000  82.5000 0.7700  52.5000 1.2100  5625.0000   0.4900
1.100000    75.000  0.3000  82.5000 0.3300  22.5000 1.2100  5625.0000   0.0900
1.100000    45.000  0.7000  49.5000 0.7700  31.5000 1.2100  2025.0000   0.4900
1.100000    45.000  0.3000  49.5000 0.3300  13.5000 1.2100  2025.0000   0.0900
0.828000    60.000  0.5000  49.6800 0.4140  30.0000 0.6856  3600.0000   0.2500
2.172000    60.000  0.5000  130.3200    1.0860  30.0000 4.7176  3600.0000   0.2500
1.500000    34.800  0.5000  52.2000 0.7500  17.4000 2.2500  1211.0400   0.2500
1.500000    85.200  0.5000  127.8000    0.7500  42.6000 2.2500  7259.0400   0.2500
1.500000    60.000  0.1640  90.0000 0.2460  9.8400  2.2500  3600.0000   0.0269
1.500000    60.000  0.8360  90.0000 1.2540  50.1600 2.2500  3600.0000   0.6989
1.500000    60.000  0.5000  90.0000 0.7500  30.0000 2.2500  3600.0000   0.2500
1.500000    60.000  0.5000  90.0000 0.7500  30.0000 2.2500  3600.0000   0.2500
1.500000    60.000  0.5000  90.0000 0.7500  30.0000 2.2500  3600.0000   0.2500
1.500000    60.000  0.5000  90.0000 0.7500  30.0000 2.2500  3600.0000   0.2500
1.500000    60.000  0.5000  90.0000 0.7500  30.0000 2.2500  3600.0000   0.2500
1.500000    60.000  0.5000  90.0000 0.7500  30.0000 2.2500  3600.0000   0.2500];


X1 = [ones(size(X,1),1) X(:,1:9)]; % Adding a row of ones to the beginning of the matrix

PreExp=X(:,1);
ActEnergy=X(:,2);
Sechenov=X(:,3);

ypred=ones(20,1);

y=[7.4079
    7.9737
```

```
    7.3604
    7.9284
    7.5561
    7.4533
    7.5018
    7.4101
    7.9946
    7.9482
    7.3561
    7.4153
    7.8095
    7.2378
    7.3749
    7.3749
    7.3749
    7.3749
    7.3749
    7.3749];

stats=regstats(y,X);

beta=stats.beta

for index=1:20
    ypred(index,1)= beta(1)+ beta(2)*PreExp(index) + beta(3)*ActEnergy(index) + beta(4)*Sechenov(index)...
    + beta(5)*(PreExp(index))*(ActEnergy(index)) + beta(6)*(PreExp(index))*(Sechenov(index)) +
beta(7)*(ActEnergy(index))*(Sechenov(index))...
    + beta(8)*(PreExp(index))^2 + beta(9)*(ActEnergy(index))^2 +beta(10)*(Sechenov(index))^2;
end

R = stats.rsquare

f = stats.fstat;

fprintf('\n')
fprintf('Regression ANOVA');
fprintf('\n\n')
```

```
fprintf('%6s','Source');
fprintf('%10s','df','SS','MS','F','P');
fprintf('\n')

fprintf('%6s','Regr');
fprintf('%10.4f',f.dfr,f.ssr,f.ssr/f.dfr,f.f,f.pval);
fprintf('\n')

fprintf('%6s','Resid');
fprintf('%10.4f',f.dfe,f.sse,f.sse/f.dfe);
fprintf('\n')

fprintf('%6s','Total');
fprintf('%10.4f',f.dfe+f.dfr,f.sse+f.ssr);
fprintf('\n')

t = stats.tstat;
CoeffTable = dataset({t.beta,'Coef'},{t.se,'StdErr'}, ...
                     {t.t,'tStat'},{t.pval,'pVal'})


TZ=20;
T=linspace(min(X(:,3)),max(X(:,3)),TZ)';

FZ=20;
F=linspace(min(X(:,1)),max(X(:,1)),FZ);

TM=repmat(T,[1,FZ]);
FM=repmat(F,[TZ,1]);

MM=zeros(TZ,FZ);

for a=1:TZ;
    for g=1:FZ;
        MM(a,g)=60;
    end
end
```

```
%The model to predict the response variable
YD=beta(1)+ beta(2).*FM + beta(3).*MM + beta(4).*TM + beta(5).*(FM).*(MM) + beta(6).*(FM).*(TM) +
beta(7).*(MM).*(TM) + beta(8).*(FM).^2 + beta(9).*(MM).^2 +beta(10).*(TM).^2;

%to make any values that are negative, zero
for d=1:20;
    for e=1:20;
        YD_new(d,e)=YD(d,e);

        if YD(d,e)<0
            YD_new(d,e)=YD(d,e);
        end
    end
end



surf(FM,TM,YD_new);
set(gca,'Xcolor',[0 0 0],'Ycolor',[0 0 0],'Zcolor',[0 0 0],'FontName','Arial','FontSize',16);
colorbar('FontName','Arial','FontSize',22,'Xcolor',[0 0 0],'Ycolor',[0 0 0],'location','eastoutside')

axis square
shading faceted
colormap jet
view(235,30)
xlabel('Ko','FontName','Arial','FontSize',22,'FontWeight','normal','Color',[0 0 0])
ylabel('Ks','FontName','Arial','FontSize',22,'FontWeight','normal','Color',[0 0 0])
zlabel('Relative error','FontName','Arial','FontSize',22,'FontWeight','normal','Color',[0 0 0])

%-----------------------------------------

figure(2)

[C,h]=contour(FM,TM,YD);
clabel(C,h,'FontName','Arial','FontSize',20,'LabelSpacing',200,'Color',[0 0 0]);
set(gca,'Xcolor',[0 0 0],'Ycolor',[0 0 0],'FontName','Arial','FontSize',16,'LineWidth',0.5);
set(h,'LineWidth',2);
```

```
axis square
shading interp
colormap jet
xlabel('Mass KOH','FontName','Arial','FontSize',22,'FontWeight','normal','Color',[0 0 0])
ylabel('Temperature /K','FontName','Arial','FontSize',22,'FontWeight','normal','Color',[0 0 0])

hold on

({'Surface and contour plot of HFPO yield (%) for molar feed ratio vs temperature'; 'at a fixed space time (120
s)'},'FontName','Arial','FontSize',20,'FontWeight','normal','Color',[0 0 0.6])
%-----------------------------------------------
figure(3)

plot(y,ypred,'ko','MarkerFaceColor','black','MarkerEdgeColor','black','MarkerSize',12)

hold on

FFDx=linspace(0,100,50);
FFDy=linspace(0,100,50);

plot(FFDx,FFDy,'k-','LineWidth',3)

set(gca,'XColor','k','YColor','k','LineWidth',0.5)

set(gca,'Ytick',0:10:50)
set(gca,'Xtick',0:10:50)

set(gca,'YTickLabel',{'0';'10';'20';'30';'40';'50'},'FontName','Arial'...
    ,'FontSize',16,'FontWeight','normal')

set(gca,'XTickLabel',{'0';'10';'20';'30';'40';'50'},'FontName','Arial'...
    ,'FontSize',16,'FontWeight','normal')

axis([0 50 0 50])
axis square
```

```
xlabel('Observed HFPO yield /%','FontName','Arial','FontSize',22,'FontWeight','normal')
ylabel('Predicted HFPO yield /%','FontName','Arial','FontSize',22,'FontWeight','normal')


B=zeros(3,3);

B(1,1)=(beta(8));
B(1,2)=(beta(5))/2;
B(1,3)=(beta(6))/2;
B(2,1)=(beta(5))/2;
B(2,2)=(beta(9));
B(2,3)=(beta(7))/2;
B(3,1)=(beta(6))/2;
B(3,2)=(beta(7))/2;
B(3,3)=(beta(10));

b=[beta(2); beta(3); beta(4)];

D=B^-1;

X0=-0.5*D*b;

X0T=X0';

Y0=beta(1)+0.5*X0T*b
```

E.3 Momentum Balance

E.3.1 Main file

```
unction uz = main(dimensions)
global ncall nx ny mmf b Ql g nu rho mu y

nx = dimensions(1);
ny = dimensions(2);
T = dimensions(3);

% Parameters shared with the ODE routine

% Initial condition (which also is consistent with the
% boundary conditions)
%Parameters
rho = 770.467;                                  %Perrys 2-116 = denisty of methanol at 97% purity
% T = 275;                                        %Assume T of 275 Kelvin
mu = exp(-25.317 + 1789.2/T + 2.069*log(T));    %Perrys 2-430 (Pa.s)
nu = mu/rho;                                    %Calculting kinematic viscosity
g = 9.81;                                       %Acceleration due to gravity(m/s^2)
b = 641*10^-6;                                  %Channel width
Ql = dimensions(4);                                %Liquid flow rate (m3/s)
Fl = 0.01;                                      %Liquid linear velocity (approximate in m/s)
% nx=5;
% ny=5;
for i=2:(nx)
    for j=1:ny
        if(i==1) u0(i,j)=0.0;
        elseif(i==ny)u0(i,j)=0;
        else u0(i,j)=Fl;
        end
    end
end
u0(:,1) = 0;
%
% Matrix conversion method flag
%
```

```
% mmf = 1 - explicit subscripting for matrix conversion
%
% mmf = 2 - Matlab reshape function
%
mmf=2;
%
% 2D to 1D matrix conversion
%
if(mmf==1)
    for i=1:nx
        for j=1:ny
            y0((i-1)*ny+j)=u0(i,j);
        end
    end
end
%
if(mmf==2)
y0=reshape(u0',1,nx*ny);
end
%
% Independent variable for ODE integration
t0=0.0;
tf=0.15;
tout=[t0:0.03:tf]';
nout=length(tout);
ncall=0;
%
% ODE integration
mf=1;
reltol=1.0e-04; abstol=1.0e-04;
options=odeset('RelTol',reltol,'AbsTol',abstol);
if(mf==1) % explicit FDs
[t,y]=ode15s(@pde_1,tout,y0,options); end
if(mf==2) ndss=4; % ndss = 2, 4, 6, 8 or 10 required
[t,y]=ode15s(@pde_2,tout,y0,options); end
if(mf==3) ndss=44; % ndss = 42, 44, 46, 48 or 50 required
[t,y]=ode15s(@pde_3,tout,y0,options); end

for it=1:nout
```

```
% 2D to 3D matrix conversion
u(it,:,:)=reshape(y(it,:),ny,nx)';
end

uz = reshape(u(nout,:,:),nx,ny);
end
```

E.3.2 Function file

```
function yt=pde_1(t,y)
%
% Function pde_1 computes the temporal derivative in the
% pseudo transient solution of Laplace's equation by explicit
% finite differences
%
% Problem parameters
global ncall nx ny mmf b Ql g nu rho yu uxx uyy mu
BB = y;
xl=0.0;
xu=b;%Width of a microchannel (m)
yl=0.0;
yu=(3 * Ql * nu/(b*g))^(1/3);      %Film thickness
%
% Initially zero derivatives in x, y, t
uxx=zeros(nx,ny); uyy=zeros(nx,ny); ut=zeros(nx,ny);
%
% 1D to 2D matrix conversion
if(mmf==1)
    for i=1:nx
        for j=1:ny
            u(i,j)=y((i-1)*ny+j);
        end
    end
end
if(mmf==2)
    u=reshape(y,ny,nx)';
end
%
% PDE
dx2=((xu-xl)/(nx-1))^2;
dy2=((yu-yl)/(ny-1))^2;
for i=1:nx
    for j=1:ny
%
% uxx
if(i==1) uxx(i,j)=0;
elseif(i==nx) uxx(i,j)=2.0*(u(i-1,j)-u(i,j))/dx2;
```

```
else uxx(i,j)=(u(i+1,j)-2.0*u(i,j)+u(i-1,j))/dx2;
end
%
% uyy
if(j~=1)&&(j~=ny)
uyy(i,j)=(u(i,j+1)-2.0*u(i,j)+u(i,j-1))/dy2;
end
%
% ut = nu(uxx + uyy) + rho*g
if(j==1)||(j==ny)ut(i,j)=0.0;
else ut(i,j)=mu*(uxx(i,j)+uyy(i,j))+ rho*g;
end
end
end
ut(1,:) = 0;

%
% 2D to 1D matrix conversion
if(mmf==1)
for i=1:nx
for j=1:ny
yt((i-1)*ny+j)=ut(i,j);
end
end
yt=yt';
end
if(mmf==2)
yt=reshape(ut',nx*ny,1);
end

% Increment calls to pde_1
ncall=ncall+1;
end
```

APPENDIX F: CHEMICAL DATA TABLE

IUPAC name	CAS number	Supplier	Supplier specified purity (%)	Determined purity (%)
Methanol	67-56-1	Laboratory Equipment and Supplies	99.9	99.6[a]
Potassium hydroxide	1310-58-3	Merck KGaA	85	-
Sodium hydroxide	1310-73-2	Merck KGaA	98	-
Propan-1-ol	71-23-8	Merck KGaA	99	99 [a]
Methyl-2,3,3,3-tetrafluoro-2-methoxypropionate	10186-63-7	ABCR GmbH and Co. KG	97	97.0 [a]
Hexafluoropropene	116-15-4	NECSA	-	99.8[b]
2,2,3-Trifluoro-3-(trifluoromethyl)-oxirane	428-59-1	NECSA	-	99.5[b]
Nitrogen	7727-37-9	Afrox	99.999	-

[a] Purity of confirmed by gas chromatography and area normalisation technique in this study.

[b] Purity of hexafluoropropene and 2,2,3-Trifluoro-3-(trifluoromethyl)-oxirane (referred to as hexafluoropropene oxide in this work) was identified using gas-chromatography by researchers at Thermodynamic Research Unit – University of KwaZulu-Natal (Dr. David Lokhat, 2012).